National Library
of Canada

Bibliothèque nationale
du Canada

Canadian Theses Service

Service des thèses canadiennes

Ottawa, Canada
K1A 0N4

NOTICE

The quality of this microform is heavily dependent upon the quality of the original thesis submitted for microfilming. Every effort has been made to ensure the highest quality of reproduction possible.

If pages are missing, contact the university which granted the degree.

Some pages may have indistinct print especially if the original pages were typed with a poor typewriter ribbon or if the university sent us an inferior photocopy.

Reproduction in full or in part of this microform is governed by the Canadian Copyright Act, R.S.C. 1970, c. C-30, and subsequent amendments.

AVIS

La qualité de cette microforme dépend grandement de la qualité de la thèse soumise au microfilmage. Nous avons tout fait pour assurer une qualité supérieure de reproduction.

S'il manque des pages, veuillez communiquer avec l'université qui a conféré le grade.

La qualité d'impression de certaines pages peut laisser à désirer, surtout si les pages originales ont été dactylographiées à l'aide d'un ruban usé ou si l'université nous a fait parvenir une photocopie de qualité inférieure.

La reproduction, même partielle, de cette microforme est soumise à la Loi canadienne sur le droit d'auteur, SRC 1970, c. C-30, et ses amendements subséquents.

NL-339 (r. 88/04) c

Canada

National Library of Canada
Canadian Theses Service
Ottawa, Canada
K1A 0N4

Bibliothèque nationale du Canada
Service des thèses canadiennes

The author has granted an irrevocable non-exclusive licence allowing the National Library of Canada to reproduce, loan, distribute or sell copies of his/her thesis by any means and in any form or format, making this thesis available to interested persons.

The author retains ownership of the copyright in his/her thesis. Neither the thesis nor substantial extracts from it may be printed or otherwise reproduced without his/her permission.

L'auteur a accordé une licence irrévocable et non exclusive permettant à la Bibliothèque nationale du Canada de reproduire, prêter, distribuer ou vendre des copies de sa thèse de quelque manière et sous quelque forme que ce soit pour mettre des exemplaires de cette thèse à la disposition des personnes intéressées.

L'auteur conserve la propriété du droit d'auteur qui protège sa thèse. Ni la thèse ni des extraits substantiels de celle-ci ne doivent être imprimés ou autrement reproduits sans son autorisation.

ISBN 0-315-55582-3

Canadä

THE UNIVERSITY OF ALBERTA

THERMO FIELD DYNAMICS OF A QUANTUM ALGEBRA AND ITS APPLICATION TO THE ANDERSON MODEL

BY

JOHN STEPHEN HEBRON

(C)

A THESIS
SUBMITTED TO THE FACULTY OF GRADUATE STUDIES AND RESEARCH IN PARTIAL FULFILLMENT OF THE REQUIREMENTS FOR THE DEGREE OF DOCTOR OF PHILOSOPHY

IN

THEORETICAL PHYSICS.

DEPARTMENT OF PHYSICS

EDMONTON, ALBERTA

FALL 1989

THE UNIVERSITY OF ALBERTA
RELEASE FORM

NAME OF AUTHOR: **John Stephen Hebron**

TITLE OF THESIS: **Thermo Field Dynamics of a Quantum Algebra and its Application to the Anderson Model**

DEGREE: **Doctor of Philosophy**

YEAR THIS DEGREE GRANTED: **1989**

Permission is hereby granted to THE UNIVERSITY OF ALBERTA LIBRARY to reproduce single copies of this thesis and to lend or sell such copies for private, scholarly, or scientific research purposes only.

The author reserves all other publication rights, and neither this thesis nor extensive extracts from it may be printed or otherwise reproduced without the author's written permission.

John Hebron

Box 1638
Didsbury, Alberta, Canada
T0M 0W0

5 August 1989

THE UNIVERSITY OF ALBERTA
FACULTY OF GRADUATE STUDIES AND RESEARCH

The undersigned certify that they have read, and recommend to the Faculty of Graduate Studies and Research for acceptance, a thesis entitled **"Thermo Field Dynamics of a Quantum Algebra and its Application to the Anderson Model"**, submitted by John Stephen Hebron in partial fulfillment of the requirements for the degree of **Doctor of Philosophy** in Theoretical Physics.

....
(Supervisor)

Piers Coleman
....

Martin Legaré
....

L B Woods
....

ANKamal
....

Date: July 5, 1989

DEDICATION

To all who feel the pain
And truly fear it,
May you break the chain
That binds your spirit.

To those who are lost
And thirst to fill their cup,
May you bear the cost
And never ever give up.

ABSTRACT

Quantum field theory was extended beyond its usual realm, by considering the situation where creation and annihilation operators do not satisfy the usual commutation relations but, rather, they form a "quantum algebra". This was done within the context of a thermal quantum field theory known as "thermo field dynamics". Most of the standard techniques of quantum field theory needed to be generalized, starting with finding an operator which annihilates the vacuum, making a generalized Wick's theorem, and developing Feynman rules. This generalization was explored by considering four models which are, in order of increasing level of difficulty, 1) a single, localized, N–fold degenerate fermionic state whose occupancy is restricted to a maximum of one fermion, 2) the first model with an interaction that merely shifts the energy of the state, 3) the single–site N–fold degenerate infinite–U Anderson model, and 4) the lattice Anderson model. The generalized Wick's theorem was found to break down, beyond a certain point in the reduction, necessitating the use of a time–splitting technique to complete the reduction. Feynman rules show a two–sector structure, having different rules in each sector; one of these sectors has very complex rules. No consistent self–energy expansion could be found for the Anderson model in this "bad" sector. Spontaneous vertices were found, which arise even in the absence of any interaction. These led to the creation of a "starting point function", which is a diagram connected to the starting point of a propagator. Non–cancelling vacuum diagrams were found. In the "bad" sector, these "vacuum diagrams" become multiply connected to the main diagrams. A method was found in which to disconnect these vacuum diagrams, yielding a renormalized perturbation expansion. Diagrammatic

analysis of the single-site and lattice Anderson models led to a topological classification of self-energies, and self-consistent Dyson equations, in the "good" sector. By ignoring the "bad" sector, limited success was found in reproducing known results. Specifically, the single-site result showed a phase transition to a Kondo resonance state at the correct Kondo temperature, and the lattice result showed a renormalized band structure with a mass enhancement comparable to that of heavy-fermion materials.

ACKNOWLEDGEMENTS

Six years have passed since I started the doctoral program at the University of Alberta. During this time, I was influenced by many good people. My supervisor, Professor Hiroomi Umezawa, inspired me greatly with his knowledge, his wealth of ideas, his enthusiasm, his kindness, and his positive outlook. I thank him for always having faith in me, even when I had lost faith in myself. Dr. Hideki Matsumoto was an invaluable resource in the initial phases of this project, before he left the U of A. His intimate technical knowledge of the intricate mathematical details of theoretical physics was most helpful. I thank Dr. John Whitehead for many stimulating conversations and for his inciteful ideas. Credit for the numerical work goes to Bob Teshima, who is a veritable wizard on the computer. For keeping me sane and making my life so much richer, I would like to acknowledge all of the graduate students and post doctoral fellows who touched my life at the U of A, especially Jim Pradko and Jackie, Dr. On Wong, Dr. Peter Piercy, Dr. Mikio Nakahara, Dr. Michele Guida and Mafalda, Ado Umezawa, Ian Hardman, Dr. Dave Jack, Mike Boyce, Drew Peterson, Eric Poisson, and George Tsoupros: a bunch of wild and crazy guys! Our time together was all too short. I miss the booby traps, hidden office furniture, night wars, night climbing, night tunneling, and general fellowship! For encouragement and moral support, during the long and sometimes torturous course of pursuing my PhD, I thank my close friends Dr. Mark Shegelski, Dr. Pierre Zakarauskas, Ron Rensink, and Jeff Creasey. To my little girls Barbie and Mindy, both of whom were born during the course of my doctoral research: you have enriched my life in ways I had never before imagined. I would like to acknowledge my wife Miriam for putting up with my being a student all these years, my

having a low income, and my being very busy all of the time. I thank her for the many times she took the kids out of the house for a few days, allowing me uninterrupted time to pursue my research. Perhaps now I can be a better husband and father. For financial support in the form of postgraduate scholarships, I am indebted to the Natural Sciences and Engineering Research Council, the Killam trustees, and the Alberta Heritage Scholarship fund. Finally, I thank my current employers at the University of Calgary Department of Mathematics and Statistics for granting me the leaves of absence necessary for completing this thesis.

This thesis was produced using the T^3 Scientific Word Processing System developed by TCI Software Research Inc., and printed on an HP Laserjet Series II printer connected to a Zenith AT microcomputer.

TABLE OF CONTENTS

CHAPTER and SECTION PAGE

1. INTRODUCTION 1
  - 1.1 Initial Motivation 1
  - 1.2 Heavy–Fermion Systems 1
  - 1.3 What Causes Heavy–Fermion Behaviour? 5
  - 1.4 The Kondo Effect 7
  - 1.5 The Anderson Model 9
  - 1.6 High T_c Superconductivity; Further Motivation to Study the Anderson Model 11
  - 1.7 What is Known About the Single–Site Anderson Model? 12
    - 1.7.1 Overview 12
    - 1.7.2 Haldane Scaling 12
    - 1.7.3 1/N Expansion 14
    - 1.7.4 Bethe Ansatz 16
    - 1.7.5 Fixed–Time–Ordering Goldstone Expansion; The Non-Crossing Approximation 17
    - 1.7.6 Functional Integral 19
    - 1.7.7 Slave Boson Method 20
    - 1.7.8 Renormalization Group and Fermi Liquid Considerations 21
  - 1.8 What is Known About the Lattice Anderson Model? 27
    - 1.8.1 Overview 27
    - 1.8.2 The Band Picture 28
    - 1.8.3 Fermi Liquid Considerations: The Luttinger Picture 33
    - 1.8.4 A Variational Approach 33

CHAPTER and SECTION PAGE

1.8.5 Fixed–Time–Ordering Goldstone Expansion; The Extended Non–Crossing Approximation 36
1.8.6 Slave Bosons and the 1/N Expansion 37
1.8.7 Other Methods 38
1.9 Revised Motivation 39
1.10 The Quantum Algebra Approach to the Anderson Model 41
1.11 Overview of This Thesis 42
2. TFD OF CANONICALLY QUANTIZED SYSTEMS; NOTATION 44
2.1 Introduction 44
2.2 What's It All About? 44
2.2.1 The Thermal Vacuum 44
2.2.2 The Tilde Field: Construction of the Vacuum 45
2.2.3 Why Is It A Pure State? 46
2.2.4 Physical Intuitions 47
2.3 Formal Construction of TFD 40
2.3.1 The Thermal State Condition 49
2.3.2 The Bogoliubov Transformation and Thermal Doublet Notation 50
2.4 Propagators and Spectral Functions 51
2.4.1 The General Form of the Thermal Propagator 51
2.4.2 The Analytic Properties of $\tilde{G}(z,\vec{k})$ 52
2.4.3 The Spectral Function 54
2.4.4 Summary 55
2.5 Perturbation Theory 55

CHAPTER and SECTION PAGE

3. TFD OF A QUANTUM ALGEBRA 57

3.1 Introduction 57

3.1.1 Canonical Quantization 57

3.1.2 Breaking Canonical Quantization; A Quantum Algebra of Eigenoperators 58

3.2 The Generalized Wick's Theorem 59

3.2.1 The Setup 59

3.2.2 Finding an Annihilation Operator 60

3.2.3 Wick's Theorem, Generalized 61

3.2.4 Zero–Energy Bosons, A Limitation 62

3.2.5 An Ambiguity in the Reduction 62

3.3 Vacuum Diagrams and the Generalized Gell–Mann Low Formula 65

3.3.1 The Most General Form of the Gell–Mann Low Formula 65

3.3.2 Why the U–Operators at $\mathcal{R}e\, t = \pm\infty$ Now Contribute Non–Cancelling Vacuum Diagrams 66

3.3.3 The Non–Commutativity of the Zero–Energy Boson Eigenoperators 69

4. LOCALIZED FERMIONIC STATES WITH RESTRICTED OCCUPANCY: A QUANTUM ALGEBRA 70

4.1 Introduction 70

4.2 The Model 70

4.2.1 Preliminary Consideration: A Non–Interacting Localized Fermion State 70

4.2.2 Restricted Occupancy: A Quantum Algebra 71

4.2.3 The Non-Canonical Quantization 73

4.3 Application of TFD: The ξ–Propagator and Sector Structure 74

4.3.1 Construction of the Vacuum 74

CHAPTER and SECTION PAGE

4.3.2 The ξ–Propagator 74

4.3.3 An Alternative: The $\xi^\dagger$ Propagator 75

4.3.4 Interpretation of the Sector Structure 76

4.4 The Multi–Point ξ–Functions 78

4.4.1 Spontaneous Vertices and Zero–Energy Bosons 78

4.4.2 The 4–Point Function: An Incomplete Reduction 79

4.5 Reduction of the Zero–Energy Boson T–Product Without the SU(N) Group; Time–Splitting 80

4.5.1 A Mistake in Previous Work Using the SU(N) Group 80

4.5.2 The Time–Splitting Technique 81

4.5.3 Derivation of Reduction Formulae for T–Products of X–Operators 82

4.5.4 A Shortcoming of the X–Operator Reduction: Multi–Point Vertices 85

4.5.5 An Alternate Set of Reduction Formulae for T–Products of X–Operators 86

4.5.6 Elimination of the Multi–Point Vertices 88

4.5.7 The Final Set of Non–SU(N) Reduction Formulae 89

4.5.8 Examples of X–Operator T–Product Reduction 90

4.6 The 4–Point ξ–Function: Completed 92

4.7 A Demonstration of the ϵ_f-μ Independence of the X–Operator Reduction 93

4.8 Reduction of the Zero–Energy Boson T–Product Using the SU(N) Group 94

4.8.1 Why Use the SU(N) Representation? 94

4.8.2 The SU(N) Algebra and its Consequences 95

CHAPTER and SECTION PAGE

4.8.3 Derivation of Reduction Formulae for T–Products of X_i–Operators 97

4.8.4 A Shortcoming of the X_i–Operator Reduction: Multi–Point Vertices 100

4.8.5 An Alternate Set of Reduction Formulae for T–Products of X_i–Operators 101

4.8.6 The Final Set of SU(N) Reduction Formulae 103

4.8.7 Examples of X_i–Operator T–Product Reduction 105

4.8.8 An Attempt to Remove the 2–Vertex Loops 106

4.8.9 Broken–Chain Examples of X_i–Operator T–Product Reduction 109

4.9 Diagrammatic Representation of Feynman Rules 112

4.9.1 The Building Blocks 112

4.9.2 The Non–SU(N) Rules 114

4.9.2.1 The ξ–Propagator 114

4.9.2.2 The X–Operator Function: Wiggle Diagrams 115

4.9.2.3 Vertex Types 116

4.9.2.4 Spin Labelling 116

4.9.2.5 Feynman Rules for Vertices 118

4.9.2.6 Feynman Rules for the n–Point ξ–Function 119

4.9.2.7 Decomposition of Wiggle Diagrams; Spin Labelling 121

4.9.2.8 Feynman Rules for Wiggle Vertices 124

4.9.2.9 Completion of Feynman Rules for the n–Point ξ–Function 124

4.9.2.10 The 2–Point, 4–Point, and 6–Point ξ–Functions 125

4.9.3 The Broken–Chain SU(N) Rules 131

4.9.3.1 Why Use This Reduction? 131

CHAPTER and SECTION PAGE

4.9.3.2 The Unbroken Chain: Wiggle Diagrams 131

4.9.3.3 Feynman Rules for Vertices 131

4.9.3.4 Feynman Rules for the n–Point ξ–Function 133

4.9.3.5 Decomposition of the Wiggle Diagrams 134

4.9.3.6 The Dotted Line 135

4.9.3.7 Feynman Rules for Wiggle Vertices 136

4.9.3.8 The 2–Wiggle, 3–Wiggle, 4–Wiggle, and 5–Wiggle 138

4.9.3.9 Completion of Feynman Rules for the n–Point ξ–Function 141

4.9.3.10 The 2–Point, 4–Point, and 6–Point ξ–Functions 141

4.10 Conclusion 147

5. AN EXACTLY SOLVABLE MODEL: SHIFTING THE ENERGY OF A CONSTRAINED FERMIONIC STATE 148

5.1 Introduction 148

5.2 The Model 148

5.3 The Fully Renormalized ξ–Propagator 151

5.4 Perturbative Calculation of the Full ξ–Propagator Ignoring the Vacuum Diagrams 151

5.5 Perturbative Calculation of the Full ξ–Propagator Using the Generalized Gell–Mann Low Formula 153

5.6 The Fully Renormalized 4–Point ξ–Function 155

5.7 Perturbative Calculation of the Full 4–Point ξ–Function Ignoring Vacuum Diagrams 156

5.8 Perturbative Calculation of the Full 4–Point ξ–Function Using the Generalized Gell–Mann Low Formula 160

5.9 Contractions Which Do Not Damp at $\mathcal{R}e\, t = \pm\infty$ 163

5.10 Conclusion 164

CHAPTER and SECTION PAGE

6. THE SINGLE IMPURITY INFINITE–U ANDERSON MODEL 166

6.1 The Model 166

6.1.1 The Hamiltonian 166

6.1.2 Chemical Potentials and the Energy Scale 167

6.1.3 The Propagators and Their Spectral Functions 168

6.1.4 Statement of the Problem 173

6.1.5 The Flat Band (D – Cutoff) Approximation 173

6.2 The Particle/Hole Sum Rule 176

6.2.1 Derivation of the Particle/Hole Sum Rule 176

6.2.2 Effect of the Particle/Hole Sum Rule On The f–Electron Spectral Function 177

6.2.3 The Particle/Hole Sum Rule With a Magnetic Interaction: A Paradox? 179

6.3 The Heisenberg Equations and the Resulting Bethe–Salpeter Equations 180

6.3.1 Derivation of the Heisenberg Equations 180

6.3.2 The Bethe–Salpeter Equation for the c–Electron 181

6.3.3 The Unitary Limit 183

6.3.4 Bethe–Salpeter Equations for the f–Electron Propagator 184

6.4 The Feynman Rules, Ignoring Vacuum Diagrams 188

6.4.1 Why Ignore the Vacuum Diagrams? 188

6.4.2 The c–Electron Propagator 188

6.4.3 The Non–SU(N) Rules 188

6.4.4 The Broken–Chain SU(N) Rules 192

6.5 "Vacuum Diagrams" and Their Effects 193

6.5.1 Are They *Really* Vacuum Diagrams? 193

CHAPTER and SECTION PAGE

6.5.2 Disconnection of the Vacuum Diagrams 198
6.5.2.1 The Hypothesis of Disconnection 198
6.5.2.2 Diagrammatic Representation of the Hypothesis 198
6.5.2.3 A Direct Non–Feynman Evaluation of the X–Operator T–Product 201
6.5.2.4 Direct Evaluation of the X–Operator T–Product Which Results When Vacuum Diagrams are Present 204
6.5.2.5 Proof of Disconnection; Confirmation of the Hypothesis 207
6.5.2.6 The Vacuum–Disconnected Perturbation Expansion 211
6.5.2.7 Modifications of the Feynman Rules 212
6.5.2.8 Examples of Vacuum Diagram Disconnection 212
6.5.3 Renormalization of the Projection Operators 216
6.6 "Regular" Vacuum Diagrams 217
6.6.1 Do the Regular Vacuum Diagrams Contribute? 217
6.6.2 Disconnection of the Regular Vacuum Diagrams 219
6.6.2.1 An Attempt, Using the SU(N) Rules 219
6.6.2.2 Partial Disconnection Using the Broken–Chain SU(N) Rules 221
6.7 The Renormalized Perturbation Expansion for $\mathcal{L}_R$ 226
6.7.1 $\mathcal{L}_R$ in Terms of the Renormalized Projection Operators 226
6.7.2 The Renormalized Feynman Rules 228
6.7.3 The Self–Consistent Calculation 228
6.8 Conclusion 229
7. RESULTS 230
7.1 The $\langle P_o \rangle$ Sector 230

CHAPTER and SECTION PAGE

7.1.1 The Renormalized Propagators, the Self–Energies, and the Starting–Point Function 230
7.1.2 Diagrammatics of the $\langle P_0 \rangle$ Sector to Three–Loop Order 233
7.1.3 The One–Loop Self–Consistent Calculation 236
7.2 The $\langle P_1 \rangle$ Sector 238
7.2.1 The Breakdown of the Self–Energy Expansion in the $\langle P_1 \rangle$ Sector 238
7.2.2 Finding a Lowest–Order Perturbative Scheme in the $\langle P_1 \rangle$ Sector 243
7.2.3 Diagrammatics of the $\langle P_1 \rangle$ Sector at Order $1/N^0$ 245
7.2.4 The $O(1/N^0)$ $\langle P_1 \rangle$ Sector Calculation 246
7.3 The Single–Site Results, Ignoring the $\langle P_1 \rangle$ Sector 247
7.3.1 Why Ignore the $\langle P_1 \rangle$ Sector? 247
7.3.2 The $\mathscr{d}_k$ Propagator and the Unitary Limit 248
7.3.3 Violation of the Particle/Hole Sum Rule 248
7.3.4 Numerical Calculations 249
7.3.5 The Kondo Solution and a Finite–T Phase Transition 257
7.3.6 Violation of the Friedel Sum Rule 259
7.3.7 Comparison to the Slave Boson Results 259
7.4 The Infinite–U Lattice Anderson Model 261
7.4.1 The Lattice Hamiltonian and the Feynman Rules 261
7.4.2 More Reason to Ignore the $\langle P_1 \rangle$ Sector 262
7.4.3 The Lattice–Renormalized Propagators, Self–Energies, and Starting–Point Function 264
7.4.4 The Lattice Dyson Equations 266
7.4.5 A Problem: Hidden Summation Restrictions 268
7.4.6 Lattice Diagrammatics to Three–Loop Order 269

CHAPTER and SECTION PAGE

7.4.7 The One–Loop Self–Consistent Lattice Calculation 270

7.4.8 Numerical Results of the Lattice Calculation 271

7.4.9 The Chemical Potential 273

1.4.10 The Mass Enhancement 274

8. CONCLUSION 276

8.1 Summary of This Thesis 276

8.2 Remarks 282

REFERENCES 284

APPENDIX A: USEFUL FORMULAE 288

APPENDIX B: VIOLATING THE CANONICAL QUANTIZATION CONDITION 292

LIST OF TABLES

TABLE PAGE

1.1 Properties of Heavy–Fermion Systems 3

LIST OF FIGURES

FIGURE PAGE

1.1 The Kondo Anomaly in Specific Heat 4
1.2 The Kondo Anomaly in Resistivity 5
1.3 Magnetic Moment Screening 6
1.4 The Kondo Resonance in the f–Electron Density of States 18
1.5 A Two–Resonance Form for the f–Electron Spectral Function 24
1.6 Typical Electronic Band Structure in a Weak Periodic Potential 28
1.7 The Flat Band (D–Cutoff) Approximation 30
1.8 Hybridization of the Conduction Band and the f–Band 31

2.1 The Sheet Structure of $\bar{G}(z,\vec{k})$ 53

4.1 Multi–Point Vertices in the X–Operator Reduction 86
4.2 The Linear Chain X–Operator Reduction 89
4.3 The Two Spontaneous Vertices 113
4.4 The $S^{\alpha\gamma}_{\epsilon_f}(t-t')$ Propagator 115
4.5 The Non–SU(N) Wiggle Diagrams 115
4.6 The Vertices 116
4.7 Non–SU(N) Spin Labelling of Diagrams 117
4.8 Non–SU(N) Feynman Rules for Vertices in the $\langle P_0\rangle$ Sector 118
4.9 Non–SU(N) Feynman Rules for Vertices in the $\langle P_1\rangle$ Sector 119
4.10a Spin Labelling the Non–SU(N) 2–Wiggle 121
4.10b Spin Labelling the Non–SU(N) 3–Wiggle 122
4.10c Spin Labelling the Non–SU(N) 4–Wiggle 122

FIGURE PAGE

4.10d Spin Labelling the Non–SU(N) 5–Wiggle 123
4.11 Non–SU(N) Feynman Rules for Wiggle Vertices 124
4.12 The 2–Point ξ–Function with Non–SU(N) Rules 125
4.13a The 4–Point ξ–Function in the $\langle P_0 \rangle$ Sector with Non–SU(N) Rules 126
4.13b The 4–Point ξ–Function in the $\langle P_1 \rangle$ Sector with Non–SU(N) Rules 127
4.14a The 6–Point ξ–Function in the $\langle P_0 \rangle$ Sector with Non–SU(N) Rules 128
4.14b The 6–Point ξ–Function in the $\langle P_1 \rangle$ Sector with Non–SU(N) Rules 129
4.15 SU(N) Feynman Rules for Vertices in the $\langle P_0 \rangle$ Sector 132
4.16 SU(N) Feynman Rules for Vertices in the $\langle P_1 \rangle$ Sector 132
4.17 Example: SU(N) Decomposition of a 15–Point Wiggle Diagram 135
4.18 Dotted Lines in a 15–Point SU(N) Wiggle Diagram 136
4.19 SU(N) Feynman Rules for Vertices Inside Wiggle Diagrams 137
4.20 The Trace Convention 138
4.21a The SU(N) 2–Wiggle Decomposition 138
4.21b The SU(N) 3–Wiggle Decomposition 139
4.21c The SU(N) 4–Wiggle Decomposition 139
4.21d The SU(N) 5–Wiggle Decomposition 140
4.22 The 4–Point ξ–Function in the $\langle P_1 \rangle$ Sector With SU(N) Rules 143
4.23 The 6–Point ξ–Function in the $\langle P_1 \rangle$ Sector With SU(N) Rules 144

6.1 The Free Conduction Electron Density of States 172
6.2 Diagrammatic Representation of the C_0 Propagator 188

FIGURE PAGE

6.3 Non–SU(N) Feynman Rules for Interaction Vertices in the $\langle P_0 \rangle$ Sector 189

6.4 Non–SU(N) Feynman Rules for Interaction Vertices in the $\langle P_1 \rangle$ Sector 190

6.5 Point–Splitting of the Cross–Vertex, Showing the Flow of Spin 191

6.6 SU(N) Feynman Rules for Interaction Vertices in the $\langle P_o \rangle$ Sector 192

6.7 SU(N) Feynman Rules for Interaction Vertices in the $\langle P_1 \rangle$ Sector 193

6.8 Diagrammatic Representation of $F_{wc}\left[S_{\varepsilon_f}, C_o\right]$ 199

6.9 Diagrammatic Representation of $V_{wc+}\left[S_{\varepsilon_f}, C_o\right]$ and $V_{wc+}\left[S_{\varepsilon_f}, C_o\right]$ 199

6.10 Connection of the "Vacuum Diagrams" to the Main Diagram 200

6.11 How the Vacuum Diagrams Might Disconnect from the Main Diagrams 201

6.12 A Decomposition of FIG. 6.10 Using Equation (6.104) 207

6.13 How FIG. 6.12 Disconnects, Confirming the Hypothesis of FIG. 6.11 210

6.14 Splitting the 3–Wiggle 213

6.15 Another Splitting of the 3–Wiggle 213

6.16 Splitting the 4–Wiggle 214

6.17 Another Splitting of the 4–Wiggle 214

6.18 Splitting the 5–Wiggle 215

6.19 Splitting the 9–Wiggle 215

6.20 Regular Vacuum Diagrams Which Vanish Using the SU(N) Trace Rules 218

6.21 A Regular Vacuum Diagram Which Does Not Vanish 218

FIGURE PAGE

6.22 Splitting the 4–Wiggle Into Two 2–Wiggles When $t_1 > t_3 > t_4 > t_2$ and $\gamma_1 = \gamma_2 = \gamma_3 = \gamma_4 = 1$ 220

6.23 Reducing the 4–Wiggle When $t_1 > t_3 > t_2 > t_4$ and $\gamma_1 = \gamma_2 = \gamma_3 = \gamma_4 = 1$ 221

6.24 Diagrammatic Decomposition of the Regular Vacuum Diagrams Which Compose $\langle P_l \rangle_R$, Using SU(N) Rules 222

6.25 Decomposition of $\mathscr{A}_R$ in the $\langle P_o \rangle$ Sector, Using SU(N) Rules and Ignoring Vacuum Diagrams at $\mathcal{R}e\, t = \pm\infty$ 224

6.26 An at Factorizing the Diagrams Which Renormalize $\langle P_l \rangle$ 225

7.1 The Self–Energy Expansion of $\mathscr{A}_R$ in the $\langle P_o \rangle$ Sector 230

7.2 f–Connection 232

7.3 Diagrammatic Representation of the Renormalized Propagators 233

7.4 A Diagram Included in the Self–Consistent One–Loop Calculation 239

7.5 A Set of n–Loop Diagrams Which All Combine at Order $1/N^0$ 240

7.6 Portions of the 5–Point Wiggle Which Contribute at Order $1/N^0$ 241

7.7 Portions of the 5–Point Wiggle Which Do Not Contribute at $O(1/N^0)$ 242

7.8 The First Order Approximation for $\mathscr{A}_R$ in the $\langle P_l \rangle$ Sector 243

7.9 A Wiggle–Line Chain Connected to a Vertex Within a Tadpole Diagram 244

7.10 A Regular Vacuum Diagram Which Renormalizes a Wiggle Line Loop 244

7.11 Diagrammatic Representation of $S_R^{(0)}(\ell=1)$ and $\dot{S}_R^{(0)}(\ell=1)$ 245

7.12 $\tilde{\varepsilon}_f$ Versus $\ell n(k_B T/|\varepsilon_f|)$ for $D = 8.33$, $N = 4$, and Various Δ 250

7.13 Γ_T Versus $\ell n(k_B T/|\varepsilon_f|)$ for $D = 8.33$, $N = 4$, and Various Δ 251

FIGURE PAGE

7.14 $\tilde{\varepsilon}_f$ Versus $\ln(k_B T/|\varepsilon_f|)$ for $D = 8.33$, $N = 15$, and Various Δ 252

7.15 Γ_T Versus $\ln(k_B T/|\varepsilon_f|)$ for $D = 8.33$, $N = 15$, and Various Δ 253

7.16 $\tilde{\varepsilon}_f$ Versus $\ln(k_B T/|\varepsilon_f|)$ for $D = 8.33$, $N = \infty$, and Various Δ 254

7.17 Γ_T Versus $\ln(k_B T/|\varepsilon_f|)$ for $D = 8.33$, $N = \infty$, and Various Δ 255

7.18 The Intersite c–Electron Propagator and its Vertices 262

7.19 Examples of Lattice Renormalization of a Self–Energy Diagram at Site n 263

7.20 Lattice Corrections 265

7.21 Diagrammatic Representation of the Renormalized Propagators 266

7.22 The Dyson Equation for C^L 267

7.23 Transformations Which Turn Single–Site Diagrams Into Lattice Diagrams 270

CHAPTER 1
INTRODUCTION

1.1 INITIAL MOTIVATION

When I started this research project in 1984, its objective was quite ambitious: to quantitatively explain the observed peculiar properties of the so-called "heavy-fermion" materials. At the time, this was a hot topic, causing considerable excitement in the international physics community. Heavy-fermion materials presented the first example of a new type of superconductivity, which could not be explained by any of the current theories. Now, of course, the hot topic is high T_c superconductors, which presents us with an even more exotic type of superconductivity. Because of the practical technological benefits of high T_c superconductors, most research on heavy fermion systems has been dropped. And yet heavy fermion behaviour is not fully understood.

1.2 HEAVY-FERMION SYSTEMS

It all started in 1979 when Steglich, et al. [1] discovered superconductivity in $CeCu_2Si_2$ at 0.5 K. This was unexpected because the Cerium atoms contain tightly bound f-electrons which act like localized magnetic moments. Near room temperatures, this lattice of localized spins obeys the Curie Weiss law for paramagnetic susceptibility. This usually leads to a magnetic ordering transition at low temperatures. A superconducting phase transition is not usually found in such a system, because the incoherent spin-flip scattering generated by local moments is strongly pair-breaking. Other anomalies of this system include a very high effective mass for the conduction electrons, ($m^* \sim 100\ m_e$ [2]), and hence the name "heavy-fermions". Somehow these highly renormalized conduction electrons screen the localized magnetic moments and their pair-breaking effects, and are responsible for a new brand of superconductivity.

The subsequent discovery of heavy-fermion superconductivity in UBe_{13} at 0.9 K (1983) [3] and in UPt_3 at 0.5 K (1984) [4] confirmed what was found in $CeCu_2Si_2$. In particular, the Uranium atoms contain tightly bound f-electrons having properties similar to those of the Cerium atoms.

Not all heavy-fermion systems are superconductors. Some of these systems, which have a very high electron effective mass, undergo a magnetic ordering transition at low temperatures, such as $NpBe_{13}$, U_2Zn_{17} , and UCd_{11} , whereas others, such as $CeAl_3$ and $CeCu_6$, show no phase transition down to 0.05 K.

A good review article on the properties of heavy-fermion metals was done in 1984 by Stewart [2]. Table 1.1 below summarizes the major properties of the prominent heavy-fermion systems.

The entries in this table require some explanation. Firstly, the low-temperature specific heat of a metal is given by:

$$C = \gamma T + \beta T^3 + (\delta T^3 \ln T) , \tag{1.1}$$

where the γ term is due to electronic excitation, the β term is due to phonon excitation, and the δ term is due to possible spin fluctuations. In a normal metal $\gamma \sim 0(1)$ mJ/f-atom mol/K^2. The high values of γ in table 1.1 indicate that the effective mass of the conduction electrons is enormous. $\gamma(0)$ means that the curve of C/T versus T^2 was extrapolated to T=0, ignoring any phase transition at low T. Stewart [2] defines a heavy-fermion system as one having $\gamma(0) > 400$ mJ/f-atom mol/K^2.

Name	Ordering	Critical T (K)	d_{f-f} (Å)	$\gamma(0)$ $\left[\frac{\text{mJ}}{\text{mol K}^2}\right]$	$\chi(0)$ $\left[10^{-3}\frac{\text{emu}}{\text{mol G}}\right]$	Comment
$CeCu_2Si_2$	super	0.5	4.1	1100	7 –?	K.A.*
UBe_{13}	super	0.9	5.13	1100	15	(K.A.)
UPt_3	super	0.5	4.1	450	7	S.F.
$NpBe_{13}$	magnetic	3.4	5.13	900 –?	56	K.A.
U_2Zn_{17}	magnetic	9.7	4.39	535	12.5	
UCd_{11}	magnetic	5.0	6.56	840	38	
$CeAl_3$	none	to .02 K	4.43	1600	36	K.A.*
$CeCu_6$	none	to .02 K	4.63	~1600	27	K.A.

Table 1.1

Properties of Heavy–Fermion Systems

The most prominent of the heavy–fermion systems are listed, along with what type of ordering they undergo, and the critical temperature of this ordering. d_{f-f} is the inter–atomic spacing of the f–electron atoms, $\gamma(0)$ is the linear coefficient of specific heat at T=0, and $\chi(0)$ is the magnetic susceptibility at T=0. Entries marked with a "?" showed a wide range of experimental variation. The comment "K.A." refers to the Kondo Anomaly, and "S.F." refers to Spin Fluctuations. "*" means that the feature is pronounced, and "( )" means that the feature is weak.

$\chi(0)$ is the magnetic susceptibility, extrapolated to T = 0, again ignoring any low temperature phase transitions. (From 100 – 300 K, the susceptibility obeys the Curie–Weiss law with large μ_{eff} ($>>\mu_B$).). Compare these $\chi(0)$ values to $\chi(0) \simeq 0.5 \times 10^{-3}$ emu/mol G for Pu [2], the f–electron atom closest to being magnetic. One may thereby see that the magnetic susceptibility is gigantic, which adds to the mystery of why some of these systems become superconducting.

d_{f-f} is the spacing between nearest neighbor f–electron atoms. Note that these values are all larger than the Hill limit, $d_o \simeq 3.25$–3.50 Å. The Hill limit [5] is defined such that when $d_{f-f} > d_o$, there is no f–electron overlap; thus the f–electrons are localized rather than itinerant, and one expects magnetism to occur.

The comments "K.A." and "S.F." in table 1.1 refer to the "Kondo Anomaly" and "Spin Fluctuations". The "S.F." for UPt_3 means that the $T^3 \ln T$ term of eq. (1.1) was observed in the specific heat of this metal. This could indicate that the superconductivity is not due to the usual BCS type singlet pairing, but could be due to triplet pairing or something more exotic.

The Kondo anomaly manifests itself as a departure from eq. (1.1) at low $T>T_c$, in that γ rises dramatically. This is illustrated in FIG. 1.1.

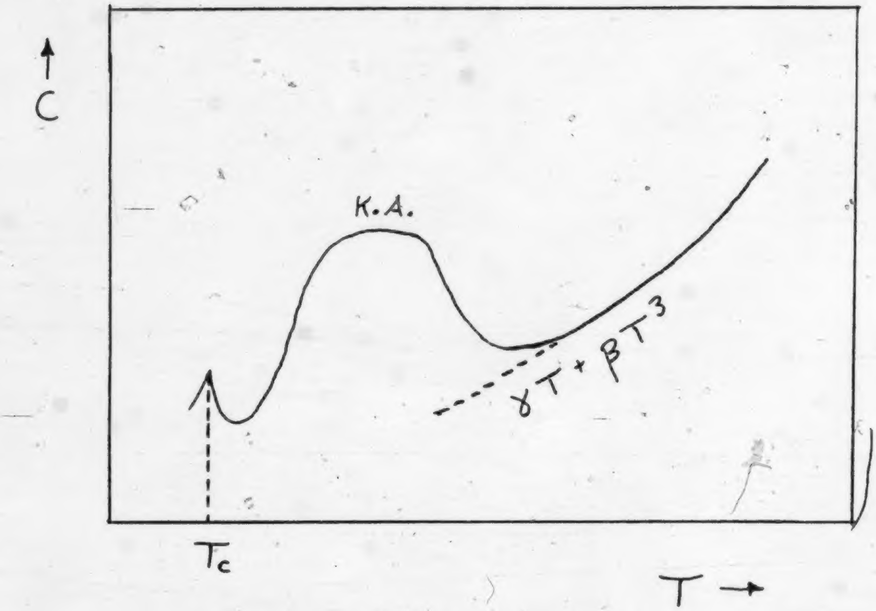

FIG. 1.1

The Kondo Anomaly in Specific Heat

At relatively low temperatures, the specific heat follows eq. (1.1). As the temperature is further lowered, the Kondo Anomaly may show up. This is labeled "K.A.". At still lower temperatures, there may be a superconducting or magnetic phase transition. This point is labeled T_c.

Another manifestation of the Kondo anomaly is a rise in resistivity at low $T>T_c$. The resistivity of a "normal" metal is given by:

$$\rho = \rho_o + BT^5, \tag{1.2}$$

where ρ_o is due to crystal defects, and the B term is due to phonon interactions. The Kondo anomaly, as a departure from eq. (1.2), is illustrated in FIG. 1.2.

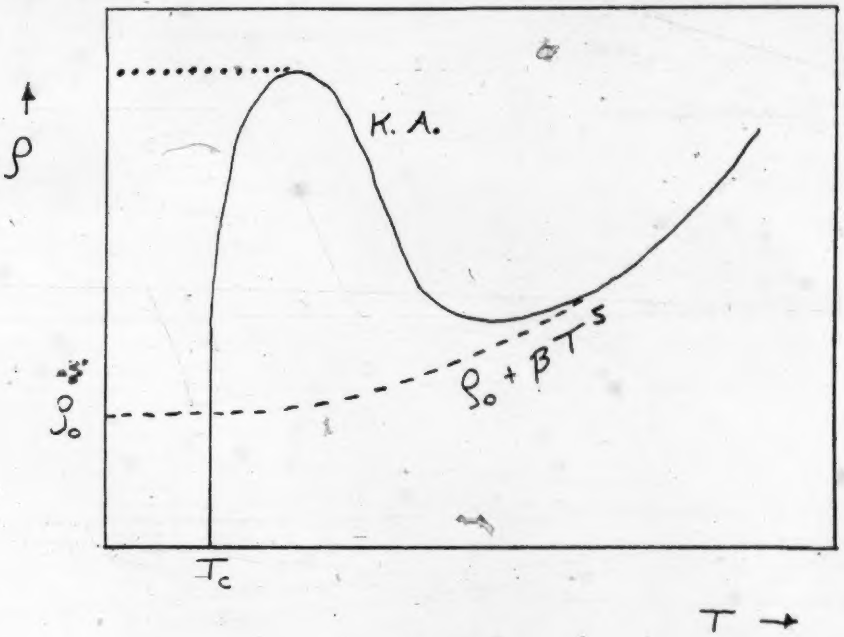

FIG. 1.2

The Kondo Anomaly in Resistivity

At relatively low temperatures, the resistivity follows eq. (1.2). As the temperature is further lowered, the Kondo Anomaly may show up. This is labeled "K.A.". At still lower temperatures, there may be a superconducting transition. This point is labeled T_c. (If there is no phase transition, then the resistivity follows the dotted line.)

1.3 WHAT CAUSES HEAVY-FERMION BEHAVIOUR?

A number of questions come to mind: 1) Why is Hill's rule violated? 2) What causes the high effective masses of the conduction electrons? 3) What causes the high magnetic susceptibility? 4) What is responsible for the Kondo Anomaly? 5) What makes these highly magnetic systems become superconducting? 6) What kind of superconductivity is it? 7) Why do some heavy fermion systems become magnetically ordered or show no ordering, rather than becoming superconducting?

Most of the above questions may be qualitatively answered by the obvious statement that there is strong hybridization between the f–electrons and the conduction electrons ("c–electrons"). The interaction between the c–electrons and the f–electron state causes a mass renormalization, which may account for the high effective mass. Hill's rule is violated because, although the f–atoms are too far apart for the f–orbitals to overlap, the f–electrons may still become itinerant due to the hybridization.

A high magnetic susceptibility at low temperatures can also be explained by the renormalization. At high temperatures, the c–electron spins will be randomized, and the f–electron spins will obey a Curie–Weiss law. Suppose that, at low temperatures, the c–electron spins screen the f–electron magnetic moment, forming a quasi–bound state, as in FIG. 1.3(a). Although this state has no net magnetic moment, one would still expect a high magnetic susceptibility due to the state becoming polarized in a magnetic field. (See FIG. 1.3(b).) At still lower temperatures, a long–range coherence may be established, causing a superconducting or a magnetic phase transition.

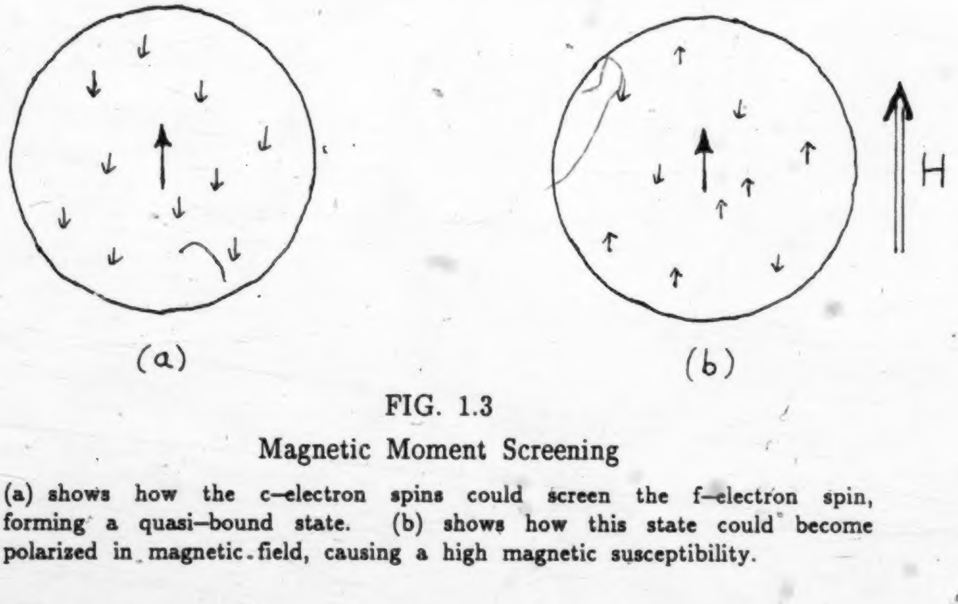

FIG. 1.3

Magnetic Moment Screening

(a) shows how the c–electron spins could screen the f–electron spin, forming a quasi–bound state. (b) shows how this state could become polarized in magnetic field, causing a high magnetic susceptibility.

The Kondo anomaly is also a result of the interaction of f–electrons with c–electrons, as explained in the next section.

Therefore, it appears that a highly renormalized, strongly interacting Fermi liquid is found as one lowers the temperature to where γ, χ, and ρ rise dramatically. It would be a great achievement to develop a microscopic model which would quantitatively predict the shapes of these curves at low temperatures. It would be an even greater achievement to show how this Fermi liquid can undergo a Bose condensation into a superconducting state, at still lower temperatures. An early review of the theoretical attempts to do this was given by Lee [6].

1.4 THE KONDO EFFECT

As the name "Kondo Anomaly" suggests, its explanation may be the well–known Kondo effect, first theorized by Kondo in 1963 [7,8].

Kondo used a Hamiltonian known as the s–d model, in which free s–wave conduction electrons interact via spin–exchange with a localized d–electron spin impurity. The free conduction electron Hamiltonian is:

$$H_o = \sum_{\mathbf{k}s} \epsilon_{\mathbf{k}} c^{\dagger}_{\mathbf{k}s} c_{\mathbf{k}s} \quad , \tag{1.3}$$

where $c^{\dagger}_{\mathbf{k}s}$ and $c_{\mathbf{k}s}$ are the creation and annihilation operators of conduction electrons with momentum $\vec{k}$, energy $\epsilon_{\mathbf{k}}$, and spin s. The interaction is given by:

$$H_{s-d} = J\, \vec{S}_c \cdot \vec{S}_d \quad , \tag{1.4a}$$

$$\vec{S}_c = \sum_{ss'} c^{\dagger}_{os}\, \vec{\sigma}_{ss'}\, c_{os'} \quad , \tag{1.4b}$$

where $c^{\dagger}_{os}$ and c_{os} are the creation and annihilation operators of conduction electrons with spin s, at the site of the d–electron impurity, $\vec{\sigma}$ are the Pauli spin matrices, and $\vec{S}_d$ is the spin operator for the d–electron impurity.

Applying perturbation theory to this Hamiltonian yields a $\ln T$ divergence in the resistivity [7,8,9,10]. The amplitude for a conduction electron of momentum $\vec{k}$ to scatter into momentum $\vec{k}'$ is given by [10]:

$$T_{k'k} \sim J\ N(0) + (J\ N(0))^2 \ln\left[\frac{D}{k_B T}\right] + \ldots \qquad (1.5)$$

where N(0) is the energy density of states at the Fermi surface, k_B is Boltzman's constant, and D is the conduction electron cutoff. (It is assumed that the conduction electrons exist in a flat energy band width 2D centered on the Fermi energy.) The higher order terms in eq. (1.5) contain higher powers of $\ln\left[\frac{D}{k_B T}\right]$.

This logarithmically divergent expression is what causes the rise in resistivity at low temperature known as the Kondo effect. Of course, at very low temperatures perturbation theory breaks down. A more careful treatment shows that the resistivity saturates to a constant value when $T << T_K$, the Kondo temperature.

One may show [10], that the anti-ferromagnetic interaction of eq. (1.4) ($J>0$) can form a bound state between the localized spin and an itinerant spin. This bound state has a binding energy E_B of the order:

$$E_B \sim D\ e^{-1/JN(0)} \quad . \qquad (1.6)$$

The Kondo ground state ($T << E_B$) is essentially non-magnetic, whereas the Curie-Weiss law is obeyed when $T >> E_B$. This would explain the screening of magnetic moments discussed in section 1.3.

Of course, the s-d model does not explain everything. It does not even fully explain the Kondo anomaly. The s-d model predicts the dotted line in FIG. 1.2, representing saturation of the divergent spin scattering. It does not explain why there is a precipitous fall in resistivity, after the Kondo rise, and yet well before the superconducting transition. This fall may well be due to "dense" or "lattice" Kondo effects. The s-d model, which considers only one impurity atom, is applicable only to systems with dilute impurities. The heavy–fermion systems, on the other hand, have a regular lattice of localized f–spins, interacting with the conduction electrons. Perhaps a "Kondo" coherence is established at very low temperatures, causing the resistivity to fall.

Another drawback of the s–d model is that it assumes the impurity site to be occupied by a single localized electron. This prohibits the possibility of hybridization interactions, which may cause the localized electrons to become itinerant. The Anderson model enables this possibility.

1.5 THE ANDERSON MODEL

First proposed by Anderson in 1961 [11], the Anderson model today still attracts much theoretical attention. It is more general than the s–d model and yet appears deceptively simple. In its simplest form, the "single–site" Anderson model, a single magnetic impurity interacts with a conduction electron gas, in that electrons may jump from the conduction band to the impurity level and vice versa. This is in contrast with the s–d model in which the impurity electron is not free to leave, and interacts with the conduction band only via spin exchange.

The single–site Anderson Hamiltonian is given by:

$$H = \sum_s \int d^3x \; c_s^\dagger(\vec{x}) \; \varepsilon(-i\vec{\nabla}) \; c_s(\vec{x}) \;+\; \varepsilon_f \sum_s f_s^\dagger f_s \;+ \\ +\; U \, f_\uparrow^\dagger f_\uparrow f_\downarrow^\dagger f_\downarrow \;+\; V \sum_s \left[c_{0s}^\dagger f_s + f_s^\dagger c_{0s} \right] \,, \tag{1.7}$$

where $c_s^\dagger(\vec{x})$ and $c_s(\vec{x})$ are the conduction electron operators with spin index s, $\varepsilon(-i\vec{\nabla}) = -\frac{\vec{\nabla}^2}{2m} - \mu$ is the free electron energy, $f_s^\dagger$ and f_s are the creation and annihilation operators of an electron of spin s in the localized f–level of the impurity atom, with $\varepsilon_f < 0$ being the energy of this state (energy 0 being the Fermi surface), U is the Coulomb repulsion between two electrons in a doubly occupied impurity level, $c^\dagger_{os}$ and c_{os} are the creation and annihilation operators of conduction electrons at the impurity site, and V is the interaction strength.

c_{os} is given by:

$$c_{os} \equiv \sqrt{\Omega}\, c_s(\vec{x}=0) \quad , \tag{1.8}$$

where $\vec{x} = 0$ is the location of the impurity atom and Ω is the volume of a unit cell of the metal. This ensures the following anti-commutation relations:

$$\left\{c_s(\vec{x}) \ , \ c^\dagger_{s'}(\vec{x}')\right\} = \delta_{ss'} \ \delta^3(\vec{x}-\vec{x}') \tag{1.9a}$$

$$\left\{c_{os} \ , \ c^\dagger_{os'}\right\} = \delta_{ss'} \ . \tag{1.9b}$$

Of course, any Dirac delta function in position space is restricted by the finite k-volume of the Brillouin zone (Ω_B) and any Dirac delta function in momentum space is restricted by the finite volume of the crystal (V_c):

$$\delta^3(\vec{x}-\vec{y}) \equiv \frac{1}{(2\pi)^3} \int_{\Omega_B} d^3k \ e^{i\vec{k}\cdot(\vec{x}-\vec{y})} = \frac{\Omega_B}{(2\pi)^3} \ \delta_{\vec{x},\vec{y}} = \frac{1}{\Omega} \ \delta_{\vec{x},\vec{y}} \tag{1.10a}$$

$$\delta^3(\vec{k}-\vec{q}) \equiv \frac{1}{(2\pi)^3} \int_{V_c} d^3x \ e^{i((\vec{k}-\vec{q})\cdot\vec{x})} = \frac{V_c}{(2\pi)^3} \ \delta_{\vec{k},\vec{q}} \ . \tag{1.10b}$$

(Natural units are used throughout this thesis: $\hbar = c = 1$.)

The f-electron operators also satisfy the usual algebra:

$$\left\{f_s \ , \ f^\dagger_{s'}\right\} = \delta_{ss'} \ . \tag{1.11}$$

It can be shown [8,9] that the s-d model may be derived from the Anderson model under certain conditions, (such as assuming the impurity state to be singly occupied). In fact, the two models are related by a canonical transformation [12]. Thus the Anderson model also shows the Kondo effect. It has the advantage that when V is sufficiently large the f-level can be broadened to the point that it overlaps the Fermi surface, such that the f-electrons become itinerant. This is called valence mixing.

The Anderson model, and its extension, the lattice Anderson model, are used extensively by theoreticians attempting to explain heavy-fermion behaviour. The single-site Anderson model is useful for explaining effects that start to show up near 10 K or 15 K, such as the Kondo anomaly. To explain the coherence effects which start to show up at still lower temperatures, one needs to use the lattice Anderson model. It is essentially the same as eq. (1.7), with the following replacements: $f_s \to f_{ns}$, $f_s^\dagger \to f_{ns}^\dagger$, $c_{os} \to c_{ns}$, $c_{os}^\dagger \to c_{ns}^\dagger$, and one sums over the site index n.

1.6 HIGH Tc SUPERCONDUCTIVITY; FURTHER MOTIVATION TO STUDY THE ANDERSON MODEL

For over a decade, the highest temperature superconductor was Nb_3Ge which has a $T_c \simeq 24$ K. One needs liquid helium to reach this temperature; this is expensive and thus technological applications of superconductivity were limited. In the summer of 1986, Bednorz and Muller [13] shocked the scientific community with their discovery of the onset of superconductivity at 30 K in a multiphase compound of $Ba_xLa_{5-x}Cu_5O_{5(3-y)}$ (for which they won the Nobel prize in 1987). The superconducting phase was identified by Takagi et al. [14] to be $La_{2-x}Ba_xCuO_{4-\delta}$. A flurry of activity began, in which various copper oxide metals were investigated. The world was further astounded when Wu, et al. [15] and Hor et al. [16] reported $T_c > 90$ K in a mixed phase compound of Y–Ba–Cu–O. This has great potential in terms of technological applications, because one no longer needs liquid helium to reach the superconducting temperature. Cheap liquid nitrogen at 77K will do the job.

Since then, many high T_c copper oxide materials have been investigated. All of these materials contain atoms such as Y and La, which have a d–electron level, somewhat similar to the f–electron level in heavy–fermion metals. It is not yet known what kind of a role, if any, this d–electron state plays in the high T_c properties. It may be important to consider the effect of this d–state, and the Anderson model may be well suited in this endeavor. Thus, one has another motivation for studying the Anderson model.

1.7 WHAT IS KNOWN ABOUT THE SINGLE–SITE ANDERSON MODEL?

1.7.1 OVERVIEW

The obvious method that comes to mind when trying to solve the system described by eq. (1.7) is to directly apply standard perturbation theory in U and V. While this has been done in the past, and may be useful for some purposes, it is not really relevant to systems in which the impurity state is a highly localized f–orbital. In this case, one would expect the Coulomb repulsion, U, to be very large. The standard procedure is to take $U \rightarrow \infty$, such that double occupancy of the f–state is forbidden.

When $U \rightarrow \infty$, the f–electron operators in eq. (1.7) transform into Hubbard operators [17]. The details of this will be described in Chapter 4 (section 4.2.2). Essentially, the Hubbard operators obey a Hubbard algebra, rather than the standard anti–commutation relations of fermion creation/annihilation operators. This means that there is no Wick's theorem and hence, conventional quantum field theoretical methods break down.

This problem has been circumvented in many ways. Below are described some of these methods, to give the reader a taste for the flavour of various approaches. Please note that this is not intended to be a complete review of the subject.

1.7.2 HALDANE SCALING

One should keep in mind that the conduction electrons important to the transport properties of a metal are those near the Fermi surface. This is because the Fermi temperature of a typical metal is 10^4 to 10^5 K; therefore at room temperatures and below, the electron gas is highly degenerate with most excitations near the Fermi surface. A good approximation is to assume the conduction band to be of width 2D centred on the Fermi surface, and to take the density of states in this band to be a constant, N(0), which is the number of momentum states per unit energy per unit cell at the Fermi level. One then has:

$$2DN(0) = 1 \ , \tag{1.12}$$

because there is one momentum state per unit cell.

Within this approximation, one finds that objects calculated will depend on the band cut–off, D. (For example, see eq. (1.5).) Haldane [18] argued that if one scales the cut–off D, the low energy physics should remain unchanged. That is, the physics should depend on certain "scaling invariants", and changing D will renormalize only the "bare" unobserved quantities.

The scaling invariants found by Haldane were Δ the interaction strength, and ε_f^* the physical f–electron energy, defined by:

$$\Delta \equiv \pi V^2 N(0) \ , \tag{1.13}$$

$$\varepsilon_f^* = \varepsilon_f + \frac{\Delta}{\pi} \ln\left[\frac{D}{\Delta}\right] \ . \tag{1.14}$$

At lowest order perturbation theory, Δ is roughly the half width at half the maximum of the renormalized f–resonance, and ε_f^* is its position. It was found that these scaling invariants may be used to classify certain regimes of behaviour for the Anderson model.

Three general regimes for the Anderson model are the empty impurity, mixed valence, and Kondo regimes. The empty impurity regime occurs when $\varepsilon_f^* >> \Delta$. This means that the f–level is above the Fermi surface and does not overlap it; thus it remains unoccupied at low temperatures. There exists a temperature T_{FL}, below which the system behaves like a Fermi liquid and has $\langle n_f \rangle \simeq 0$, where n_f is the number of electrons occupying the f–state.

The mixed valence regime occurs when $|\epsilon_f^*| \lesssim \Delta$, such that the f–level overlaps the Fermi surface. In this case the system becomes a Fermi liquid when $T \lesssim \Delta$. It is called mixed valence, fluctuating valence, or intermediate valence, because $\langle n_f \rangle$ is non–integral, even at T=0.

The Kondo regime occurs when $-\epsilon_f^* >> \Delta$, such that the f–level is well below the Fermi surface. Haldane found that there exists a temperature $\tilde{T} >> \Delta$, below which $\langle n_f \rangle \simeq 1$, and thus the Anderson model becomes equivalent to the s–d model, using the Schrieffer–Wolff transformation [12]. Furthermore, below a Kondo temperature $T_K << \Delta$, a Fermi liquid is formed in which the local moment is quenched. This is the Kondo bound state described in section 1.4.

1.7.3 1/N EXPANSION

In virtually all perturbative approaches to solving the Anderson model, one encounters great difficulty. It has been found that some of the fog is lifted by considering a large–N expansion, where N is the degeneracy of the localized state. The Anderson Hamiltonian of eq. (1.7) assumes N=2; an extension of this to the general N ("spin J") case is given as follows:

$$H = \sum_m \int d^3x \; c_m^\dagger(\vec{x}) \; \epsilon(-i\vec{\nabla}) \; c_m(\vec{x}) \; + \; \epsilon_f \, n_f \; + \; + \; \frac{U}{2} \, n_f \, (n_f - 1) \; + \; \sqrt{\frac{2}{N}} \, V \sum_m \left[c_{om}^\dagger \, f_m + f_m^\dagger \, c_{om} \right] \; , \qquad (1.15)$$

where

$$n_f \equiv \sum_m f_m^\dagger \, f_m \; , \qquad (1.16)$$

m = –J, –J+1, ... J, and N = 2J+1.

Although this model is vastly simplified, it may be justified as follows. Firstly, the f–electron is in an L=3 orbital angular momentum state, and has spin 1/2, so that the angular momenta may couple to form a J=5/2 or J=7/2 total angular momentum state, (assuming these are good quantum numbers and ignoring crystal field effects). This means N=6 or N=8, which is enough justification to start with $N = \infty$ and do a 1/N expansion.

Secondly, the conduction electrons ***really*** only have spin 1/2, but most authors pretend that they have spin J in order to keep the interaction simple. That is, one starts with two conduction electron bands, which couple to the f–electron bands with a scaling invariant strength of $\Delta = \pi V^2 N(0)$. Then one splits the two c–bands into N c–bands. If they ***each*** couple to the f–bands with a strength of Δ, then the total hybridization energy will be $\frac{N}{2}\Delta$. This is not realistic; the total interaction strength should remain the same. Therefore V has been multiplied by a factor of $\sqrt{\frac{2}{N}}$ in eq. (1.15).

Thirdly, the splitting of the two c–bands into N c–bands may be justified by imagining a spherical harmonic expansion of the c–electron wave–functions about the impurity site.

The N–fold degenerate infinite–U Anderson model will show a Kondo effect in the same manner as the spin 1/2 infinite–U Anderson model. For example, in the Kondo regime ($\langle n_f \rangle \simeq 1$), the N–fold degenerate infinite–U Anderson model transforms into the Coqblin–Schrieffer model [19], which is a generalization of the s–d model to the spin–J case.

Many authors have studied the 1/N expansion in the Anderson model such as Gunnarson and Schonhammer in 1983 [20] and Sur and Ramakrishnan in 1982 [21], and found it to considerably simplify things. Some low temperature properties were found to be exact in the $N \to \infty$ limit by Rasul and Hewson in 1984 [22]. However, there are problems which arise, such as infrared divergences [23], which bring the 1/N expansion into question. A finite temperature phase transition is known to appear in an infinite N calculation [24,25]. This artifact will be washed out due to infrared effects at finite N.

1.7.4 BETHE ANSATZ

The Bethe Ansatz is a technique useful for diagonalizing the Anderson model. The method is exact, subject to the degree to which the resulting integral equations can be solved numerically. Extensive reviews of the Bethe Ansatz technique applied to the Kondo problem and the spin 1/2 Anderson model have been given by Andrei, Furuya, and Lowenstein [26], and Tsvelick and Wiegmann [27], and Okiji and Kawakami [28]. This method was also applied to the N–fold degenerate, infinite–U Anderson model by Schlottmann [29, 30 ,31] in 1984.

The Bethe Ansatz method proves very useful for calculating static T=0 groundstate properties, such as the groundstate energy and magnetic susceptibility $\chi(0)$. It has also had success in the calculation of thermodynamic properties, such as the magnetic susceptibility $\chi(T)$ and the specific heat C(T). This method confirms the scaling regimes of Haldane, the Kondo behaviour, and the Fermi liquid behaviour.

If the Bethe Ansatz method is exact, a logical question to ask is, “Why does one need to bother with perturbative methods and the 1/N expansion?”. There are many reasons, the foremost of which is that the Bethe Ansatz will not work on the lattice Anderson model; it is only useful in the single impurity case. The main reason, then, for developing a perturbative scheme, is to find a method which is extendible to the lattice case.

Secondly, the Bethe Ansatz is only good for calculating the static quantities mentioned above. To calculate dynamical quantities such as the f–electron density of states $\sigma(\omega)$, and the dynamical magnetic susceptibility $\chi(\omega)$, one needs a different method.

The greatest usefulness of the Bethe Ansatz technique is perhaps to serve as an exact check on the correctness of perturbative methods.

1.7.5 FIXED–TIME–ORDERING GOLDSTONE EXPANSION; THE NON–CROSSING APPROXIMATION

As previously noted in section 1.7.1, the f–electron operators do not obey the standard anti–commutation relations. This precludes using the usual Feynman techniques of evaluating T–products of operators, because the anti–commutation of one f–electron (Hubbard) operator past another will introduce an extra operator. This is bad news. It has been avoided by many authors, using a fixed–time–ordering Goldstone expansion of the partition function. The ordering of operators is preserved, thereby avoiding the extra operators that arise due to the quantum algebra.

Keiter and Kimball [32] pioneered the Goldstone expansion method for the spin 1/2 Anderson model in 1971. The method was extended in 1983 by Kuramoto [33] to self–consistently avoid previous singularities, and encompass both the mixed valence and Kondo regimes of the spin J, infinite–U Anderson model. Kuramoto introduces the "non–crossing approximation" (NCA), in which certain diagrams are dropped. (Namely, those having conduction electron lines which cross.) This approximation ensures that the f–state cannot be more than singly occupied; ie. it models the infinite–U behaviour. Not only that, but the NCA is self–consistent, calculable, and becomes increasingly accurate for large N, (which is a motivation for the 1/N expansion). Expressions were obtained for the f–electron density of states and the dynamical magnetic susceptibility.

Numerical results of Kuramoto's method were given by Kojima, Kuramoto, and Tachiki in 1984 [34]. Graphs of the f–electron density of states were presented for both the mixed valence and Kondo regimes. These are qualitatively reproduced in Figs. 1.4(a) – (d).

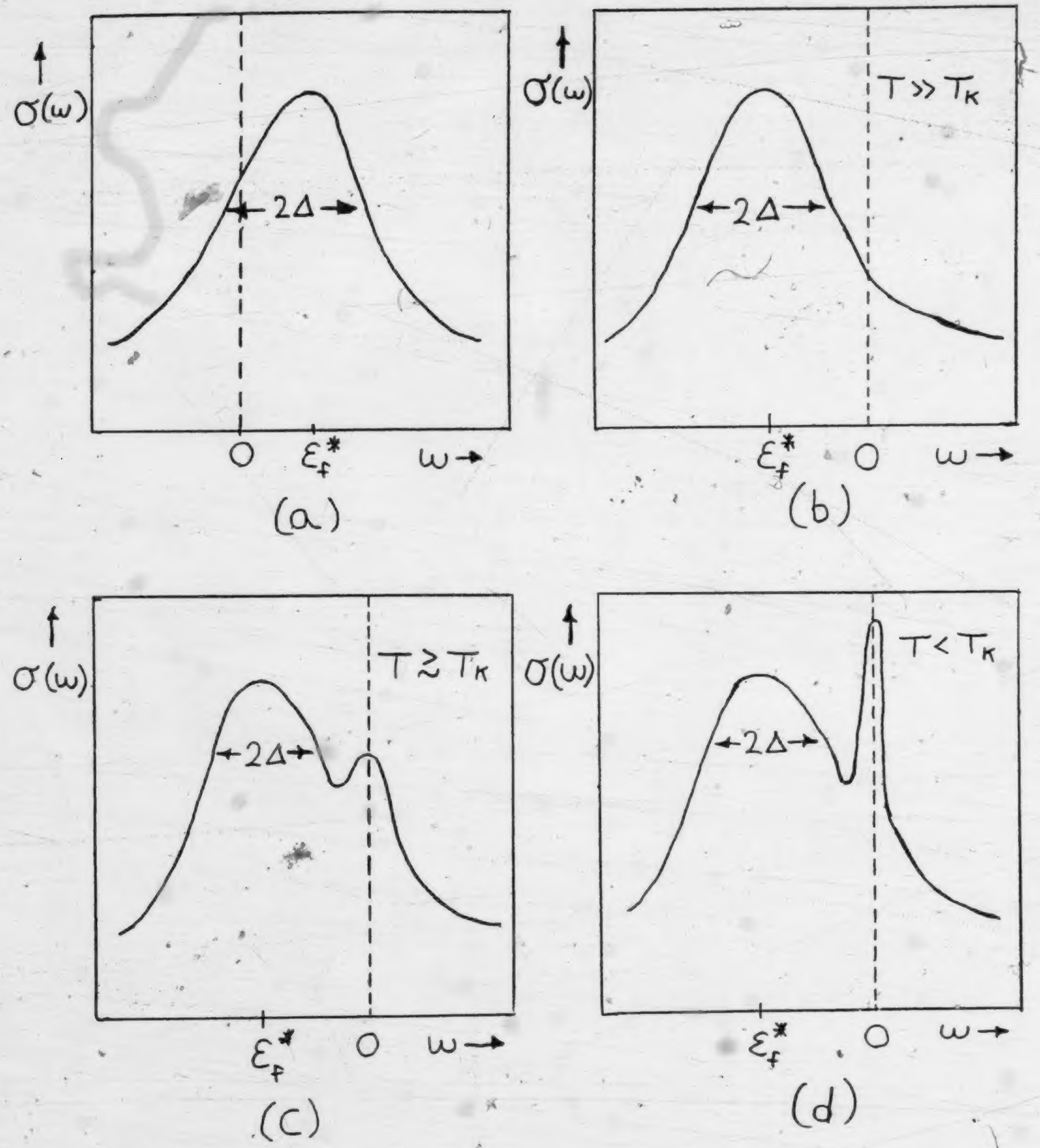

Fig. 1.4

The Kondo Resonance in the f–Electron Density of States

The density of states $\sigma(\omega)$ is plotted versus the energy ω. ε_f^* is the physical (renormalized) f–electron energy and Δ is the interaction strength. (a) shows the mixed valence regime. (b) to (d) show the Kondo regime as the temperature is lowered, illustrating the formation of the Kondo resonance.

Fig. 1.4(a) illustrates the mixed valence regime. Here $\varepsilon_f^* \sim \Delta$ so that the f–resonance overlaps the Fermi surface, as described by Haldane (see section 1.7.2). FIG. 1.4(b) illustrates the Kondo regime when $T >> T_K$. Here the f–level ε_f^* is considerably below the Fermi energy, again conforming to Haldane's conditions. As the temperature is lowered, a second peak starts to appear, at the Fermi surface, as illustrated in FIG. 1.4(c). When $T < T_K$, this peak sharpens into a very narrow resonance, as illustrated in FIG. 1.4(d). This feature is very important because it is the electrons at the Fermi surface which determine the transport properties of the metal. It could explain the very high effective masses observed in heavy–fermion materials.

In a similar approach to Kuramoto's NCA, Zhang and Lee [35] (1983), self–consistently applied the Goldstone expansion of Keiter and Kimball to the N–fold degenerate, infinite–U Anderson model. A systematic 1/N expansion for the free energy was obtained, and numerical results for static properties were found to be consistent with the Bethe Ansatz results.

The narrow Kondo resonance at the Fermi surface was confirmed by the calculations of Bickers, Cox and Wilkins [36] (1985).

1.7.6 FUNCTIONAL INTEGRAL

Read and Newns [24] (1983) used a functional integral method to develop a large–N expansion for the Coqblin–Schrieffer model. (This is the Kondo limit of the N–fold degenerate infinite–U Anderson model.) Rather than imposing the $n_f = 1$ condition by modifying the algebra of the operators, the condition was imposed by introducing a constraint field. Results for $\chi(0)$, $\gamma(0)$, and E_o (the groundstate energy) were found to be in good agreement with the N–fold degenerate Bethe Ansatz results.

It is interesting to note that when $N \rightarrow \infty$, the solution (which becomes *exact*) is a broken symmetry state with $\langle \sum_m f_m^\dagger c_{om} \rangle \neq 0$ [37]. This broken symmetry state appears as a saddle point of the functional integral.

1.7.7 SLAVE BOSON METHOD

Coleman [25] (1984) modified the N–fold degenerate, infinite–U Anderson model, by replacing the Hubbard operators by the product of a fermion operator and a boson operator. The boson operator creates (annihilates) a "slave boson" every time the fermion operator annihilates (creates) an f–electron. Thus the slave boson keeps track of the f–electron "hole". It turns out that this is a faithful representation of the Hubbard algebra, when one imposes the condition Q=1, where

$$Q = \sum_m f_m^\dagger f_m + b^\dagger b \; . \tag{1.17}$$

Here b is the slave boson operator and f_m is the f–electron operator. Q keeps track of the total number of f–electrons and f–electron holes. By constraining it to Q=1, the infinite–U behaviour is modelled because $0 \leq n_f \leq 1$.

Coleman's model is more general than the Anderson model, in that it exists in various disjoint subspaces of integral Q. Of course, only the Q=1 subspace is physical and corresponds to the Anderson model. In order to project out this subspace, a chemical potential λ is introduced to the grand canonical ensemble.

By taking a large–N limit, vertex corrections could be dropped, and Coleman obtained results identical to those of the NCA Goldstone expansions discussed in sect. 1.7.5. In particular, the f–electron density of states showed the same structure as obtained by Kuramoto and illustrated in FIGS. 1.4(a)–(d).

An advantage of Coleman's method is that the b– and f–operators obey the standard boson/fermion commutation/anti–commutation relations, rather than the quantum algebra of the Hubbard operators.

Another advantage of the slave boson method, is that it can be extended in a manner that effectively deals with the infrared divergence problems of the 1/N expansion mentioned in section 1.7.3. Coleman discusses this in refs. [37] (1985) and [38] (1987). Following the functional integral method of Read and Newns, introduced in sect. 1.7.6, Coleman considers the 1/N expansion about a mean field, broken symmetry state, which appears as a saddle point of the constrained functional integral. The mean field is that of the boson operator. When N is finite, unbound Goldstone phase fluctuations of the boson field restore the symmetry, in a manner in which infrared divergences can be cancelled. Coleman describes the Kondo state as an "almost broken symmetry", because the fluctuations are sufficiently weak that many properties of the broken symmetry state are preserved.

There is one hitch to all of this. When $Q=1$, true mean field behaviour does not develop, and the 1/N expansion is invalidated. Coleman therefore considers a macroscopic occupation of the f–level, such that when $N \to \infty$, $q \equiv Q/N$ remains finite.

In 1985 Coleman and Andrei [39] diagonalized the slave boson Anderson model using the Bethe Ansatz technique. Solving this for finite q yielded results in good agreement with the finite q, 1/N expansion. It was shown that the large–N limit in the infinite–U Anderson model does ***not*** exist, unless q remains finite.

1.7.8 RENORMALIZATION GROUP AND FERMI LIQUID CONSIDERATIONS

Renormalization group techniques have been used to study the Kondo problem. An excellent review of this method and its application to solving the s–d model is given by Wilson [40]. He shows that the coupling constant J of eq. (1.4) is renormalized by spin fluctuations spanning many decades of frequency. Call this renormalized interaction $\tilde{J}(T)$. At high temperatures,

$\tilde{J}(T)$ logarithmically goes to zero as $1/\ln(T/T_0)$, and the system becomes asymptotically free. T_0 is a dynamical scale which comes from the s–d model, and is roughly the Kondo temperature. The region of $T>T_0$ is called the "weak coupling regime", where perturbation theory is valid. On the other hand, when $T<T_0$, the system enters the "strong coupling regime" where perturbation theory breaks down, because $\tilde{J}(T)$ diverges logarithmically as $T \rightarrow 0$. This infinitely strong anti–ferromagnetic coupling indicates that the localized ↑ (↓) spin traps a ↓ (↑) spin conduction electron to form a singlet bound state.

Nozières [41] realized that although this singlet state cannot be broken, it can still be polarized by virtual excitations. Thus one has an interacting conduction electron gas. This led Nozières to describe the low–temperature fixed point, of the renormalization group approach to the s–d model, as a local Fermi liquid.

Noting that the infinite–U Anderson model becomes the s–d model in the low–T Kondo regime, one should find this system also described as a local Fermi liquid. Therefore, the graph of Fig. 1.4(d), obtained from both the NCA and slave boson methods of self consistent perturbation theory, should be consistent with a Fermi liquid description, if these methods are to be considered valid in the strong coupling regime.

What is a Fermi liquid? It is an extension of a Fermi gas, in which interactions adiabatically renormalize the system, such that it can be described by quasi–particles, the number of which is equal to the original number of particles in the non–interacting gas. It is assumed that these quasi–particles form an excitation spectrum analogous to that of a free Fermi gas, i.e. there is a Fermi surface. The concept was first introduced by Landau [42] and is extensively reviewed in the textbook of Abrikosov, Gorkov, and Dzyaloshinski [43]. Landau's Fermi liquid theory was extended by Newns and Hewson [44], to a local Fermi liquid theory applicable to mixed valence systems.

A simple check on the validity of results which should conform to the Fermi liquid approach, is that they should satisfy the Friedel sum rule [41, 44, 45]. The Friedel sum rule states simply:

$$n_f = \frac{N}{\pi}\,\eta(0)\ , \tag{1.18}$$

where n_f is the mean number of f–electrons in the impurity level, $\eta(0)$ is the scattering phase shift at the Fermi surface (ω=0), and N=2J+1 is the degeneracy of the f–state, (ie. the number of channels in the resonance). The scattering phase shift $\eta(\omega)$ may be written in terms of the full f–electron propagator $G_f(\omega)$, as follows [46]:

$$\eta(\omega) = \mathcal{Im}\ \ell n\left[G_F^{+}(\omega)\right] + \pi\ . \tag{1.19}$$

(G^+ refers to the $+i\delta$ component of the thermal propagator G, with thermal filling factors removed. There is also a $-i\delta$ component. See sect. 2.4 for the details of thermal propagators.)

What does this imply for the graph of FIG. 1.4(d)? Let us assume that the 2–peak structure may be embodied in a full f–electron propagator, which is the sum of two simple resonances:

$$G_F^{+}(\omega) = \frac{Z}{\omega - \varepsilon_f^{*} + i\Delta} + \frac{Z_K}{\omega - \varepsilon_K + i\Delta_K} \tag{1.20}$$

Here Δ is the half–width at half–maximum of the main peak of weight Z centred at energy ε_f^* , and Δ_K is the half–width at half–maximum of the Kondo peak [illegible] weight Z_K centred at energy ε_K near the Fermi surface.

The density of states associated with a propagator $G(\omega)$ is found by taking $\sigma(\omega) = -\frac{1}{\pi}\,\mathcal{Im}\,G^+(w)$. Thus the density of states associated with eq. (1.20) is given by:

$$\sigma(\omega) = \frac{Z}{\pi} \frac{\Delta}{(\omega - \varepsilon_f^*)^2 + \Delta^2} + \frac{Z_K}{\pi} \frac{\Delta_K}{(\omega - \varepsilon_K)^2 + \Delta_K^2} \quad . \tag{1.21}$$

This is plotted in FIG. 1.5.

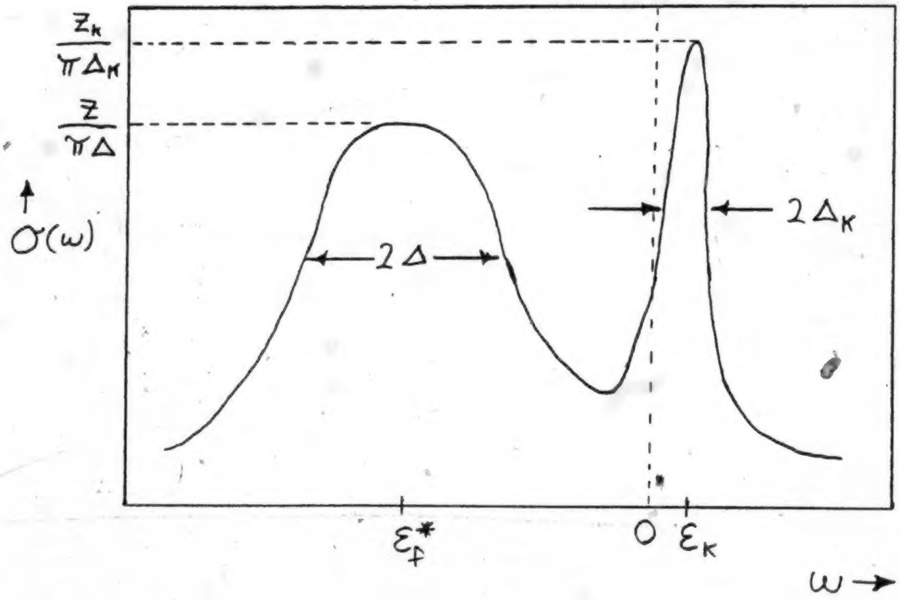

FIG. 1.5

A Two–Resonance Form for the f–Electron Spectral Function

Eq. (1.21) for the f–electron density of states (spectral function) is plotted above versus the energy ω. ε_f^* is the position of the renormalized f–electron level, having width Δ, and ε_K is the position of the Kondo peak, having width Δ_K.

Near the Fermi surface (ω=0), we assume that the Kondo resonance gives the dominant contribution, whereas the main peak is negligible. Then the phase shift of eq. (1.19) becomes:

$$\eta(\omega)\Big|_{\omega\sim 0} \simeq \tan^{-1}\left[\frac{\Delta_K}{\varepsilon_K - \omega}\right] + \pi\,\theta(\omega - \varepsilon_K) \quad . \tag{1.22}$$

Note that the Z_K drops out of this expression, by virtue of the logarithm in eq. (1.19). Inserting this expression into the Friedel sum rule of eq. (1.18), one finds:

$$n_f = N\left[\frac{1}{\pi} \tan^{-1} \left[\frac{\Delta_K}{\varepsilon_K}\right] + \theta(-\varepsilon_K) \right] . \tag{1.23}$$

Another sum rule which must be satisfied is the particle–hole sum rule. That is:

$$n_f + n_h = 1 , \tag{1.24}$$

where n_h is the number of hole states of the impurity atom. At T=0, one finds (see sect. 6.2):

$$n_f\Big|_{T=0} = N \int_{-\infty}^{0} d\omega\ \sigma(\omega) , \tag{1.25}$$

$$n_h\Big|_{T=0} = \int_{0}^{\infty} d\omega\ \sigma(\omega) . \tag{1.26}$$

That is, at T=0, the f–spectrum is filled up to the Fermi energy, therefore one integrates from $-\infty$ to 0, to find the total occupied spectral weight, and multiplies by N for the N spins. The total unoccupied spectral weight is given by integrating from 0 to ∞; here there is no factor of N because the hole states have no spin.

A useful identity when considering eqs. (1.25)–(1.26) is that the standard resonance form has a total weight of 1:

$$\int_{-\infty}^{\infty} d\omega \left[\frac{1}{\pi}\right] \frac{\Delta}{(\omega - E)^2 + \Delta^2} = 1 . \tag{1.27}$$

Let us first consider the spin 1/2, N=2 case. We know that in the Kondo limit $n_f \simeq 1$. Therefore let us assume $n_f = 1-\delta$ and $n_h = \delta$, where δ is a small number. From the Friedel sum rule of eq. (1.23), one obtains $\tan^{-1}\left[\frac{\Delta_K}{\varepsilon_K}\right] = \frac{\pi}{2} - \frac{\pi}{2}\delta$, and therefore:

$$\frac{\varepsilon_K}{\Delta_K} \simeq \frac{\pi}{2}\delta . \tag{1.28}$$

The Kondo resonance is thus situated just slightly above the Fermi level, and overlaps it. Using this in eq. (1.26) along with eq. (1.27), one finds $n_h \simeq Z_K/2$, and therefore:

$$Z_K \simeq 2\delta \quad . \tag{1.29}$$

Assuming the main resonance to be deep enough below the Fermi surface that virtually all of its spectral weight is confined to $\omega<0$, eq. (1.25) with eq. (1.27) yields $n_f \simeq 2Z + Z_K/2$, and therefore:

$$Z \simeq \frac{1}{2} - \delta \quad . \tag{1.30}$$

The T=0 strong coupling behaviour for the spin 1/2, infinite–U Anderson model is thus straightforward: The main peak at ε_f^* has a weight slightly less than 1/2. The Kondo peak has a small weight and is located slightly above the Fermi level, overlapping it. As we force the system progressively deeper into the Kondo regime by lowering ε_f^*, the main peak weight will progressively approach 1/2, the centre of the Kondo peak will progressively approach the Fermi surface, and its weight will progressively approach 0.

Let us now consider the large–N case. Again we assume $n_f = 1-\delta$ and $n_h = \delta$, where δ is a small number. From the Friedel sum rule of eq. (1.23), one obtains $\tan^{-1}\left[\frac{\Delta_K}{\varepsilon_K}\right] = \frac{\pi}{N}(1-\delta)$, and therefore:

$$\frac{\Delta_K}{\varepsilon_K} \simeq \frac{\pi}{N}(1-\delta) \quad . \tag{1.31}$$

Contrast this to eq. (1.28); the Kondo resonance is no longer centred on the Fermi energy, rather, it is sufficiently above the Fermi energy that only a very small part of it dips below $\omega=0$. We may then assume that the integral of eq. (1.26) covers the whole Kondo resonance and none of the main resonance, whereas the integral of eq. (1.25) covers the whole main resonance and none of the Kondo resonance. With the use of eq. (1.27), eq. (1.25) therefore yields $n_f \simeq NZ$, and eq. (1.26) yields $n_h \simeq Z_k$. Therefore:

$$Z \simeq \frac{1-\delta}{N} \quad , \tag{1.32}$$

$$Z_K \simeq \delta \quad . \tag{1.33}$$

The picture that emerges, in the T=0 strong coupling limit of the large

N, infinite–U Anderson model, is as follows: The main peak at ε_f^* has a weight slightly less than 1/N. The Kondo peak has a small weight, is located above the Fermi surface, and is sufficiently narrow that only a small part of it overlaps the Fermi surface. As we force the system progressively deeper into the Kondo regime by lowering ε_f^* , the main peak weight will progressively approach 1/N, and the weight of the Kondo peak will progressively approach 0, but the peak remains above the Fermi surface with only a small portion overlapping it.

1.8 WHAT IS KNOWN ABOUT THE LATTICE ANDERSON MODEL?

1.8.1 OVERVIEW

The inherent difficulties of the single–site Anderson model are carried over into the lattice Anderson model. Although the lattice does not further complicate the Hubbard algebra, problems are compounded by having this local algebra exist at each Lanthanide or Actinide site in the lattice. Many of the methods described in section 1.7 have been extended to the lattice case, with limited success. Single–site perturbative schemes, such as the 1/N expansion in its various guises, are not generally suitable for explaining periodic behaviour, such as band structure and Fermi surface effects. In order to retrieve the periodic behaviour from these perturbative schemes, one must perform an infinite order resummation of multi–site diagrams, and there is no exact diagonalization method, such as the Bethe Ansatz, with which to compare the results. For example, one finds from the 1/N expansion that the single impurity term is of order $1/N^0$, the 2–impurity term is of order 1/N , the 3–impurity term is of order $1/N^2$, etc. [47].

Some of what is known and what has been done is briefly reviewed below. Again, this review is not intended to be complete. An extensive bibliography of the various methods applied to the lattice Anderson model is contained within the quoted references of ref. [47].

1.8.2 THE BAND PICTURE

Typical free-electron bands in a weak periodic potential are illustrated in FIG. 1.6. (See any solid state physics textbook, eg. ref. [48].)

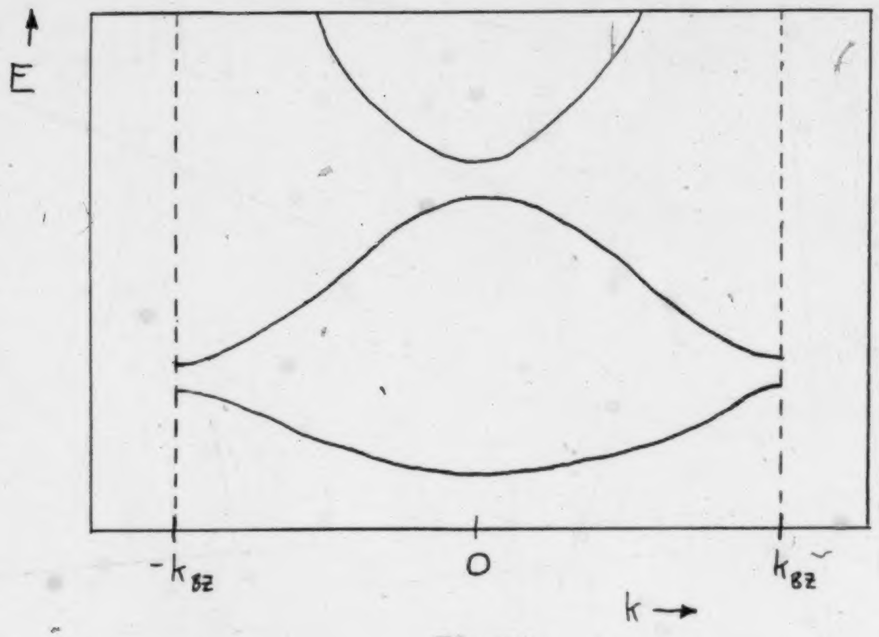

Fig. 1.6

Typical Electronic Band Structure in a Weak Periodic Potential

This is a graph of the Energy, E, versus the momentum, k, of conduction electrons in a typical metal. k_{BZ} is the edge of the first Brillouin zone.

The wave number k cannot be greater than k_{BZ} , the Brillouin zone edge, because that is where the wavelength of the electrons equals the lattice spacing. Thus the parabolic shape of the free electron dispersion is reflected back into the first Brillouin zone. Band gaps occur at k_{BZ} due to small crystal field effects. Each band can hold a maximum of 2 electrons/unit cell. At T=0, the bands are filled up to the Fermi energy, E_F . We assume that the valence is very nearly an odd number, so that the Fermi level occurs roughly in the middle of a band.

Of course, the situation is much more complicated in 3 dimensions due to different lattice spacings, and hence different k_{BZ}, in different directions. The one–dimensional picture of FIG. 1.6 will suffice, though, when the Fermi level is roughly in the middle of a band.

In the single–site Anderson model, conduction electrons from the Fermi band (ie. the band containing the Fermi energy) interacted with a localized f–electron level. The c–electron operators in eq. (1.7) were assumed to apply only to the Fermi band; the lower bands do not interact with the impurity level. Furthermore, the f–level was sufficiently close to the Fermi level that, for the purpose of calculation, the band could be confined to a region of width 2D having a constant density of states. This picture is illustrated in FIG. 1.7.

The single–site Anderson model calculation is a scattering problem. A conduction electron of momentum $\vec{k}$ scatters off the impurity site into a state of momentum $\vec{k}'$. Momentum will not be conserved, because the f–electron state is a localized one carrying no momentum.

In contrast, the full f–electron propagator in the lattice Anderson model ***will*** carry momentum: an electron in an f–state at site i can jump into the conduction band, travel to an unoccupied f–state at site j and drop into it. Because the f–electron states exist in a regular lattice, they will be describable as Bloch waves, and thus momentum will be conserved. The problem is no longer one of scattering, but of one band (c–electrons) interacting with another band (f–electrons).

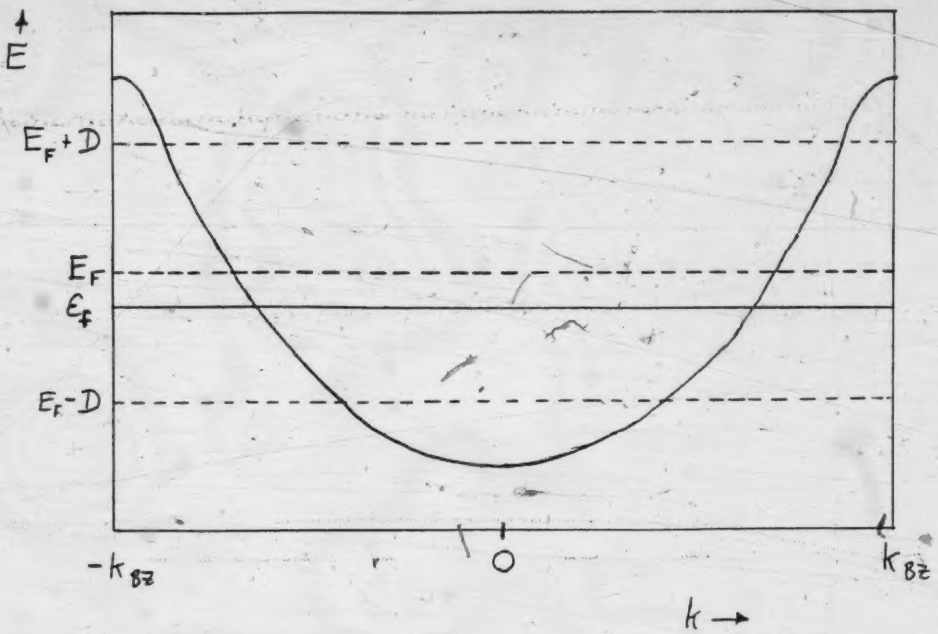

FIG. 1.7

The Flat Band (D–Cutoff) Approximation

The conduction band and the f–electron level are plotted. Assuming that the Fermi level (E_F) is close to the middle of the band, and that the f–electron level (ε_f) is relatively close to E_F, then the conduction electron band may be approximated as a featureless energy band of width 2D, having a constant density of states.

The picture of FIG. 1.7 may still be valid, in that the D–cutoff approximation may be okay for the purpose of calculating how the two bands affect each other. Let me clarify this. The original bands with no interaction appear as in FIG. 1.7. When the interaction is switched on, the shapes of the bands will remain approximately the same, except in the small regions where the bands cross. To calculate what happens in these small regions, one may use the D–cutoff approximation. Once the calculation has been done, we go back to the original picture, and modify only the small crossing regions. The standard result of such a band interaction is illustrated in FIG. 1.8.

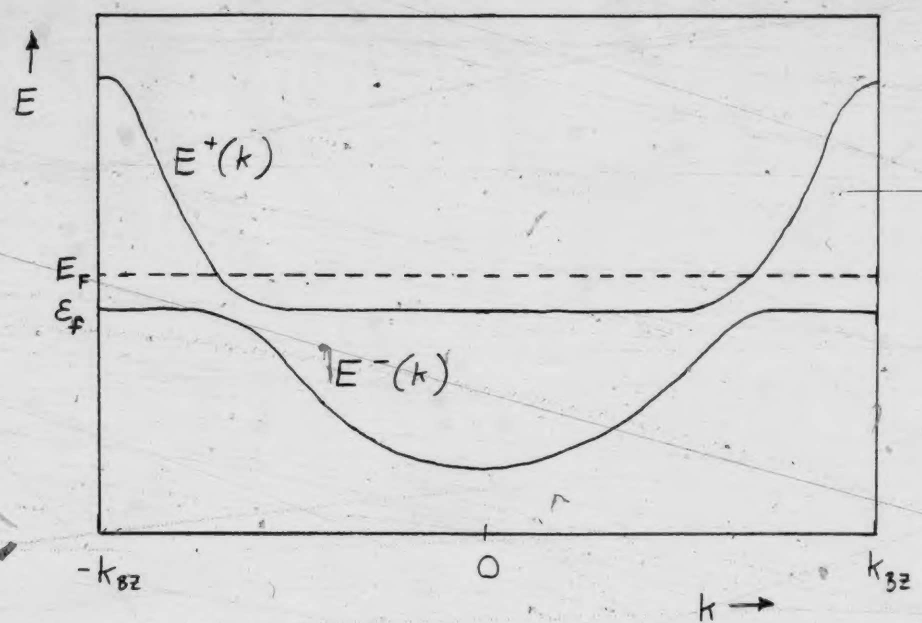

FIG. 1.8

Hybridization of the Conduction Band and the f–Band

This illustrates a typical band interaction. In this case, the conduction electron band interacts with the f–electron band at the crossing regions. This results in the formation of two hybrid bands, $E^+(k)$ and $E^-(k)$.

There will be two bands formed, $E^+(k)$ and $E^-(k)$. In this particular example, $E^+(k)$ has c–like character at high $|k|$ and f–like character at low $|k|$, whereas $E^-(k)$ has c–like character at low $|k|$ and f–like character at high $|k|$. Ignoring any widths which may be introduced, the c and f propagators, $G_c(\omega,k)$ and $G_f(\omega,k)$, will have the following forms:

$$G_c(\omega,k) = \frac{Z_c^+(k)}{\omega - E^+(k) + i\delta} + \frac{Z_c^-(k)}{\omega - E^-(k) + i\delta} , \qquad (1.34)$$

$$G_f(\omega,k) = \frac{Z_f^+(k)}{\omega - E^+(k) + i\delta} + \frac{Z_f^-(k)}{\omega - E^-(k) + i\delta} . \qquad (1.35)$$

(As before, we ignore any thermal filling factors and consider only the $+i\delta$ components.)

Here $Z_c^+(k)$ will be small for small $|k|$, $Z_c^-(k)$ will be small for large

$|k|$, $Z_f^+(k)$ will be small for large $|k|$, and $Z_f^-(k)$ will be small for small $|k|$.

Care is required in using this picture, for a number of reasons. Firstly, one may *not* assume that these two bands can accommodate the usual 2 electrons/unit cell. In the bare picture of FIG. 1.7, the c–band can accommodate a maximum of 2 electrons/unit cell, but the f–band can accommodate only 1 electron/unit cell, due to the infinite Coulomb repulsion. Therefore a maximum total of 3 electrons/unit cell can be accommodated by the two bands. This will hold true in FIG. 1.8 as well. We must assume that the E^+ band can hold a maximum of x electrons/unit cell, and the E^- band can hold a maximum of y electrons/unit cell, such that x+y=3. x and y will be determined by the calculation.

Secondly, at T=0, electrons will fill these bands up to a level of E_F^* to accommodate the *actual* valence, which will be close to two: one electron from the f–band and one electron from the c–band. Thus, the Fermi level E_F will be renormalized to a new level E_F^*.

Thirdly, we have ignored any widths which are introduced by the interaction. The picture of FIG. 1.8 may still be valid if the widths are small, and $E^+(k)$ and $E^-(k)$ are considered to be the positions of the peaks of the resonances.

Fourthly, this picture is valid only in the weak coupling regimes. In a strong coupling regime there may be a Kondo resonance appearing at the Fermi level, as in the single–site case.

Fifthly, in a Fermi liquid regime there will be Fermi liquid relations which must be satisfied, in the same manner in which the Friedel sum rule must be satisfied by the single–site solution at low T.

1.8.3 FERMI LIQUID CONSIDERATIONS: THE LUTTINGER PICTURE

In sect. 1.7.8, it was stated that the solution of the single–site Anderson model, in the strong coupling regime, should be described as a local Fermi liquid. Specifically, it should satisfy the Friedel sum rule. Presumably, the lattice Anderson model will also have a strong coupling regime. This regime should, in the absence of a phase transition to a superconducting or magnetically ordered state, be described as a periodic Fermi liquid [47]. For this purpose, the Luttinger [49] picture of a periodic Fermi liquid is very useful.

Features of the Luttinger picture are as follows [47]: Firstly, there exists a Fermi surface, which manifests itself by a T=0 discontinuity in the conduction electron density of states. Secondly, quasi–electrons at this T=0 Fermi surface have infinite lifetimes. That is, the imaginary part of the pole of the T=0 conduction electron propagator should go to zero as k goes to k_F, where k_F is the Fermi momentum. Thirdly, the system must obey the Luttinger sum rule. This rule is simply that the total number of quasi–particle states enclosed by the Fermi surface must equal the number of electrons in the metal.

The Luttinger sum rule was implicitly assumed in the discussion of section 1.8.2. One finds that the Luttinger picture is very similar to the band picture, especially near the Fermi surface. Combining the band picture with the Luttinger conditions should serve as a useful tool for analyzing the Lattice Anderson model.

1.8.4 A VARIATIONAL APPROACH

B.H. Brandow [47] (1986) considered a variational approach to determining the ground state (T=0) of the spin 1/2 lattice Anderson model. The variational approach consists of introducing a trial wave function, and then minimizing the expectation value of the Hamiltonian, by varying the parameters of the trial wave function. Both a 1–parameter and a 2–parameter trial wave function were considered, chosen to conform to the Luttinger picture of a Fermi liquid, and maintaining a close correspondence to band theory. The quasi–particles were all assumed to have infinite lifetimes.

For the purpose of illustration, Brandow first considered the U=0 case, which is a simple 2–band interaction, as illustrated in FIG. 1.8. The two bands were found to have the following form:

$$E^{\pm}(k) = \frac{1}{2}\left[\, \varepsilon_c(k) + \varepsilon_f \pm \sqrt{(\varepsilon_c(k) - \varepsilon_f)^2 + 4V^2}\,\right] , \qquad (1.36)$$

where ε_f is the energy of the f–electron state, $\varepsilon_c(k)$ is the energy of the c–electron band at momentum k, and V is the strength of the interaction.

Next, Brandow considered the U=∞ case with a 1–parameter trial wave function. In this approximation, the different impurity sites interact only via the Pauli exclusion principle, causing destructive interference which inhibits long range correlations. The results show three regimes corresponding to the empty impurity, mixed valence, and Kondo regimes of the single–site model. As in the U=0 case, a 2–band structure is found, satisfying eq. (1.36) with the following substitutions:

$$\varepsilon_f \rightarrow \tilde{\varepsilon}_f = \varepsilon_f + \mu , \qquad (1.37a)$$

$$V \rightarrow \tilde{V} = V\sqrt{1-n_f} . \qquad (1.37b)$$

Here μ is a renormalization of the chemical potential, and n_f is the renormalized occupation of the localized f–state. In the Kondo regime, $1-n_f$ becomes exponentially small.

The picture that arises then is that of a "renormalized band" structure. The standard band hybridization illustrated in FIG. 1.8 shows a band gap centred on ε_f , between the top of the E^- band and the bottom of the E^+ band. This picture is still valid, except that the band gap is renormalized by a factor of $1-n_f$, and the gap will be centred on $\tilde{\varepsilon}_f$. This gap thus becomes exponentially small in the Kondo regime. The renormalization of the bands also causes an enhancement of the effective mass of the quasi-particles, which can be about $O(10^2)$ in the Kondo regime.

By considering the f-weight of the quasi-particles, the f-electron spectral function was found to consist of 2 sharp peaks separated by a band gap centred on $\tilde{\varepsilon}_f$. In the Kondo regime, $\tilde{\varepsilon}_f$ becomes the Fermi energy, and the two sharp peaks correspond to the Kondo peak of the single-site case, illustrated in FIG. 1.4d. The broad peak of FIG. 1.4d, below the Fermi surface, is expected to come from a non-quasi-particle, continuum contribution to the spectral function, but these calculations were incomplete.

Brandow's 2-parameter refinement of the 1-parameter results shows the same qualitative features as above, except that there is now a significant quasi-particle contribution to the f-electron spectral function, at the bare ε_f, in the Kondo regime. This corresponds to the broad peak of FIG. 1.4d below the Fermi surface. (As in the 1-parameter case, one also expects a non-quasi-particle contribution to this peak.)

This method shows that there is a close link between the single-site and lattice Anderson models, and yet it also shows periodic Fermi liquid properties conforming to the Luttinger picture. Its major disadvantage is that it ***assumes*** a form for the trial wave function which satisfies the Luttinger conditions, rather than having the Luttinger properties fall naturally from a solution with no assumptions. This excludes the possibility of other non-Fermi-liquid ground states, such as heavy-fermion superconductivity.

1.8.5 FIXED–TIME–ORDERING GOLDSTONE EXPANSION; THE EXTENDED NON–CROSSING APPROXIMATION

The Goldstone expansion method of Keiter and Kimball [32] was mentioned in sect. 1.7.5 in the context of the single–site Anderson model. Grewe and Keiter [50] extended this method to the spin 1/2 lattice model, using Goldstone diagrams for on–site processes and Feynman diagrams for inter–site processes. Site summations are complicated by certain restrictions, which make it difficult to do the necessary infinite order resummations. A scheme was found for doing the infinite order resummations, which leads to Brillouin–Wigner–type self–consistency equations. An examination of the single–site f–electron spectral function shows a quasi–particle spike above a broad background continuum. There was no calculation of the band structure. Another disadvantage of this method is that there exist singularities which must be regularized.

Kuramoto's self–consistent extension of the Goldstone expansion methods and his "non–crossing approximation" were discussed in sect. 1.7.5. Kuramoto has also extended his NCA to the lattice Anderson model, resulting in the "extended non–crossing approximation" (XNCA) [51]. As in the NCA, use is made of large N. Use is also made of large Z, where Z is the number of effective neighbors for a site in the lattice.

Heavy fermion behaviour is discussed in terms of the Kondo regime. One finds the Kondo effect occurring as the temperature is lowered, followed by band formation at still lower temperatures. Kuramoto's calculation of the band structure yields the same form as obtained by Brandow, and discussed in sect. 1.8.4. There is a difference, though, in that the renormalization factor of $1-n_f$ is replaced by a factor a_f , which is considerably smaller than $1-n_f$ in the Kondo regime. This yields a higher effective mass enhancement, ($\sim O(10^3)$).

Kuramoto finds $a_f = 1-n_f$ only in the zeroth order of the 1/N expansion, and in fact Brandow finds that the renormalization factor decreases in the 2-parameter calculation.

Kuramoto thus confirms that there may be a renormalized band structure responsible for heavy fermion behaviour. An advantage of his method is that there is also a regime in which magnetic ordering can occur.

1.8.6 SLAVE BOSONS AND THE 1/N EXPANSION

Coleman's slave boson method was discussed in sect. 1.7.7, in the context of the large-N, single-site Anderson model. This method has also been extended to the large-N lattice Anderson model. Read and Newns [52], used a slave boson, functional integral approach to calculate the mean field ($N \to \infty$) limit of the lattice Anderson model. This led to a renormalized band structure identical to that of Brandow discussed in sect. 1.8.4. (Actually, Read and Newns found this before Brandow.) Also, the f-electron spectral function showed the same 2-spike, separated by a gap, structure. In the large-N limit, the lattice results were found to compare closely to the single-site results.

Auerbach and Levin [53] confirmed the renormalized band structure, and performed the O(1/N) fluctuation corrections to the Kondo lattice mean field theory. Corrections to the magnetic susceptibility and specific heat were found to conform to known Fermi liquid identities, which were in turn related to Ward identities. The specific heat also showed a $T^3 \ln T$ term, such as that found in experimental observations of UPt_3. The low temperature resistivity was found to contain a T^2 term.

As discussed in sect. 1.7.7, true mean field behaviour does not develop unless the f-level is macroscopically occupied, such that Q/N remains finite. Another problem with Q=1, is that intersite correlations become a 1/N effect, as discussed in sect. 1.8.1, and will vanish from the mean field theory. This problem can be overcome by taking Q/N finite, thus preserving intersite interactions, and developing a useful 1/N expansion. [38]

Coleman [38] considered both the 2–site and the many–site Anderson models, in the context of finite Q/N. The 2–site solution showed a Fermi liquid with two Kondo resonances, having different widths and different positions. The many–site solution showed the renormalized band structure of Read and Newns [52], with the renormalization parameter given by the expectation value of the slave boson field. The effects of O(1/N) fluctuations on the 2–site and many–site solutions was also presented.

1.8.7 OTHER METHODS

There are various authors who have tried other methods of approaching the lattice Anderson model. As noted in sect. 1.8.1, this is not intended to be a complete review. This section will serve to illustrate only a couple of other methods of interest.

Roberts and Stevens [54] developed a Green's function method for the spin 1/2 lattice Anderson model with finite U. The U term is retained as part of H_o, the "free" hamiltonian, and thus Wick's theorem breaks down. This breakdown occurs for the same reasons as presented in sect. 1.7.1: the operators obey an algebra, involving anti–commutators which do not yield a c–number. Roberts and Stevens get around this by approximating the anti–commutators by their thermal averages, thus restoring a Wick's theorem. This leads to a simplified diagrammatic expansion and Dyson equations which can be solved for the c–electron and f–electron propagators. These show a renormalized band picture very similar to that obtained by other authors in the preceding sections. As shown by Brandow (sect. 1.8.4), the f–electron spectral function consists of two sharp spikes separated by a gap. Roberts and

Stevens show that the Fermi level lies below this gap.

Another finite–U method of interest, for the spin 1/2 lattice Anderson model, was formulated by Koyama and Tachiki [55]. Self–energy and vertex functions were defined at T=0, and Dyson equations were constructed to conform to the Ward–Takahashi relations derived from spin rotational invariance. Numerical calculations of the f–electron spectral function were performed, yielding a 2–peak structure. There appeared a very narrow quasi–particle peak (infinite lifetime) at the Fermi surface, which was thought to be responsible for the heavy fermion behaviour. Various choices of parameters showed that this peak causes an effective mass enhancement, which conforms to the observed experimental values. The second peak, which is broader and occurs above the Fermi surface, is a resonance peak (finite lifetime), which is thought to correspond to the single–impurity Kondo peak. It was argued that as the temperature is raised, there occurs a crossover from heavy fermion behaviour to dilute Kondo behaviour, in which the quasi–particle peak would disappear, leaving only the Kondo resonance peak.

1.9 REVISED MOTIVATION

Various approaches to the Anderson model were described in sections 1.7 and 1.8, and yet none of these methods have adequately dealt with the Hubbard algebra of the operators. The perturbative approaches get around this problem in one of three ways: 1) the algebra is avoided by using a fixed–time–ordering Goldstone expansion combined with the non–crossing approximation; 2) the algebra is re–represented in terms of slave bosons; or 3) the algebra is removed by taking the thermal average of the anti–commutators. The first method precludes the use of Feynman diagrams, and the NCA is only valid in the large–N limit. The second method uses a 1/N expansion about a mean field of the slave bosons, which is only valid for a macroscopic occupation of the f–level. The third method is also a mean field theory, the mean field being the anti–commutators.

In spite of these drawbacks, the above methods have been very successful. It may not be necessary to develop a Feynman diagram method, which deals with the quantum algebra honestly and thoroughly. Nevertheless, that is the intent of this thesis.

Nobody before has thoroughly developed perturbative quantum field theory in the context of a quantum algebra. There are many questions to answer: How does one construct a Wick's theorem? How does one find an operator which annihilates the vacuum? How does one construct a propagator and Feynman rules? What new features arise? How does one perform the renormalization? These questions probe into the very core of quantum field theory, and one may expect that most of the standard techniques will need to be modified or generalized.

This project may or may not lead to new results on the Anderson model. But the extensive results of the other authors will serve as a check on the correctness of this approach. Once the quantum algebra approach is established, it may find uses in other domains of quantum field theory, ranging from condensed matter physics to high energy physics.

The initial motivation of sect. 1.1 has been changed. I am no longer attempting to explain the observed properties of heavy fermion materials. Rather, I am trying to establish the quantum algebra approach as a viable field theoretic tool, by applying it to the Anderson model, and hopefully reproducing some of the established results.

1.10 THE QUANTUM ALGEBRA APPROACH TO THE ANDERSON MODEL

A Wick's theorem for a general quantum algebra was found in 1984 by Matsumoto and Umezawa [56], in the context of thermo field dynamics [57], which is a real–time finite–temperature quantum field theory. An attempt was made by Matsumoto and Umezawa [58], to apply this to the spin 1/2 Anderson model. It was found that there were certain conditions under which the generalized Wick's theorem broke down, necessitating the use of a time–splitting technique. Feynman rules were found to be very complicated, having spontaneous vertices even without an interaction, and having a sector structure with different rules in each sector.

This work on the spin 1/2 Anderson model was extended by Matsumoto, Umezawa, and Whitehead [59], to the general spin J case. They claimed that the Feynman rules were a direct extension of those for the spin 1/2 case. But they were wrong. The spin J case is considerably more complicated.

This is not the only problem with the method. It was later realized by Whitehead et al. [60], that these first attempts had overlooked an essential constituent of the perturbation expansion, namely, vacuum diagrams which do not cancel. A number of simple examples were given, showing how these vacuum diagrams arise in a quantum algebra, how they affect the perturbation expansion, and how to calculate them. Unfortunately, these examples are all too simple; they do not illustrate how one would apply the method to a more complex system, such as the Anderson model.

The quantum algebra approach to the Anderson model was thereby left in a very unsatisfactory state. The purpose of this thesis is to consistently present the method of thermo field dynamics of a quantum algebra, correctly apply it to the Anderson model, showing the full complication of the spin J rules, demonstrate how the vacuum diagrams are essential to correctly renormalizing the theory, and, hopefully, disentangle the perturbation expansion.

1.11 OVERVIEW OF THIS THESIS

Because most of the people who have worked on the Anderson model do not know thermo field dynamics (TFD), chapter 2 was designed to introduce TFD and summarize its essential features. Chapter 3 then goes into the details of TFD of a quantum algebra: how the generalized Wick's theorem is constructed, what its limitations are, how non–cancelling vacuum diagrams arise, and what the vacuum diagrams do to the perturbation formula.

The major complication in the Anderson model comes not from the hybridization interaction of f–electrons with conduction electrons, but rather, from the infinite Coulomb repulsion U, which restricts the f–state to a maximum occupancy of 1. It is therefore instructive to firstly consider this constrained f–state with no c–electrons and no interaction. This is the purpose of Chapter 4.

Chapter 4 shows how the spontaneous vertices arise, explicitly constructs the propagator and multi–point functions, and sets out systematic Feynman rules. The N–fold degenerate (spin J) case is quite extensively covered. It is very complicated and two sets of rules are laid out, which depend upon whether or not one wishes to represent the algebra in terms of the SU(N) group. The time–splitting technique (which must be used when the generalized Wick's theorem fails) is shown in full detail. Vacuum diagrams do not arise because there is no interaction.

Chapter 5 serves to illustrate the effects of the vacuum diagrams, and how the renormalization works. This is done by adding a very simple interaction to the model of chapter 4: a shift of energy. Of course, this is exactly solvable, and thereby serves as a check on the correctness of the renormalization procedure.

These methods are applied to the single impurity, infinite–U, N–fold degenerate Anderson model in Chapter 6. Vacuum diagram effects turn out to be much more complicated than in chapter 5, because these "vacuum diagrams" become connected to the main diagrams. Most of this chapter is spent analyzing how to disconnect these vacuum diagrams. Finally, a renormalized perturbation formula is obtained.

Chapter 7 shows results of this method. Renormalized diagrammatics of both the single–site and lattice Anderson models are presented. A self–consistent 1–loop calculation is performed for both of these models.

Finally, chapter 8 summarizes the thesis and makes conclusions regarding the usefulness of this novel approach to the Anderson model.

CHAPTER 2

TFD OF CANONICALLY QUANTIZED SYSTEMS; NOTATION

2.1 INTRODUCTION

The following is a very brief summary of equilibrium thermo field dynamics (TFD), intended to establish the formalism, conventions, and notation used throughout this thesis. An extension of this framework to the case of a quantum algebra will be presented in chapter 3. Readers who desire a more detailed description of TFD are referred to the excellent book by H. Umezawa, et al. [57]. The notation of this thesis differs somewhat from that of ref. [57], in that the chemical potential μ is kept explicit. Too often μ is buried by taking it to be the zero point of the energy scale; this hides the essential role that μ plays in TFD.

2.2 WHAT'S IT ALL ABOUT?

2.2.1 THE THERMAL VACUUM

The essence of TFD is that the thermal average of operators may be expressed as a thermal vacuum expectation value. That is, one constructs a thermal vacuum $|0(\beta)\rangle$ at temperature T ($\beta = 1/k_B T$), such that:

$$\langle 0(\beta)|A|0(\beta)\rangle \equiv \frac{\mathrm{Tr}\left[e^{-\beta(H-\mu N)}\,A\right]}{\mathrm{Tr}\left[e^{-\beta(H-\mu N)}\right]}, \tag{2.1}$$

corresponding to the grand canonical ensemble of statistical mechanics; where H is the full Hamiltonian of the system, N is the number operator, μ is the chemical potential, A is a generic operator, and the trace is taken over all states. The advantage of this method is that one has a thermal quantum field theory in which the operator relations and Feynman propagator methods of zero–temperature field theory may be used.

2.2.2 THE TILDE FIELD: CONSTRUCTION OF THE VACUUM

In order to mathematically realize the construction of eq. (2.1), one must double the operator degrees of freedom: With every operator, A, is associated a "tilde conjugate" operator, $\tilde{A}$, which is independent of A. That is,

$$[A_1\ ,\ \tilde{A}_2]_\rho = 0 \quad , \tag{2.2}$$

where we define

$$[A\ ,\ B]_\rho \equiv AB-\rho BA \quad , \tag{2.3}$$

where $\rho=1$ for boson commutation, and $\rho=-1$ for fermion anti–commutation, depending on the nature of A and B. The tilde conjugate operators act in the tilde conjugate space which is orthogonal to the non–tilde space.

Let us consider a typical canonically quantized field whose physical states at T=0 may be described by creation operators $a^\dagger_{k\sigma}$ of definite momentum k and spin σ, operating on an empty vacuum $|0\rangle$. By introducing $\tilde{a}^\dagger_{k\sigma}$ and its vacuum $|\tilde{0}\rangle$, one may construct $|0(\beta)\rangle$:

$$|0(\beta)\rangle =$$

$$= \frac{1}{\sqrt{Z}}\sum_{n=0}^{\infty}\ \sum_{\{k,\sigma\}} e^{-\beta(H-\mu N)/2}\ a^\dagger_{k_1\sigma_1}a^\dagger_{k_2\sigma_2}\cdots a^\dagger_{k_n\sigma_n}\tilde{a}^\dagger_{k_1\sigma_1}\tilde{a}^\dagger_{k_2\sigma_2}\cdots\tilde{a}^\dagger_{k_n\sigma_n}|0,\tilde{0}\rangle \ , \tag{2.4}$$

where

$$Z \equiv \mathrm{Tr}\left[e^{-\beta(H-\mu N)}\right] \equiv$$

$$\equiv \sum_{n=0}^{\infty}\ \sum_{\{k,\sigma\}} \langle 0|a_{k_1\sigma_1}a_{k_2\sigma_2}\cdots a_{k_n\sigma_n}\,e^{-\beta(H-\mu N)}\ a^\dagger_{k_n\sigma_n}\cdots a^\dagger_{k_2\sigma_2}a^\dagger_{k_1\sigma_1}|0\rangle \ . \tag{2.5}$$

By virtue of eq. (2.2), only the diagonal momentum states participate in $\langle 0(\beta)|A|0(\beta)\rangle$, and eq. (2.1) is obviously satisfied.

2.2.3 WHY IS IT A PURE STATE?

Paradoxically, $|0(\beta)\rangle$ is a pure state rather than a mixed state. This is contrary to what one would expect from the density matrix formulation of statistical quantum mechanics: Rather than being described by a ket vector $|\Psi\rangle$, a statistical (mixed) state is described by a density matrix ρ_D , which is a hermitian operator that determines the observables of a system via:

$$\langle A\rangle = \mathrm{Tr}\left[\rho_D A\right]. \tag{2.6}$$

To illustrate, consider a simple spin system in which the Hilbert space is spanned by the two states $|\uparrow\rangle = \begin{bmatrix}1\\0\end{bmatrix}$ and $|\downarrow\rangle = \begin{bmatrix}0\\1\end{bmatrix}$ in the z–basis. Observable quantities are:

$$\left.\begin{aligned} s_x &= \tfrac{1}{2}\mathrm{Tr}\left[\rho_D\sigma_x\right] \\ s_y &= \tfrac{1}{2}\mathrm{Tr}\left[\rho_D\sigma_y\right] \\ s_z &= \tfrac{1}{2}\mathrm{Tr}\left[\rho_D\sigma_z\right] \end{aligned}\right\} , \tag{2.7}$$

where $\sigma_x = \begin{bmatrix}0 & 1\\1 & 0\end{bmatrix}$, $\sigma_y = \begin{bmatrix}0 & -i\\i & 0\end{bmatrix}$, and $\sigma_z = \begin{bmatrix}1 & 0\\0 & -1\end{bmatrix}$. This yields the following form for the density matrix:

$$\rho_D = \begin{bmatrix}\tfrac{1}{2}+s_z & s_x-is_y\\ s_x+is_y & \tfrac{1}{2}-s_z\end{bmatrix}. \tag{2.8}$$

There are no conditions on s_x, s_y, and s_z (other than $-\tfrac{1}{2} < s_i < \tfrac{1}{2}$). In particular, one could have $s_x = s_y = s_z = \tfrac{1}{2}$; this is only possible in a mixed state.

A pure state in this spin system, on the other hand, is described by a state vector $|\Psi\rangle$ as follows:

$$|\Psi\rangle = \sqrt{\tfrac{1}{2}+s_z}\; e^{i\theta}|\uparrow\rangle + \sqrt{\tfrac{1}{2}-s_z}\; e^{i\theta'}|\downarrow\rangle \ , \tag{2.9}$$

where

$$\left.\begin{aligned} s_z &= \tfrac{1}{2}\langle\Psi|\sigma_z|\Psi\rangle \\ s_y &= \tfrac{1}{2}\langle\Psi|\sigma_y|\Psi\rangle = \sqrt{\tfrac{1}{4}-s_z^2}\,\sin(\theta'-\theta) \\ s_x &= \tfrac{1}{2}\langle\Psi|\sigma_x|\Psi\rangle = \sqrt{\tfrac{1}{4}-s_z^2}\,\cos(\theta'-\theta) \end{aligned}\right\} . \qquad (2.10)$$

The condition on this pure state is $s_x^2 + s_y^2 + s_z^2 = \tfrac{1}{4}$. For example, if $s_z = \tfrac{1}{2}$, then $s_x = s_y = 0$.

Evidently, there is a fundamental distinction between a pure state and a mixed state. How can the statistical thermal vacuum be written as a pure state? It was done through the introduction of the tilde space. One may do the same with any mixed state as follows. Suppose the Hilbert space is spanned by the basis vectors $|\Phi_i\rangle$; we introduce the tilde Hilbert space spanned by the basis vectors $|\tilde{\Phi}_i\rangle$. Then the mixed state may be written as a pure state vector $|\Psi\rangle$ as follows:

$$|\Psi\rangle = \sqrt{\rho_D}\sum_i |\Phi_i\rangle \otimes |\tilde{\Phi}_i\rangle \qquad (2.11)$$

such that $\langle\Psi|A|\Psi\rangle = \mathrm{Tr}\left[\rho_D\, A\right]$.

Although $|0(\beta)\rangle$ is a pure state, there are still fluctuations, in the same manner that one finds fluctuations in the grand canonical ensemble; namely via $|\langle 0(\beta)|A|0(\beta)\rangle|^2 - |\langle 0(\beta)|A^2|0(\beta)\rangle|$.

2.2.4 PHYSICAL INTUITIONS

The thermal "vacuum" is actually a linear superposition of all possible states of all possible particles; it is not the vacuum state of the $a_{k\sigma}$ operator. But it *is* the vacuum state of the $\alpha_{k\sigma}$ operator which may be obtained via a Bogoliubov transformation:

$$\alpha_{k\sigma} = a_{k\sigma}\exp\left[\beta(\omega_{k\sigma}-\mu)/2\right] - \tilde{a}^{\dagger}_{k\sigma} , \qquad (2.12)$$

where $\left[H, a_{k\sigma}\right] = -\omega_{k\sigma}a_{k\sigma}$ such that $\alpha_{k\sigma}|0(\beta)\rangle = 0$. When the system has an infinite number of degrees of freedom, $|0(\beta)\rangle$ is unitarily inequivalent to

$|0,\tilde{0}\rangle$, ie. the Bogoliubov transformation takes one to a different Fock space. This can have far reaching consequences. (See ref. [57].)

The Hamiltonian which describes the dynamics of the thermal system is given by $\hat{H}$, where

$$\hat{H} \equiv H - \tilde{H} \qquad (2.13)$$

such that $\hat{H}|0(\beta)\rangle = 0$.

In this sense the $\tilde{a}^{\dagger}_{k\sigma}$ operators may be thought of as the creators of hole states of negative energy. Then the Bogoliubov transformation of eq. (2.12) has a simple physical interpretation: $\alpha^{\dagger}_{k\sigma}$ creates a *thermal* quantum, partly by putting an extra *zero temperature* particle into the thermal vacuum, and partly by removing a *zero temperature* hole state from the thermal vacuum. This "thermal quantum" is to be considered as one "extra" quantum, above that distribution maintained by the thermal reservoir at temperature T. Thus α_k annihilates this "extra" quantum. But the state $|0(\beta)\rangle$ contains only the equilibrium distribution of quanta, thus there are no "extra" thermal quanta to annihilate: this is why α_k annihilates the thermal vacuum.

Similarly, we may construct the operators $\tilde{\alpha}_{k\sigma}$ and $\tilde{\alpha}^{\dagger}_{k\sigma}$ which annihilate and create thermal holes, a thermal hole being one less quantum than the equilibrium distribution. For the same reasons as above, $\tilde{\alpha}_{k\sigma}$ also annihilates $|0(\beta)\rangle$.

In short, we have eight operator classes: $a_{k\sigma}$, $a^{\dagger}_{k\sigma}$, $\tilde{a}_{k\sigma}$, and $\tilde{a}^{\dagger}_{k\sigma}$, which are the annihilation and creation operators of zero–temperature particles and holes, and $\alpha_{k\sigma}$, $\alpha^{\dagger}_{k\sigma}$, $\tilde{\alpha}_{k\sigma}$, and $\tilde{\alpha}^{\dagger}_{k\sigma}$, which are the annihilation and creation operators of thermal quanta and holes. Because the tilde operators describe hole states, we have the following tilde conjugation rules:

$$\left.\begin{aligned} (c_1A_1 + c_2A_2)^{\sim} &= c_1^* \tilde{A}_1 + c_2^* \tilde{A}_2 \\ (A_1A_2)^{\sim} &= \tilde{A}_1\tilde{A}_2 \\ \tilde{\tilde{A}} &= \bar{\sigma}_A \; A \end{aligned}\right\} , \qquad (2.14)$$

where A is a generic operator, c is a c–number, and $\bar{\sigma}_A$ is a phase factor.

One should be careful of the physical intuitions presented above. Hole states at T=0 created by $\tilde{a}^{\dagger}_{k\sigma}$ are not physically observable particles. Conversely, the thermal hole state at T>0 created by $\tilde{\alpha}^{\dagger}_{k\sigma}$ *is* physically observable, but *only* that component of it which operates in the non–tilde space. One might then be led to conclude that the tilde conjugate space does not have physical significance, and that it is merely a mathematical trick. This view is too naive. The tilde degrees of freedom are actually very important, because they represent hidden variables which self–consistently control the thermal state of the system, eliminating the need for a reservoir [61]. By choosing the appropriate representation of a quantum field, (from an infinite class of unitarily inequivalent representations), one can place the system in *any* thermal state. This includes non–equilibrium situations. For a good review of the recent work done on non–equilibrium thermo field dynamics, see ref. [61].

2.3 FORMAL CONSTRUCTION OF TFD

2.3.1 THE THERMAL STATE CONDITION

The most general construction of equilibrium TFD is to start with doubling the operator degrees of freedom according to the tilde conjugation rules given in eqs. (2.14) and (2.2). Then, rather than explicitly construct the vacuum as in eqs. (2.4) and (2.5), one introduces temperature via a general relation called the "thermal state condition" as follows:

$$e^{\beta\mu\hat{N}/2} \; A(t+i\beta/2) \; e^{-\beta\mu\hat{N}/2} \; |0(\beta)\rangle = \hat{\sigma} \; \tilde{A}^{\dagger}(t)|0(\beta)\rangle \tag{2.15}$$

where $A(z) \equiv e^{i\hat{H}z} \, A \, e^{-i\hat{H}z}$ is time-evolved according to the full Hamiltonian ($\hat{H} = H-\tilde{H}$), $\hat{N} = N-\tilde{N}$, and $\hat{\sigma}$ is a phase operator. (Here we are assuming $[H,N] = 0$.) The thermal state condition is considered to be the most fundamental relation in TFD; it embodies the physics of equilibrium systems. (Modifications of the thermal state condition have lead to non-equilibrium TFD, which is reviewed in ref. [61].)

The choice of the phase operator $\hat{\sigma}$ is related to the choice of the double tilde-conjugate phase factor $\bar{\sigma}_A$ (see eq. (2.14)). The general rules for choosing $\hat{\sigma}$ and $\bar{\sigma}_A$ are given in ref. [62]. For the purposes of this thesis, the following choice is made:

$$\hat{\sigma} = (-1)^{\frac{1}{2}\hat{N}_F(\hat{N}_F+1)} \tag{2.16}$$

$$\bar{\sigma}_A = \rho_A \tag{2.17}$$

where $\hat{N}_F \equiv N_F - \tilde{N}_F$ is the fermion number operator, and $\rho_A = 1$ for bosonic A and $\rho_A = -1$ for fermionic A.

2.3.2 THE BOGOLIUBOV TRANSFORMATION AND THERMAL DOUBLET NOTATION

If $A = a_{\mathbf{k}\sigma}$ where $a_{\mathbf{k}\sigma}$ is a fermion or boson annihilation operator which diagonalizes H such that its time dependence is $a_{\mathbf{k}\sigma}(t) = a_{\mathbf{k}\sigma}\exp\left[-i\omega_{\mathbf{k}\sigma}t\right]$, then the thermal state condition, eq. (2.15), becomes:

$$\exp\left[\beta(\omega_{\mathbf{k}\sigma}-\mu)/2\right] \; a_{\mathbf{k}\sigma}|0(\beta)\rangle = \tilde{a}^{\dagger}_{\mathbf{k}\sigma}|0(\beta)\rangle \tag{2.18a}$$

and

$$\exp\left[-\beta(\omega_{\mathbf{k}\sigma}-\mu)/2\right] \; a^{\dagger}_{\mathbf{k}\sigma}|0(\beta)\rangle = \rho_a \; \tilde{a}_{\mathbf{k}\sigma}|0(\beta)\rangle \; . \tag{2.18b}$$

(Here we assume that the fermion number of $a_{\mathbf{k}\sigma}$ is 0 for bosonic $a_{\mathbf{k}\sigma}$ and -1 for fermionic $a_{\mathbf{k}\sigma}$.)

Following eq. (2.12), we may construct the thermal operators as follows:

$$\alpha_{\mathbf{k}\sigma} = \frac{e^{\beta(\omega_{\mathbf{k}\sigma}-\mu)/2} a_{\mathbf{k}\sigma} - \tilde{a}^{\dagger}_{\mathbf{k}\sigma}}{\sqrt{e^{\beta(\omega_{\mathbf{k}\sigma}-\mu)} - \rho_a}} , \tag{2.19a}$$

$$\tilde{\alpha}_{\mathbf{k}\sigma} = \frac{e^{\beta(\omega_{\mathbf{k}\sigma}-\mu)/2} \tilde{a}_{\mathbf{k}\sigma} - \rho_a a^{\dagger}_{\mathbf{k}\sigma}}{\sqrt{e^{\beta(\omega_{\mathbf{k}\sigma}-\mu)} - \rho_a}} , \tag{2.19b}$$

where the normalization has been chosen to preserve the commutation relations.

It is useful to introduce the thermal doublet notation as follows:

$$A^{\gamma} \equiv \begin{bmatrix} A \\ \tilde{A}^{\dagger} \end{bmatrix}^{\gamma} . \tag{2.20}$$

Then the Bogoliubov transformation of eqs. (2.19) acquires the following simple matrix form:

$$a^{\gamma}_{k\sigma} = \sum_{\eta=1}^{2} U_a^{\gamma\eta}(k,\sigma;\mu)\alpha^{\eta}_{k\sigma} , \tag{2.21a}$$

where

$$U_a(k,\sigma;\mu) = \frac{1}{\sqrt{e^{\beta(\omega_{k\sigma}-\mu)} - \rho_a}} \begin{bmatrix} e^{\beta(\omega_{k\sigma}-\mu)/2} & 1 \\ \rho_a & e^{\beta(\omega_{k\sigma}-\mu)/2} \end{bmatrix} . \tag{2.21b}$$

2.4 PROPAGATORS AND SPECTRAL FUNCTIONS

2.4.1 THE GENERAL FORM OF THE THERMAL PROPAGATOR

Using eq. (2.21a), one finds the following general form for fermion (F) and boson (B) Feynman propagators:

$$\langle 0(\beta)|\mathrm{T}\ \Psi^{\alpha}(\vec{x},t)\ \Psi^{\gamma\dagger}(\vec{x}',t')|0(\beta)\rangle \equiv$$

$$\equiv i\int\frac{d\omega}{2\pi}\int\frac{d^3k}{(2\pi)^3}\,e^{-i\omega(t-t')}\,e^{i\,\vec{k}\cdot(\vec{x}-\vec{x}')}\,G^{\alpha\gamma}(\omega,\vec{k};\mu) \qquad (2.22a)$$

where

$$G_F^{\alpha\gamma}(\omega,\vec{k};\mu) = \left[U_F(\omega-\mu)\ \bar{G}_F(\omega,\vec{k})\ U_F^{\dagger}(\omega-\mu)\right]^{\alpha\gamma}, \qquad (2.22b)$$

$$G_B^{\alpha\gamma}(\omega,\vec{k};\mu) = \left[U_B(\omega-\mu)\ \tau\ \bar{G}_B(\omega,\vec{k})\ U_B^{\dagger}(\omega-\mu)\right]^{\alpha\gamma}, \qquad (2.22c)$$

and

$$\tau \equiv \begin{bmatrix} 1 & 0 \\ 0 & -1 \end{bmatrix}, \qquad (2.22d)$$

U_F (U_B) is the fermion (boson) Bogoliubov transformation matrix,

$$U_{\rho}(\omega) = \frac{1}{\sqrt{e^{\beta\omega}-\rho}}\begin{bmatrix} e^{\beta\omega/2} & 1 \\ \rho & e^{\beta\omega/2} \end{bmatrix}, \qquad (2.23)$$

corresponding to $\rho=-1$ $(\rho=1)$, and $\bar{G}_{F(B)}(\omega,\vec{k})$ is a diagonal 2 x 2 matrix. A notation used throughout this thesis is that a "barred" propagator, $\bar{G}$, is the propagator G which has been stripped of its thermal U matrices.

Application of the spectral theorem for type 1 fields [57] yields the following form for $\bar{G}_{F(B)}(\omega,\vec{k})$:

$$\bar{G}_{F(B)}^{\alpha\gamma}(\omega,\vec{k}) = \int d\kappa\ \sigma_{G_{F(B)}}(\kappa,\vec{k})\ \frac{1}{\omega-\kappa+i\delta\tau^{\alpha\gamma}}, \qquad (2.24)$$

where δ is a positive infinitesimal and $\sigma_G(\kappa,\vec{k})$ is the spectral function of the propagator $G(\omega,\vec{k};\mu)$. (Only type 1 fields will be used in this thesis.) In general, $\sigma_G(\kappa,\vec{k})$ will also depend on β.

2.4.2 THE ANALYTIC PROPERTIES OF $\bar{G}(z,\vec{k})$

The analytic properties of $\bar{G}(z,\vec{k})$ for complex z (as defined by eq. (2.24)) are as follows: $\bar{G}^{\gamma\gamma}(z,\vec{k})$ is defined on four half-sheets connected by a branch cut at $\mathcal{Im}\,z = -\tau^{\gamma\gamma}\delta$; it is analytic in the first sheet which is composed of two half-sheets, the upper one, 1U, ($\mathcal{Im}\, z > -\tau^{\gamma\gamma}\delta$) and the lower one, 1L, ($\mathcal{Im}\, z < -\tau^{\gamma\gamma}\delta$); any poles of $\bar{G}^{\gamma\gamma}(z,\vec{k})$ occur in the second sheet, which is obtained from the first sheet by analytic continuation through the branch cut. For example, G_{2L} is the analytic continuation of G_{1U}, and G_{2U} is the analytic continuation of G_{1L}. This structure is illustrated in FIG. 2.1.

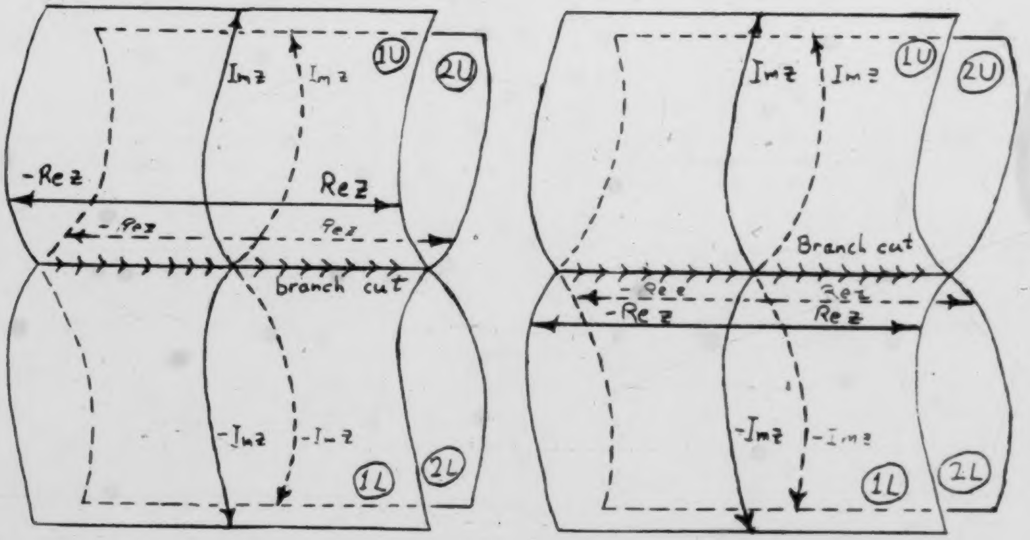

(a) (b)

FIG. 2.1

The Sheet Structure of $\bar{G}(z,\vec{k})$

The two upper half sheets are labeled 1U and 2U, and the two lower half sheets are labeled 1L and 2L. $\bar{G}(z,\vec{k})$ is analytic in sheets 1U and 1L; any poles occur in sheets 2U and 2L. (a) shows the sheet structure for $\bar{G}^{11}$, which has the branch cut below the $\mathcal{Re}\, z$ axis. (b) shows the sheet structure for $\bar{G}^{22}$, which has the branch cut above the $\mathcal{Re}\, z$ axis.

Note from eq. (2.24) that

$$\bar{G}^{\gamma\gamma}(z^{*}-i\delta\tau^{\gamma\gamma},\vec{k}) = \left[\bar{G}^{\gamma\gamma}(z-i\delta\tau^{\gamma\gamma},\vec{k})\right]^{*} . \tag{2.25}$$

Thus, $\bar{G}^{\gamma\gamma}_{1L}$ is a complex conjugated reflection of $\bar{G}^{\gamma\gamma}_{1U}$ through the branch cut; the same relation holds between $\bar{G}^{\gamma\gamma}_{2L}$ and $\bar{G}^{\gamma\gamma}_{2U}$. Also, eq. (2.24) shows that there is a relation between $\bar{G}^{11}$ and $\bar{G}^{22}$:

$$\left[\bar{G}^{11}(z^*,\vec{k})\right]^* = \bar{G}^{22}(z,\vec{k}) \quad , \tag{2.26}$$

which shows that $\bar{G}^{22}$ is a complex conjugated reflection of $\bar{G}^{11}$ through the $\mathcal{R}e\, z$ axis. Therefore, only $\bar{G}^{11}_{1U}$ and its analytic continuation $\bar{G}^{11}_{2L}$ are unique; all other pieces of $\bar{G}^{\gamma\gamma}$ are determined through eqs. (2.25) and (2.26).

In general, there is a smooth transition between $\bar{G}^{\gamma\gamma}_{1U}$ and $\bar{G}^{\gamma\gamma}_{2L}$, (or between $\bar{G}^{\gamma\gamma}_{1L}$ and $\bar{G}^{\gamma\gamma}_{2U}$), but there is a jump, or "discrepancy", between $\bar{G}^{\gamma\gamma}_{1U}$ and $\bar{G}^{\gamma\gamma}_{1L}$ (or between $\bar{G}^{\gamma\gamma}_{2U}$ and $\bar{G}^{\gamma\gamma}_{2L}$), as one crosses the branch cut.

The union of $\bar{G}^{11}_{1U}$ with $\bar{G}^{11}_{2L}$ is a smooth function $\bar{G}^{11}_{1U/2L}$, which will be called $\bar{G}^{11}$ for short. $\bar{G}^{11}(z,\vec{k})$ is analytic above and including the Re z axis but may have poles below the $\mathcal{R}e\, z$ axis. Similarly, the union of $\bar{G}^{22}_{1L}$ with $\bar{G}^{22}_{2U}$ is a smooth function $\bar{G}^{22}_{1L/2U}$, which will be called $\bar{G}^{22}$ for short. $\bar{G}^{22}(z,\vec{k})$ is analytic below and including the $\mathcal{R}e\, z$ axis, but may have poles above the $\mathcal{R}e\, z$ axis.

From eq. (2.24), the discrepancy may be found:

$$\bar{G}^{11}_{1U}(\omega-i\delta+i\delta',\vec{k}) - \bar{G}^{11}_{1L}(\omega-i\delta-i\delta',\vec{k}) =$$

$$= \int d\kappa\; \sigma_G(\kappa,\vec{k}) \left[\frac{1}{\omega-\kappa+i\delta'} - \frac{1}{\omega-\kappa-i\delta'}\right] = -2\pi i\; \sigma_G(\omega,\vec{k}) \ . \tag{2.27}$$

Using this with eq. (2.25), we may obtain the spectral function in a simple manner:

$$\sigma_G(\omega,\vec{k}) = -\frac{1}{\pi}\, \mathcal{I}m\left[\bar{G}^{11}(\omega,\vec{k})\right] \ . \tag{2.28}$$

2.4.3 THE SPECTRAL FUNCTION

The spectral function $\sigma_G(\omega,\vec{k})$ is a non-negative quantity which gives the density of states (per unit energy, at energy ω and momentum $\vec{k}$) which contribute to particles propagated by G. Nothing is said here about the occupation of these states; this depends on the temperature and is determined by the thermal U matrices. Both the density of states and the occupation of these states will depend on the temperature. The thermal U matrices carry the chemical potential, which determines where the Fermi energy (or Bose condensation energy) will be.

2.4.4 SUMMARY

Some simple properties of the propagators and the U matrices are summarized in appendix A, section A.1.

2.5 PERTURBATION THEORY

As illustrated in eq. (2.22), the formalism of Feynman propagators is preserved in TFD. One also finds the Gell–Mann Low formula of perturbation theory extended in a straightforward fashion:

$$\langle 0(\beta)|\, T\, A_1^{\alpha_1}(t_1) \ldots A_n^{\alpha_n}(t_n)\, |0(\beta)\rangle =$$

$$= \frac{\langle 0,\beta|\, T\, \hat{U}(\infty,-\infty)\, \mathcal{A}_1^{\alpha_1}(t_1) \ldots \mathcal{A}_n^{\alpha_n}(t_n)\, |0,\beta\rangle}{\langle 0,\beta|\, T\, \hat{U}(\infty,-\infty)\, |0,\beta\rangle}\,, \tag{2.29a}$$

where

$$\hat{U}(\infty,-\infty) = T \exp\left[-i\int_{-\infty}^{\infty} dt\, \hat{\mathcal{H}}_I(t)\right]\,, \tag{2.29b}$$

and $\hat{H}_I$ ($\equiv H_I - \tilde{H}_I$) is the interaction Hamiltonian. Operators on the left hand side of the equation are time–evolved according to the full Hamiltonian:

$$A^{\alpha}(t) \equiv e^{i\hat{H}t}\, A^{\alpha}\, e^{-i\hat{H}t}\,, \qquad \hat{H} \equiv H - \tilde{H}\,; \tag{2.29c}$$

whereas operators on the right hand side of the equation are time–evolved according to the free Hamiltonian:

$$\left.\begin{aligned} \mathcal{A}^{\alpha}(t) &\equiv e^{i\hat{H}_o t}\, A^{\alpha}\, e^{-i\hat{H}_o t}\,, \\ \hat{\mathcal{H}}_I(t) &\equiv e^{i\hat{H}_o t}\, \hat{H}_I\, e^{-i\hat{H}_o t}\,, \\ \hat{H}_o &\equiv H_o - \tilde{H}_o \end{aligned}\right\} \tag{2.29d}$$

Similarly, $|0(\beta)\rangle$ is the thermal vacuum of the full Hamiltonian H, whereas $|0,\beta\rangle$ is the thermal vacuum of the free Hamiltonian H_o .

The vacuum diagrams of $\hat{U}(\infty,-\infty)$ in the numerator cancel the vacuum diagrams of the denominator in the usual way. (In fact, one finds in general that all vacuum diagrams in eq. (2.29a) are naturally zero. [63,64]) Wick's theorem is also applied in the usual manner, leading to a perturbation expansion similar to the zero–temperature one.

One thereby sees a very close relationship between the formalisms of TFD and zero–temperature quantum field theory, which is not so evident in the imaginary time (Matsubara) method of thermal quantum field theory.

CHAPTER 3
TFD OF A QUANTUM ALGEBRA

3.1 INTRODUCTION

3.1.1 CANONICAL QUANTIZATION

One of the most fundamental premises of quantum field theory is the canonical quantization condition. To illustrate, we consider a generic field $\Psi(\vec{x},t)$ and its Lagrangian density $\mathscr{L}(\Psi,\dot{\Psi};\vec{x},t)$ where $\dot{\Psi}(\vec{x},t) \equiv d\Psi(\vec{x},t)/dt$. The canonical momentum $\Pi_{\Psi}(\vec{x},t)$ is obtained via:

$$\Pi_{\Psi}(\vec{x},t) \equiv \frac{\delta \, \mathscr{L}(\Psi,\dot{\Psi};\vec{x},t)}{\delta \, \dot{\Psi}(\vec{x},t)} \tag{3.1}$$

One imposes the canonical quantization condition by:

$$\Big[\, \Psi(\vec{x},t) \; , \; \Pi_{\Psi}(\vec{x}\,',t) \, \Big]_{\rho} = i \, \delta^{3}(\vec{x}-\vec{x}\,') \tag{3.2}$$

where we use the commutator ($\rho=1$) for boson fields and the anti–commutator ($\rho=-1$) for fermion fields.

When Ψ is expanded in terms of creation and annihilation operators, ($a^{\dagger}_{k\sigma}$ and $a_{k\sigma}$), the canonical quantization condition usually leads to the simple harmonic oscillator algebra, namely:

$$\Big[\, a_{k\sigma} \, , \, a^{\dagger}_{k'\sigma'} \Big]_{\rho} = \delta^{3}(\vec{k}-\vec{k}') \; \delta_{\sigma\sigma'} \quad , \tag{3.3a}$$

$$\Big[\, a_{k\sigma} \, , \, a_{k'\sigma'} \Big]_{\rho} = \Big[\, a^{\dagger}_{k\sigma} \, , \, a^{\dagger}_{k'\sigma'} \Big]_{\rho} = 0 \quad , \tag{3.3b}$$

where the hamiltonian is given by:

$$H = \sum_{\sigma} \int d^{3}k \; \omega_{k\sigma} \, a^{\dagger}_{k\sigma} \, a_{k\sigma} \tag{3.4}$$

The assumption behind these equations is that $\mathscr{L}$ is a bilinear function of Ψ and $\dot{\Psi}$. If there exists other terms which are not bilinear, one usually assumes they are small and treats them using perturbation theory. That is, eqs. (3.1) to (3.3) are still valid, but eq. (3.4) applies only to H_o, the free part of the Hamiltonian. The rest of the Hamiltonian, H_I, is treated as a perturbation.

3.1.2 BREAKING CANONICAL QUANTIZATION: A QUANTUM ALGEBRA OF EIGENOPERATORS

What happens if there exist non–bilinear terms so strong that they cannot be treated as a perturbation? Then they must be included as part of H_o. Eqs. (3.1) to (3.3) are still valid but eq. (3.4) for H_o is not. That is, $a_{k\sigma}$ no longer has the simple time dependence, $a_{k\sigma}(t) = a_{k\sigma}\, e^{-i\omega_{k\sigma}t}$, and one cannot obtain the propagators; one is stuck.

A possible way out of this dilemma is to find an operator transformation to a new set of operators, ξ_i, such that

$$[\, H_o \,,\, \xi_i \,] = -\, \omega_i \xi_i \quad . \tag{3.5}$$

These "eigenoperators" will have the familiar time dependence, $\xi_i(t) = \xi_i e^{-i\omega_i t}$, but eqs. (3.3) will no longer be valid, leading to a "quantum algebra":

$$[\, \xi_i \,,\, \xi_j \,]_\rho = C_{ijk}\xi_k \quad , \tag{3.6}$$

where C_{ijk} is a c–number.

One may then introduce an eigenfield $\Xi_i(\vec{x},t)$ which is expanded in terms of the eigenoperator ξ_i. If one now rewrites the full Hamiltonian H in terms of these eigenfields, one may obtain the Heisenberg equations for the Ξ_i fields via:

$$[\, H \,,\, \Xi_i \,] = -\, i \frac{\partial}{\partial t}\, \Xi_i(\vec{x},t) \quad . \tag{3.7}$$

Suppose one wishes to find a Lagrangian for this system in terms of the Ξ_i fields. Firstly one needs to find a canonical momentum for Ξ_i. In general, it is not possible to find an operator Π_{Ξ_j} such that Ξ_i and Π_{Ξ_j} satisfy the canonical quantization condition (eq. (3.2)); such a thing may not exist.

Yet, it is still sometimes possible to find a Lagrangian in terms of Ξ_i, such that its Euler–Lagrange equations agree with the Heisenberg equations of eq. (3.7). One may then obtain the canonical momentum Π_{Ξ_j} using eq. (3.1). *But*, Ξ_i and Π_{Ξ_j} will not satisfy the usual canonical quantization condition; the right hand side of eq. (3.2) will in general involve other operators:

$$\left[\Xi_i(\vec{x},t) \ , \ \Pi_{\Xi_j}(\vec{x}',t) \right]_\rho \neq i\delta^3(\vec{x}-\vec{x}')\ \delta_{ij} \ . \tag{3.8}$$

(An illustration of how this is possible is given in Appendix B.)

The eigenfields, in general, violate the canonical quantization condition. If this language is too strong, then one may simply say that there is no Lagrangian and we don't have a canonical formalism. In any case, one must be very careful in using the standard formalism of conventional quantum field theory.

In this chapter, it is shown how one extends the formalism of thermo field dynamics (TFD) to apply to this unconventional and perhaps perilous situation.

3.2 THE GENERALIZED WICK'S THEOREM

3.2.1 THE SETUP

Consider a Hamiltonian which has some non–bilinear terms which are strong, and some interaction terms which are weak, in addition to the free bilinear terms. We wish to formulate a perturbation theory in which the free bilinear terms and the strong non–bilinear terms are grouped under H_o, and the interaction terms are grouped under H_I. As in eqs. (3.5) and (3.6), one rewrites the Hamiltonian in terms of the eigenoperators ξ_i of eigenenergy ω_i :

$$\left[H_o \ , \ \xi_i \right] = -\omega_i \ \xi_i \ , \tag{3.9a}$$

$$[\ \xi_i\ ,\ \xi_j\ ]_\rho = C_{ijk}\ \xi_k\ . \tag{3.9b}$$

(It is assumed that the algebra is closed.) Then one constructs an interaction representation, and attempts perturbation theory.

3.2.2 FINDING AN ANNIHILATION OPERATOR

Because ξ_i satisfies a quantum algebra, it is not an annihilation operator, (i.e. it does not annihilate the vacuum), and thus one does not have a Wick's theorem for reducing a time-ordered product of ξ-operators. This is where TFD comes to the rescue. As shown by eq. (2.15), one may use the thermal state condition to construct an annihilator of the thermal vacuum, from ***any*** operator, even ξ_i:

$$\xi_{i\beta}(t)\ \ \alpha\ \ e^{\beta\mu\hat{N}/2}\ \xi_i\left[t + \frac{i\beta}{2}\right]\ e^{-\beta\mu\hat{N}/2} - \hat{\sigma}\ \xi_i^\dagger(t)\ , \tag{3.10}$$

such that $\xi_{i\beta}(t)|0,\beta\rangle = 0$.

Although the standard annihilation operator of the simple harmonic oscillator algebra obeys $\left[\ \mu N\ ,\ a_{k\sigma}\right] = -\mu\ a_{k\sigma}$, this does not necessarily hold true for a general eigenoperator. One would expect

$$[\ \mu N\ ,\ \xi_i\ ] = -\ \eta_i\ \mu\ \xi_i\ , \tag{3.11}$$

where η_i could be 1, –1, or 0, depending on whether ξ_i annihilates a particle, creates a particle, or commutes with N. Therefore, the thermal annihilation operator, $\xi_{i\beta}$, has the simple form of eqs. (2.21) with $\mu \rightarrow \eta_i\mu$, as follows:

$$\xi_i^\gamma = U_i^{\gamma\eta}(\eta_i\mu)\ \xi_{i\beta}^\eta \tag{3.12a}$$

where

$$U_i(\eta_i\mu) = \frac{1}{\sqrt{e^{\beta(\omega_i-\eta_i\mu)} - \rho_i}} \begin{bmatrix} e^{\beta(\omega_i-\eta_i\mu)/2} & 1 \\ \rho_i & e^{\beta(\omega_i-\eta_i\mu)/2} \end{bmatrix} \tag{3.12b}$$

(As in sect. 2.3.2., we have assumed that ξ_i has a fermion number of 0 for bosonic ξ_i and -1 for fermionic ξ_i.)

3.2.3 WICK'S THEOREM, GENERALIZED

Using this annihilation operator, a generalized Wick's theorem may be obtained at finite temperature. This was first done in refs. [56] and [58]. The result is quoted below:

$$\langle 0,\beta|T\ \xi_a^{\alpha}(t)\ \xi_{a_1}^{\alpha_1}(t_1)\ \ldots\ \xi_{a_n}^{\alpha_n}(t_n)\ |0,\beta\rangle =$$
$$= \sum_j P_j \Big[G_a(t-t_j)\ T_a T_{aa_j} \Big]^{\alpha\alpha_j} C_{aa_jb}\ \langle 0,\beta|T\ \xi_{a_1}^{\alpha_1}(t_1)\ \ldots\ \xi_b^{\alpha_j}(t_j)\ \ldots\ \xi_{a_n}^{\alpha_n}(t_n)|0,\beta\rangle \qquad (3.13)$$

where G_a is the propagator of ξ_a , given by

$$G_a^{\alpha\gamma}(t-t_j) = i\int \frac{d\omega}{2\pi}\, e^{-i\omega(t-t_j)}\ G_a^{\alpha\gamma}(\omega,\eta_a\mu)\ , \qquad (3.14a)$$

$$G_a^{\alpha\gamma}(\omega,\eta_a\mu) = \left[U_a(\omega-\eta_a\mu)\ \frac{T_a}{\omega - \omega_a + i\delta\tau}\ U_a^{\dagger}(\omega-\eta_a\mu) \right]^{\alpha\gamma}, \qquad (3.14b)$$

$$T_a = \begin{cases} 1 : & \text{fermionic } \xi_a \\ \tau : & \text{bosonic } \xi_a \end{cases}, \qquad (3.15a)$$

$$T_{aa_j} = \begin{cases} 1 : & \text{fermionic } \xi_a \text{ and } \xi_{a_j} \\ \tau : & \text{otherwise} \end{cases}, \qquad (3.15b)$$

$$U_a(\omega) = \frac{1}{\sqrt{e^{\beta\omega} - \rho_a}} \begin{pmatrix} e^{\beta\omega/2} & 1 \\ \rho_a & e^{\beta\omega/2} \end{pmatrix}, \qquad (3.16)$$

and $P_j \equiv (-1)^{N_j}$ where N_j is the number of fermion anti-commutations required to bring ξ_a to the immediate left of ξ_{a_j}. (Again, we assume that if ξ_a is fermionic, then its fermion number is -1.) Note that the propagator G_a has the same form as eqs. (2.22) to (2.24) for a canonically quantized field, with a spectral function given by:

$$\sigma_a(\omega) = \delta(\omega - \omega_a) \ . \tag{3.17}$$

The difference in the reduction formula is that $\xi_{a_j}^{\alpha_j}(t_j)$ is replaced by $C_{aa_jb}\ \xi_b^{\alpha_j}(t_j)$ due to the quantum algebra, rather than being replaced by 1. A spontaneous vertex at t_j is thereby introduced, even without an interaction; this greatly complicates the Feynman rules.

3.2.4 ZERO–ENERGY BOSONS, A LIMITATION

Further complications arise when the algebra contains a subset of zero–energy bosonic eigenoperators $\{n_i\}$, such that

$$\left[\ H_o\ ,\ n_i\ \right] = \left[\ N\ ,\ n_i\ \right] = 0\ , \tag{3.18}$$

yielding $\omega_{n_i} = \eta_{n_i} = 0$, and a spectral function of $\sigma_{n_i}(\omega) = \delta(\omega)$. Upon using eq. (A.18), eq. (3.14b) becomes:

$$G_{n_i}(\omega) = U_B(\omega)\ \frac{\tau}{\omega + i\delta\tau}\ U_B(\omega), \tag{3.19a}$$

$$= \tau\ \frac{\mathcal{P}}{\omega} - i\pi\ U_B^2(0)\ \delta(\omega), \tag{3.19b}$$

where $U_B^2(0)$ is clearly divergent, and the reduction formula breaks down.

Thus, with the use of eq. (3.13), a T–product of eigenoperators, ξ_i , may be reduced to a T–product of 0–energy bosonic eigenoperators, n_i , but no further. To further reduce the T–product of n_i–operators requires special techniques which will be specific to the individual problem being considered.

3.2.5 AN AMBIGUITY IN THE REDUCTION

It is interesting to note that there is an ambiguity in the generalized Wick's theorem of eq. (3.13). The reduction is defined to start with the leftmost operator in the T–product, ξ_a , and the first propagator obtained is that of ξ_a . The ambiguity lies in choosing which operator will sit at the far left. A different choice will lead to a completely different reduction, although one expects the end result to be the same.

As an example, suppose one has three eigenoperators, defined such that

$$\left[\, H-\mu N \,,\, \xi_j \,\right] = -\left[\, E_j - \eta_j\mu \,\right] \xi_j \,, \qquad j = 1,2,3 \,, \tag{3.20}$$

?

$$\{\, \xi_1 \,,\, \xi_2 \,\} = \xi_3 \,, \tag{3.21}$$

where ξ_1 and ξ_2 are fermionic and ξ_3 is bosonic.

Then eq. (3.13) yields:

$$\langle 0,\beta|T\ \xi_1^\alpha(t)\ \xi_2^\gamma(t')|0,\beta\rangle = G_1^{\alpha\gamma}(t-t')\ \langle 0,\beta|\xi_3^\gamma(t')|0,\beta\rangle =$$

$$= -\langle 0,\beta|T\ \xi_2^\gamma(t')\ \xi_1^\alpha(t)|0,\beta\rangle = -G_2^{\gamma\alpha}(t'-t)\langle 0,\beta|\xi_3^\alpha(t)|0,\beta\rangle \,, \tag{3.22}$$

where $G_1^{\alpha\gamma}$ is the propagator of ξ_1 with energy E_1 and $G_2^{\gamma\alpha}$ is the propagator of ξ_2 with energy E_2.

On the surface there appears to be a contradiction: with one choice of the reduction, a particle with energy E_1 is being propagated; with another choice of the reduction a particle with energy E_2 is being propagated.

To resolve this, one notes $[H,\{\xi_1,\xi_2\}] = -(E_1+E_2)\{\xi_1,\xi_2\}$, therefore $E_3 = E_1+E_2$. Also $[\mu N,\{\xi_1,\xi_2\}] = -\mu(\eta_1+\eta_2)\{\xi_1,\xi_2\}$, therefore $\eta_3 = \eta_1 + \eta_2$. Now, one uses the thermal state condition, eq. (2.15):

$$\hat{\sigma}\ \tilde{\xi}_3^\dagger|0,\beta\rangle = \xi_3|0,\beta\rangle\ e^{(E_3-\eta_3\mu)\beta/2} \tag{3.23}$$

Let $\langle 0,\beta|\xi_3|0,\beta\rangle \equiv c$. One finds: $\langle 0,\beta|\tilde{\xi}_3^\dagger|0,\beta\rangle = [\langle 0,\beta|\xi_3^\dagger|0,\beta\rangle]^\sim = [\langle 0,\beta|\xi_3|0,\beta\rangle^*]^\sim = \tilde{c}^* = c$. Therefore:

$$\langle 0,\beta|\xi_3|0,\beta\rangle = \langle 0,\beta|\tilde{\xi}_3^\dagger|0,\beta\rangle \ . \tag{3.24}$$

But, from eq. (3.23):

$$\langle 0,\beta|\xi_3|0,\beta\rangle = \sigma\ e^{-(E_3-\eta_3\mu)\beta/2}\ \langle 0,\beta|\tilde{\xi}_3{}^\dagger|0,\beta\rangle \,, \tag{3.25}$$

where σ is the phase factor given by $\hat{\sigma}\ \tilde{\xi}_3^\dagger|0,\beta\rangle = \sigma\ \tilde{\xi}_3^\dagger|0,\beta\rangle$.

There are only two ways that eq. (3.24) can be consistent with eq. (3.25). One way is to have $\langle 0,\beta|\xi_3|0,\beta\rangle = 0$, in which case the contradiction of eq. (3.22) is trivially resolved. The other way is to have ξ_3

being a zero-energy bosonic eigenoperator such that $E_3 = \eta_3 = 0$ and $\sigma = 1$. (See eq. (2.16).)

With the second choice, one has:

$$E_2 = -E_1 \;,\quad \eta_2 = -\,\eta_1 \tag{3.26a}$$

$$\xi_2 = \xi_1^\dagger \;, \tag{3.26b}$$

in which case, eq. (3.22) becomes:

$$G_\xi^{\alpha\gamma}(t-t') = -G_{\xi\dagger}^{\gamma\alpha}(t'-t) \;. \tag{3.27}$$

To convince oneself that this is true, one uses eqs. (3.14) – (3.16) to write:

$$G_\xi^{\alpha\gamma}(t-t') = i\int \frac{d\omega}{2\pi}\, e^{-i\omega(t-t')}\left[U_F(\omega-\mu)\,\frac{1}{\omega-E_1+i\delta\tau}\,U_F^\dagger(\omega-\mu)\right]^{\alpha\gamma}, \tag{3.28}$$

where U_F is given by eq. (3.16) with $\rho = -1$, and we assume that ξ has a fermion number of –1, and $\eta_\xi = 1$. To write $G_{\xi\dagger}$, one must realize that the form of eq. (3.16) is no longer valid: $\xi_2 = \xi_1^\dagger$ has a fermion number of +1, rather than –1, and $\hat{\sigma}$ (eq. (2.16)) in the thermal state condition acquires the opposite sign. If one re-derives the thermal Bogoliubov transformation as in sect. 2.3.2., one finds

$$U_{\xi\dagger}(\omega) = U_F^\dagger(\omega) \;. \tag{3.29}$$

Using this with eqs. (3.26), one obtains

$$G_{\xi\dagger}^{\gamma\alpha}(t'-t) = i\int \frac{d\omega}{2\pi}\, e^{-i\omega(t'-t)}\left[U_F^\dagger(\omega+\mu)\,\frac{1}{\omega+E_1+i\delta\tau}\,U_F(\omega+\mu)\right]^{\gamma\alpha}, \tag{3.30}$$

Transforming $\omega \to -\omega$, and using the properties of $U_F(\omega)$ and $G_F(\omega)$ given in eqs. (A.11) and (A.17), one finds that eq. (3.27) is true. Thus there is no contradiction in eq. (3.22); the alternate methods of performing the reduction are equivalent.

3.3 VACUUM DIAGRAMS AND THE GENERALIZED GELL–MANN LOW FORMULA

3.3.1 THE MOST GENERAL FORM OF THE GELL–MANN LOW FORMULA

In section 2.5 the Gell–Mann Low formula of perturbation theory in TFD was presented, and it was stated that the vacuum diagrams cancel in the usual way. When dealing with a quantum algebra though, this situation changes. It was first realized by Whitehead, et al. [60], that one can have vacuum diagrams which do not cancel, due to the presence of zero–energy boson eigenoperators. In this section, it is shown how these vacuum diagrams arise.

Careful derivation of the Gell–Mann Low formula leads to the following expression [60]:

$$\langle 0(\beta)|\mathrm{T}[\mathrm{A}_1^{\alpha_1}(t_1)\mathrm{A}_2^{\alpha_2}(t_2)\ \ldots\ \mathrm{A}_n^{\alpha_n}(t_n)|0(\beta)\rangle =$$

$$\frac{\langle 0,\beta|\mathrm{U}(\infty-i\beta/2,\infty)\mathrm{T}\left[\hat{\mathrm{U}}(\infty,-\infty)\mathbb{A}_1^{\alpha_1}(t_1)\mathbb{A}_2^{\alpha_2}(t_2)\ \ldots\ \mathbb{A}_n^{\alpha_n}(t_n)\right]\mathrm{U}(-\infty,-\infty+i\beta/2)|0,\beta\rangle}{\langle 0,\beta|\mathrm{U}(\infty-i\beta/2,\infty)\hat{\mathrm{U}}(\infty,-\infty)\mathrm{U}(-\infty,-\infty+i\beta/2)|0,\beta\rangle} \tag{3.31}$$

where $|0(\beta)\rangle$ is the thermal vacuum of the full hamiltonian, $|0,\beta\rangle$ is the thermal vacuum of the free Hamiltonian, $\mathrm{A}^{\alpha}(t)$ is A^{α} time evolved using $\hat{\mathrm{H}}$, and $\mathbb{A}^{\alpha}(t)$ is A^{α} time evolved using $\hat{\mathrm{H}}_o$. Here,

$$\hat{\mathrm{U}}(t_2,t_1) \equiv \mathrm{T}\ \exp\left[-i\int_{t_1}^{t_2}dt\ \hat{\mathscr{H}}_{\mathrm{I}}(t)\right] , \tag{3.32}$$

where $\hat{\mathscr{H}}_{\mathrm{I}}(t)$ is $\hat{\mathrm{H}}_{\mathrm{I}}$ time evolved using $\hat{\mathrm{H}}_o$, and

$$\mathrm{U}(z_2,z_1) \equiv \mathrm{T}_z\ \exp\left[-i\int_{z_1}^{z_2}dt\ \mathscr{H}_{\mathrm{I}}(t)\right] . \tag{3.33}$$

Recall that $\hat{\mathrm{H}} \equiv \mathrm{H}-\tilde{\mathrm{H}}$.

Upon comparison of eqs. (2.29) to (3.31), one finds a notable difference, namely the presence of the U–operators at $\mathcal{R}e\,t = \pm\infty$. They arise due to the change of vacuum from $|0(\beta)\rangle$ on the left hand side, to $|0,\beta\rangle$ on the right hand side. In fact, one may relate this to the ratio of the full partition function Z to the free partition function Z_0 as follows [60]:

$$\frac{Z}{Z_0} = \langle 0,\beta|\, U(\infty-\tfrac{i\beta}{2},\infty)\ \hat{U}(\infty,-\infty)\ U(-\infty,-\infty+\tfrac{i\beta}{2})\,|0,\beta\rangle \quad . \tag{3.34}$$

3.3.2 WHY THE U–OPERATORS AT $\mathcal{R}e\,t = \pm\infty$ NOW CONTRIBUTE: NON–CANCELLING VACUUM DIAGRAMS

Why were these U–operators ignored in eq. (2.29)? The reason is that for the usual canonically quantized fields, the U terms in the numerator cancel the U terms in the denominator, thus they can be dropped. An analysis of why this cancellation occurs in the usual case but not in the quantum algebra case follows below.

Suppose one uses eq. (3.31) along with the generalized Wick's theorem, eq. (3.13), to obtain a perturbation expansion in terms of propagators of non–zero–energy eigenoperators $G_a^{\alpha\gamma}(t-t')$. Any contraction of the $\hat{U}$ or $\hat{\mathcal{A}}$ terms with a U term at $\mathcal{R}e\,t = \pm\infty$ will yield a $G_a^{\alpha\gamma}(\pm\infty\mp ib)$ term, where $0\le b\le\beta/2$. From eq. (3.14a), one has

$$G_a^{\alpha\gamma}(t{=}\pm\infty) = i\int\frac{d\omega}{2\pi}\, e^{\mp i\infty\omega}\, G_a^{\alpha\gamma}(\omega), \tag{3.35}$$

and it is clear that the infinitely rapid oscillations of the $e^{\mp i\infty\omega}$ term will average to zero when performing the integration, assuming $G_a^{\alpha\gamma}(\omega)$ is a smooth function which decays as $\omega \to \pm\infty$. This assumption is not entirely true because $G_a^{\alpha\gamma}(\omega)$ has a pole at $\omega = \omega_a$. To circumvent this problem, one assumes that $|t|\to\infty$ in U before the $\delta\to 0$ limit is taken in $G_a^{\alpha\gamma}(\omega)$; thus $G_a^{\alpha\gamma}(\omega)$ is still smooth compared to the scale of the $e^{\mp i\infty\omega}$ oscillations. A similar argument applies for $G_a^{\alpha\gamma}(\pm\infty\mp ib)$ except one has a discrete Fourier transform in the ib direction. One thereby finds that all $G_a^{\alpha\gamma}(\pm\infty\mp ib)$ terms are zero.

The above analysis shows that the U terms at $\mathcal{R}e\,t = \pm\infty$ contract only within themselves and do ***not*** connect to the $\hat{U}$ or $\hat{\mathcal{A}}$ terms via a non–zero–energy propagator, G_a. *(Note: There are exceptions to this rule. See sect. 5.9.)* Thus we may perform the reduction of the $\hat{U}$ and $\hat{\mathcal{A}}$ terms, leaving the U terms at $\mathcal{R}e\,t = \pm\infty$ alone, until all the non–zero–energy eigenoperators have been exhausted. All that will be left are the U terms and the zero–energy boson eigenoperators. The final result of such a process is given below:

$$\langle 0(\beta)|\,T\Big[A_1^{\alpha_1}(t_1)\;A_2^{\alpha_2}(t_2)\;\dots\;A_n^{\alpha_n}(t_n)\Big]\,|0(\beta)\rangle =$$

$$= \frac{\displaystyle\sum_{\text{w.c.}}\int d\{t'\}\;F_{\text{w.c.}}^{\{\alpha'\}\{\alpha\}}(G_a;\{t'\};\{t\})\;N_{\text{w.c.}}^{\{\alpha'\}}(\{t'\})}{\displaystyle\sum_{\text{v.w.c.}}\int d\{t''\}\;F_{\text{v.w.c.}}^{\{\alpha''\}}(G_a;\{t''\})\;N_{\text{v.w.c.}}^{\{\alpha''\}}(\{t''\})},$$

$$N_{\text{w.c.}}^{\{\alpha'\}}(\{t'\}) \equiv \langle 0,\beta|\,U(\infty-\tfrac{i\beta}{2},\infty)\,T\Big[n_i^{\alpha_i'}(t_i')\;\dots\;n_j^{\alpha_j'}(t_j')\Big]_{\text{w.c.}}\,U(-\infty,-\infty+\tfrac{i\beta}{2})\,|0,\beta\rangle$$

$$N_{\text{v.w.c.}}^{\{\alpha''\}}(\{t''\}) \equiv \langle 0,\beta|\,U(\infty-\tfrac{i\beta}{2},\infty)\,T\Big[n_k^{\alpha_k''}(t_k'')\;\dots\;n_m^{\alpha_m''}(t_m'')\Big]_{\text{v.w.c.}}\,U(-\infty,-\infty+\tfrac{i\beta}{2})\,|0,\beta\rangle \qquad (3.36)$$

where the "w.c." represents all possible sets of Wick contractions using eq. (3.13), and "v.w.c." represents all possible sets of Wick contractions which lead to vacuum diagrams. $F_{\text{w.c.}}^{\{\alpha'\}\{\alpha\}}(G_a;\{t'\};\{t\})$ includes all connected and disconnected Feynman diagrams formed from the non–zero–energy propagators G_a; a particular set of Wick contractions which form an $F_{\text{w.c.}}$ term will leave a particular set of zero–energy boson eigenoperators $\Big[n_i^{\alpha_i'}(t_i')\dots n_j^{\alpha_j'}(t_j')\Big]_{\text{w.c.}}$ in the T–product. Similarly, $F_{\text{v.w.c.}}^{\{\alpha''\}}(G_a;\{t''\})$ contains all vacuum diagrams and $\Big[n_k^{\alpha_k''}(t_k'')\dots n_m^{\alpha_m''}(t_m'')\Big]_{\text{v.w.c.}}$ are the zero–energy boson eigenoperators left behind by a particular set of vacuum Wick contractions. (Note that $n_i^\alpha(t)$, being a zero–energy eigenoperator, has no explicit time dependence; it is the ***ordering*** of these operators which depends on time.)

Now it is obvious why the U terms are dropped in the usual case: In a canonically quantized field theory there are no zero–energy boson eigenoperators, thus $[\ldots]_{w.c.}$ and $[\ldots]_{v.w.c}$ are replaced by 1 in eq. (3.36), causing the cancellation of the U terms. Also the vacuum diagrams $F_{v.w.c}$ cancel the vacuum diagrams in $F_{w.c.}$, leaving behind only the connected Feynman diagrams $F_{c.w.c.}$.

In a quantum algebra with zero–energy boson eigenoperators, the situation is much more complex, as shown by eq. (3.36). Firstly, the U terms, which contract only within themselves, yield extra vacuum diagrams. Secondly, these contractions will leave behind more zero–energy boson eigenoperators. Thirdly, the generalized Wick's theorem does not work for zero–energy boson eigenoperators. Fourthly, it is not clear that even the regular vacuum diagrams will cancel because all the "disconnected" diagrams are actually connected to the n_i^α–operators.

Fifthly, this whole method must be applied very carefully, because there *do* arise [illegible] in which contractions of ξ_a with the U terms at $\mathcal{R}e\, t = \pm\infty$ [illegible] damp out, in spite of the above argument. (See sect. 5.9).

3.3.3 THE NON–COMMUTATIVITY OF ZERO–ENERGY BOSON EIGENOPERATORS

In ref. [60], it was assumed that the zero–energy boson eigenoperators are mutually commuting, ie. $[n_i, n_j] = 0$. Then one may simultaneously diagonalize H_o and the set $\{n_i\}$ such that $|0,\beta\rangle$ may be written as a linear superposition of eigenstates of the set $\{n_i\}$: $|0,\beta\rangle = \sum_j |0,\beta;j\rangle / \sum_j$. In this case, the evaluation of eq. (3.36) is trivial: the zero–energy boson eigen–operators are replaced by their eigenvalues in each eigenstate $|0,\beta;j\rangle$.

Unfortunately, life is not so simple. In the case of the Anderson model, one finds $[n_i, n_j] \neq 0$, which makes things very complicated. These problems are not insurmountable. Reduction formulae for the T–products of n_i–operators can be found using a time–splitting technique, and one may also find a way to deal with the vacuum diagrams; although their structure is vastly more intricate than in ref. [60]. All this is presented later.

Before diving into the deep end, let us wet our feet by considering a greatly simplified model. In Chapter 4, we look at a non–interacting localized fermionic state with restricted occupancy. Then, in Chapter 5, we consider an exactly solvable perturbation of this system: a shift of energy. It isn't until Chapter 6 that the real Anderson model is presented.

CHAPTER 4

LOCALIZED FERMIONIC STATES WITH RESTRICTED OCCUPANCY: A QUANTUM ALGEBRA

4.1 INTRODUCTION

Many new concepts were introduced in Chapter 3: a generalized Wick's theorem, spontaneous vertices, a generalized Gell–Mann Low formula, vacuum diagrams which don't cancel, and zero–energy boson eigenoperators for which the reduction formula doesn't work. To familiarize the reader with the generalized Wick's theorem, spontaneous vertices, and how to reduce the zero–energy boson eigenoperator T–product, a simple model is presented. Exposition of the generalized Gell–Mann Low formula and non–cancelling vacuum diagrams is deferred to Chapter 5.

The model presented in the present chapter is essentially the Anderson model of a localized, N–fold degenerate, f–electron state with limited occupancy, in which the interaction with conduction electrons (hybridization) is not present. The analysis of this model provides a foundation on which to build the analysis of the real Anderson model in Chapter 6.

4.2 THE MODEL

4.2.1 PRELIMINARY CONSIDERATION: A NON–INTERACTING LOCALIZED FERMION STATE

The physical system described by the usual Anderson model is a lattice of rare earth or Actinide atoms in an alloy with other metallic atoms. The f–electron orbitals of the rare earth or actinide atoms are highly localized states which interact with the conduction electron gas to produce interesting effects, as described in Chapter 1.

For now, it is assumed that there is no lattice and there are no conduction electrons; all that remains is a single localized f–electron state of energy ϵ_f, described by the following Hamiltonian:

$$H_o = \epsilon_f \sum_m f_m^\dagger f_m \, . \tag{4.1}$$

Here m is the z–component of the total angular momentum, J, of the f–electron state; m = –J, –J+1, ... J . We shall loosely refer to J as the "spin" of the f–electron and N (≡2J+1) as the degeneracy. The f and $f^\dagger$ are the usual fermion creation and annihilation operators satisfying

$$\left\{ f_m \, , f_{m'}^\dagger \right\} = \delta_{mm'} \, . \tag{4.2}$$

They operate on a Fock space spanned by the states $|0\rangle$, $|m_1\rangle$, $|m_1 m_2\rangle$, $|m_1 m_2 m_3\rangle$, ... $|m_1 m_2 \ldots m_n\rangle$, where $m_i \neq m_j$ for all i and j in the ket.

4.2.2 RESTRICTED OCCUPANCY: A QUANTUM ALGEBRA

To be more realistic, one should include the effects of the Coulomb repulsion, U, between electrons of different m in the f–state. This will introduce a non–bilinear term into the Hamiltonian, as in eq. (1.15). Because the f–state is highly localized, the coulomb repulsion will be large, and this term cannot be treated as a perturbation. Thus one has the situation that was discussed in sect. 3.1.2.

As was proposed in sect. 3.1.2, one may construct all the eigenoperators and rewrite the problem in terms of these transformed operators. This was done in ref. [58] for the N = 2 case, and the general N case was illustrated in ref. [59]. Let us take a simpler approach by assuming U is infinite; i.e. multiple occupation of the f–state is forbidden. This restricts the Fock space to the sub–space spanned by $|0\rangle$ and $|m\rangle$. The unit operator on this space is given by:

$$\mathbf{1} \equiv |0\rangle\langle 0| + \sum_{m} |m\rangle\langle m| \, . \tag{4.3}$$

When f and $f^{\dagger}$ are restricted to this space, they become:

$$\xi_m \equiv f_m \, \mathbf{1} = |0\rangle\langle m| \, , \tag{4.4}$$

$$\xi_m^{\dagger} \equiv f_m^{\dagger} \, \mathbf{1} = |m\rangle\langle 0| \, . \tag{4.5}$$

One finds:

$$\left\{ \xi_m \, , \, \xi_{m'}^{\dagger} \right\} = \delta_{mm'} |0\rangle\langle 0| + |m'\rangle\langle m| \equiv M_{mm'} \neq \delta_{mm'} \, \mathbf{1} \, , \tag{4.6}$$

and therefore the f–electron operators no longer obey standard fermion anti-commutation rules. But they are still eigenoperators with eigenenergy ϵ_f because,

$$H_o \, \mathbf{1} = \epsilon_f \sum_m f_m^{\dagger} \, f_m \, \mathbf{1} = \epsilon_f \sum_m |m\rangle\langle m| = \epsilon_f \sum_m \xi_m^{\dagger} \, \xi_m \, , \tag{4.7}$$

and

$$\left[H_o \, , \, \xi_m \right] = \epsilon_f \sum_{m'} \left[\xi_{m'}^{\dagger} \xi_{m'} \, , \, \xi_m \right] = - \epsilon_f \sum_{m'} \left\{ \xi_{m'}^{\dagger} \, , \, \xi_m \right\} \xi_{m'} =$$

$$= - \epsilon_f \sum_{m'} M_{mm'} \, \xi_{m'} = - \epsilon_f \, \xi_m \tag{4.8}$$

(Here one notes from eqs. (4.6) and (4.4) that $M_{mm'} \, \xi_{m'} = \delta_{mm'} \, \xi_{m'}$.) Thus, one has eigenoperators which form a quantum algebra, as discussed in chapter 3.

Note that the U term is not explicitly present in the Hamiltonian of eq. (4.7). The effects of infinite–U are manifest by the algebra of the ξ_m and $\xi_m^{\dagger}$ operators. This is an example of a non–bilinear Hamiltonian being made bilinear, at the expense of complicating the algebra of the operators. This infinite–U bilinearization was done the "quick and easy" way, rather than using the method of ref. [58], in which all the eigenoperators at finite U were constructed.

4.2.3 THE NON-CANONICAL QUANTIZATION

Note that ξ and M satisfy the conditions of eq. (B.9) appendix B, for consistently breaking the canonical quantization condition. Thus the system may be described by the following Lagrangian:

$$L = \sum_m \xi_m^\dagger(t) \left[i \frac{\partial}{\partial t} - \varepsilon_f \right] \xi_m(t) \ , \tag{4.9}$$

and the canonical momentum of $\xi_m(t)$ is given by:

$$\Pi_{\xi_m}(t) = \frac{\delta L}{\delta \dot{\xi}_m(t)} = i \ \xi_m^\dagger(t) \ . \tag{4.10}$$

Note that the Euler Lagrange equations of L, namely

$$\begin{gathered} \left[i \frac{\partial}{\partial t} - \varepsilon_f \right] \xi_m(t) = 0 \ , \\ \left[- i \frac{\partial}{\partial t} - \varepsilon_f \right] \xi_m^\dagger(t) = 0 \ , \end{gathered} \tag{4.11}$$

agree with the Heisenberg equation, $\frac{d}{dt} \xi_m(t) = i\left[H_o , \xi_m(t) \right]$, as shown by eq. (4.8).

But one doesn't have the usual canonical quantization conditions. That is, one has

$$\left\{ \xi_m(t) , \Pi_{m'}(t) \right\} = i \ M_{mm'}(t) \tag{4.12}$$

rather than $\{ \xi_m(t) , \Pi_{m'}(t) \} = i\delta_{mm'}$. In fact an operator Π_m which would satisfy this latter condition does not exist in the Fock space.

One therefore has the situation discussed in sect. 3.1.2: the eigenfields violate the canonical quantization condition.

4.3 APPLICATION OF TFD: THE ξ-PROPAGATOR AND SECTOR STRUCTURE

4.3.1 CONSTRUCTION OF THE VACUUM

As in eq. (2.4), one may construct the thermal vacuum of H_o, yielding the following simple form:

$$|0,\beta\rangle = \frac{1}{\sqrt{Z_{\varepsilon_f}}} \left[\, |0\ \tilde{0}\rangle + e^{-\beta(\varepsilon_f-\mu)/2} \sum_m |m\ \tilde{m}\rangle \right] , \tag{4.13a}$$

where

$$Z_{\varepsilon_f} \equiv 1 + N\, e^{-\beta(\varepsilon_f-\mu)} \tag{4.13b}$$

4.3.2 THE ξ-PROPAGATOR

We define the propagator in this vacuum to be

$$\mathcal{S}^{\alpha\gamma}_{mm'}(t,t') \equiv \langle 0,\beta|\ T\ \xi^{\alpha}_{m}(t)\ \xi^{\dagger\gamma}_{m'}(t')\ |0,\beta\rangle . \tag{4.14}$$

Using the generalized Wick's theorem of eq. (3.13), one finds:

$$\mathcal{S}^{\alpha\gamma}_{mm'}(t,t') = S^{\alpha\gamma}_{\varepsilon_f}(t-t')\ \langle 0,\beta|\ T\ M^{\gamma}_{mm'}(t')\ |0,\beta\rangle , \tag{4.15}$$

where $M_{mm'}$ is given by eq. (4.6), and

$$S^{\alpha\gamma}_{\varepsilon_f}(t-t') = i\int \frac{d\omega}{2\pi}\, e^{-i\omega(t-t')}\ S^{\alpha\gamma}_{\varepsilon_f}(\omega;\mu) , \tag{4.16a}$$

$$S^{\alpha\gamma}_{\varepsilon_f}(\omega;\mu) = \left[\ U_F(\omega-\mu)\ \bar{S}_{\varepsilon_f}(\omega)\ U^{\dagger}_F(\omega-\mu)\ \right]^{\alpha\gamma} , \tag{4.16b}$$

$$\bar{S}_{\varepsilon_f}(\omega) \equiv \frac{1}{\omega - \varepsilon_f + i\delta\tau} , \tag{4.16c}$$

where $U_F(\omega)$ is defined in eq. (3.16) with $\rho = -1$.

Using eqs. (4.6) and (4.13), one finds

$$\langle 0,\beta|M^{\gamma}_{mm'}|0,\beta\rangle = \delta_{mm'} \left[\ \langle P_o\rangle + \frac{1}{N}\langle P_1\rangle\ \right] , \tag{4.17a}$$

where

$$\langle P_o \rangle \equiv \langle 0,\beta | P_o | 0,\beta \rangle \ , \tag{4.17b}$$

$$\langle P_1 \rangle \equiv \langle 0,\beta | P_1 | 0,\beta \rangle \ , \tag{4.17c}$$

and

$$P_o \equiv |0\rangle\langle 0| \ , \tag{4.17d}$$

$$P_1 \equiv \sum_m |m\rangle\langle m| \ . \tag{4.17e}$$

Here P_o is the zero–particle projection operator and P_1 is the one–particle projection operator. Upon using eq. (4.13), one finds:

$$\langle P_o \rangle \equiv \frac{1}{1 + N\, e^{-\beta(\varepsilon_f - \mu)}} \ , \tag{4.18a}$$

$$\langle P_1 \rangle \equiv \frac{N\, e^{-\beta(\varepsilon_f - \mu)}}{1 + N\, e^{-\beta(\varepsilon_f - \mu)}} \ . \tag{4.18b}$$

In summary,

$$\boxed{\mathcal{S}^{\alpha\gamma}_{mm'}(t,t') = \delta_{mm'}\, S^{\alpha\gamma}_{\varepsilon_f}(t-t') \left[\ \langle P_o \rangle + \frac{1}{N} \langle P_1 \rangle \ \right]} \ . \tag{4.19}$$

This illustrates the concepts presented in sect. 3.2. The generalized Wick's theorem was used to reduce the T–product of ξ–operators to a T–product of zero–energy boson eigenoperators; in this case only one zero–energy boson eigenoperator $M^{\alpha}_{mm'}$ was left behind. Then this zero energy boson T–product was evaluated directly from the structure of $|0,\beta\rangle$ without having to devise one of the special techniques alluded to at the end of sect. 3.2.4.

4.3.3 AN ALTERNATIVE: THE $\xi^{\dagger}$ PROPAGATOR

As discussed in sect. 3.2.5, there is an ambiguity in the reduction, depending on which operator is chosen to be leftmost in the T–product. Eq. (4.19) was derived starting with ξ^{α} as the leftmost operator. Alternatively, one may write

$$\mathcal{G}^{\alpha\gamma}_{mm'}(t,t') = - \langle 0,\beta| T\, \xi^{\dagger\gamma}_{m'}(t')\, \xi^{\alpha}_{m}(t)\, |0,\beta\rangle \ , \qquad (4.20)$$

and use the generalized Wick's theorem, eq. (3.13), to obtain:

$$\mathcal{G}^{\alpha\gamma}_{mm'}(t,t') = - S^{\gamma\alpha}_{\tilde{\epsilon}_f}(t'-t)\, \delta_{mm'} \left[\langle P_0\rangle + \frac{1}{N} \langle P_1\rangle \right] , \qquad (4.21)$$

where

$$S^{\gamma\alpha}_{\tilde{\epsilon}_f}(t'-t) \equiv i\int \frac{d\omega}{2\pi}\, e^{-i\omega(t'-t)} \left[U^{\dagger}_{F}(\omega+\mu)\, \frac{1}{\omega+\tilde{\epsilon}_f+i\delta\tau}\, U_{F}(\omega+\mu) \right]^{\gamma\alpha} \qquad (4.22)$$

As in eq. (3.27),

$$S^{\alpha\gamma}_{\tilde{\epsilon}_f}(t-t') = - S^{\gamma\alpha}_{\tilde{\epsilon}_f}(t'-t) \ , \qquad (4.23)$$

and the two methods of doing the reduction are equivalent.

As a convention, we will always start the reduction with the ξ-operator rather than the $\xi^{\dagger}$-operator.

4.3.4 INTERPRETATION OF THE SECTOR STRUCTURE

Note that the ξ propagator has a two-sector structure. The $\langle P_0\rangle$ sector contains the 0-particle contribution of the zero-energy boson T-product, and the $\langle P_1\rangle$ sector contains the 1-particle contribution of the zero-energy boson T-product. These are ***not*** the 0-particle and 1-particle contributions of the propagator itself. To find the 0- and 1-particle contributions of the propagator, one must choose a particular time-ordering (ie. $\xi^{\dagger}_m\, \xi_m = |m\rangle\langle m|$ projects out the 1-particle subspace and whereas $\xi_m\, \xi^{\dagger}_m = |0\rangle\langle 0|$ projects out the 0-particle subspace.)

Let us calculate the 0-particle and 1-particle contributions of the propagator. From eqs. (4.14) and (4.4)-(4.5), one finds:

$$\langle P_0\rangle = \lim_{\delta\to 0^+} \mathcal{G}^{11}_{mm}(t\, ,\, t-\delta) \ , \qquad (4.24a)$$

$$\langle P_1\rangle = - N \lim_{\delta\to 0^+} \mathcal{G}^{11}_{mm}(t, t+\delta) \qquad (4.24b)$$

Now let us check this for consistency by using eq. (4.19).

$$\langle P_o \rangle = \lim_{\delta \to 0^+} S^{11}_{\varepsilon_f}(\delta) \left[\langle P_o \rangle + \frac{1}{N} \langle P_1 \rangle \right] , \tag{4.25a}$$

$$\langle P_1 \rangle = - N \lim_{\delta \to 0^+} S^{11}_{\varepsilon_f}(-\delta) \left[\langle P_o \rangle + \frac{1}{N} \langle P_1 \rangle \right] . \tag{4.25b}$$

Using eqs. (4.16) and (3.16):

$$S^{11}_{\varepsilon_f}(\pm\delta) = i \int \frac{d\omega}{2\pi} e^{\mp i\omega\delta} \left[\frac{e^{\beta(\omega-\mu)}}{e^{\beta(\omega-\mu)}+1} \frac{1}{\omega-\varepsilon_f+i\delta} + \frac{1}{e^{\beta(\omega-\mu)}+1} \frac{1}{\omega-\varepsilon_f-i\delta} \right]$$

$$= \begin{cases} \dfrac{e^{\beta(\varepsilon_f-\mu)}}{e^{\beta(\varepsilon_f-\mu)}+1} , & \text{for } + \delta \\ -\dfrac{1}{e^{\beta(\varepsilon_f-\mu)}+1} , & \text{for } - \delta \end{cases} \tag{4.26}$$

Therefore:

$$\langle P_o \rangle = \frac{e^{\beta(\varepsilon_f-\mu)}}{e^{\beta(\varepsilon_f-\mu)} + 1} \left[\langle P_o \rangle + \frac{1}{N} \langle P_1 \rangle \right] , \tag{4.27a}$$

$$\langle P_1 \rangle = \frac{-N}{e^{\beta(\varepsilon_f-\mu)} + 1} \left[\langle P_o \rangle + \frac{1}{N} \langle P_1 \rangle \right] . \tag{4.27b}$$

This is consistent with $\langle P_o \rangle$ and $\langle P_1 \rangle$ given by eqs. (4.18).

By use of the techniques of chapter 3, we have obtained the Feynman propagator for a localized f–state in the infinite–U Anderson model without hybridization. Preserving the Feynman formalism is not without cost; we have a propagator in which the occupied and unoccupied states are mixed together. This is a major difference between our method and the other methods: virtually all other methods keep the propagators of the occupied and unoccupied states distinct. Further serious complications arise when one considers multi–point functions. These will be discussed in sect. 4.4.

4.4 THE MULTI-POINT ξ-FUNCTIONS

4.4.1 SPONTANEOUS VERTICES AND ZERO-ENERGY BOSONS

As found in eq. (4.19), the 2-point function has a form which differs from the 2-point functions of the usual canonical quantum field theory, namely, there is a sector structure. What about the multi-point functions?

Now it becomes necessary to use the full algebra, which is obtained from eq. (4.6) as:

$$\left\{ \xi_m , \xi^\dagger_{m'} \right\} = M_{mm'} , \tag{4.28a}$$

$$\left[\xi_{m''} , M_{mm'} \right] = -\delta_{mm''} \xi_{m'} + \delta_{m''m'} \xi_m \tag{4.28b}$$

Suppose one uses this in the generalized Wick's theorem of eq. (3.13). A typical contraction of ξ with $\xi^\dagger$ leaves behind an M in the T product, as illustrated below:

$$\langle 0,\beta | T \ldots \xi^{\alpha_2}_{m_2}(t_2) \underbrace{\xi^{\alpha_1}_{m_1}(t_1) \, \xi^{\dagger\gamma_1}_{m'_1}(t'_1)}_{} \xi^{\dagger\gamma_2}_{m'_2}(t'_2) \ldots |0,\beta\rangle =$$

$$= S^{\alpha_1\gamma_1}_{\epsilon_f}(t_1-t'_1) \langle 0,\beta | T \ldots \xi^{\alpha_2}_{m_2}(t_2) M^{\gamma_1}_{m_1m'_1}(t'_1) \xi^{\dagger\gamma_2}_{m'_2}(t'_2) \ldots |0,\beta\rangle \tag{4.29}$$

Now one has the choice of leaving the M until all the rest of the ξ's have been used up, or contracting the M with another ξ. The first choice leaves behind a T-product of M's, as follows:

$$\langle 0,\beta | T \ldots \underbrace{\xi^{\alpha_2}_{m_2}(t_2) \, M^{\gamma_1}_{m_1m'_1}(t'_1) \, \xi^{\dagger\gamma_2}_{m'_2}(t'_2)}_{} \ldots |0,\beta\rangle =$$

$$= S^{\alpha_2\gamma_2}_{\epsilon_f}(t_2-t'_2) \langle 0,\beta | T \ldots M^{\gamma_1}_{m_1m'_1}(t'_1) M^{\gamma_2}_{m_2m'_2}(t'_2) \ldots |0,\beta\rangle , \tag{4.30}$$

whereas the second choice introduces a 3-point vertex as follows

$$\langle 0,\beta|\mathrm{T}\ \ldots\ \underbrace{\xi^{\alpha_2}_{m_2}(t_2)\ M^{\gamma_1}_{m_1 m_1'}(t_1')}\ \xi^{\dagger\gamma_2}_{m_2'}(t_2')\ \ldots\ |0,\beta\rangle =$$

$$= S^{\alpha_2\gamma_1}_{\varepsilon_f}(t_2-t_1')\ \varepsilon^{\gamma_1}\left[-\delta_{m_1 m_1'}\,\delta_{m_2\ell}+\delta_{m_2 m_1'}\,\delta_{m_1\ell}\right]\times$$

$$\times\ \langle 0,\beta|\mathrm{T}\ \ldots\ \xi^{\gamma_1}_{\ell}(t_1')\ \xi^{\dagger\gamma_2}_{m_2'}(t_2')\ \ldots\ |0,\beta\rangle\ , \qquad (4.31)$$

where ε^{γ} is defined by:

$$\left.\begin{aligned}\varepsilon^{(1)} &= 1\\ \varepsilon^{(2)} &= -1\end{aligned}\right\}. \qquad (4.32)$$

One is therefore faced with two major complications. The first is how to reduce the T-product of M's; the second is that a 3-point vertex arises spontaneously, ***without any interaction terms***.

4.4.2 THE 4-POINT ξ-FUNCTION: AN INCOMPLETE REDUCTION

Let us illustrate the 4-point function. Using the generalized Wick's theorem (and keeping in mind our convention of starting the reduction with the ξ's rather than $\xi^{\dagger}$'s), one obtains:

$$\Gamma^{\alpha_1\alpha_2\gamma_1\gamma_2}_{4\,m_1 m_2 m_1' m_2'}(t_1,t_2,t_1',t_2') \equiv \langle 0,\beta|\mathrm{T}\ \xi^{\alpha_1}_{m_1}(t_1)\ \xi^{\dagger\gamma_1}_{m_1'}(t_1')\ \xi^{\alpha_2}_{m_2}(t_2)\ \xi^{\dagger\gamma_2}_{m_2'}(t_2')\ |0,\beta\rangle$$

$$= S^{\alpha_1\gamma_1}_{\varepsilon_f}(t_1-t_1')\ S^{\alpha_2\gamma_2}_{\varepsilon_f}(t_2-t_2')\ \langle 0,\beta|\mathrm{T}\ M^{\gamma_1}_{m_1 m_1'}(t_1')\ M^{\gamma_2}_{m_2 m_2'}(t_2')\ |0,\beta\rangle\ +$$

$$-\ S^{\alpha_1\gamma_2}_{\varepsilon_f}(t_1-t_2')\ S^{\alpha_2\gamma_1}_{\varepsilon_f}(t_2-t_1')\ \langle 0,\beta|\mathrm{T}\ M^{\gamma_1}_{m_2 m_1'}(t_1')\ M^{\gamma_2}_{m_1 m_2'}(t_2')\ |0,\beta\rangle\ +$$

$$+\ S^{\alpha_1\gamma_1}_{\varepsilon_f}(t_1-t_1')\ S^{\alpha_2\gamma_1}_{\varepsilon_f}(t_2-t_1')\ \varepsilon^{\gamma_1}\ S^{\gamma_1\gamma_2}_{\varepsilon_f}(t_1'-t_2')\ \times$$

$$\times\left[-\delta_{m_1 m_1'}\,\delta_{m_2\ell}+\delta_{m_2 m_1'}\,\delta_{m_1\ell}\right]\langle 0,\beta|\mathrm{T}\ M^{\gamma_2}_{\ell m_2'}(t_2')\ |0,\beta\rangle\ +$$

$$-\ S^{\alpha_1\gamma_2}_{\varepsilon_f}(t_1-t_2')\ S^{\alpha_2\gamma_2}_{\varepsilon_f}(t_2-t_2')\ \varepsilon^{\gamma_2}\ S^{\gamma_2\gamma_1}_{\varepsilon_f}(t_2'-t_1')\ \times$$

$$\times\left[-\delta_{m_1 m_2'}\,\delta_{m_2\ell}+\delta_{m_2 m_2'}\,\delta_{m_1\ell}\right]\langle 0,\beta|\mathrm{T}\ M^{\gamma_1}_{\ell m_1'}(t_1')\ |0,\beta\rangle\ . \qquad (4.33)$$

The expectation value of a single M is given simply by eq. (4.17a). But the expectation value of the product of two or more M's is a problem because the M's do not, in general, commute:

$$[\, M_{mm'} \,,\, M_{\bar{m}\bar{m}'} \,] = \delta_{m\bar{m}'} |m'\rangle\langle\bar{m}| - \delta_{\bar{m}m'} |\bar{m}'\rangle\langle m| \tag{4.34}$$

Although the M's do not depend on time, their ***ordering*** does, and thus any attempt to directly evaluate the T–product will result in a θ–function dependent expression. In keeping with the spirit of the Feynman formalism, we wish to express the T–product of M–operators in terms of Feynman propagators. But M is a zero–energy bosonic operator and thus our generalized Wick's theorem will not work. Nevertheless, reduction formulae may be found using a special time–splitting technique, as illustrated in the next section.

4.5 REDUCTION OF THE ZERO-ENERGY BOSON T-PRODUCT WITHOUT THE SU(N) GROUP: TIME-SPLITTING

4.5.1 A MISTAKE IN PREVIOUS WORK USING THE SU(N) GROUP

A time–splitting technique for reducing the T–product of M–operators was first introduced in ref. [58] for the spin $\frac{1}{2}$ case. The quantum algebra was re–expressed in terms of the generators of the SU(2) group so that one had **1**'s and σ_j matrices at the vertices, rather than spin delta functions.

In ref. [59], this method was incorrectly extended to the spin J case. The authors re–expressed the quantum algebra in terms of the generators of the SU(N) group so that one had **1**'s and λ_j matrices at the vertices, they then claimed that the Feynman diagram expansion is virtually the same as for the spin $\frac{1}{2}$ case. Their mistake was in claiming $\mathrm{Tr}(\lambda_i\lambda_j\lambda_k) = -\mathrm{Tr}(\lambda_j\lambda_i\lambda_k)$. This is ***not*** true in general, because the SU(N) algebra has symmetric structure factors when $N > 2$.

When one uses the SU(N) algebra correctly, one finds the general spin Feynman diagram expansion considerably more complicated than for the N = 2 case. This will be presented in sect. 4.8. For simplicity let us first consider the Feynman expansion without the SU(N) group; in this section we will leave the algebra in the delta function form of eqs. (4.28).

4.5.2 THE TIME–SPLITTING TECHNIQUE

Define the operator $X_{m'm}$ as follows:

$$\xi^{\dagger}_{m'}\ \xi_m \equiv |m'\rangle\langle m| \equiv X_{m'm} \quad . \tag{4.35}$$

Using this with eq. (4.17d), one may rewrite eq. (4.6) as:

$$\left\{ \xi_m\ ,\ \xi^{\dagger}_{m'} \right\} \equiv M_{mm'} = \delta_{mm'}\ P_o + X_{m'm} \quad . \tag{4.36}$$

Noting that $X_{m'm}$ acts only in the P_1 subspace and that $P_oP_1 = 0$, a T–product of M–operators acquires the following form:

$$\begin{aligned} \langle 0,\beta|\,T\ M^{\gamma_i}_{m_i m_i'}(t_i')\ M^{\gamma_j}_{m_j m_j'}(t_j') \ldots M^{\gamma_\ell}_{m_\ell m_\ell'}(t_\ell')\ |0,\beta\rangle &= \\ = \delta_{m_i m_i'}\ \delta_{m_j m_j'} \cdots \delta_{m_\ell m_\ell'}\ \langle P_o\rangle &+ \\ + \langle 0,\beta|\,T\ X^{\gamma_i}_{m_i' m_i}(t_i')\ X^{\gamma_j}_{m_j' m_j}(t_j') \ldots X^{\gamma_\ell}_{m_\ell' m_\ell}(t_\ell')\ |0,\beta\rangle & \quad . \end{aligned} \tag{4.37}$$

When eq. (4.35) is written as a thermal doublet, it becomes:

$$X^{\gamma}_{m'm} = P^{\gamma}\ \xi^{\dagger\gamma}_{m'}\ \xi^{\gamma}_{m} \quad , \tag{4.38}$$

where P^{γ} is the thermal ordering operator: $P^{(1)} = 1$ and $P^{(2)}$ reverses the order of the operators. (This follows directly from the definition of the thermal doublet in eq. (2.20).) When $X^{\gamma}_{m'm}$ appears inside a T product, as in eq. (4.37), it may be written as:

$$X^{\gamma}_{m'm}(t) = T\ \varepsilon^{\gamma}\ \xi^{\dagger\gamma}_{m'}(t+\varepsilon^{\gamma}\delta)\ \xi^{\gamma}_{m}(t) \quad , \tag{4.39}$$

where δ is an infinitesimal and ε^{γ} is defined in eq. (4.32). The time t has been "split" into two times: t and $t + \varepsilon^{\gamma}\delta$. This is the essence of the time–

splitting technique.

4.5.3 DERIVATION OF REDUCTION FORMULAE FOR T-PRODUCTS OF X-OPERATORS

It is useful to start with a finite time-splitting, and then take the limit as the splitting becomes infinitesimal. We therefore introduce the following operator:

$$X^{\gamma\alpha}_{m'm}(t',t) \equiv T\, \epsilon^{\alpha}\, \xi^{\dagger\gamma}_{m'}(t')\, \xi^{\alpha}_{m}(t)\ , \tag{4.40a}$$

where

$$X^{\gamma\gamma}_{m'm}(t+\epsilon^{\gamma}\delta,t) = X^{\gamma}_{m'm}(t) \tag{4.40b}$$

Noting that:

$$\left[\, \xi_{m''}\ ,\ X_{m'm}\, \right] = \delta_{m''m'}\ \xi_{m}\ , \tag{4.41}$$

one may use the generalized Wick's theorem of eq. (3.13) to obtain

$$\langle 0,\beta|\ T\ \xi^{\alpha}_{m}(t)\ X^{\gamma_j}_{m'_j m_j}(t'_j)\ \ldots\ X^{\gamma_1}_{m'_1 m_1}(t'_1)\ \xi^{\dagger\gamma}_{m'}(t')\ |0,\beta\rangle =$$

$$= S^{\alpha\gamma}_{\epsilon_f}(t-t')\ \langle 0,\beta|\ T\ X^{\gamma_j}_{m'_j m_j}(t'_j)\ \ldots\ X^{\gamma_1}_{m'_1 m_1}(t'_1)\ M^{\gamma}_{mm'}(t')\ |0,\beta\rangle\ +$$

$$+ \sum_k S^{\alpha\gamma_k}_{\epsilon_f}(t-t'_k)\ \epsilon^{\gamma_k}\ \delta_{mm'_k}\ \cdot$$

$$\cdot\ \langle 0,\beta|\ T\ X^{\gamma_j}_{m'_j m_j}(t'_j)\ \ldots\ \xi^{\gamma_k}_{m_k}(t'_k)\ \ldots\ X^{\gamma_1}_{m'_1 m_1}(t'_1)\ \xi^{\dagger\gamma}_{m'}(t')\ |0,\beta\rangle \tag{4.42}$$

In the first term, note that only the component of M in the P_1 subspace contributes (assuming there is a non-zero number of X-operators in the T-product). In the second term, we will use eq. (4.40a); let us do this on the left-hand side as well. Eq. (4.42) becomes:

$$\boxed{\begin{aligned}&\langle 0,\beta|\ T\ X^{\gamma\alpha}_{m'm}(t',t)\ X^{\gamma_j}_{m_j'm_j}(t_j')\ \ldots\ X^{\gamma_\ell}_{m_\ell'm_\ell}(t_\ell')\ |0,\beta\rangle =\\ &= -\varepsilon^{\alpha}\ S^{\alpha\gamma}_{\varepsilon_f}(t-t')\ \langle 0,\beta|\ T\ X^{\gamma}_{m'm}(t')\ X^{\gamma_j}_{m_j'm_j}(t_j')\ \ldots\ X^{\gamma_\ell}_{m_\ell'm_\ell}(t_\ell')\ |0,\beta\rangle\ +\\ &\qquad + \sum_k \varepsilon^{\alpha}\ S^{\alpha\gamma_k}_{\varepsilon_f}(t-t_k')\ \delta_{mm_k'}\ \times\\ &\qquad \times\ \langle 0,\beta|\ T\ X^{\gamma\gamma_k}_{m'm_k}(t',t_k')\ X^{\gamma_j}_{m_j'm_j}(t_j')\ \overset{\overset{k}{\smile}}{\ldots}\ X^{\gamma_\ell}_{m_\ell'm_\ell}(t_\ell')\ |0,\beta\rangle\quad ,\end{aligned}}$$

(4.43)

where the $\overset{k}{\smile}$ means that the $X^{\gamma_k}_{m_k'm_k}(t_k')$ term is missing.

If one now lets $\alpha=\gamma\equiv\gamma_i$, $t'=t+\varepsilon^{\gamma}\delta\equiv t_i'$, $m'\equiv m_i'$, $m\equiv m_i$, and uses eq. (4.40b), one obtains:

$$\begin{aligned}&\langle 0,\beta|T\ X^{\gamma_i}_{m_i'm_i}(t_i')\ X^{\gamma_j}_{m_j'm_j}(t_j')\ \ldots\ X^{\gamma_\ell}_{m_\ell'm_\ell}(t_\ell')\ |0,\beta\rangle =\\ &= -\varepsilon^{\gamma_i}\ S^{\gamma_i\gamma_i}_{\varepsilon_f}(-\varepsilon^{\gamma_i}\delta)\ \langle 0,\beta|T\ X^{\gamma_i}_{m_i'm_i}(t_i')\ X^{\gamma_j}_{m_j'm_j}(t_j')\ \ldots\ X^{\gamma_\ell}_{m_\ell'm_\ell}(t_\ell')\ |0,\beta\rangle\ +\\ &\qquad \sum_k \varepsilon^{\gamma_i}\ S^{\gamma_i\gamma_k}_{\varepsilon_f}(t_i'-t_k')\ \delta_{m_im_k'}\ \times\\ &\qquad \times\ \langle 0,\beta|T\ X^{\gamma_i\gamma_k}_{m_i'm_k}(t_i',t_k')\ X^{\gamma_j}_{m_j'm_j}(t_j')\ \overset{\overset{k}{\smile}}{\ldots}\ X^{\gamma_\ell}_{m_\ell'm_\ell}(t_\ell')\ |0,\beta\rangle\quad .\end{aligned}\tag{4.44}$$

Upon using eqs. (4.16) for the $S^{\gamma\gamma}_{\varepsilon_f}$ propagator, along with eq. (3.16) for the U_F matrix, one finds:

$$-\varepsilon^{\gamma}\ S^{\gamma\gamma}_{\varepsilon_f}(-\varepsilon^{\gamma}\delta) = f_F(\varepsilon_f-\mu)\ ,\tag{4.45}$$

where $f_F(\omega)$ is the Fermi distribution function ($f_F(\omega) = 1/[e^{\beta\omega}+1]$). cf. eq. (4.26). Therefore, eq. (4.44) becomes:

$$\boxed{\begin{aligned} &\langle 0,\beta|\mathrm{T}\; X^{\gamma_i}_{m'_i m_i}(t'_i)\; X^{\gamma_j}_{m'_j m_j}(t'_j)\;\ldots\; X^{\gamma_\ell}_{m'_\ell m_\ell}(t'_\ell)\;|0,\beta\rangle = \\ &= \frac{1}{f_p(-\epsilon_f+\mu)}\sum_k \epsilon^{\gamma_i}\, S^{\gamma_i\gamma_k}_{\epsilon_f}(t'_i-t'_k)\;\delta_{m_i m'_k}\;\cdot \\ &\cdot\;\langle 0,\beta|\mathrm{T}\; X^{\gamma_i\gamma_k}_{m'_i m_k}(t'_i,t'_k)\; X^{\gamma_j}_{m'_j m_j}(t'_j)\;\overset{k}{\ldots}\; X^{\gamma_\ell}_{m'_\ell m_\ell}(t'_\ell)\;|0,\beta\rangle \end{aligned}}$$

(4.46)

Eqs. (4.43) and (4.46) are the reduction formulae; they may be used to reduce a T–product of two or more X^{γ}–operators to a sum of Feynman propagator products, multiplied ultimately by the expectation value of an $X^{\gamma\gamma'}$. This final expectation value is evaluated directly from the definition eq. (4.40).

$$\begin{aligned} \langle 0,\beta|\mathrm{T}\; X^{\gamma\alpha}_{m'm}(t',t)\;|0,\beta\rangle &= \epsilon^{\alpha}\;\langle 0,\beta|\mathrm{T}\;\xi^{\dagger\gamma}_{m'}(t')\;\xi^{\alpha}_{m}(t)\;|0,\beta\rangle = \\ &= -\,\epsilon^{\alpha}\;\mathcal{S}^{\alpha\gamma}_{mm'}(t,t') \end{aligned} \tag{4.47}$$

Using the $\mathcal{S}$ propagator given by eq. (4.19), one finds

$$\langle 0,\beta|\mathrm{T}\; X^{\gamma\alpha}_{m'm}(t',t)\;|0,\beta\rangle = -\,\delta_{mm'}\;\epsilon^{\alpha}\;S^{\alpha\gamma}_{\epsilon_f}(t-t')\left[\langle P_0\rangle + \frac{1}{N}\langle P_1\rangle\right]$$

(4.48)

As mentioned before, the X^{γ}–operators act only in the 1–particle subspace. If one wishes to keep the interpretation of sect. 4.3.4, namely that the sector structure arises from the 0– and 1–particle contribution of the zero–energy boson T–product, then eq. (4.48) should be rewritten in terms of $\langle P_1\rangle$ only. This is accomplished through the following relations, (see eqs. (4.18))

$$\langle P_0\rangle = \left[\langle P_0\rangle + \frac{1}{N}\langle P_1\rangle\right] f_p(-(\epsilon_f-\mu)) \tag{4.49a}$$

$$\langle P_1\rangle = N\left[\langle P_0\rangle + \frac{1}{N}\langle P_1\rangle\right] f_p(\epsilon_f-\mu) \tag{4.49b}$$

Using eq. (4.49b) in eq. (4.48), one obtains

$$\boxed{\langle 0,\beta|\,T\; X^{\gamma\alpha}_{m'm}(t',t)\,|0,\beta\rangle = -\,\delta_{mm'}\,\varepsilon^{\alpha}\; S^{\alpha\gamma}_{\varepsilon_f}(t-t')\;\frac{\langle P_1\rangle}{N\, f_F(\varepsilon_f-\mu)}\;.} \tag{4.50}$$

A complete reduction of the T–product of 2 or more X–operators may be obtained using eqs. (4.43), (4.46) and (4.50).

4.5.4 A SHORTCOMING OF THE X–OPERATOR REDUCTION: MULTI–POINT VERTICES

Although the above reduction is complete, it is diagrammatically inconvenient. Look at eqs. (4.43) and (4.46). Upon studying these equations, the following properties of the reduction are revealed:

1) The reduction is composed of closed loops of S_{ε_f} propagators.

2) The second term in eq. (4.43) will insert an extra S_{ε_f} propagator on a loop under construction, which makes the loop bigger.

3) The first term in eq. (4.43) will close a loop under construction, leaving the starting point of the initial reduction $(X^{\gamma_i}(t_i'))$, as the starting point of any further reduction. A further reduction will start a new loop.

4) A loop under construction is always started and finished at $X^{\gamma_i}(t_i')$. That is, ***all*** loops are connected together at a single multi–point vertex: $X^{\gamma_i}(t_i')$.

The picture that emerges is illustrated in FIG. 4.1. One has a product of closed S_{ε_f} loops of varying size all connected together at a single multi–point vertex. Not only is this hard to draw but it is virtually impossible to calculate.

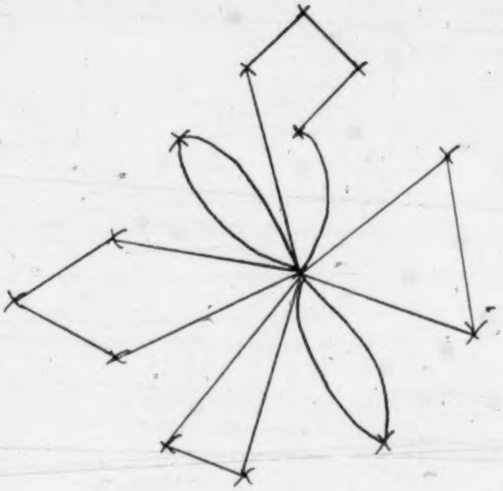

FIG. 4.1

Multi–Point Vertices in the X–Operator Reduction

The reduction formulae for T–products of X–operators, as given by eqs. (4.43) and (4.46), yield multi–point vertices as illustrated. This particular example shows a diagram from the 14–point X–function. Each time point is drawn as a cross. Each S_{ε_f} propagator is drawn as a line. Note the 12–point vertex which appears at time t_i'.

4.5.5 AN ALTERNATE SET OF REDUCTION FORMULAE FOR T–PRODUCTS OF X–OPERATORS

As previously noted (sect. 3.2.5 and 4.3.3), there is an ambiguity in the generalized Wick's theorem, which depends on which operator is chosen to be leftmost in the T–product. This ambiguity is manifestly illustrated by FIG. 4.1: it is the leftmost X–operator which forms the multi–point vertex.

In fact, is is not necessary that the X–operator reduction have the form of FIG. 4.1 at all. This construction resulted from choosing $X^{\gamma}_{m'm}(t')$ in the first term of eq. (4.43) to be the leftmost operator. If one chooses a different operator to be leftmost in the first term of eq. (4.43), then one has the possibility of producing many multi–point vertices, rather than just one. This would apparently complicate matters even further!

Fortunately, a careful choice of the reduction can eliminate all multi–point vertices greater than 4–point, leaving a linear chain of connected S_{ε_f} loops.

In the interest of deriving this kind of reduction, we first derive a pair of reduction formulae analogous to eqs. (4.43) and (4.46), using the $\xi^\dagger$ propagator of sect. 4.3.3.

Noting that

$$\left[\xi^\dagger_{m'}\ ,\ X_{m'm}\right] = -\,\delta_{m'm}\ \xi^\dagger_{m'}\ , \tag{4.51}$$

eq. (4.42) becomes:

$$\begin{aligned}
&\langle 0,\beta|\ T\ \xi^\alpha_m(t)\ X^{\gamma_j}_{m_j'm_j}(t_j')\ \ldots\ X^{\gamma_\ell}_{m_\ell'm_\ell}(t_\ell')\ \xi^{\dagger\gamma}_{m'}(t')\ |0,\beta\rangle =\\
&= -\ \langle 0,\beta|\ T\ \xi^{\dagger\gamma}_{m'}(t')\ X^{\gamma_j}_{m_j'm_j}(t_j')\ \ldots\ X^{\gamma_\ell}_{m_\ell'm_\ell}(t_\ell')\ \xi^\alpha_m(t)\ |0,\beta\rangle =\\
&= -\ S^{\gamma\alpha}_{\bar{\varepsilon}_f}(t'-t)\ \langle 0,\beta|\ T\ X^{\gamma_j}_{m_j'm_j}(t_j')\ \ldots\ X^{\gamma_\ell}_{m_\ell'm_\ell}(t_\ell')\ M^\alpha_{mm'}(t)\ |0,\beta\rangle\ +\\
&\qquad + \sum_k\ S^{\gamma\gamma_k}_{\bar{\varepsilon}_f}(t'-t_k')\ \varepsilon^{\gamma_k}\ \delta_{m'm_k}\ \times\\
&\langle 0,\beta|\ T\ X^{\gamma_j}_{m_j'm_j}(t_j')\ \ldots\ \xi^{\dagger\gamma_k}_{m_k'}(t_k')\ \ldots\ X^{\gamma_\ell}_{m_\ell'm_\ell}(t_\ell')\ \xi^\alpha_m(t)\ |0,\beta\rangle\ .
\end{aligned} \tag{4.52}$$

Performing the operations that led from eq. (4.42) to eq. (4.43) and using eq. (4.23) for the $S_{\bar{\varepsilon}_f}$ propagator, one finds:

$$\boxed{\begin{aligned}
&\langle 0,\beta|\ T\ X^{\gamma\alpha}_{m'm}(t',t)\ X^{\gamma_j}_{m_j'm_j}(t_j')\ \ldots\ X^{\gamma_\ell}_{m_\ell'm_\ell}(t_\ell')\ |0,\beta\rangle =\\
&= -\ \varepsilon^\alpha\ S^{\alpha\gamma}_{\varepsilon_f}(t-t')\ \langle 0,\beta|\ T\ X^\alpha_{m'm}(t)\ X^{\gamma_j}_{m_j'm_j}(t_j')\ \ldots\ X^{\gamma_\ell}_{m_\ell'm_\ell}(t_\ell')\ |0,\beta\rangle\ +\\
&\qquad + \sum_k \varepsilon^{\gamma_k}\ S^{\gamma_k\gamma}_{\varepsilon_f}(t_k'-t')\ \delta_{m'm_k}\ \times\\
&\times\ \langle 0,\beta|\ T\ X^{\gamma_k\alpha}_{m_k'm}(t_k',t)\ X^{\gamma_j}_{m_j'm_j}(t_j')\ \overset{k}{\ldots}\ X^{\gamma_\ell}_{m_\ell'm_\ell}(t_\ell')\ |0,\beta\rangle\ .
\end{aligned}}$$

(4.53)

7

If one now lets $\alpha = \gamma \equiv \gamma_i$, $t' = t + \varepsilon^{\gamma}\delta \equiv t_i'$, $m' \equiv m_i'$, $m \equiv m_i$, and uses eq. (4.40b), one obtains:

$$\langle 0,\beta | T\, X^{\gamma_i}_{m_i' m_i}(t_i')\, X^{\gamma_j}_{m_j' m_j}(t_j') \dots X^{\gamma_\ell}_{m_\ell' m_\ell}(t_\ell')\, |0,\beta\rangle =$$

$$= -\varepsilon^{\gamma_i} S^{\gamma_i\gamma_i}_{\varepsilon_f}(-\varepsilon^{\gamma_i}\delta)\, \langle 0,\beta | T\, X^{\gamma_i}_{m_i' m_i}(t_i')\, X^{\gamma_j}_{m_j' m_j}(t_j') \dots X^{\gamma_\ell}_{m_\ell' m_\ell}(t_\ell')\, |0,\beta\rangle +$$

$$+ \sum_k \varepsilon^{\gamma_k} S^{\gamma_k\gamma_i}_{\varepsilon_f}(t_k'-t_i')\, \delta_{m_i' m_k} \times$$

$$\times \langle 0,\beta | T\, X^{\gamma_k\gamma_i}_{m_k' m_i}(t_k',t_i')\, X^{\gamma_j}_{m_j' m_j}(t_j') \overset{k}{\dots} X^{\gamma_\ell}_{m_\ell' m_\ell}(t_\ell')\, |0,\beta\rangle \, . \qquad (4.54)$$

Finally making use of eq. (4.45), one gets:

$$\boxed{\begin{aligned} &\langle 0,\beta | T\, X^{\gamma_i}_{m_i' m_i}(t_i')\, X^{\gamma_j}_{m_j' m_j}(t_j') \dots X^{\gamma_\ell}_{m_\ell' m_\ell}(t_\ell')\, |0,\beta\rangle = \\ &= \frac{1}{f_F(-\varepsilon_f+\mu)} \sum_k \varepsilon^{\gamma_k} S^{\gamma_k\gamma_i}_{\varepsilon_f}(t_k'-t_i')\, \delta_{m_i' m_k} \times \\ &\times \langle 0,\beta | T\, X^{\gamma_k\gamma_i}_{m_k' m_i}(t_k',t_i')\, X^{\gamma_j}_{m_j' m_j}(t_j') \overset{k}{\dots} X^{\gamma_\ell}_{m_\ell' m_\ell}(t_\ell')\, |0,\beta\rangle \, . \end{aligned}}$$

(4.55)

Equations (4.53) and (4.55) are the alternate set of reduction formulae, to be compared to eqs. (4.43) and (4.46). Studying the alternate set reveals properties identical to the former set as described in sect. 4.5.4. Specifically, one has the multi-point construction of FIG. 4.1.

4.5.6 ELIMINATION OF THE MULTI-POINT VERTICES

A more tractable set of reduction formulae is found by using eq. (4.43) of the former reduction with eq. (4.55) of the alternate reduction. A study of these two equations reveals that the starting point of a loop under construction is removed from the T-product. It is the second point of a loop under construction which will form the starting point of the next loop. Thus the multi-point vertex structure of FIG. 4.1 has been transformed into a linear chain of loops of varying sizes, *with the condition that the loops are linked together at the second vertex of each successive loop.* This is illustrated in FIG. 4.2.

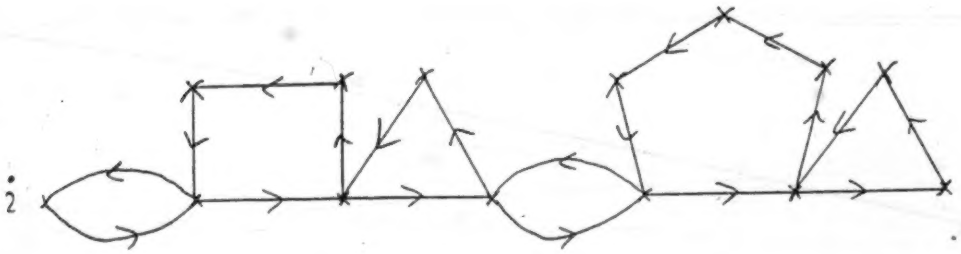

FIG. 4.2

The Linear Chain X–Operator Reduction

A T–product of X–operators may be reduced in terms of linear chain diagrams, using eqs. (4.43) and (4.55). This particular example comes from the reduction of the 14–point X–function. Each time point is represented by a cross. Each $S_{\epsilon f}$ propagator is represented by a line. The arrows point from the $\xi^\dagger$ end of the propagator towards the ξ end. "i" marks the starting point of the reduction, at time t_i' . Note that each link of the chain occurs at the second vertex of each successive loop.

4.5.7 THE FINAL SET OF NON–SU(N) REDUCTION FORMULAE

FIG. 4.2 is much easier to draw than FIG. 4.1, and is presumably easier to calculate, although the end result of both reductions should be the same. Let us therefore use the reduction of FIG. 4.2.

Collecting eqs. (4.55), (4.43), (4.50), (4.37) and (4.17a), one has the final set of reduction formulae which is to be used:

$$\boxed{\langle 0,\beta | M^{\gamma}_{mm'}(t) | 0,\beta \rangle = \delta_{mm'} \left[\langle P_o \rangle + \frac{1}{N} \langle P_1 \rangle \right]} \tag{4.56a}$$

$$\boxed{\begin{array}{c}
\langle 0,\beta| T\ M^{\gamma_i}_{m_i m_i'}(t_i')\ M^{\gamma_j}_{m_j m_j'}(t_j') \ldots M^{\gamma_\ell}_{m_\ell m_\ell'}(t_\ell')\ |0,\beta\rangle = \\
= \delta_{m_i m_i'}\ \delta_{m_j m_j'} \cdots \delta_{m_\ell m_\ell'}\ \langle P_o\rangle + \\
+\ \langle 0,\beta| T\ X^{\gamma_i}_{m_i' m_i}(t_i')\ X^{\gamma_j}_{m_j' m_j}(t_j') \ldots X^{\gamma_\ell}_{m_\ell' m_\ell}(t_\ell')\ |0,\beta\rangle
\end{array}} \tag{4.56b}$$

$$\boxed{\begin{array}{c}
\langle 0,\beta| T\ X^{\gamma_i}_{m_i' m_i}(t_i')\ X^{\gamma_j}_{m_j' m_j}(t_j') \ldots X^{\gamma_\ell}_{m_\ell' m_\ell}(t_\ell')\ |0,\beta\rangle = \\
= \dfrac{1}{f_F(-\varepsilon_f+\mu)} \sum_k \varepsilon^{\gamma_k}\ S^{\gamma_k \gamma_i}_{\varepsilon_f}(t_k'-t_i')\ \delta_{m_i' m_k} \times \\
\times \langle 0,\beta| T\ X^{\gamma_k \gamma_i}_{m_k' m_i}(t_k', t_i')\ X^{\gamma_j}_{m_j' m_j}(t_j') \overset{k}{\ldots} X^{\gamma_\ell}_{m_\ell' m_\ell}(t_\ell')\ |0,\beta\rangle
\end{array}} \tag{4.56c}$$

$$\boxed{\begin{array}{c}
\langle 0,\beta|\ T\ X^{\gamma\alpha}_{m' m}(t',t)\ X^{\gamma_j}_{m_j' m_j}(t_j') \ldots X^{\gamma_\ell}_{m_\ell' m_\ell}(t_\ell')\ |0,\beta\rangle = \\
= -\ \varepsilon^{\alpha}\ S^{\alpha\gamma}_{\varepsilon_f}(t-t')\ \langle 0,\beta|\ T\ X^{\gamma}_{m' m}(t')\ X^{\gamma_j}_{m_j' m_j}(t_j') \ldots X^{\gamma_\ell}_{m_\ell' m_\ell}(t_\ell')\ |0,\beta\rangle + \\
+ \sum_k \varepsilon^{\alpha}\ S^{\alpha\gamma_k}_{\varepsilon_f}(t-t_k')\ \delta_{m m_k'} \times \\
\times\ \langle 0,\beta|\ T\ X^{\gamma\gamma_k}_{m' m_k}(t',t_k')\ X^{\gamma_j}_{m_j' m_j}(t_j') \overset{k}{\ldots} X^{\gamma_\ell}_{m_\ell' m_\ell}(t_\ell')\ |0,\beta\rangle
\end{array}} \tag{4.56d}$$

$$\boxed{\langle 0,\beta| T\ X^{\gamma\alpha}_{m' m}(t',t) |0,\beta\rangle = -\ \delta_{m m'}\ \varepsilon^{\alpha}\ S^{\alpha\gamma}_{\varepsilon_f}(t-t')\ \frac{\langle P_1\rangle}{N\ f_F(\varepsilon_f-\mu)}} \tag{4.56e}$$

4.5.8 EXAMPLES OF X-OPERATOR T-PRODUCT REDUCTION

In this section, the reduction formulae of eqs. (4.56) will be applied to some specific examples. To facilitate this, we make the following definitions:

$$\langle 0,\beta|\mathrm{T}\, X^{\gamma_i}_{m'_i m_i}(t'_i)\, X^{\gamma_j}_{m'_j m_j}(t'_j)\, \ldots\, X^{\gamma_\ell}_{m'_\ell m_\ell}(t'_\ell)\, |0,\beta\rangle \equiv \langle i\, j \ldots \ell\rangle \tag{4.57}$$

$$G_{\varepsilon_f}(i\, j \ldots \ell) \equiv$$

$$\equiv -\frac{\varepsilon^{\gamma_i}\, S^{\gamma_i\gamma_j}_{\varepsilon_f}(t'_i-t'_j)\ \varepsilon^{\gamma_j}\, S^{\gamma_j\gamma_k}_{\varepsilon_f}(t'_j-t'_k)\ \varepsilon^{\gamma_k} \ldots \varepsilon^{\gamma_\ell}\, S^{\gamma_\ell\gamma_i}_{\varepsilon_f}(t'_\ell-t'_i)}{f_F(-\varepsilon_f+\mu)} \tag{4.58}$$

One obtains the following:

$$\boxed{\langle i\, j\rangle = \delta_{m_i m'_j}\, \delta_{m_j m'_i}\, G_{\varepsilon_f}(i\, j)\, \frac{\langle P_1\rangle}{N\, f_F(\varepsilon_f-\mu)}} \tag{4.59}$$

$$\boxed{\begin{aligned} \langle i\, j\, k\rangle = \Big\{ & \delta_{m'_i m_j}\, \delta_{m'_j m_k}\, \delta_{m'_k m_i} \Big[G_{\varepsilon_f}(i\, j)\, G_{\varepsilon_f}(j\, k) + G_{\varepsilon_f}(i\, k\, j)\Big] + \\ & + \delta_{m'_i m_k}\, \delta_{m'_k m_j}\, \delta_{m'_j m_i} \Big[G_{\varepsilon_f}(i\, k)\, G_{\varepsilon_f}(k\, j) + G_{\varepsilon_f}(i\, j\, k)\Big] \Big\} \frac{\langle P_1\rangle}{N\, f_F(\varepsilon_f-\mu)} \end{aligned}} \tag{4.60}$$

$$\boxed{\begin{aligned} \langle i\, j\, k\, \ell\rangle = \Big\{ & \delta_{m'_i m_j}\, \delta_{m'_j m_k}\, \delta_{m'_k m_\ell}\, \delta_{m'_\ell m_i} \Big[G_{\varepsilon_f}(i\, j)\, G_{\varepsilon_f}(j\, k)\, G_{\varepsilon_f}(k\, \ell) + \\ & + G_{\varepsilon_f}(i\, j)\, G_{\varepsilon_f}(j\, \ell\, k) + G_{\varepsilon_f}(i\, \ell\, j)\, G_{\varepsilon_f}(j\, k) + G_{\varepsilon_f}(i\, \ell\, k\, j)\Big] + \\ & + \text{all permutations of } j,k,\ell \Big\} \frac{\langle P_1\rangle}{N\, f_F(\varepsilon_f-\mu)} \end{aligned}} \tag{4.61}$$

$$\boxed{\begin{aligned} & \langle i\, j\, k\, \ell\, m\rangle = \\ & = \Big\{ \delta_{m'_i m_j} \delta_{m'_j m_k} \delta_{m'_k m_\ell} \delta_{m'_\ell m_m} \delta_{m'_m m_i} \Big[G_{\varepsilon_f}(i\, j)\, G_{\varepsilon_f}(j\, k)\, G_{\varepsilon_f}(k\, \ell)\, G_{\varepsilon_f}(\ell\, m) + \\ & + G_{\varepsilon_f}(i\, j)\, G_{\varepsilon_f}(j\, k)\, G_{\varepsilon_f}(k\, m\, \ell) + G_{\varepsilon_f}(i\, j)\, G_{\varepsilon_f}(j\, m\, k)\, G_{\varepsilon_f}(k\, \ell) + \\ & + G_{\varepsilon_f}(i\, j)\, G_{\varepsilon_f}(j\, m\, \ell\, k) + G_{\varepsilon_f}(i\, m\, j)\, G_{\varepsilon_f}(j\, k)\, G_{\varepsilon_f}(k\, \ell) + \\ & + G_{\varepsilon_f}(i\, m\, j)\, G_{\varepsilon_f}(j\, \ell\, k) + G_{\varepsilon_f}(i\, m\, \ell\, j)\, G_{\varepsilon_f}(j\, k) + \\ & + G_{\varepsilon_f}(i\, m\, \ell\, k\, j)\Big] + \text{all permutations of } j,k,l,m \Big\} \frac{\langle P_1\rangle}{N\, f_F(\varepsilon_f-\mu)} \end{aligned}} \tag{4.62}$$

The pattern that emerges is very straightforward. These examples are sufficient; the reader should now be able to write down the general form of the T-product of any number of X-operators.

Using this reduction method, we are now ready to complete our analysis of the 4-point function.

4.6 THE 4-POINT ξ-FUNCTION: COMPLETED

In section 4.4.2, the 4-point ξ-function was presented. The result given in eq. (4.33) was incomplete because we did not yet have a reduction formula for the T-product of zero-energy bosonic eigenoperators. Using eqs. (4.56a), (4.56b), and (4.59), the reduction may be completed, yielding:

$$
\begin{aligned}
&\Gamma_{4\,m_1 m_2 m_1' m_2'}^{\alpha_1\alpha_2\gamma_1\gamma_2}(t_1,t_2,t_1',t_2') = \\
&= S_{\varepsilon_f}^{\alpha_1\gamma_1}(t_1-t_1')\; S_{\varepsilon_f}^{\alpha_2\gamma_2}(t_2-t_2')\; \delta_{m_1m_1'}\; \delta_{m_2m_2'}\; \langle P_o\rangle\; + \\
&- S_{\varepsilon_f}^{\alpha_1\gamma_2}(t_1-t_2')\; S_{\varepsilon_f}^{\alpha_2\gamma_1}(t_2-t_1')\; \delta_{m_1m_2'}\; \delta_{m_2m_1'}\; \langle P_o\rangle\; + \\
&+ S_{\varepsilon_f}^{\alpha_1\gamma_1}(t_1-t_1')\; S_{\varepsilon_f}^{\alpha_2\gamma_2}(t_2-t_2')\; \delta_{m_1m_2'}\; \delta_{m_2m_1'}\; G_{\varepsilon_f}^{\gamma_1\gamma_2}(t_1',t_2')\; \frac{\langle P_1\rangle}{N\; f_F(\varepsilon_f-\mu)} \\
&- S_{\varepsilon_f}^{\alpha_1\gamma_2}(t_1-t_2')\; S_{\varepsilon_f}^{\alpha_2\gamma_1}(t_2-t_1')\; \delta_{m_1m_1'}\; \delta_{m_2m_2'}\; G_{\varepsilon_f}^{\gamma_1\gamma_2}(t_1',t_2')\; \frac{\langle P_1\rangle}{N\; f_F(\varepsilon_f-\mu)} \\
&+ S_{\varepsilon_f}^{\alpha_1\gamma_1}(t_1-t_1')\; S_{\varepsilon_f}^{\alpha_2\gamma_1}(t_2-t_1')\; \varepsilon^{\gamma_1}\; S_{\varepsilon_f}^{\gamma_1\gamma_2}(t_1'-t_2')\; \times \\
&\times \left[-\delta_{m_1m_1'}\; \delta_{m_2m_2'} + \delta_{m_1m_2'}\; \delta_{m_2m_1'}\right] \left[\langle P_o\rangle + \frac{1}{N}\langle P_1\rangle\right] + \\
&- S_{\varepsilon_f}^{\alpha_1\gamma_2}(t_1-t_2')\; S_{\varepsilon_f}^{\alpha_2\gamma_2}(t_2-t_2')\; \varepsilon^{\gamma_2}\; S_{\varepsilon_f}^{\gamma_2\gamma_1}(t_2'-t_1')\; \times \\
&\times \left[-\delta_{m_1m_2'}\; \delta_{m_2m_1'} + \delta_{m_1m_1'}\; \delta_{m_2m_2'}\right] \left[\langle P_o\rangle + \frac{1}{N}\langle P_1\rangle\right] \qquad (4.63)
\end{aligned}
$$

One may see from the structure of this 4-point function that even in this simple non-interacting model, the situation is greatly complicated by the spontaneous vertices and zero-energy bosons, which arise from the generalized Wick's formula.

Feynman rules for the general n-point ξ-function will be presented in section 4.9. Before this, we first consider some more properties of the zero–energy boson reduction.

4.7 A DEMONSTRATION OF THE $\varepsilon_f-\mu$ INDEPENDENCE OF THE X–OPERATOR REDUCTION

From the definition of the X–operator in eq. (4.35), it is obvious that an X–operator T–product acts only in the P_1 subspace. Using the explicit representation of the thermal vacuum given in eq. (4.13a), one finds:

$$\langle 0,\beta|T\, X^{\gamma_i}_{m_i' m_i}(t_i')\, X^{\gamma_j}_{m_j' m_j}(t_j') \ldots X^{\gamma_\ell}_{m_\ell' m_\ell}(t_\ell')|0,\beta\rangle =$$

$$= \frac{e^{-\beta(\varepsilon_f-\mu)}}{1+N\, e^{-\beta(\varepsilon_f-\mu)}} \sum_{mm'} \langle m\,\tilde{m}|T\, X^{\gamma_i}_{m_i' m_i}(t_i')\, X^{\gamma_j}_{m_j' m_j}(t_j') \ldots X^{\gamma_\ell}_{m_\ell' m_\ell}(t_\ell')|m'\,\tilde{m}'\rangle. \tag{4.64}$$

This expectation value is obviously just a product of spin delta–functions and time θ–functions; the spin delta–functions depend on the time–ordering and the γ's. (For an explicit representation, see eq. (6.100).) The only dependence on $\varepsilon_f-\mu$ is in the factor multiplying the expectation value; this factor is simply $\langle P_1\rangle/N$.

Therefore, upon removing the factor $\langle P_1\rangle/N$ from the final result of the reduction of a T–product of X–operators, one must have an $(\epsilon_f-\mu)$–independent expression. Applying this to the examples in sect. 4.5.8 one finds the following $\epsilon_f-\mu$ independent expressions:

Eg. 1. $$\frac{1}{f_F(\varepsilon_f-\mu)}\, G_{\varepsilon_f}(i\,j)$$

Eg. 2. $$\frac{1}{f_F(\varepsilon_f-\mu)} \left[G_{\varepsilon_f}(i\,j)\, G_{\varepsilon_f}(j\,k) + G_{\varepsilon_f}(i\,k\,j)\right]$$

Eg. 3. $$\frac{1}{f_F(\varepsilon_f-\mu)} \Big[G_{\varepsilon_f}(i\,j)\, G_{\varepsilon_f}(j\,k)\, G_{\varepsilon_f}(k\,\ell) +$$
$$+ G_{\varepsilon_f}(i\,j)\, G_{\varepsilon_f}(j\,\ell\,k) + G_{\varepsilon_f}(i\,\ell\,j)\, G_{\varepsilon_f}(j\,k) + G_{\varepsilon_f}(i\,\ell\,k\,j)\Big]$$

Eg. 4.
$$\frac{1}{f_F(\varepsilon_f-\mu)}\Big[G_{\varepsilon_f}(i\,j)\;G_{\varepsilon_f}(j\,k)\;G_{\varepsilon_f}(k\,\ell)\;G_{\varepsilon_f}(\ell\,m)\;+$$
$$+\;G_{\varepsilon_f}(i\,j)\;G_{\varepsilon_f}(j\,k)\;G_{\varepsilon_f}(k\,m\,\ell)\;+\;G_{\varepsilon_f}(i\,j)\;G_{\varepsilon_f}(j\,m\,k)\;G_{\varepsilon_f}(k\,\ell)\;+$$
$$+\;G_{\varepsilon_f}(i\,j)\;G_{\varepsilon_f}(j\,m\,\ell\,k)\;+\;G_{\varepsilon_f}(i\,m\,j)\;G_{\varepsilon_f}(j\,k)\;G_{\varepsilon_f}(k\,\ell)\;+$$
$$+\;G_{\varepsilon_f}(i\,m\,j)\;G_{\varepsilon_f}(j\,\ell\,k)\;+\;G_{\varepsilon_f}(i\,m\,\ell\,j)\;G_{\varepsilon_f}(j\,k)\;+\;G_{\varepsilon_f}(i\,m\,\ell\,k\,j)\Big]\;.$$

In these expressions, one may replace $\varepsilon_f-\mu$ by any value which is convenient.

4.8 REDUCTION OF THE ZERO-ENERGY BOSON T-PRODUCT USING THE SU(N) GROUP

4.8.1 WHY USE THE SU(N) REPRESENTATION?

As shown in eq. (4.37), the T–product of M–operators reduces simply into a $\langle P_o\rangle$ term and a T–product of X–operators which acts only in the P_1 subspace. The T–product of X–operators may be reduced into linear chains of ξ loops, as shown by the examples in sect. 4.5.8. Why should we complicate matters by representing the simple algebra of eqs. (4.28) in terms of the generators of the SU(N) group?

A major shortcoming of the reduction presented in sect. 4.5 is that it does not lend itself to a self–energy expansion. For example, suppose that there is an interaction term in the Hamiltonian which allows ξ to interact with another field φ. Normally, this would give the ξ propagator a 1–particle irreducible self–energy. But all the interaction vertices introduce an M–operator which may in turn produce an X–operator. The reduction presented in sect. 4.5 shows that all the X–operator vertices are connected to each other via linear chains of ξ loops. Thus any set of 1–particle irreducible diagrams becomes multiply connected when the X–operator T–product is reduced. (This only happens in the P_1 subspace. In the P_o subspace there is no problem.)

Using the SU(N) representation has the advantage of a self-energy expansion, as will be shown below. The reason this is possible is evident from eq. (4.64). The X-operator T-product is merely a product of spin delta-functions and time theta-functions. There is no reason this must be represented by chains connecting all X-vertices; other reductions schemes exist in which groups of X-vertices disconnect from other groups of X-vertices, restoring the concept of 1-particle irreducible self-energy diagrams. (Still, one should be careful, because a diagram which is 1-particle irreducible in the P_o sector is not necessarily 1-particle irreducible in the P_1 sector. It depends on how the X-vertices are grouped in the reduction.)

Although using the SU(N) representation naturally introduces disconnected diagrams in the X-operator reduction, this benefit does not come for free: the SU(N) rules are very complicated. They are derived below.

4.8.2 THE SU(N) ALGEBRA AND ITS CONSEQUENCES

In ref. [59], a normalization of $\mathrm{Tr}[\lambda_i \lambda_j] = N\ \delta_{ij}$ was assumed for the generators λ_j of the SU(N) group. (Eq. (26) of this reference states $\mathrm{Tr}[\lambda_i \lambda_j] = \delta_{ij}$ but this is a misprint.) In this thesis we shall take the following normalization:

$$\mathrm{Tr}[\lambda_i \lambda_j] = 2\ \delta_{ij}\ . \tag{4.65}$$

This normalization is consistent with the Pauli spin matrices (SU(2)) and the Gell-Mann matrices (SU(3)), and conforms to the normalization generally used by particle physicists. (For example, see ref. [65].)

The generators λ_j are N^2-1 traceless Hermitian $N \times N$ matrices satisfying the following algebra:

$$[\lambda_i\, , \lambda_j] = 2i\ f_{ijk}\ \lambda_k\ , \tag{4.66}$$

$$\{\lambda_i\, , \lambda_j\} = \frac{4}{N}\ \delta_{ij}\ \mathbb{1} + 2\ d_{ijk}\ \lambda_k\ , \tag{4.67}$$

where f_{ijk} are totally anti-symmetric structure factors and d_{ijk} are totally symmetric structure factors. The rules of ref. [59] are incorrect because they ignored d_{ijk} and assumed $\mathrm{Tr}(\lambda_i\lambda_j\lambda_k) = -\mathrm{Tr}(\lambda_k\lambda_j\lambda_i)$. Actually,

$$\mathrm{Tr}(\lambda_i\lambda_j\lambda_k) = 2(i\, f_{ijk} + d_{ijk}) \; . \tag{4.68}$$

Further properties of the SU(N) group are summarized in sect. A.2 of appendix A.

Using eq. (A.46), the algebra of eq. (4.28) may be rewritten:

$$\left\{\xi_m \, , \, \xi^\dagger_{m'}\right\} = M_{mm'} \tag{4.69}$$

$$\begin{aligned}\left[\xi_{m''} \, , \, M_{mm'}\right] &= \left[-\,\delta_{mm'}\,\delta_{m''\ell} + \delta_{m''m'}\,\delta_{m\ell}\right]\xi_\ell = \\ &= \left[-\left[1-\frac{1}{N}\right]\delta_{mm'}\,\delta_{m''\ell} + \frac{1}{2}\sum_j \lambda_j^{mm'}\lambda_j^{m''\ell}\right]\xi_\ell \; .\end{aligned} \tag{4.70}$$

If one multiplies eq. (A.45) by $\xi^\dagger_\ell\,\xi_{\ell'}$ and sums over ℓ and ℓ', one finds an expression for $X_{m'm}$:

$$X_{m'm} = \frac{1}{N}\,\delta_{mm'}\,P_1 + \frac{1}{2}\sum_i \lambda_i^{mm'} X_i \; , \tag{4.71}$$

where

$$X_i \equiv \sum_{\ell\ell'} \xi^\dagger_\ell\,\lambda_i^{\ell\ell'}\,\xi_{\ell'} = \sum_{\ell\ell'} |\ell\rangle\,\lambda_i^{\ell\ell'}\,\langle\ell'| \; , \tag{4.72}$$

and $P_1 = \sum_m |m\rangle\langle m|$ is the 1-particle projection operator.

Eq. (4.36) for $M_{mm'}$ may thus be written terms of the X_i-operators as follows:

$$M_{mm'} = \delta_{mm'}\left[P_o + \frac{1}{N}P_1\right] + \frac{1}{2}\sum_i \lambda_i^{mm'} X_i \tag{4.73}$$

Noting that P_o and P_1 are 0-energy eigenoperators, one may use the thermal state condition (eq. (2.15)) to declare that

$$\left.\begin{aligned} P_o^\gamma|0,\beta\rangle &= P_o|0,\beta\rangle \\ P_1^\gamma|0,\beta\rangle &= P_1|0,\beta\rangle \end{aligned}\right\} \tag{4.74}$$

Noting also that $P_o^2 = P_o$, $P_1^2 = P_1$, $P_oP_1 = P_1P_o = 0$, $P_oX_i = X_iP_o = 0$, and $P_1X_i = X_iP_1 = X_i$, one finds that a $\mathcal{T}$-product of M-operators acquires the following form:

$$\langle 0,\beta| T\ M^{\gamma_i}_{m_i m_i'}(t_i')\ M^{\gamma_j}_{m_j m_j'}(t_j') \ldots M^{\gamma_\ell}_{m_\ell m_\ell'}(t_\ell')\ |0,\beta\rangle =$$

$$= \delta_{m_i m_i'}\ \delta_{m_j m_j'} \cdots \delta_{m_\ell m_\ell'}\ \langle P_o\rangle + \frac{\delta_{m_i m_i'}}{N}\ \frac{\delta_{m_j m_j'}}{N} \cdots \frac{\delta_{m_\ell m_\ell'}}{N}\ \langle P_1\rangle +$$

$$\sum_k \frac{\delta_{m_i m_i'}}{N}\ \frac{\delta_{m_j m_j'}}{N}\ \overset{k}{\underset{-}{\ldots}}\ \frac{\delta_{m_\ell m_\ell'}}{N}\ \frac{1}{2} \sum_{i_k} \lambda^{m_k m_k'}_{i_k}\ \langle 0,\beta|\ X^{\gamma_k}_{i_k}\ |0,\beta\rangle +$$

$$\sum_{k_1<k_2} \frac{\delta_{m_i m_i'}}{N}\ \frac{\delta_{m_j m_j'}}{N}\ \overset{k_1\ \ k_2}{\overset{\vee\ \ \ \vee}{\cdots\cdots\cdots}}\ \frac{\delta_{m_\ell m_\ell'}}{N}\ \frac{1}{2^2} \sum_{i_{k_1} i_{k_2}} \lambda^{m_{k_1} m_{k_1}'}_{i_{k_1}}\ \lambda^{m_{k_2} m_{k_2}'}_{i_{k_2}} \times$$

$$\times\ \langle 0,\beta| T\ X^{\gamma_{k_1}}_{i_{k_1}}(t_{i_{k_1}}')\ X^{\gamma_{k_2}}_{i_{k_2}}(t_{i_{k_2}}')|0,\beta\rangle + \ldots +$$

$$+ \frac{1}{2}\sum_{i_i} \frac{1}{2}\sum_{i_j} \cdots \frac{1}{2}\sum_{i_\ell} \lambda^{m_i m_i'}_{i_i}\ \lambda^{m_j m_j'}_{i_j} \cdots \lambda^{m_\ell m_\ell'}_{i_\ell} \times$$

$$\times\ \langle 0,\beta| T\ X^{\gamma_i}_{i_i}(t_i')\ X^{\gamma_j}_{i_j}(t_j') \ldots X^{\gamma_\ell}_{i_\ell}(t_\ell')|0,\beta\rangle\ . \qquad (4.75)$$

This expression is to be compared to eq. (4.37) from the non–SU(N) rules. Although eq. (4.75) is more complicated, it does have the advantage that the X–operator T–product is broken up into a $\langle P_1\rangle$ term, plus other disconnected terms involving the T–product of X_i–operators. This yields the possibility of a self–energy expansion in the P_1 sector, if one can argue that higher order X_i T–products are a perturbation on lower order X_i T–products.

These issues will be dealt with later. Let us now turn to the problem of deriving reduction formulae for X_i–operator T–products.

4.8.3 DERIVATION OF REDUCTION FORMULAE FOR T–PRODUCTS OF X_i–OPERATORS

Following section 4.5.3, we use the method of time–splitting. To facilitate this we introduce the following operator:

$$X_i^{\gamma\alpha}(t',t) \equiv T\, \varepsilon^\alpha \sum_{\ell'\ell} \xi_{\ell'}^{\dagger\gamma}(t')\, \lambda_i^{\ell'\ell}\, \xi_\ell^\alpha(t)\ , \tag{4.76}$$

where

$$X_i^{\gamma\gamma}(t+\varepsilon^\gamma\delta,t) = X_i^\gamma(t) \equiv P^\gamma \sum_{\ell'\ell} \xi_{\ell'}^{\dagger\gamma}(t)\, \lambda_i^{\ell'\ell}\, \xi_\ell^\gamma(t) = P^\gamma\, \xi^{\dagger\gamma}(t)\, \lambda_i^\gamma\, \xi^\gamma(t)\ , \tag{4.77}$$

P^γ is the thermal ordering operator (see eq. (4.38), $\lambda_i^{(1)} = \lambda_i$, and $\lambda_i^{(2)} = \lambda_i^T$, the transposed λ_i matrix. To be more general, we also introduce the following operators:

$$X_A^{\gamma\alpha}(t',t) \equiv T\, \varepsilon^\alpha \sum_{\ell'\ell} \xi_{\ell'}^{\dagger\gamma}(t')\, A^{\ell'\ell}\, \xi_\ell^\alpha(t)\ , \tag{4.78}$$

where

$$X_A^{\gamma\gamma}(t+\varepsilon^\gamma\delta,t) = X_A^\gamma(t)\ , \tag{4.79}$$

$$X_A(t) \equiv \sum_{\ell'\ell} \xi_{\ell'}^\dagger(t)\, A^{\ell'\ell}\, \xi_\ell(t)\ , \tag{4.80}$$

and A is an arbitrary N×N matrix.

Noting that:

$$\left[\xi_m\ , X_A\right] = \sum_\ell A^{m\ell}\, \xi_\ell\ , \tag{4.81}$$

one may use the generalized Wick's theorem of eq. (3.13) to obtain:

$$\begin{aligned} &\langle 0,\beta|T\ \xi_m^\alpha(t)\, X_{A_j}^{\gamma_j}(t_j') \ldots X_{A_\ell}^{\gamma_\ell}(t_\ell')\, \xi_{m'}^{\dagger\gamma}(t')|0,\beta\rangle = \\ &= S_{\varepsilon_f}^{\alpha\gamma}(t-t')\ \langle 0,\beta|T\ X_{A_j}^{\gamma_j}(t_j') \ldots X_{A_\ell}^{\gamma_\ell}(t_\ell')\, M_{mm'}^\gamma(t')|0,\beta\rangle + \\ &+ \sum_k S_{\varepsilon_f}^{\alpha\gamma_k}(t-t_k')\varepsilon^{\gamma_k}\langle 0,\beta|T\ X_{A_j}^{\gamma_j}(t_j') \ldots [A_k \xi^{\gamma_k}(t_k')]_m \ldots X_{A_\ell}^{\gamma_\ell}(t_\ell')\, \xi_{m'}^{\dagger\gamma}(t')|0,\beta\rangle \end{aligned} \tag{4.82}$$

In the first term, note that only the component of M in the P_1 subspace contributes, (assuming there is a non-zero number of X-operators in the T-product).

Let us multiply both sides of eq. (4.82) by $-\epsilon^\alpha\ A_i^{m'm}$ and sum over m' and m, using definitions (4.78) and (4.80). We obtain:

$$\boxed{\begin{aligned}
&\langle 0,\beta|\ T\ X^{\gamma\alpha}_{A_i}(t',t)\ X^{\gamma_j}_{A_j}(t'_j)\ \dots\ X^{\gamma_\ell}_{A_\ell}(t'_\ell)\ |0,\beta\rangle = \\
&= -\,\varepsilon^{\alpha}\ S^{\alpha\gamma}_{\varepsilon_f}(t-t')\ \langle 0,\beta|\ T\ X^{\gamma}_{A_i}(t')\ X^{\gamma_j}_{A_j}(t'_j)\ \dots\ X^{\gamma_\ell}_{A_\ell}(t'_\ell)\ |0,\beta\rangle\ + \\
&+ \sum_k \varepsilon^{\alpha}\ S^{\alpha\gamma_k}_{\varepsilon_f}(t-t'_k)\ \langle 0,\beta|\ T\ X^{\gamma\gamma_k}_{A_iA_k}(t',t'_k)\ X^{\gamma_j}_{A_j}(t'_j)\ \overset{k}{\dots}\ X^{\gamma_\ell}_{A_\ell}(t'_\ell)\ |0,\beta\rangle\ ,
\end{aligned}}\tag{4.83}$$

where the $\overset{k}{\dots}$ means that the $X^{\gamma_k}_{A_k}(t'_k)$ term is missing.

If one now lets $\alpha = \gamma \equiv \gamma_i$, $t' = t + \varepsilon^{\gamma}\delta \equiv t'_i$, and uses eq. (4.79), one obtains:

$$\begin{aligned}
&\langle 0,\beta|T\ X^{\gamma_i}_{A_i}(t'_i)\ X^{\gamma_j}_{A_j}(t'_j)\ \dots\ X^{\gamma_\ell}_{A_\ell}(t'_\ell)\ |0,\beta\rangle = \\
&= -\,\varepsilon^{\gamma_i}\ S^{\gamma_i\gamma_i}_{\varepsilon_f}(-\varepsilon^{\gamma_i}\delta)\ \langle 0,\beta|T\ X^{\gamma_i}_{A_i}(t'_i)\ X^{\gamma_j}_{A_j}(t'_j)\ \dots\ X^{\gamma_\ell}_{A_\ell}(t'_\ell)\ |0,\beta\rangle\ + \\
&\sum_k \varepsilon^{\gamma_i}\ S^{\gamma_i\gamma_k}_{\varepsilon_f}(t'_i-t'_k)\ \langle 0,\beta|T\ X^{\gamma_i\gamma_k}_{A_iA_k}(t'_i,t'_k)\ X^{\gamma_j}_{A_j}(t'_j)\ \overset{k}{\dots}\ X^{\gamma_\ell}_{A_\ell}(t'_\ell)\ |0,\beta\rangle\ .
\end{aligned}\tag{4.84}$$

Upon using eq. (4.45), the above equation becomes:

$$\boxed{\begin{aligned}
&\langle 0,\beta|T\ X^{\gamma_i}_{A_i}(t'_i)\ X^{\gamma_j}_{A_j}(t'_j)\ \dots\ X^{\gamma_\ell}_{A_\ell}(t'_\ell)\ |0,\beta\rangle = \\
&= \frac{1}{f_F(-\varepsilon_f+\mu)} \sum_k \varepsilon^{\gamma_i}\ S^{\gamma_i\gamma_k}_{\varepsilon_f}(t'_i-t'_k)\ \times \\
&\times\ \langle 0,\beta|T\ X^{\gamma_i\gamma_k}_{A_iA_k}(t'_i,t'_k)\ X^{\gamma_j}_{A_j}(t'_j)\ \overset{k}{\dots}\ X^{\gamma_\ell}_{A_\ell}(t'_\ell)\ |0,\beta\rangle\ .
\end{aligned}}\tag{4.85}$$

Eqs. (4.83) and (4.85) are the reduction formulae; they may be used to reduce a T–product of two or more X^{γ}_{i}–operators to a sum of Feynman propagator products, multiplied ultimately by the expectation value of an $X_A^{\gamma\gamma'}$. This final expectation value is evaluated directly from the definition, eq. (4.78).

$$\langle 0,\beta|\mathrm{T}\ X_A^{\gamma\alpha}(t',t)\ |0,\beta\rangle = \varepsilon^{\alpha}\sum_{\ell'\ell} A^{\ell'\ell}\ \langle 0,\beta|\mathrm{T}\ \xi_{\ell'}^{\dagger\gamma}(t')\ \xi_{\ell}^{\alpha}(t)\ |0,\beta\rangle =$$

$$= -\ \varepsilon^{\alpha}\sum_{\ell'\ell} A^{\ell'\ell}\ \mathcal{S}_{\ell\ell'}^{\alpha\gamma}(t,t')\ . \tag{4.86}$$

Using the $\mathcal{S}$ propagator given by eq. (4.19), one finds:

$$\langle 0,\beta|\mathrm{T}\ X_A^{\gamma\alpha}(t',t)\ |0,\beta\rangle = -\ \varepsilon^{\alpha}\ S_{\varepsilon_f}^{\alpha\gamma}(t-t')\ \mathrm{Tr}(A)\ \left[\langle P_o\rangle + \frac{1}{N}\ \langle P_1\rangle\right] . \tag{4.87}$$

As discussed in sect. 4.5.3, eq. (4.87) should be written in terms of $\langle P_1\rangle$ only, because the X_A–operator T–products act only in the P_1 sector. This is accomplished by using eq. (4.49b) in the above expression, yielding:

$$\boxed{\langle 0,\beta|\mathrm{T}\ X_A^{\gamma\alpha}(t',t)|0,\beta\rangle = -\ \varepsilon^{\alpha}\ S_{\varepsilon_f}^{\alpha\gamma}(t-t')\ \mathrm{Tr}(A)\ \frac{\langle P_1\rangle}{N\ f_F(\varepsilon_f-\mu)}\ .} \tag{4.88}$$

A complete reduction of the T–product of 2 or more X_i–operators may be obtained using eqs. (4.83), (4.85), and (4.88).

4.8.4. A SHORTCOMING OF THE X_i–OPERATOR REDUCTION: MULTI–POINT VERTICES

Although the above reduction is complete, it is diagrammatically inconvenient. The story is very similar to what happened in sect. 4.5.4. Studying the reduction formulae reveals the following properties:

1) The reduction is composed of closed loops of S_{ε_f} propagators, with a λ matrix at each vertex, a final trace being taken over all λ's.

2. The second term in eq. (4.83) will insert an extra S_{ε_f} propagator on a

loop under construction, which makes the loop bigger.

3. The first term in eq. (4.83) will close a loop under construction, leaving the starting point of the initial reduction ($X^{\gamma_i}(t_i')$), as the starting point of any further reduction. A further reduction will start a new loop.
4. A loop under construction is always started and finished at $X^{\gamma_i}(t_i')$. That is, all loops are connected together at a single multi-point vertex: $X^{\gamma_i}(t_i')$.

The picture that emerges is virtually the same one that was found in sect. 4.5.4, and is illustrated in FIG. 4.1. One has an appalling product of closed S_{ε_f} loops of varying size all connected together at a single multi-point vertex.

4.8.5 AN ALTERNATE SET OF REDUCTION FORMULAE FOR T-PRODUCTS OF X_i-OPERATORS

Proceeding as in sect. 4.5.5, we derive a pair of reduction formulae analogous to eqs. (4.83) and (4.85), using the $\xi^\dagger$ propagator of sect. 4.3.3.

Noting that

$$\left[\xi_m^\dagger , X_A\right] = - \sum_\ell \xi_\ell^\dagger A^{\ell m} , \tag{4.89}$$

eq. (4.82) becomes:

$$\begin{aligned} &\langle 0,\beta | T\ \xi_m^\alpha(t)\ X_{A_j}^{\gamma_j}(t_j') \ldots X_{A_\ell}^{\gamma_\ell}(t_\ell')\ \xi_{m'}^{\dagger\gamma}(t') | 0,\beta\rangle = \\ &- \langle 0,\beta | T\ \xi_{m'}^{\dagger\gamma}(t')\ X_{A_j}^{\gamma_j}(t_j') \ldots X_{A_\ell}^{\gamma_\ell}(t_\ell')\ \xi_m^\alpha(t) | 0,\beta\rangle \\ &= - S_{\bar\varepsilon_f}^{\gamma\alpha}(t'-t)\ \langle 0,\beta | T\ X_{A_j}^{\gamma_j}(t_j') \ldots X_{A_\ell}^{\gamma_\ell}(t_\ell')\ M_{mm'}^\alpha(t) | 0,\beta\rangle + \\ &+ \sum_k S_{\bar\varepsilon_f}^{\gamma\gamma_k}(t'-t_k')\varepsilon^{\gamma_k} \langle 0,\beta | T\ X_{A_j}^{\gamma_j}(t_j') \ldots [\xi^{\dagger\gamma_k}(t_k')A_k]_{m'} \ldots X_{A_\ell}^{\gamma_\ell}(t_\ell')\ \xi_m^\alpha(t) | 0,\beta\rangle . \end{aligned} \tag{4.90}$$

Performing the operations that led from eq. (4.82) to eq. (4.83), and using eq. (4.23) for the $S_{\bar{\varepsilon}_f}$ propagator, one finds:

$$\boxed{\begin{aligned} &\langle 0,\beta|\ T\ X^{\gamma\alpha}_{A_i}(t',t)\ X^{\gamma_j}_{A_j}(t_j')\ \ldots\ X^{\gamma_\ell}_{A_\ell}(t_\ell')\ |0,\beta\rangle = \\ &= -\ \varepsilon^{\alpha}\ S^{\alpha\gamma}_{\varepsilon_f}(t-t')\ \langle 0,\beta|\ T\ X^{\alpha}_{A_i}(t)\ X^{\gamma_j}_{A_j}(t_j')\ \ldots\ X^{\gamma_\ell}_{A_\ell}(t_\ell')\ |0,\beta\rangle\ + \\ &+\sum_k \varepsilon^{\gamma_k}\ S^{\gamma_k\gamma}_{\varepsilon_f}(t_k'-t')\langle 0,\beta|\ T\ X^{\gamma_k\alpha}_{A_kA_i}(t_k',t)\ X^{\gamma_j}_{A_j}(t_j')\ \overset{k}{\ldots}\ X^{\gamma_\ell}_{A_\ell}(t_\ell')\ |0,\beta\rangle\ . \end{aligned}} \tag{4.91}$$

If one now lets $\alpha = \gamma \equiv \gamma_i$, $t' = t + \epsilon^{\gamma}\delta \equiv t_i'$, and uses eq. (4.79), one obtains:

$$\begin{aligned} &\langle 0,\beta|T\ X^{\gamma_i}_{A_i}(t_i')\ X^{\gamma_j}_{A_j}(t_j')\ \ldots\ X^{\gamma_\ell}_{A_\ell}(t_\ell')\ |0,\beta\rangle = \\ &= -\ \varepsilon^{\gamma_i}\ S^{\gamma_i\gamma_i}_{\varepsilon_f}(-\varepsilon^{\gamma_i}\delta)\ \langle 0,\beta|T\ X^{\gamma_i}_{A_i}(t_i')\ X^{\gamma_j}_{A_j}(t_j')\ \ldots\ X^{\gamma_\ell}_{A_\ell}(t_\ell')\ |0,\beta\rangle\ + \\ &+\sum_k \varepsilon^{\gamma_k}\ S^{\gamma_k\gamma_i}_{\varepsilon_f}(t_k'-t_i')\ \langle 0,\beta|T\ X^{\gamma_k\gamma_i}_{A_kA_i}(t_k',t_i')\ X^{\gamma_j}_{A_j}(t_j')\ \overset{k}{\ldots}\ X^{\gamma_\ell}_{A_\ell}(t_\ell')\ |0,\beta\rangle\ . \end{aligned} \tag{4.92}$$

Upon using eq. (4.45), the above equation becomes:

$$\boxed{\begin{aligned} &\langle 0,\beta|T\ X^{\gamma_i}_{A_i}(t_i')\ X^{\gamma_j}_{A_j}(t_j')\ \ldots\ X^{\gamma_\ell}_{A_\ell}(t_\ell')\ |0,\beta\rangle = \\ &= \frac{1}{f_F(-\varepsilon_f+\mu)}\sum_k \varepsilon^{\gamma_k}\ S^{\gamma_k\gamma_i}_{\varepsilon_f}(t_k'-t_i')\ \times \\ &\times\ \langle 0,\beta|T\ X^{\gamma_k\gamma_i}_{A_kA_i}(t_k',t_i')\ X^{\gamma_j}_{A_j}(t_j')\ \overset{k}{\ldots}\ X^{\gamma_\ell}_{A_\ell}(t_\ell')\ |0,\beta\rangle\ . \end{aligned}} \tag{4.93}$$

Equations (4.91) and (4.93) are the alternate set of reduction formulae, to be compared to eqs. (4.83) and (4.85). Studying the alternate set reveals properties identical to the former set as described in sect. 4.8.4. Specifically, one again has the multi–point construction of FIG. 4.1.

4.8.6 THE FINAL SET OF SU(N) REDUCTION FORMULAE

The situation that presents itself is very similar to what happens for the non–SU(N) case. In particular, the multi–point vertices may be eliminated by using eq. (4.83) of the former reduction with eq. (4.93) of the alternate reduction. A study of these two equations reveals that the starting point of a loop under construction is removed from the T–product. It is the second point of a loop under construction which will form the starting point of the next loop. As in the non–SU(N) case, the multi–point vertex structure of FIG. 4.1 has been transformed into a linear chain of loops of varying sizes, with the condition that the loops are linked together at the second vertex of each successive loop. This is illustrated in FIG. 4.2 (see pg. 89).

This is the reduction scheme to be used in this thesis. For convenience the complete set of reduction formulae, (eqs. (4.56a), (4.75), (4.93), (4.83), and (4.88)), is collected below.

$$\boxed{\langle 0,\beta | M^{\gamma}_{mm'}(t) | 0,\beta \rangle = \delta_{mm'} \left[\langle P_o \rangle + \frac{1}{N} \langle P_1 \rangle \right]} \tag{4.94a}$$

$$\boxed{\begin{aligned}
&\langle 0,\beta|\mathrm{T}\; M^{\gamma_1}_{m_1m'_1}(t'_1)\; M^{\gamma_2}_{m_2m'_2}(t'_2)\;\ldots\; M^{\gamma_\ell}_{m_\ell m'_\ell}(t'_\ell)\;|0,\beta\rangle =\\
&= \Big[\, \langle P_o\rangle + \frac{1}{N^{\ell}}\,\langle P_1\rangle \,\Big] \prod_{i=1}^{\ell} \delta_{m_i m'_i} +\\
&+ \frac{1}{N^{\ell-1}}\sum_{k=1}^{\ell} \delta_{m_1m'_1}\;\delta_{m_2m'_2}\;\overset{k}{\cdots}\;\delta_{m_\ell m'_\ell}\;\frac{1}{2}\sum_{i_k}\lambda^{m_km'_k}_{i_k}\;\langle 0,\beta|\;X^{\gamma_k}_{i_k}\;|0,\beta\rangle +\\
&+ \frac{1}{N^{\ell-2}}\sum_{k_1<k_2} \delta_{m_1m'_1}\;\delta_{m_2m'_2}\;\overset{\substack{k_1\;\,k_2\\ \vee\;\;\,\vee}}{\cdots\cdots\cdots}\;\delta_{m_\ell m'_\ell}\;\frac{1}{2^2}\sum_{i_{k_1}i_{k_2}}\lambda^{m_{k_1}m'_{k_1}}_{i_{k_1}}\;\lambda^{m_{k_2}m'_{k_2}}_{i_{k_2}}\;\times\\
&\times\;\langle 0,\beta|\mathrm{T}\;X^{\gamma_{k_1}}_{i_{k_1}}(t'_{i_{k_1}})\;X^{\gamma_{k_2}}_{i_{k_2}}(t'_{i_{k_2}})|0,\beta\rangle + \ldots +\\
&+ \frac{1}{2^{\ell}}\sum_{\{i\}}\lambda^{m_1m'_1}_{i_i}\;\lambda^{m_2m'_2}_{i_2}\;\ldots\;\lambda^{m_\ell m'_\ell}_{i_\ell}\;\times\\
&\times\;\langle 0,\beta|\mathrm{T}\;X^{\gamma_1}_{i_i}(t'_1)\;X^{\gamma_2}_{i_2}(t'_2)\;\ldots\;X^{\gamma_\ell}_{i_\ell}(t'_\ell)|0,\beta\rangle
\end{aligned}}$$

(4.94b)

$$\boxed{\begin{aligned}
&\langle 0,\beta|\mathrm{T}\;X^{\gamma_i}_{\Lambda_i}(t'_i)\;X^{\gamma_j}_{\Lambda_j}(t'_j)\;\ldots\;X^{\gamma_\ell}_{\Lambda_\ell}(t'_\ell)\;|0,\beta\rangle =\\
&= \frac{1}{f_F(-\varepsilon_f+\mu)}\sum_{k}\varepsilon^{\gamma_k}\;S^{\gamma_k\gamma_i}_{\varepsilon_f}(t'_k-t'_i)\;\times\\
&\times\;\langle 0,\beta|\mathrm{T}\;X^{\gamma_k\gamma_i}_{\Lambda_k\Lambda_i}(t'_k,t'_i)\;X^{\gamma_j}_{\Lambda_j}(t'_j)\;\overset{k}{\cdots}\;X^{\gamma_\ell}_{\Lambda_\ell}(t'_\ell)\;|0,\beta\rangle
\end{aligned}}$$

(4.94c)

$$\boxed{\begin{aligned}
&\langle 0,\beta|\;\mathrm{T}\;X^{\gamma\alpha}_{\Lambda_i}(t',t)\;X^{\gamma_j}_{\Lambda_j}(t'_j)\;\ldots\;X^{\gamma_\ell}_{\Lambda_\ell}(t'_\ell)\;|0,\beta\rangle =\\
&= -\,\varepsilon^{\alpha}\;S^{\alpha\gamma}_{\varepsilon_f}(t-t')\;\langle 0,\beta|\;\mathrm{T}\;X^{\gamma}_{\Lambda_i}(t')\;X^{\gamma_j}_{\Lambda_j}(t'_j)\;\ldots\;X^{\gamma_\ell}_{\Lambda_\ell}(t'_\ell)\;|0,\beta\rangle +\\
&+ \sum_{k}\varepsilon^{\alpha}\;S^{\alpha\gamma_k}_{\varepsilon_f}(t-t'_k)\;\langle 0,\beta|\;\mathrm{T}\;X^{\gamma\gamma_k}_{\Lambda_i\Lambda_k}(t',t'_k)\;X^{\gamma_j}_{\Lambda_j}(t'_j)\;\overset{k}{\cdots}\;X^{\gamma_\ell}_{\Lambda_\ell}(t'_\ell)\;|0,\beta\rangle
\end{aligned}}$$

(4.94d)

$$\boxed{\langle 0,\beta|\mathrm{T}\ X_{\Lambda}^{\gamma\alpha}(t',t)|0,\beta\rangle = -\,\varepsilon^{\alpha}\ S_{\varepsilon_f}^{\alpha\gamma}(t-t')\ \mathrm{Tr}(A)\ \frac{\langle P_1\rangle}{N\ f_F(\varepsilon_f-\mu)}} \tag{4.94e}$$

Using eq. (4.77) with eq. (4.94e), one finds that the second term of eq. (4.94b) disappears because $\mathrm{Tr}(\lambda_i) = 0$.

4.8.7 EXAMPLES OF X_i–OPERATOR T–PRODUCT REDUCTION

In this section, the reduction formulae of eqs. (4.94) will be applied to some specific examples. To facilitate this, we make the following definition:

$$\langle 0,\beta|\mathrm{T}\ X_i^{\gamma_i}(t_i')\ X_j^{\gamma_j}(t_j')\ \dots\ X_\ell^{\gamma_\ell}(t_\ell')|0,\beta\rangle \equiv \langle i\, j \dots \ell\rangle_\lambda \quad , \tag{4.95}$$

where the λ is to distinguish this T–product from the corresponding $\langle i\, j \dots \ell\rangle$ of eq. (4.57) in the non–SU(N) rules. We will also use definition (4.58) for $G_{\varepsilon_f}(i\, j \dots \ell)$.

One obtains the following:

$$\boxed{\langle i\rangle_\lambda = 0} \tag{4.96}$$

$$\boxed{\langle i\, j\rangle_\lambda = \mathrm{Tr}(\lambda_j\lambda_i)\ G_{\varepsilon_f}(i\, j)\ \frac{\langle P_1\rangle}{N\ f_F(\varepsilon_f-\mu)}} \tag{4.97}$$

$$\boxed{\begin{aligned}\langle i\, j\, k\rangle_\lambda = \Big\{ &\mathrm{Tr}(\lambda_k\lambda_j\lambda_i)\ \Big[G_{\varepsilon_f}(i\, j)\ G_{\varepsilon_f}(j\, k) + G_{\varepsilon_f}(i\, k\, j)\Big] + \\ &+ \mathrm{Tr}(\lambda_j\lambda_k\lambda_i)\ \Big[G_{\varepsilon_f}(i\, k)\ G_{\varepsilon_f}(k\, j) + G_{\varepsilon_f}(i\, j\, k)\Big]\Big\}\ \frac{\langle P_1\rangle}{N\ f_F(\varepsilon_f-\mu)}\end{aligned}} \tag{4.98}$$

$$\boxed{\begin{aligned} \langle i\,j\,k\,\ell\rangle_\lambda = \Big\{ & \mathrm{Tr}(\lambda_\ell \lambda_k \lambda_j \lambda_i) \Big[G_{\varepsilon_f}(i\,j)\, G_{\varepsilon_f}(j\,k)\, G_{\varepsilon_f}(k\,\ell) + \\ & + G_{\varepsilon_f}(i\,j)\, G_{\varepsilon_f}(j\,\ell\,k) + G_{\varepsilon_f}(i\,\ell\,j)\, G_{\varepsilon_f}(j\,k) + G_{\varepsilon_f}(i\,\ell\,k\,j) \Big] + \\ & + \text{all permutations of } j,k,\ell \Big\} \frac{\langle P_1\rangle}{N\, f_F(\varepsilon_f-\mu)} \end{aligned}} \tag{4.99}$$

$$\boxed{\begin{aligned} & \langle i\,j\,k\,\ell\,m\rangle_\lambda = \\ & = \Big\{ \mathrm{Tr}(\lambda_m \lambda_\ell \lambda_k \lambda_j \lambda_i) \Big[G_{\varepsilon_f}(i\,j)\, G_{\varepsilon_f}(j\,k)\, G_{\varepsilon_f}(k\,\ell)\, G_{\varepsilon_f}(\ell\,m) + \\ & + G_{\varepsilon_f}(i\,j)\, G_{\varepsilon_f}(j\,k)\, G_{\varepsilon_f}(k\,m\,\ell) + G_{\varepsilon_f}(i\,j)\, G_{\varepsilon_f}(j\,m\,k)\, G_{\varepsilon_f}(k\,\ell) + \\ & + G_{\varepsilon_f}(i\,j)\, G_{\varepsilon_f}(j\,m\,\ell\,k) + G_{\varepsilon_f}(i\,m\,j)\, G_{\varepsilon_f}(j\,k)\, G_{\varepsilon_f}(k\,\ell) + \\ & + G_{\varepsilon_f}(i\,m\,j)\, G_{\varepsilon_f}(j\,\ell\,k) + G_{\varepsilon_f}(i\,m\,\ell\,j)\, G_{\varepsilon_f}(j\,k) + \\ & + G_{\varepsilon_f}(i\,m\,\ell\,k\,j) \Big] + \text{all permutations of } j,k,\ell,m \Big\} \frac{\langle P_1\rangle}{N\, f_F(\varepsilon_f-\mu)} \end{aligned}} \tag{4.100}$$

The pattern that emerges is very similar to that of eqs. (4.59)–(4.62), the difference being that the δ–functions are replaced by a trace of λ–matrices.

4.8.8 AN ATTEMPT TO REMOVE THE 2–VERTEX LOOPS

As the 2–vertex loops $G_{\varepsilon_f}(i\,j)$ are actually time–independent (see eq. (4.124)), it was hoped that the SU(N) representation would remove them, breaking up the chain, and thereby introducing disconnected diagrams. But the above examples show that the 2–vertex loops remain. In the interest of removing them, let us insert eq. (4.94d) into eq. (4.94c):

$$\langle 0,\beta|T\; X^{\gamma_i}_{A_i}(t'_i)\; X^{\gamma_j}_{A_j}(t'_j)\;\dots\; X^{\gamma_\ell}_{A_\ell}(t'_\ell)\;|0,\beta\rangle =$$

$$=\sum_k G_{\varepsilon_f}(i\,k)\;\langle 0,\beta|T\; X^{\gamma_k}_{A_kA_i}(t'_k)\; X^{\gamma_j}_{A_j}(t'_j)\;\overset{k}{\check{\dots}}\; X^{\gamma_\ell}_{A_\ell}(t'_\ell)|0,\beta\rangle\;+$$

$$+\;\frac{1}{f_F(-\varepsilon_f+\mu)}\sum_{k_1k_2}\varepsilon^{\gamma_{k_1}}\; S^{\gamma_{k_1}\gamma_i}_{\varepsilon_f}(t'_{k_1}-t'_i)\;\varepsilon^{\gamma_i}\; S^{\gamma_i\gamma_{k_2}}_{\varepsilon_f}(t'_i-t'_{k_2})\;\times$$

$$\times\;\langle 0,\beta|T\; X^{\gamma_{k_1}\gamma_{k_2}}_{A_{k_1}A_iA_{k_2}}(t'_{k_1},t'_{k_2})\; X^{\gamma_j}_{A_j}(t'_j)\;\dots\overset{k_1}{\vee}\dots\overset{k_2}{\vee}\dots\; X^{\gamma_\ell}_{A_\ell}(t'_\ell)\;|0,\beta\rangle\;. \tag{4.101}$$

Now let us insert eq. (4.91) into eq. (4.85):

$$\langle 0,\beta|T\; X^{\gamma_i}_{A_i}(t'_i)\; X^{\gamma_j}_{A_j}(t'_j)\;\dots\; X^{\gamma_\ell}_{A_\ell}(t'_\ell)\;|0,\beta\rangle =$$

$$=\sum_k G_{\varepsilon_f}(i\,k)\;\langle 0,\beta|T\; X^{\gamma_k}_{A_iA_k}(t'_k)\; X^{\gamma_j}_{A_j}(t'_j)\;\overset{k}{\check{\dots}}\; X^{\gamma_\ell}_{A_\ell}(t'_\ell)|0,\beta\rangle\;+$$

$$+\;\frac{1}{f_F(-\varepsilon_f+\mu)}\sum_{k_1k_2}\varepsilon^{\gamma_{k_2}}\; S^{\gamma_{k_2}\gamma_i}_{\varepsilon_f}(t'_{k_2}-t'_i)\;\varepsilon^{\gamma_i}\; S^{\gamma_i\gamma_{k_1}}_{\varepsilon_f}(t'_i-t'_{k_1})\;\times$$

$$\times\;\langle 0,\beta|T\; X^{\gamma_{k_2}\gamma_{k_1}}_{A_{k_2}A_iA_{k_1}}(t'_{k_2},t'_{k_1})\; X^{\gamma_j}_{A_j}(t'_j)\;\dots\overset{k_1}{\vee}\dots\overset{k_2}{\vee}\dots\; X^{\gamma_\ell}_{A_\ell}(t'_\ell)\;|0,\beta\rangle\;. \tag{4.102}$$

Equations (4.101) and (4.102) should be the same. Changing $k_1 \longleftrightarrow k_2$ in the second term of one equation will give the second term of the other equation. Therefore the first terms of these two equations should be equal.

Using eq. (4.71) for $X_{m'm}$, one finds:

$$X_A = \sum_{m'm} X_{m'm}\; A^{m'm} = \frac{1}{N}\,\mathrm{Tr}(A)\; P_1 + \frac{1}{2}\sum_i \mathrm{Tr}(A\lambda_i)\; X_i\;. \tag{4.103}$$

Using this on the 1st terms of eqs. (4.101) and (4.102) one obtains:

$$\langle 0,\beta|T\; X^{\gamma_k}_{A_kA_i}(t'_k)\;\dots\;|0,\beta\rangle = \frac{1}{N}\,\mathrm{Tr}(A_kA_i)\;\langle 0,\beta|\;\dots\;|0,\beta\rangle\;+$$

$$+\;\frac{1}{2}\sum_c \mathrm{Tr}(A_kA_i\lambda_c)\;\langle 0,\beta|T\; X^{\gamma_k}_c(t'_k)\;\dots\;|0,\beta\rangle\;, \tag{4.104}$$

$$\langle 0,\beta| T\, X^{\gamma_k}_{A_i A_k}(t_k') \ldots |0,\beta\rangle = \frac{1}{N}\,\mathrm{Tr}(A_i A_k)\, \langle 0,\beta| \ldots |0,\beta\rangle + $$

$$+ \frac{1}{2}\sum_c \mathrm{Tr}(A_i A_k \lambda_c)\, \langle 0,\beta| T\, X^{\gamma_k}_c(t_k') \ldots |0,\beta\rangle \quad . \tag{4.105}$$

Let us insert these expressions into eqs. (4.101) and (4.102), then add the two equations together and divide by two. One obtains:

$$\boxed{\begin{aligned}
&\langle 0,\beta| T\, X^{\gamma_i}_i(t_i')\, X^{\gamma_j}_j(t_j') \ldots X^{\gamma_\ell}_\ell(t_\ell')\, |0,\beta\rangle = \\
&\sum_k G_{\varepsilon_f}(i\,k)\, \frac{1}{N}\,\mathrm{Tr}(\lambda_k\lambda_i)\, \langle 0,\beta| T\, X^{\gamma_j}_j(t_j') \overset{k}{\ldots} X^{\gamma_\ell}_\ell(t_\ell')\, |0,\beta\rangle + \\
&+\sum_k G_{\varepsilon_f}(i\,k) \sum_c d_{ikc}\, \langle 0,\beta| T\, X^{\gamma_k}_c(t_k')\, X^{\gamma_j}_j(t_j') \overset{k}{\ldots} X^{\gamma_\ell}_\ell(t_\ell')\, |0,\beta\rangle + \\
&+ \frac{1}{f_F(-\varepsilon_f+\mu)} \sum_{k_1 k_2} \varepsilon^{\gamma_{k_1}}\, S^{\gamma_{k_1}\gamma_i}_{\varepsilon_f}(t_{k_1}'-t_i')\, \varepsilon^{\gamma_i}\, S^{\gamma_i\gamma_{k_2}}_{\varepsilon_f}(t_i'-t_{k_2}') \times \\
&\times \langle 0,\beta| T\, X^{\gamma_{k_1}\gamma_{k_2}}_{k_1 i\, k_2}(t_{k_1}',t_{k_2}')\, X^{\gamma_j}_j(t_j') \ldots\overset{k_1}{\vee}\ldots\overset{k_2}{\vee}\ldots X^{\gamma_\ell}_\ell(t_\ell')\, |0,\beta\rangle \;.
\end{aligned}}$$

(4.106)

Here use was made of eq. (A.24) for d_{ijk}. This reduction formula should be used along with eq. (4.94d) in which eq. (4.103) has been inserted:

$$\boxed{\begin{aligned}
&\langle 0,\beta|\; T\, X^{\gamma\alpha}_A(t',t)\, X^{\gamma_j}_j(t_j') \ldots X^{\gamma_\ell}_\ell(t_\ell')\, |0,\beta\rangle = \\
&= -\,\varepsilon^\alpha\, S^{\alpha\gamma}_{\varepsilon_f}(t-t')\, \frac{1}{N}\,\mathrm{Tr}(A)\, \langle 0,\beta|\; T\, X^{\gamma_j}_j(t_j') \ldots X^{\gamma_\ell}_\ell(t_\ell')\, |0,\beta\rangle + \\
&-\,\varepsilon^\alpha\, S^{\alpha\gamma}_{\varepsilon_f}(t-t')\, \frac{1}{2}\sum_c \mathrm{Tr}(A\lambda_c)\, \langle 0,\beta|\; T\, X^{\gamma}_c(t')\, X^{\gamma_j}_j(t_j') \ldots X^{\gamma_\ell}_\ell(t_\ell') |0,\beta\rangle + \\
&+ \sum_k \varepsilon^\alpha\, S^{\alpha\gamma_k}_{\varepsilon_f}(t-t_k')\, \langle 0,\beta|\; T\, X^{\gamma\gamma_k}_{Ak}(t',t_k')\, X^{\gamma_j}_j(t_j') \overset{k}{\ldots} X^{\gamma_\ell}_\ell(t_\ell')\, |0,\beta\rangle \;.
\end{aligned}}$$

(4.107)

In the spin $\frac{1}{2}$ case, the SU(2) group has no symmetric structure factors: $d_{ijk} = 0$, and thus the second term of eq. (4.106) drops out. Then eqs. (4.106) and (4.107) become identical to eqs. (4.15) and (4.18) of ref. [58].

In the spin J case, eq. (4.107) corresponds to eq. (36) of ref. [59] and eq. (4.106) corresponds to eq. (39) of ref. [59]. Note that eq. (39) of ref. [59] is missing the d_{ikc} term. The symmetric structure factor means that the diagrammatic structure is not the same as in the spin $\frac{1}{2}$ case. In particular, we have not succeeded in removing the 2–vertex loop from the chain, although we have succeeded in breaking up the chain some more. The cost of this has been to further complicate the Feynman rules.

4.8.9 BROKEN–CHAIN EXAMPLES OF X_i–OPERATOR T–PRODUCT REDUCTION

The examples presented in section 4.8.7 gave reductions of T–products of X_i–operators in terms of linear chains of S_{ε_f} loops. The chains were not broken. Using eqs. (4.106) and (4.107) as our reduction formulae, we obtain reductions of T–products of X_i–operators in which the chains are broken up, facilitating a self–energy expansion. In this section some specific examples are presented.

$$\boxed{\langle i \rangle_\lambda = 0} \tag{4.108}$$

$$\boxed{\langle i\,j \rangle_\lambda = \mathrm{Tr}(\lambda_i \lambda_j)\; G_{\varepsilon_f}(i\,j)\, \frac{\langle P_1 \rangle}{N\, f_F(\varepsilon_f - \mu)}} \tag{4.109}$$

$$\boxed{\begin{aligned} \langle i\,j\,k \rangle_\lambda = \Big\{ &\mathrm{Tr}(\lambda_k \lambda_j \lambda_i)\; G_{\varepsilon_f}(k\,j\,i) + \mathrm{Tr}(\lambda_i \lambda_j \lambda_k)\; G_{\varepsilon_f}(i\,j\,k) + \\ &+ d_{ijb}\; \mathrm{Tr}(\lambda_b \lambda_k)\; G_{\varepsilon_f}(i\,j)\; G_{\varepsilon_f}(j\,k) + \\ &+ d_{ikb}\; \mathrm{Tr}(\lambda_b \lambda_j)\; G_{\varepsilon_f}(i\,k)\; G_{\varepsilon_f}(k\,j) \Big\} \frac{\langle P_1 \rangle}{N\, f_F(\varepsilon_f - \mu)} \end{aligned}} \tag{4.110}$$

$$\boxed{\begin{gathered}
\langle i\,j\,k\,\ell\rangle_\lambda = \frac{1}{N}\,\mathrm{Tr}(\lambda_i\lambda_j)\;G_{\varepsilon_f}(i\,j)\;\langle k\,\ell\rangle_\lambda\;+\\
+\Big\{\,\mathrm{Tr}(\lambda_i\lambda_j\lambda_k\lambda_\ell)\;G_{\varepsilon_f}(i\,j\,k\,\ell)\;+\\
+\frac{1}{2}\,\mathrm{Tr}(\lambda_i\lambda_j\lambda_c\lambda_k)\;\mathrm{Tr}(\lambda_c\lambda_\ell)\;G_{\varepsilon_f}(i\,j\,k)\;G_{\varepsilon_f}(k\,\ell)\;+\\
+\;d_{ijb}\;\mathrm{Tr}(\lambda_b\lambda_k\lambda_\ell)\;G_{\varepsilon_f}(i\,j)\;G_{\varepsilon_f}(j\,k\,\ell)\;+\\
d_{ijb}\;d_{bkc}\;\mathrm{Tr}(\lambda_c\lambda_\ell)\;G_{\varepsilon_f}(i\,j)\;G_{\varepsilon_f}(j\,k)\;G_{\varepsilon_f}(k\,\ell)\,\Big\}\;\frac{\langle P_1\rangle}{N\,f_F(\varepsilon_f-\mu)}\;+\\
+\text{ all \textbf{\textit{distinct}} permutations of } j,k,\ell
\end{gathered}}
\tag{4.111}$$

$$\boxed{\begin{gathered}
\langle i\,j\,k\,\ell\,m\rangle_\lambda = \frac{1}{N}\,\mathrm{Tr}(\lambda_i\lambda_j)\;G_{\varepsilon_f}(i\,j)\;\langle k\,\ell\,m\rangle_\lambda\;+\\
+\frac{1}{N}\,\mathrm{Tr}(\lambda_i\lambda_j\lambda_k)\;G_{\varepsilon_f}(i\,j\,k)\;\langle \ell\,m\rangle_\lambda\;+\\
+\frac{1}{N}\,d_{ija}\;\mathrm{Tr}(\lambda_a\lambda_k)\;G_{\varepsilon_f}(i\,j)\;G_{\varepsilon_f}(j\,k)\;\langle \ell\,m\rangle_\lambda\;+\\
+\Big\{\,\mathrm{Tr}(\lambda_i\lambda_j\lambda_k\lambda_\ell\lambda_m)\;G_{\varepsilon_f}(i\,j\,k\,\ell\,m)\;+\\
+\frac{1}{2}\,\mathrm{Tr}(\lambda_i\lambda_j\lambda_k\lambda_c\lambda_\ell)\;\mathrm{Tr}(\lambda_c\lambda_m)\;G_{\varepsilon_f}(i\,j\,k\,\ell)\;G_{\varepsilon_f}(\ell\,m)\;+\\
+\frac{1}{2}\,\mathrm{Tr}(\lambda_i\lambda_j\lambda_b\lambda_k)\;\mathrm{Tr}(\lambda_b\lambda_\ell\lambda_m)\;G_{\varepsilon_f}(i\,j\,k)\;G_{\varepsilon_f}(k\,\ell\,m)\;+\\
+\frac{1}{2}\,\mathrm{Tr}(\lambda_i\lambda_j\lambda_b\lambda_k)\;d_{b\ell c}\;\mathrm{Tr}(\lambda_c\lambda_m)\;G_{\varepsilon_f}(i\,j\,k)\;G_{\varepsilon_f}(k\,\ell)\;G_{\varepsilon_f}(\ell\,m)\;+\\
+\;d_{ija}\;\mathrm{Tr}(\lambda_a\lambda_k\lambda_\ell\lambda_m)\;G_{\varepsilon_f}(i\,j)\;G_{\varepsilon_f}(j\,k\,\ell\,m)\;+\\
+\;d_{ija}\,\frac{1}{2}\,\mathrm{Tr}(\lambda_a\lambda_k\lambda_c\lambda_\ell)\;\mathrm{Tr}(\lambda_c\lambda_m)\;G_{\varepsilon_f}(i\,j)\;G_{\varepsilon_f}(j\,k\,\ell)\;G_{\varepsilon_f}(\ell\,m)\;+\\
+\;d_{ija}\;d_{akb}\;\mathrm{Tr}(\lambda_b\lambda_\ell\lambda_m)\;G_{\varepsilon_f}(i\,j)\;G_{\varepsilon_f}(j\,k)\;G_{\varepsilon_f}(k\,\ell\,m)\;+\\
+\;d_{ija}d_{akb}d_{b\ell c}\;\mathrm{Tr}(\lambda_c\lambda_m)\;G_{\varepsilon_f}(i\,j)G_{\varepsilon_f}(j\,k)G_{\varepsilon_f}(k\,\ell)G_{\varepsilon_f}(\ell\,m)\,\Big\}\;\frac{\langle P_1\rangle}{N\,f_F(\varepsilon_f-\mu)}\;+\\
+\text{ all \textbf{\textit{distinct}} permutations of } j,k,\ell,m
\end{gathered}}
\tag{4.112}$$

Here "distinct permutations" means that $\langle i\,j\,k\,\ldots\rangle$ is invariant under permutations of $i,j,k\ldots$; thus for example, we don't permute k,ℓ,m in the first term of eq. (4.112).

Let us denote the unbroken chains in $\langle i\,j\ldots\rangle$ by $\{i\,j\ldots\}$. There is a factor of $\frac{1}{N}$ arising each time the chain is broken. We therefore absorb this $\frac{1}{N}$ into the definition of $\{i\,j\ldots\}$, along with the $\frac{1}{N}$ from $\frac{\langle P_1\rangle}{N\, f_F(\varepsilon_f-\mu)}$. From eqs. (4.109) – (4.112), one finds:

$$\langle i\,j\rangle_\lambda = \{i\,j\}\,\frac{\langle P_1\rangle}{f_F(\varepsilon_f-\mu)} \tag{4.113}$$

$$\langle i\,j\,k\rangle_\lambda = \{i\,j\,k\}\,\frac{\langle P_1\rangle}{f_F(\varepsilon_f-\mu)} \tag{4.114}$$

$$\langle i\,j\,k\,\ell\rangle_\lambda = \Big[\,\{i\,j\,k\,\ell\} + \{i\,j\}\{k\,\ell\} + \{i\,k\}\{j\,\ell\} + \{i\,\ell\}\{j\,k\}\,\Big]\,\frac{\langle P_1\rangle}{f_F(\varepsilon_f-\mu)} \tag{4.115}$$

$$\begin{aligned}\langle i\,j\,k\,\ell\,m\rangle_\lambda = \Big[\,&\{i\,j\,k\,\ell\,m\} + \{i\,j\,k\}\{\ell\,m\} + \{i\,j\,\ell\}\{k\,m\} + \{i\,j\,m\}\{k\,\ell\} + \\ &+ \{i\,k\,\ell\}\{j\,m\} + \{i\,k\,m\}\{j\,\ell\} + \{i\,\ell\,m\}\{j\,k\} + \{i\,j\}\{k\,\ell\,m\} + \\ &+ \{i\,k\}\{j\,\ell\,m\} + \{i\,\ell\}\{j\,k\,m\} + \{i\,m\}\{j\,k\,\ell\}\,\Big]\,\frac{\langle P_1\rangle}{f_F(\varepsilon_f-\mu)}\,.\end{aligned} \tag{4.116}$$

The general term may be written as follows:

$$\langle j_1 j_2 \cdots j_n\rangle_\lambda = \sum_{\substack{\alpha+\beta+\ldots+\gamma=n \\ \text{all distinct subsets}}} \{j_{a_1}\cdots j_{a_\alpha}\}\,\{j_{b_1}\cdots j_{b_\beta}\}\cdots\{j_{c_1}\cdots j_{c_\gamma}\}\,\frac{\langle P_1\rangle}{f_F(\varepsilon_f-\mu)} \tag{4.117}$$

where the meaning of "distinct subsets" is illustrated by:

$$\left.\begin{array}{c}\{j_{a_1}\cdots j_{a_\alpha}\}\,\{j_{b_1}\cdots j_{b_\beta}\} = \{j_{b_1}\cdots j_{b_\beta}\}\,\{j_{a_1}\cdots j_{a_\alpha}\} \\ \{j_{a_1}\cdots j_{a_\alpha}\} = \{P(j_{a_1}\cdots j_{a_\alpha})\}\end{array}\right\} \tag{4.118}$$

where P is the permutation operator.

Examples of $\{j_1\ldots j_n\}$ are given below:

$$\{i\,j) = \frac{1}{N}\,\mathrm{Tr}(\lambda_i\lambda_j)\;G_{\varepsilon_f}(i\,j) \tag{4.119}$$

$$\begin{aligned}\{i\,j\,k\} = \frac{1}{N}\Big\{ & \mathrm{Tr}(\lambda_k\lambda_j\lambda_i)\, G_{\varepsilon_f}(k\,j\,i) + \mathrm{Tr}(\lambda_i\lambda_j\lambda_k)\, G_{\varepsilon_f}(i\,j\,k) + \\ & + d_{ijb}\, \mathrm{Tr}(\lambda_b\lambda_k)\, G_{\varepsilon_f}(i\,j)\, G_{\varepsilon_f}(j\,k) + d_{ikb}\, \mathrm{Tr}(\lambda_b\lambda_j)\, G_{\varepsilon_f}(i\,k)\, G_{\varepsilon_f}(k\,j) \Big\}\end{aligned} \tag{4.120}$$

$$\begin{aligned}\{i\,j\,k\,l\} = \frac{1}{N}\Big\{ & \mathrm{Tr}(\lambda_i\lambda_j\lambda_k\lambda_\ell)\, G_{\varepsilon_f}(i\,j\,k\,\ell) + \\ & + \tfrac{1}{2}\, \mathrm{Tr}(\lambda_i\lambda_j\lambda_c\lambda_k)\, \mathrm{Tr}(\lambda_c\lambda_\ell)\, G_{\varepsilon_f}(i\,j\,k)\, G_{\varepsilon_f}(k\,\ell) + \\ & + d_{ijb}\, \mathrm{Tr}(\lambda_b\lambda_k\lambda_\ell)\, G_{\varepsilon_f}(i\,j)\, G_{\varepsilon_f}(j\,k\,\ell) + \\ & + d_{ijb}\, d_{bkc}\, \mathrm{Tr}(\lambda_c\lambda_\ell)\, G_{\varepsilon_f}(i\,j)\, G_{\varepsilon_f}(j\,k)\, G_{\varepsilon_f}(k\,\ell) + \text{all permutations of } j,k,\ell \Big\}\end{aligned} \tag{4.121}$$

$$\begin{aligned}\{i\,j\,k\,\ell\,m\} = \frac{1}{N}\Big\{ & \mathrm{Tr}(\lambda_i\lambda_j\lambda_k\lambda_\ell\lambda_m)\, G_{\varepsilon_f}(i\,j\,k\,\ell\,m) + \\ & + \tfrac{1}{2}\, \mathrm{Tr}(\lambda_i\lambda_j\lambda_k\lambda_c\lambda_\ell)\, \mathrm{Tr}(\lambda_c\lambda_m)\, G_{\varepsilon_f}(i\,j\,k\,\ell)\, G_{\varepsilon_f}(\ell\,m) + \\ & + \tfrac{1}{2}\, \mathrm{Tr}(\lambda_i\lambda_j\lambda_b\lambda_k)\, \mathrm{Tr}(\lambda_b\lambda_\ell\lambda_m)\, G_{\varepsilon_f}(i\,j\,k)\, G_{\varepsilon_f}(k\,\ell\,m) + \\ & + \tfrac{1}{2}\, \mathrm{Tr}(\lambda_i\lambda_j\lambda_b\lambda_k)\, d_{b\ell c}\, \mathrm{Tr}(\lambda_c\lambda_m)\, G_{\varepsilon_f}(i\,j\,k)\, G_{\varepsilon_f}(k\,\ell)\, G_{\varepsilon_f}(\ell\,m) + \\ & + d_{ija}\, \mathrm{Tr}(\lambda_a\lambda_k\lambda_\ell\lambda_m)\, G_{\varepsilon_f}(i\,j)\, G_{\varepsilon_f}(j\,k\,\ell\,m) + \\ & + d_{ija}\, \tfrac{1}{2}\, \mathrm{Tr}(\lambda_a\lambda_k\lambda_c\lambda_\ell)\, \mathrm{Tr}(\lambda_c\lambda_m)\, G_{\varepsilon_f}(i\,j)\, G_{\varepsilon_f}(j\,k\,\ell)\, G_{\varepsilon_f}(\ell\,m) + \\ & + d_{ija}\, d_{akb}\, \mathrm{Tr}(\lambda_b\lambda_\ell\lambda_m)\, G_{\varepsilon_f}(i\,j)\, G_{\varepsilon_f}(j\,k)\, G_{\varepsilon_f}(k\,\ell\,m) + \\ & + d_{ija} d_{akb} d_{b\ell c}\, \mathrm{Tr}(\lambda_c\lambda_m)\, G_{\varepsilon_f}(i\,j) G_{\varepsilon_f}(j\,k) G_{\varepsilon_f}(k\,\ell) G_{\varepsilon_f}(\ell\,m) + \\ & + \text{all permutations of } j,k,\ell,m \Big\}\end{aligned} \tag{4.122}$$

4.9 DIAGRAMMATIC REPRESENTATION OF FEYNMAN RULES

4.9.1 THE BUILDING BLOCKS

Feynman diagrams in this model are composed of $S^{\alpha\gamma}_{\varepsilon_f}(t-t')$ propagators and X or X_i-operator T-products connected together at spontaneous vertices.

The S_{ε_f} propagators are defined in terms of the ξ–operator T–product as in sect. 4.3.2. The choice of whether we use X or X_i–operator T–products depends on whether we use non–SU(N) or SU(N) rules, respectively. We will represent S_{ε_f} propagators by solid lines, and X or X_i–operator T–products by wiggly lines. Of course, the wiggly lines may be decomposed into linear chains of solid line loops as in FIG 4.2, but this is in general very complicated. The wiggly lines are a useful shorthand when considering the diagrammatics, although they must be decomposed into their S_{ε_f} components in an actual calculation.

There are two types of spontaneous vertices which arise: the non–wiggle vertex and the wiggle vertex. These are illustrated in FIG. 4.3. The non–wiggle vertex connects three S_{ε_f} lines, and the wiggle vertex connects an S_{ε_f} line to a wiggle line.

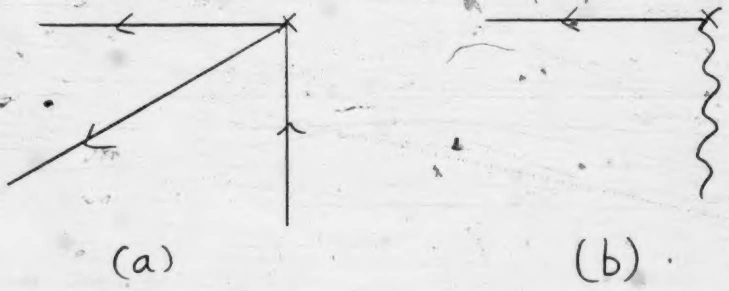

FIG. 4.3

The Two Spontaneous Vertices

This shows the two spontaneous vertices which arise in the absence of any interaction. (a) illustrates the spontaneous non–wiggle vertex. (b) illustrates the spontaneous wiggle vertex.

The details of these vertices depend on whether one uses the SU(N) rules or the non–SU(N) rules, and will be discussed below.

There also exist vertices which start and end an S_{ϵ_f} propagator which stands alone, ie. it is not connected to any other S_{ϵ_f} lines or wiggle lines. These vertices will be called the non–spontaneous vertices. They too have certain rules which will be discussed below.

A major difference between this theory and the usual quantum field theory is the sector structure. As discussed in sect. 4.3.4, there is a $\langle P_o \rangle$ sector and a $\langle P_1 \rangle$ sector. Each sector has its own Feynman rules. For example, the wiggly lines appear only in the $\langle P_1 \rangle$ sector.

The diagrammatic procedure is as follows. Construct all the Feynman diagrams in the $\langle P_o \rangle$ sector using the appropriate rules for propagators and vertices. Then multiply by an overall factor which is specific to the $\langle P_o \rangle$ sector. Repeat this process for $\langle P_1 \rangle$ sector, and add the two expressions.

The details, using non–SU(N) rules and SU(N) rules are presented in the following sections.

4.9.2 THE NON–SU(N) RULES

4.9.2.1 The ξ–Propagator

The $S^{\alpha\gamma}_{\epsilon_f}(t-t')$ propagator will be represented by a solid line with an arrow directed from t' to t, t' being the $\xi^{\dagger\gamma}$ end of the propagator, and t being the ξ^{α} end of the propagator. The $\xi^{\dagger\gamma}$ end (tail) of the propagator will be represented by a cross. This is the end which, by convention, may form a spontaneous vertex. At the tip of the propagator will be a small circle, but only if it ends in ξ^{α} and not a spontaneous vertex. This is illustrated in FIG. 4.4. If the tip of the propagator ends in a spontaneous vertex, then it will be a cross as well.

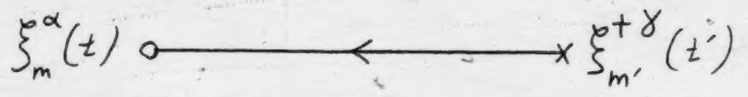

FIG. 4.4
The $S^{\alpha\gamma}_{\varepsilon_f}(t-t')$ Propagator

4.9.2.2 The X–Operator Function: Wiggle Diagrams

The n–point X–operator function $\langle j_1 j_2 \cdots j_n \rangle$ will be represented by n wiggly lines radiating out from a central point and ending in n crosses. This is illustrated in FIGS. 4.5a to 4.5d.

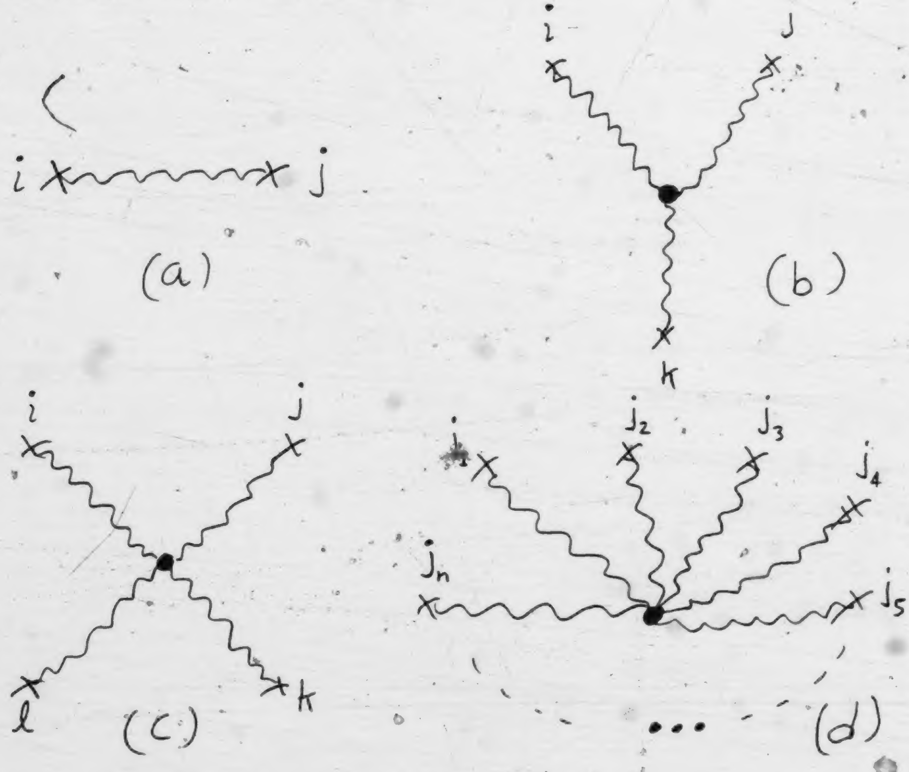

FIG. 4.5
The Non–SU(N) Wiggle Diagrams

(a) illustrates $\langle i\, j \rangle$, the 2–wiggle. (b) illustrates $\langle i\, j\, k \rangle$, the 3–wiggle. (c) illustrates $\langle i\, j\, k\, \ell \rangle$, the 4–wiggle. (d) illustrates $\langle j_1 j_2 \cdots j_n \rangle$, the n–wiggle. These represent the 2–, 3–, 4–, and n–point X–operator functions.

4.9.2.3 Vertex Types

There are four types of vertices: one dot vertex and three cross vertices. These are illustrated in FIG. 4.6. One cross vertex is non–spontaneous, another is a spontaneous non–wiggle vertex, and the other is a spontaneous wiggle vertex.

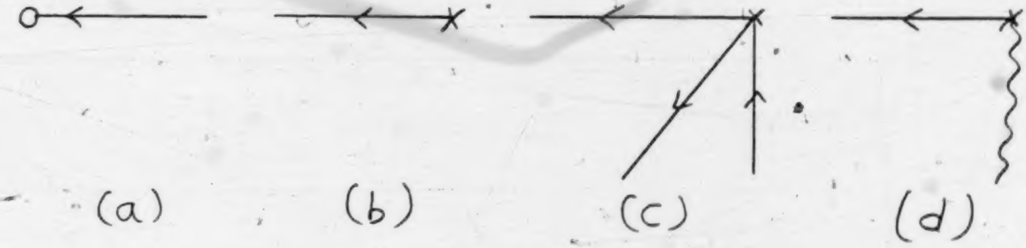

FIG. 4.6
The Vertices

(a) is the dot vertex, which represents the ξ end of the propagator. By convention, it never forms a spontaneous vertex. (b) is the non–spontaneous cross vertex. (c) is the spontaneous non–wiggle vertex. (d) is the spontaneous wiggle vertex.

4.9.2.4 Spin Labeling

Before presenting the rules for vertices, we must spin–label the diagrams. This is somewhat confusing, because the spin of an $S^{\alpha\gamma}_{\epsilon_f}(t-t')$ propagator is that of $\xi^{\alpha}_{m}(t)$ rather than $\xi^{\dagger\gamma}_{m'}(t')$. (This comes from the nature of the generalized Wick's theorem, eq. (3.13).) Therefore S_{ϵ_f} lines ending in a dot will be labeled with m, which is the spin of the $\xi^{\alpha}_{m}(t)$ sitting at the dot. The dot itself is not labeled with spin. The cross, though, will be labeled with m′, which is the spin of the $\xi^{\dagger\gamma}_{m'}(t')$ sitting at the cross. S_{ϵ_f} lines ending in a spontaneous vertex will be labeled with a dummy spin, ℓ. Spin labeling is illustrated in FIGS. 4.7a – 4.7c.

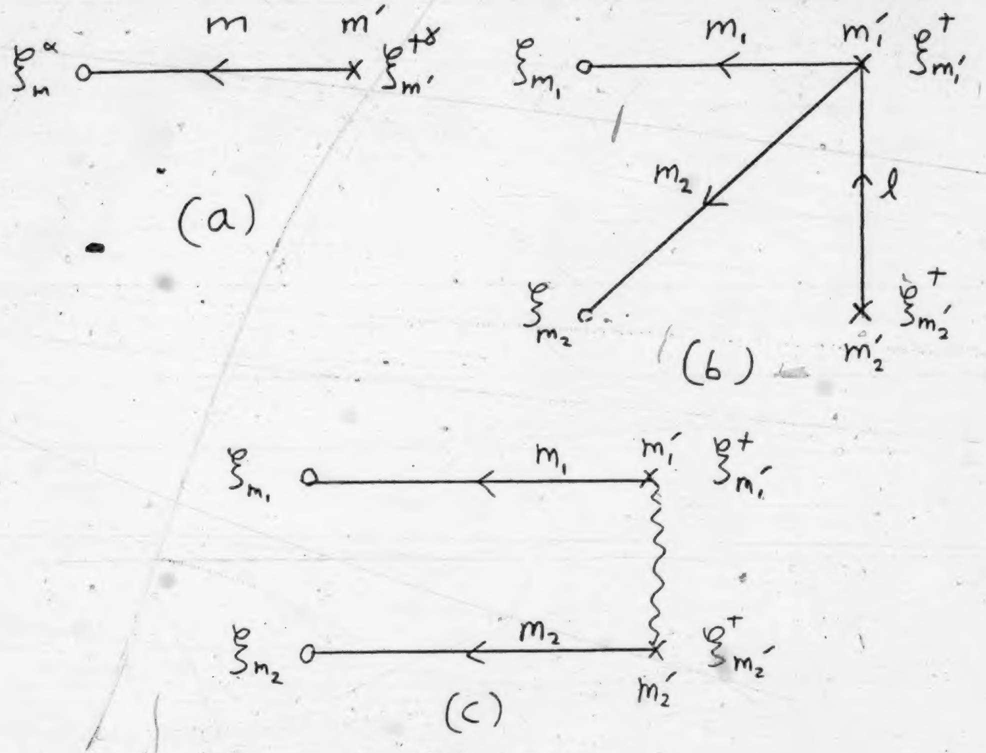

FIG. 4.7

Non–SU(N) Spin Labeling of Diagrams

Lines carry the spin of the ξ–operator. Crosses carry the spin of the $\xi^\dagger$–operator. The dot is not labeled. (a) shows the spin labeling of the S_{ε_f} propagator. (b) shows the spin labeling of a spontaneous non–wiggle vertex. Note the dummy spin ℓ which arises spontaneously. (c) shows the spin labeling of wiggle line vertices.

Note that the wiggle lines are not labeled by spin until they have been decomposed into their component S_{ε_f} lines. This will be shown below.

As usual, the vertices will also be labeled with α and γ the thermal indices, as well as with t and t′. In the Fourier representation, each S_{ε_f} line will carry energy and there will be energy conservation at each vertex. This labeling has been suppressed in order to clarify the spin labeling. The wiggle lines are not labeled by energy until they have been decomposed into their component S_{ε_f} lines.

4.9.2.5 Feynman Rules for Vertices

The Feynman rules for vertices in the $\langle P_o \rangle$ sector are illustrated in FIG. 4.8. A dot vertex has no effect other than multiplication by 1. There are only 2 types of cross vertices in the $\langle P_o \rangle$ sector: the non–spontaneous one and the spontaneous non–wiggle one. The former cross vertex carries only $\delta_{mm'}$ where m is the spin of the S_{ε_f} line and m′ is the spin of the cross. The spontaneous non–wiggle vertex carries $(-\delta_{m_1m_1'}\delta_{m_2\ell} + \delta_{m_1\ell}\delta_{m_2m_1'})\varepsilon^{\gamma}$, where m_1' is the spin label of the cross, ℓ is the dummy spin label of the S_{ε_f} line which is incoming, and m_1 and m_2 are the spin labels of the S_{ε_f} lines which are outgoing. The outgoing lines differ in that the m_1 line comes from the initial contraction of $\xi^{\alpha_1}_{m_1}$ with $\xi^{\dagger\gamma}_{m_1'}$ whereas the m_2 line comes from the secondary contraction of $\xi^{\alpha_2}_{m_2}$ with $M^{\gamma}_{m_1m_1'}$. Here $\varepsilon^{(1)} = 1$ and $\varepsilon^{(2)} = -1$. Note that wiggle lines do not appear in the $\langle P_o \rangle$ sector.

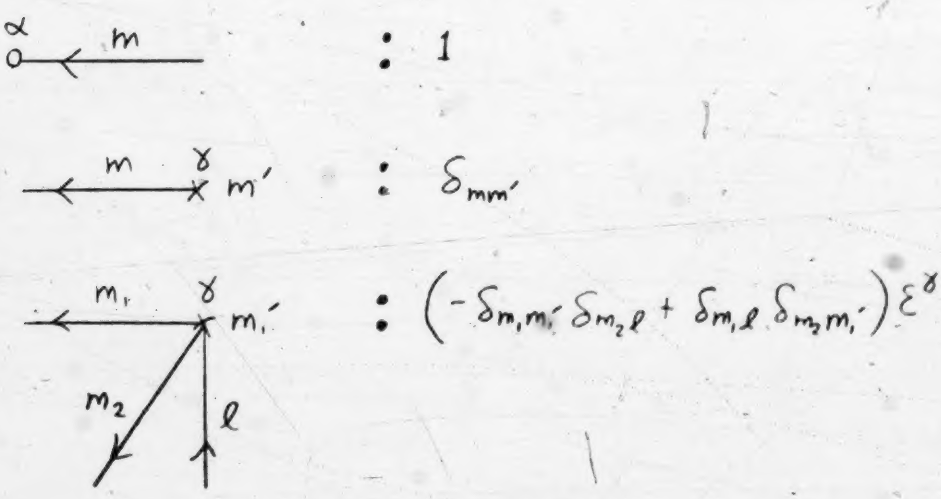
α
m
: 1
m
γ
m′
: $\delta_{mm'}$
m_1
γ
m_1'
: $(-\delta_{m_1m_1'}\delta_{m_2\ell} + \delta_{m_1\ell}\delta_{m_2m_1'})\varepsilon^{\gamma}$
m_2
ℓ

FIG. 4.8

Non–SU(N) Feynman Rules for Vertices in the $\langle P_o \rangle$ Sector

The Feynman rules for vertices in the $\langle P_1 \rangle$ sector are illustrated in FIG. 4.9. They are very similar to the rules in the $\langle P_o \rangle$ sector, except that this sector has the wiggle vertex as well. The details of the wiggle vertex will be shown when the wiggle diagrams are decomposed.

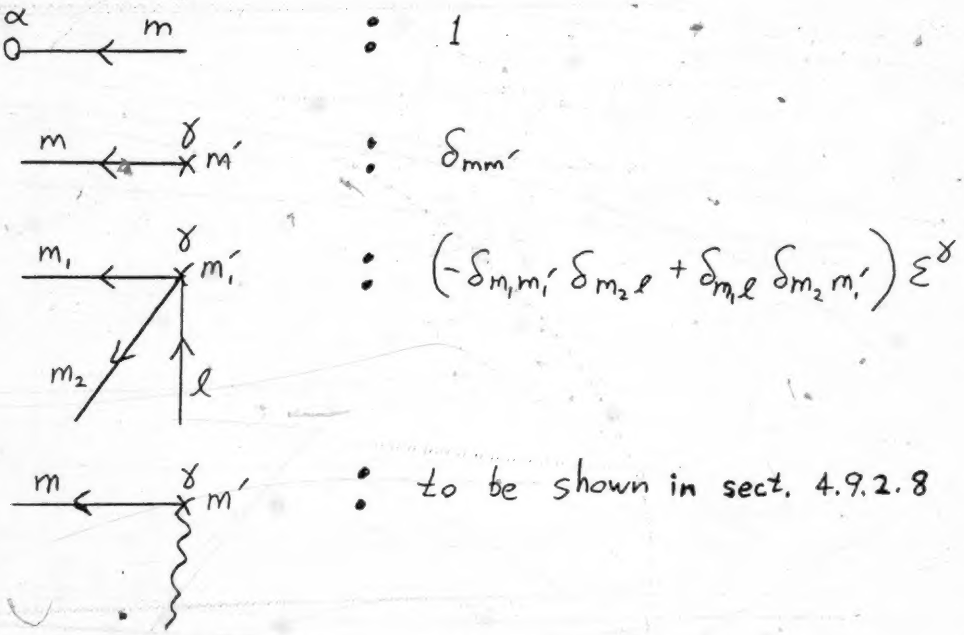
α
m
: 1
m
γ
m′
: $\delta_{mm'}$
m₁
γ
m₁′
m₂
ℓ
: $\left(-\delta_{m_1 m_1'}\delta_{m_2 \ell} + \delta_{m_1 \ell}\delta_{m_2 m_1'}\right)\varepsilon^{\gamma}$
m
γ
m′
: to be shown in sect. 4.9.2.8

FIG. 4.9

Non–SU(N) Feynman Rules for Vertices in the $\langle P_1 \rangle$ Sector

4.9.2.6 Feynman Rules for the n–Point ξ–function

Construction of diagrams for the n–point ξ–function proceeds according to the following rules:

1) Define:

$$\Gamma^{\{\alpha\}\{\gamma\}}_{n\{m\}\{m'\}}(\{t\},\{t'\}) \equiv$$

$$\equiv \langle 0,\beta| T\, \xi^{\alpha_1}_{m_1}(t_1)\, \xi^{\dagger\,\gamma_1}_{m_1'}(t_1')\, \xi^{\alpha_2}_{m_2}(t_2)\, \xi^{\dagger\,\gamma_2}_{m_2'}(t_2') \ldots \xi^{\alpha_{n/2}}_{m_{n/2}}(t_{n/2})\, \xi^{\dagger\,\gamma_{n/2}}_{m_{n/2}'}(t_{n/2}')|0,\beta\rangle \tag{4.123}$$

2) Draw $\frac{n}{2}$ dots and $\frac{n}{2}$ crosses.

3) Start with the $\langle P_o \rangle$ sector. Draw lines connecting the dots and crosses according to the rules for vertices in FIG 4.8. There are no restrictions on how many crosses form spontaneous vertices, other than the fact that at least one cross must remain as a non-spontaneous vertex.

4) Note that the S_{ε_f} lines are not allowed to form closed loops. (Such loops are only allowed in the decomposition of the wiggle diagrams which appear in the $\langle P_1 \rangle$ sector.)

5) Spin label all lines and crosses as in FIG. 4.7.

6) Keep in mind that each dot and cross is also labelled by thermal index and time.

7) For each line write $S^{\alpha\gamma}_{\varepsilon_f}(t-t')$.

8) For each vertex use the vertex factors shown in FIG. 4.8.

9) The overall sign of the diagram is determined by the anti-commutation of ξ-operators in the T-product.

10) A completed diagram carries an overall factor of $<P_o>$.

11) Now do the $\langle P_1 \rangle$ sector. Construct a diagram identical to one which appears in the $\langle P_o \rangle$ sector and spin label it as before.

12) Suppose there are p non-spontaneous cross vertices, where $1 \leq p \leq n/2$. These vertices must be connected by a p-point wiggle-line diagram, $\langle j_1 j_2 \cdots j_p \rangle$.

13. If there is only one non-spontaneous cross vertex, then it remains as is. Thus there is a maximum of one non-spontaneous cross vertex per diagram, and it app[illegible] only when there are no wiggle lines.

14) For each non-wiggle vertex, use the vertex factors shown in FIG. 4.9.

15) A completed diagram with no wiggle vertices carries an overall factor of $\langle P_1 \rangle / N$.

16) The rules for wiggle diagrams are discussed below.

4.9.2.7 Decomposition of Wiggle Diagrams; Spin Labelling

Wiggle–line diagrams are decomposed as in FIG. 4.2. A starting point of the reduction is chosen and labelled "i" (or "1"). The i (or 1) vertex is the start of a linear chain of loops connecting all vertices. It is the second vertex of each loop which forms the link to the next loop. In keeping with the above spin labelling, we label the lines by m, the spin of the ξ^{α}_{m} operator, and we label the crosses by m′, the spin of the $\xi^{\gamma\dagger}_{m'}$ operator. Note that $X_{m'm} = \xi^{\dagger}_{m'}\xi_{m}$ in the reduction formulae of eqs. (4.56).

Eq. (4.56c) comes from the alternate reduction, in which S_{ε_f} carries the spin of $\xi^{\dagger}_{m'_i}$ rather than ξ_{m_i}. But the equation has $\delta_{m'_i m_k}$, so one may say that S_{ε_f} carries a spin of m_k. Eq. (4.56d) comes from the regular reduction, so S_{ε_f} carries a spin of m. Thus one finds that the S_{ε_f} line incoming to vertex i carries spin m_i, and the line incoming to vertex k carries spin m_k. Continuing this analysis reveals the spin labelling illustrated in FIGS. 4.10(a) – 4.10(d).

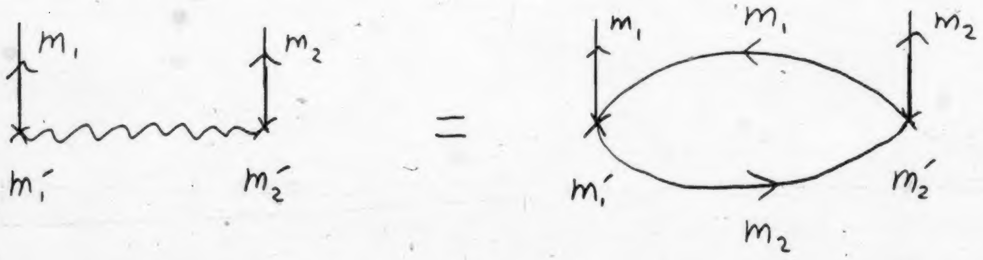

FIG. 4.10(a)
Spin Labelling the Non–SU(N) 2–Wiggle

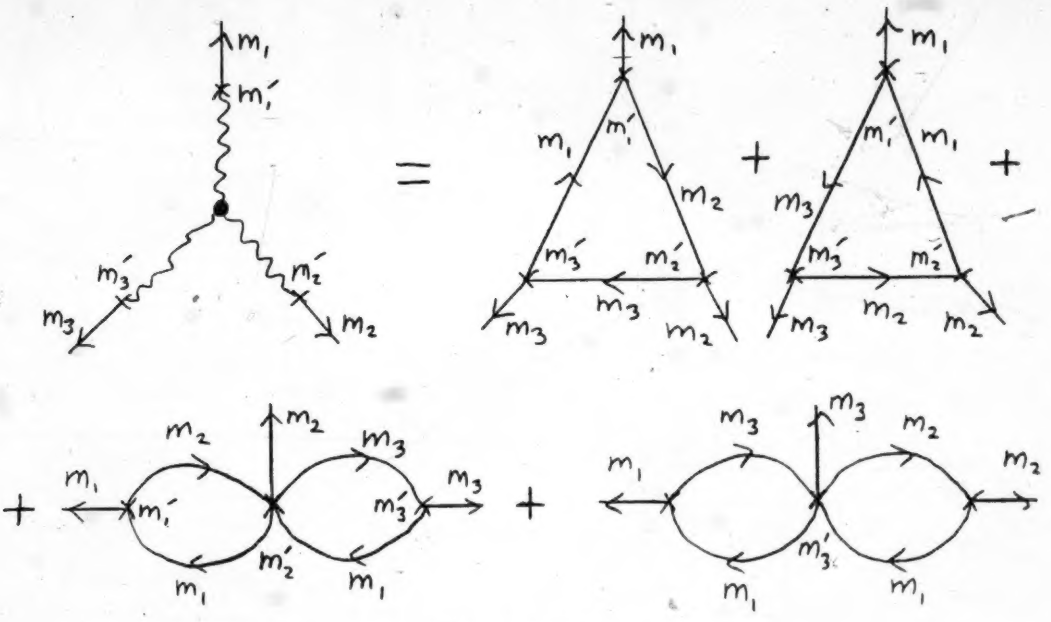
m_1
m_1'
m_3'
m_2'
m_3
m_2
=
+
+
+
m_1
m_2
m_3
m_1'
m_2'
m_3'

FIG. 4.10(b)
Spin Labeling the Non–SU(N) 3–Wiggle

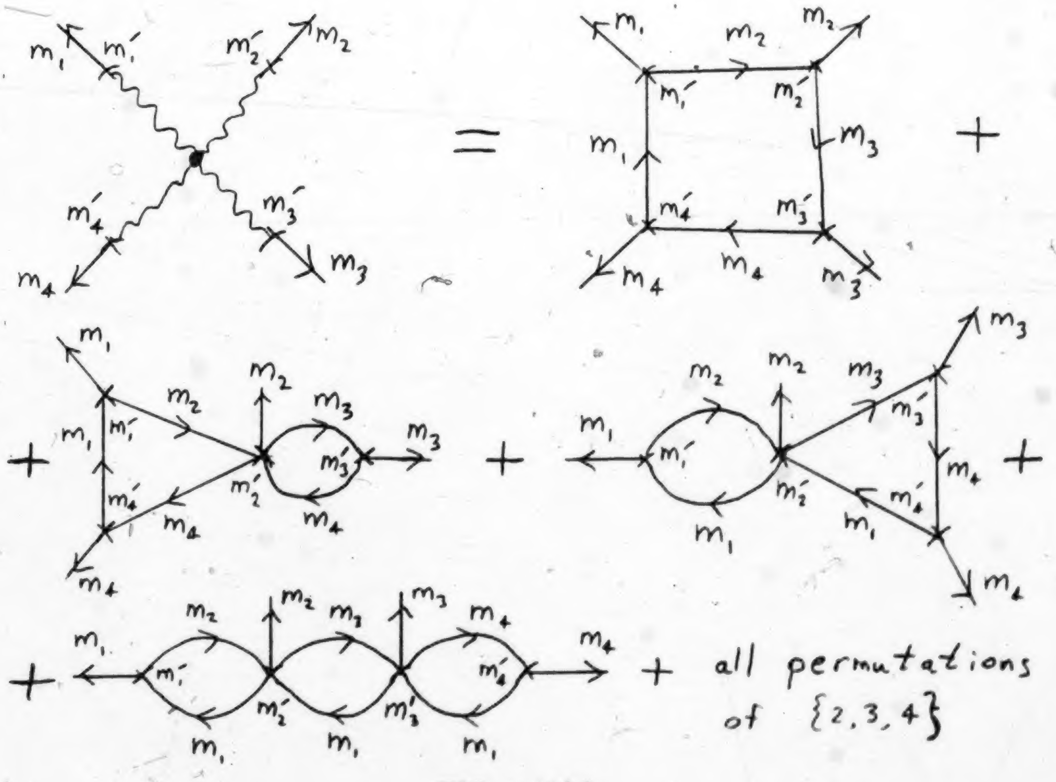
m_1
m_1'
m_2'
m_2
m_4'
m_3'
m_4
m_3
=
+
+
+
+
m_1
m_2
m_3
m_4
m_1'
m_2'
m_3'
m_4'
+ all permutations of {2,3,4}

FIG. 4.10(c)
Spin Labeling the Non–SU(N) 4–Wiggle

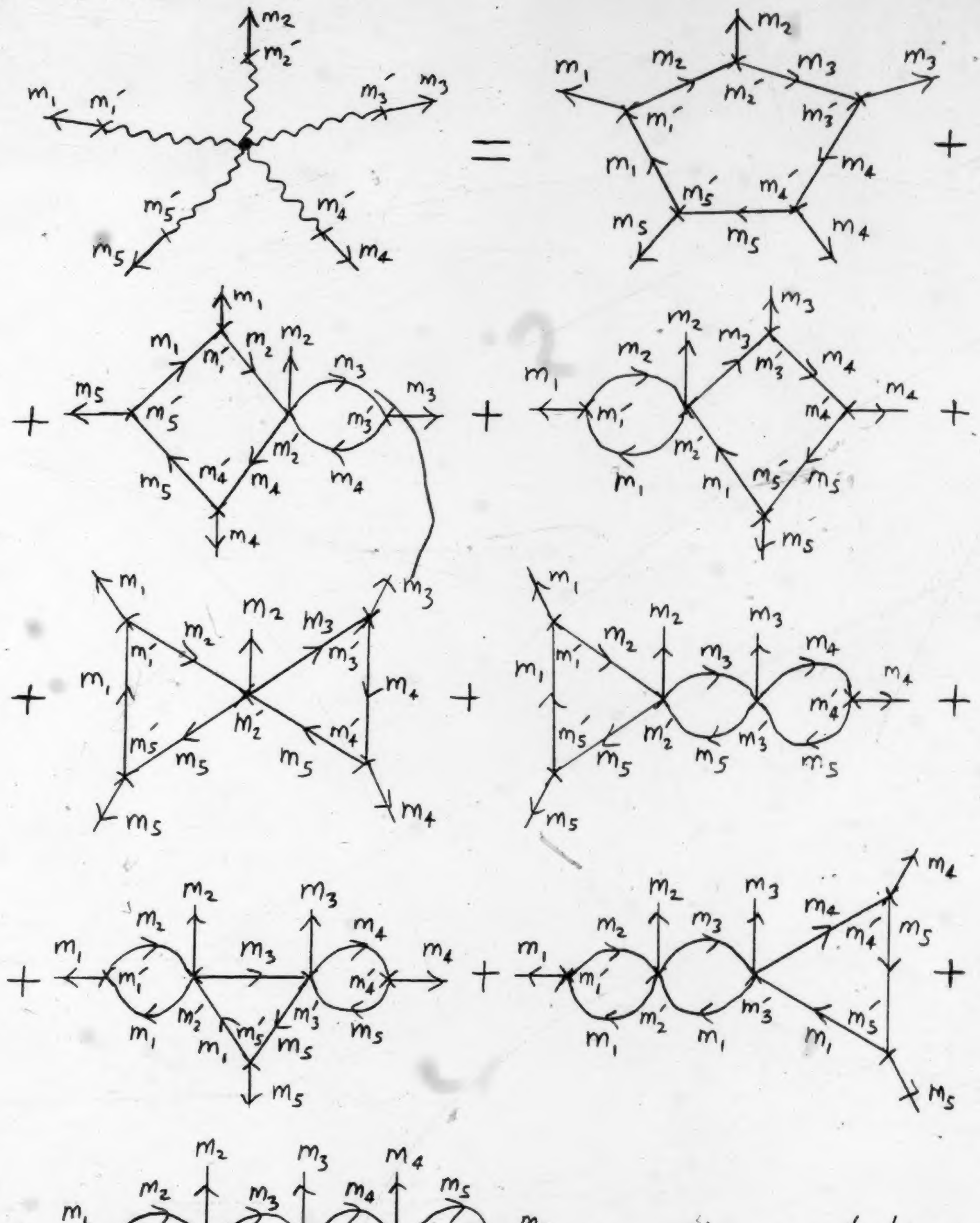
m_1
m_1'
m_2
m_2'
m_3
m_3'
m_4
m_4'
m_5
m_5'
=
+
+ all permutations of {2,3,4,5}

FIG. 4.10(d)
Spin Labeling the Non–SU(N) 5–Wiggle

4.9.2.8 Feynman Rules for Wiggle Vertices

The above illustrates that the vertex between S_{ε_f} and a wiggle line is actually either a 3–point or a 5–point S_{ε_f} vertex. The Feynman rules for these wiggle vertices are illustrated in FIGS. 4.11a – 4.11b.

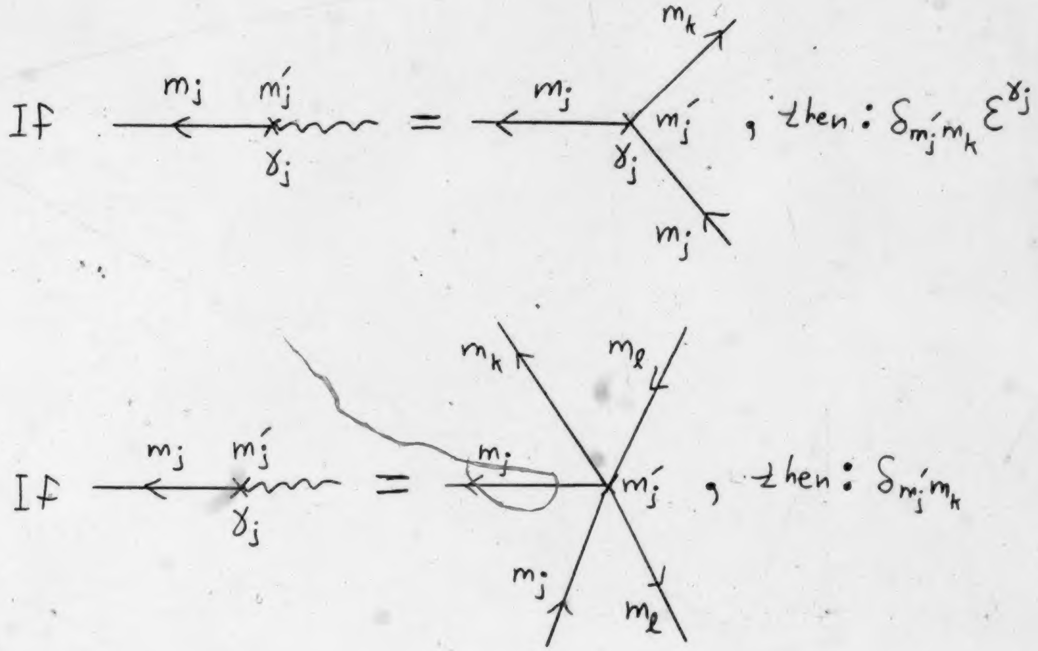
If
m_j
m_j'
γ_j
=
m_j
m_k
m_j'
γ_j
m_j
, then: $\delta_{m_j' m_k} \varepsilon^{\gamma_j}$
If
m_j
m_j'
γ_j
=
m_j
m_k
m_ℓ
m_j'
m_j
m_ℓ
, then: $\delta_{m_j' m_k}$

FIG. 4.11
Non–SU(N) Feynman Rules for Wiggle Vertices

An n–point X–operator T–product is diagrammatically decomposed and labeled as in FIG. 4.10, using the vertex factors of FIG. 4.11, with a $-1/f_F(-\varepsilon_f+\mu)$ for each loop, and carrying an overall factor of $\langle P_1\rangle/N\, f_F(\varepsilon_f-\mu)$.

4.9.2.9 Completion of Feynman Rules for the n–point ξ–Function

We are now ready to complete the non–SU(N) Feynman rules for the n–point ξ–function:

15) Decompose wiggle diagrams into all possible linear chains of loops,

choosing a vertex i (or 1) to be fixed as the starting point of the chain, and permuting over all other vertices. The link between two loops must occur at the second vertex of each successive loop.

17) Spin label the lines which form the loops as in FIG. 4.10.

18. For each line which forms part of a loop write $S^{\alpha\gamma}_{\tilde{\varepsilon}_f}(t-t')$, where $\tilde{\varepsilon}_f$ may be chosen arbitrarily.

19. For each loop vertex, use the vertex factors shown in FIG. 4.11.

20) Each complete loop carries an overall factor of $-1/f_F(-\tilde{\varepsilon}_f+\mu)$, where $\tilde{\varepsilon}_f$ has the same value as chosen in step 18.

21) A completed diagram which has wiggle lines carries an overall factor of $\dfrac{\langle P_1\rangle}{N\, f_F(\tilde{\varepsilon}_f-\mu)}$, where $\tilde{\varepsilon}_f$ has the same value as chosen in step 18.

4.9.2.10 The 2–Point, 4–Point, and 6–Point ξ–Functions

The application of these Feynman rules is illustrated for the 2–point, 4–point, and 6–point ξ–functions in FIGS. 4.12 – 4.14 below:

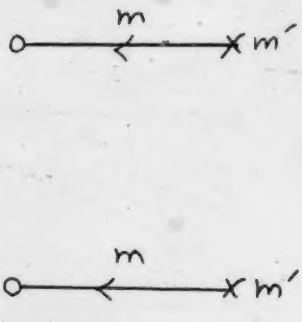

$$= \delta_{mm'}\, S^{\alpha\gamma}_{\varepsilon_f}(t-t')\, \langle P_0 \rangle$$

(a)

$$= \delta_{mm'}\, S^{\alpha\gamma}_{\varepsilon_f}(t-t')\, \frac{\langle P_1 \rangle}{N}$$

(b)

FIG. 4.12

The 2–Point ξ-Function with Non–SU(N) Rules

(a) shows the rules in the $\langle P_0\rangle$ sector. (b) shows the rules in the $\langle P_1\rangle$ sector.

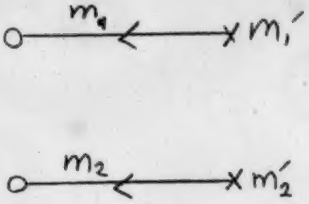

$$= \delta_{m_1 m_1'} \delta_{m_2 m_2'} S_{\varepsilon_f}^{\alpha_1\gamma_1}(t_1 - t_1') S_{\varepsilon_f}^{\alpha_2\gamma_2}(t_2 - t_2') \langle P_0 \rangle$$

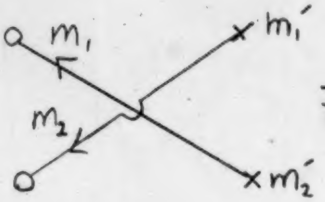

$$= -\delta_{m_1 m_2'} \delta_{m_2 m_1'} S_{\varepsilon_f}^{\alpha_1\gamma_2}(t_1 - t_2') S_{\varepsilon_f}^{\alpha_2\gamma_1}(t_2 - t_1') \langle P_0 \rangle$$

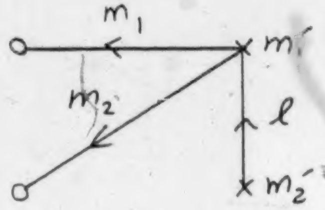

$$= \left(-\delta_{m_1 m_1'} \delta_{m_2 l} + \delta_{m_1 l} \delta_{m_2 m_1'}\right) \varepsilon^{\gamma_1} \delta_{l m_2'} \times$$

$$\times S_{\varepsilon_f}^{\alpha_1\gamma_1}(t_1 - t_1') S_{\varepsilon_f}^{\alpha_2\gamma_1}(t_2 - t_1') S_{\varepsilon_f}^{\gamma_1\gamma_2}(t_1' - t_2') \langle P_0 \rangle .$$

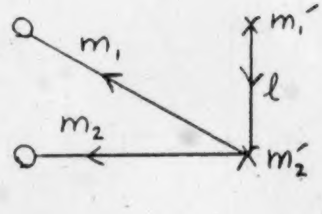

$$= -\left(-\delta_{m_1 m_2'} \delta_{m_2 l} + \delta_{m_1 l} \delta_{m_2 m_2'}\right) \varepsilon^{\gamma_2} \delta_{l m_1'} \times$$

$$\times S_{\varepsilon_f}^{\alpha_1\gamma_2}(t_1 - t_2') S_{\varepsilon_f}^{\alpha_2\gamma_2}(t_2 - t_2') S_{\varepsilon_f}^{\gamma_2\gamma_1}(t_2' - t_1') \langle P_0 \rangle$$

FIG. 4.13(a)
The 4–Point ξ-Function in the $\langle P_0 \rangle$ Sector with Non–SU(N) Rules

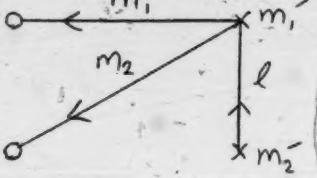

$$= \left(-\delta_{m_1 m_1'}\delta_{m_2 \ell} + \delta_{m_1 \ell}\delta_{m_2 m_1'}\right)\varepsilon^{\gamma_1}\delta_{\ell m_2'} \times$$
$$\times\, S^{\alpha_1\gamma_1}_{\varepsilon_f}(t_1-t_1')\, S^{\alpha_2\gamma_1}_{\varepsilon_f}(t_2-t_1')\, S^{\gamma_1\gamma_2}_{\varepsilon_f}(t_1'-t_2')\,\frac{\langle P_1\rangle}{N}$$

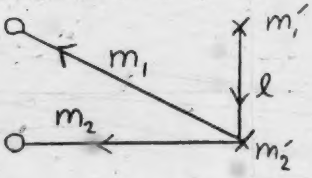

$$= -\left(-\delta_{m_1 m_2'}\delta_{m_2 \ell} + \delta_{m_1 \ell}\delta_{m_2 m_2'}\right)\varepsilon^{\gamma_2}\delta_{\ell m_1'} \times$$
$$\times\, S^{\alpha_1\gamma_2}_{\varepsilon_f}(t_1-t_2')\, S^{\alpha_2\gamma_2}_{\varepsilon_f}(t_2-t_2')\, S^{\gamma_2\gamma_1}_{\varepsilon_f}(t_2'-t_1')\,\frac{\langle P_1\rangle}{N}$$

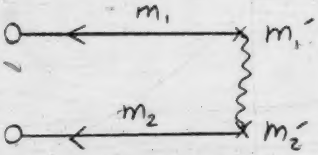

$$=$$

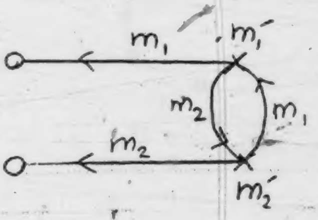

$$=$$

$$= \delta_{m_1' m_2}\delta_{m_2' m_1}\varepsilon^{\gamma_1}\varepsilon^{\gamma_2} S^{\alpha_1\gamma_1}_{\varepsilon_f}(t_1-t_1')\, S^{\alpha_2\gamma_2}_{\varepsilon_f}(t_2-t_2') \times$$
$$\times(-)\frac{S^{\gamma_1\gamma_2}_{\tilde{\varepsilon}_f}(t_1'-t_2')\, S^{\gamma_2\gamma_1}_{\tilde{\varepsilon}_f}(t_2'-t_1')}{f_F(-\tilde{\varepsilon}_f+\mu)}\;\frac{\langle P_1\rangle}{N f_F(\tilde{\varepsilon}_f-\mu)}$$

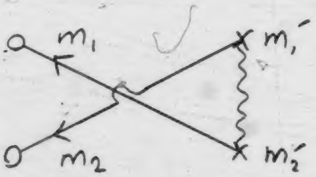

$$=$$

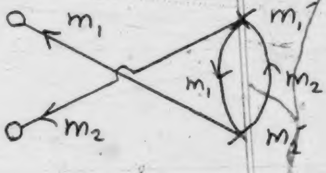

$$=$$

$$= -\delta_{m_1' m_1}\delta_{m_2' m_2}\varepsilon^{\gamma_1}\varepsilon^{\gamma_2} S^{\alpha_1\gamma_2}_{\varepsilon_f}(t_1-t_2')\, S^{\alpha_2\gamma_1}_{\varepsilon_f}(t_2-t_1') \times$$
$$\times(-)\frac{S^{\gamma_1\gamma_2}_{\tilde{\varepsilon}_f}(t_1'-t_2')\, S^{\gamma_2\gamma_1}_{\tilde{\varepsilon}_f}(t_2'-t_1')}{f_F(-\tilde{\varepsilon}_f+\mu)}\;\frac{\langle P_1\rangle}{N f_F(\tilde{\varepsilon}_f-\mu)}$$

FIG. 4.13(b)

The 4–Point ξ-Function in the $\langle P_1\rangle$ Sector with Non–SU(N) Rules

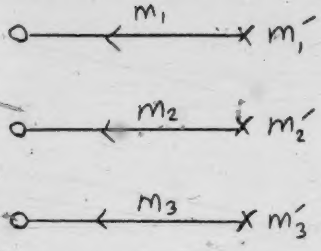

$$= \delta_{m_1 m_1'}\,\delta_{m_2 m_2'}\,\delta_{m_3 m_3'}\,S^{\alpha_1\gamma_1}_{\varepsilon_f}(t_1 - t_1') \times$$
$$\times\, S^{\alpha_2\gamma_2}_{\varepsilon_f}(t_2 - t_2')\,S^{\alpha_3\gamma_3}_{\varepsilon_f}(t_3 - t_3')\,\langle P_0\rangle$$

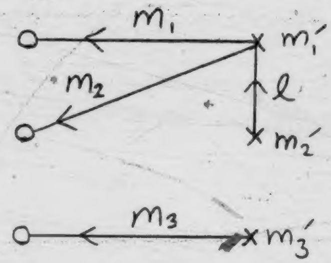

$$= \left(-\delta_{m_1 m_1'}\,\delta_{m_2 \ell} + \delta_{m_1 \ell}\,\delta_{m_2 m_1'}\right)\varepsilon^{\gamma_1}\,\delta_{\ell m_2'}\,\delta_{m_3 m_3'} \times$$
$$\times\, S^{\alpha_1\gamma_1}_{\varepsilon_f}(t_1 - t_1')\,S^{\alpha_2\gamma_1}_{\varepsilon_f}(t_2 - t_1')\,S^{\gamma_1\gamma_2}_{\varepsilon_f}(t_1' - t_2') \times$$
$$\times\, S^{\alpha_3\gamma_3}_{\varepsilon_f}(t_3 - t_3')\,\langle P_0\rangle$$

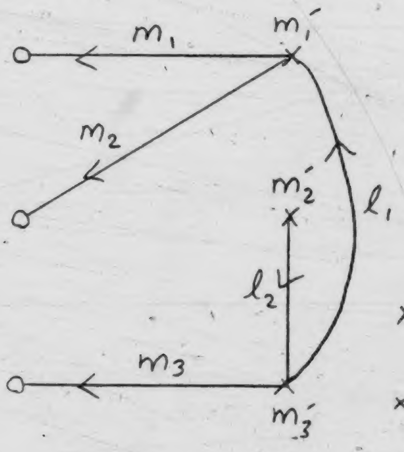

$$= \left(-\delta_{m_1 m_1'}\,\delta_{m_2 \ell_1} + \delta_{m_1 \ell_1}\,\delta_{m_2 m_1'}\right)\varepsilon^{\gamma_1} \times$$
$$\times \left(-\delta_{m_3 m_3'}\,\delta_{\ell_1 \ell_2} + \delta_{m_3 \ell_2}\,\delta_{\ell_1 m_3'}\right)\varepsilon^{\gamma_3}\,\delta_{\ell_2 m_2'} \times$$
$$\times\, S^{\alpha_1\gamma_1}_{\varepsilon_f}(t_1 - t_1')\,S^{\alpha_2\gamma_1}_{\varepsilon_f}(t_2 - t_1')\,S^{\gamma_1\gamma_3}_{\varepsilon_f}(t_1' - t_3') \times$$
$$\times\, S^{\alpha_3\gamma_3}_{\varepsilon_f}(t_3 - t_3')\,S^{\gamma_3\gamma_2}_{\varepsilon_f}(t_3' - t_2')\,\langle P_0\rangle$$

FIG. 4.14(a)

The 6-Point ξ-Function in the $\langle P_0\rangle$ Sector with Non-SU(N) Rules

To this set of diagrams must be added the set of diagrams covering all permutations of m_1', m_2', m_3'.

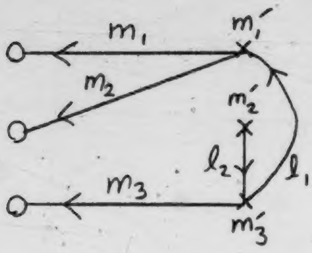
m₁
m₁′
m₂
m₂′
l₂
l₁
m₃
m₃′

$$= \left(-\delta_{m_1 m_1'}\delta_{m_2 l_1} + \delta_{m_1 l_1}\delta_{m_2 m_1'}\right)\varepsilon^{\gamma_1}\times$$
$$\times\left(-\delta_{m_3 m_3'}\delta_{l_1 l_2} + \delta_{m_3 l_2}\delta_{l_1 m_3'}\right)\varepsilon^{\gamma_3}\delta_{l_2 m_2'}\times$$
$$\times S^{\alpha_1\gamma_1}_{\varepsilon_f}(t_1-t_1')\,S^{\alpha_2\gamma_1}_{\varepsilon_f}(t_2-t_1')\,S^{\gamma_1\gamma_3}_{\varepsilon_f}(t_1'-t_3')\times$$
$$\times S^{\alpha_3\gamma_3}_{\varepsilon_f}(t_3-t_3')\,S^{\gamma_3\gamma_2}_{\varepsilon_f}(t_3'-t_2')\,\frac{\langle P_1\rangle}{N}$$

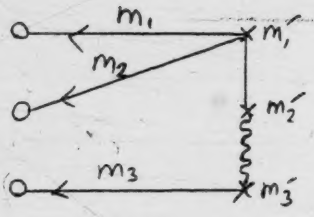
m₁
m₁′
m₂
m₂′
m₃
m₃′

$=$

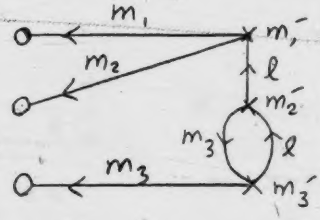
m₁
m₁′
m₂
l
m₂′
m₃
l
m₃
m₃′

$=$

$$= \left(-\delta_{m_1 m_1'}\delta_{m_2 l} + \delta_{m_1 l}\delta_{m_2 m_1'}\right)\varepsilon^{\gamma_1}\delta_{m_2' m_3}\delta_{m_3' l}\,\varepsilon^{\gamma_2}\varepsilon^{\gamma_3}\times$$
$$\times S^{\alpha_1\gamma_1}_{\varepsilon_f}(t_1-t_1')\,S^{\alpha_2\gamma_1}_{\varepsilon_f}(t_2-t_1')\,S^{\gamma_1\gamma_2}_{\varepsilon_f}(t_1'-t_2')\,S^{\alpha_3\gamma_3}_{\varepsilon_f}(t_3-t_3')\times$$
$$\times(-)\frac{S^{\gamma_2\gamma_3}_{\tilde{\varepsilon}_f}(t_2'-t_3')\,S^{\gamma_3\gamma_2}_{\tilde{\varepsilon}_f}(t_3'-t_2')}{f_F(-\tilde{\varepsilon}_f+\mu)}\;\frac{\langle P_1\rangle}{N\,f_F(\tilde{\varepsilon}_f-\mu)}$$

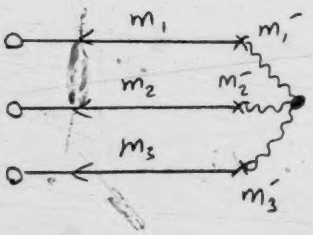
m₁
m₁′
m₂
m₂′
m₃
m₃′

$=$

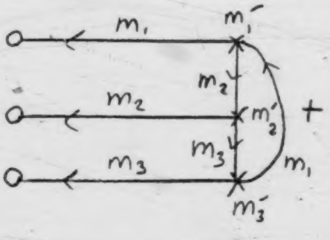
m₁
m₁′
m₂
m₂
m₂′
m₃
m₃
m₁
m₃′

$+$

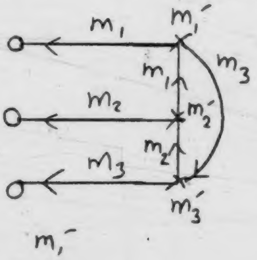
m₁
m₁′
m₁
m₃
m₂
m₂′
m₂
m₃
m₃′

$+$

$+$

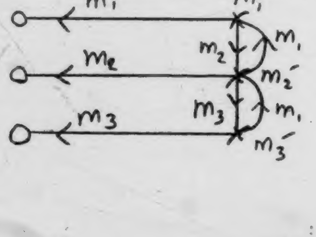
m₁
m₁′
m₂
m₁
m₂
m₂′
m₃
m₃
m₁
m₃′

$+$

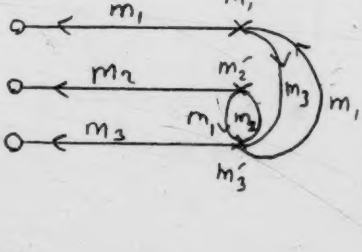
m₁
m₁′
m₂
m₂′
m₃
m₁
m₁
m₂
m₃
m₃′

$=$

FIG. 4.14(b)

The 6–Point ξ-Function in the $\langle P_1\rangle$ Sector with Non–SU(N) Rules

This Figure is continued on the next page.

$$= \delta_{m_1' m_2}\delta_{m_2' m_3}\delta_{m_3' m_1}\,\xi^{\gamma_1}\xi^{\gamma_2}\xi^{\gamma_3}\,S_{\varepsilon_f}^{\alpha_1\gamma_1}(t_1-t_1')\,S_{\varepsilon_f}^{\alpha_2\gamma_2}(t_2-t_2')\,S_{\varepsilon_f}^{\alpha_3\gamma_3}(t_3-t_3')\times$$

$$\times(-)\,\frac{S_{\tilde\varepsilon_f}^{\gamma_1\gamma_3}(t_1'-t_3')\,S_{\tilde\varepsilon_f}^{\gamma_3\gamma_2}(t_3'-t_2')\,S_{\tilde\varepsilon_f}^{\gamma_2\gamma_1}(t_2'-t_1')}{f_F(-\tilde\varepsilon_f+\mu)}\;\frac{\langle P_1\rangle}{N f_F(\tilde\varepsilon_f-\mu)}+$$

$$+\,\delta_{m_1' m_3}\delta_{m_3' m_2}\delta_{m_2' m_1}\,\xi^{\gamma_1}\xi^{\gamma_2}\xi^{\gamma_3}\,S_{\varepsilon_f}^{\alpha_1\gamma_1}(t_1-t_1')\,S_{\varepsilon_f}^{\alpha_2\gamma_2}(t_2-t_2')\,S_{\varepsilon_f}^{\alpha_3\gamma_3}(t_3-t_3')\times$$

$$\times(-)\,\frac{S_{\tilde\varepsilon_f}^{\gamma_1\gamma_2}(t_1'-t_2')\,S_{\tilde\varepsilon_f}^{\gamma_2\gamma_3}(t_2'-t_3')\,S_{\tilde\varepsilon_f}^{\gamma_3\gamma_1}(t_3'-t_1')}{f_F(-\tilde\varepsilon_f+\mu)}\;\frac{\langle P_1\rangle}{N f_F(\tilde\varepsilon_f-\mu)}+$$

$$+\,\delta_{m_1' m_2}\delta_{m_2' m_3}\delta_{m_3' m_1}\,\xi^{\gamma_1}\xi^{\gamma_3}\,S_{\varepsilon_f}^{\alpha_1\gamma_1}(t_1-t_1')\,S_{\varepsilon_f}^{\alpha_2\gamma_2}(t_2-t_2')\,S_{\varepsilon_f}^{\alpha_3\gamma_3}(t_3-t_3')\times$$

$$\times(-)^2\,\frac{S_{\tilde\varepsilon_f}^{\gamma_1\gamma_2}(t_1'-t_2')\,S_{\tilde\varepsilon_f}^{\gamma_2\gamma_1}(t_2'-t_1')}{f_F(-\tilde\varepsilon_f+\mu)}\;\frac{S_{\tilde\varepsilon_f}^{\gamma_2\gamma_3}(t_2'-t_3')\,S_{\tilde\varepsilon_f}^{\gamma_3\gamma_2}(t_3'-t_2')}{f_F(-\tilde\varepsilon_f+\mu)}\;\frac{\langle P_1\rangle}{N f_F(\tilde\varepsilon_f-\mu)}+$$

$$+\,\delta_{m_1' m_3}\delta_{m_3' m_2}\delta_{m_2' m_1}\,\xi^{\gamma_1}\xi^{\gamma_2}\,S_{\varepsilon_f}^{\alpha_1\gamma_1}(t_1-t_1')\,S_{\varepsilon_f}^{\alpha_2\gamma_2}(t_2-t_2')\,S_{\varepsilon_f}^{\alpha_3\gamma_3}(t_3-t_3')\times$$

$$\times(-)^2\,\frac{S_{\tilde\varepsilon_f}^{\gamma_1\gamma_3}(t_1'-t_3')\,S_{\tilde\varepsilon_f}^{\gamma_3\gamma_1}(t_3'-t_1')}{f_F(-\tilde\varepsilon_f+\mu)}\;\frac{S_{\tilde\varepsilon_f}^{\gamma_2\gamma_3}(t_2'-t_3')\,S_{\tilde\varepsilon_f}^{\gamma_3\gamma_2}(t_3'-t_2')}{f_F(-\tilde\varepsilon_f+\mu)}\;\frac{\langle P_1\rangle}{N f_F(\tilde\varepsilon_f-\mu)}.$$

FIG. 4.14(b) Continued

The 6–Point ξ-Function in the $\langle P_1\rangle$ Sector with Non–SU(N) Rules

This Figure is continued from the last page. To this set of diagrams must be added the set of diagrams covering all permutations of m_1', m_2', m_3'.

4.9.3 THE BROKEN–CHAIN SU(N) RULES

4.9.3.1 Why Use This Reduction?

Examples of the broken–chain SU(N) reduction were presented in sect. 4.8.9. Although the rules are more complicated, there is the advantage of disconnected diagrams in the $\langle P_1 \rangle$ sector. In this section, therefore, the diagrammatic broken–chain SU(N) rules are presented.

4.9.3.2 The Unbroken Chain: Wiggle Diagrams

As in the non–SU(N) rules, the $S^{\alpha\gamma}_{\varepsilon_f}(t-t')$ propagator is expressed as in FIG. 4.4, and spin labelled as in FIG. 4.7.

On the other hand, the wiggle–lines are different. It is the unbroken chain $\{j_1 j_2 \cdots j_n\}$ which is represented by n wiggly lines radiating out from a central point and ending in n crosses. The n–point X_i–operator function $\langle j_1 j_2 \cdots j_n \rangle_\lambda$ is decomposed in terms of the unbroken chains via eq. (4.117). Thus FIG. 4.5 is valid, provided one replaces $\langle j_1 j_2 \cdots j_n \rangle$ by $\{j_1 j_2 \cdots j_n\}$.

4.9.3.3. Feynman Rules for Vertices

The SU(N) rules have the same vertices as illustrated in FIG. 4.6, and the same spin labelling as presented in FIG. 4.7. The vertex factors, though, are different. We illustrate them below in FIG. 4.15 for the $\langle P_o \rangle$ sector. The dot and non–spontaneous cross vertex factors are the same as in FIG. 4.8. But the spontaneous non–wiggle vertex is different, it carries $\left[-\left[1 - \frac{1}{N}\right]\delta_{m_1 m_1'}\delta_{m_2 \ell} + \frac{1}{2}\sum_j \lambda_j^{m_1 m_1'} \lambda_j^{m_2 \ell}\right]\varepsilon^{\gamma}$. This is equivalent to $\left[-\delta_{m_1 m_1'}\delta_{m_2 \ell} + \delta_{m_1 \ell}\delta_{m_2 m_1'}\right]\varepsilon^{\gamma}$. As before, wiggle lines do not appear in the $\langle P_o \rangle$ sector.

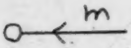

: 1

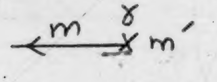

: $\delta_{mm'}$

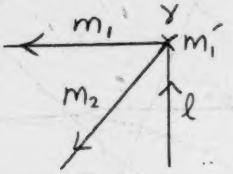

: $$\left[-\left(1-\frac{1}{N}\right)\delta_{m_1m_1'}\delta_{m_2\ell}+\frac{1}{2}\sum_j \lambda_j^{m_1m_1'}\lambda_j^{m_2\ell}\right]\varepsilon^\gamma \equiv$$

$$\equiv\left[-\left(1-\frac{1}{N}\right)\mathbb{1}\otimes\mathbb{1}+\frac{1}{2}\lambda_j\otimes\lambda_j\right]\varepsilon^\gamma$$

FIG. 4.15

SU(N) Feynman Rules for Vertices in the $\langle P_0\rangle$ Sector

The Feynman rules for vertices in the $\langle P_1\rangle$ sector are illustrated in FIG. 4.16. They are very similar to the rules in the $\langle P_0\rangle$ sector, except that this sector has the wiggle vertex as well. The wiggle vertex factor is $\frac{1}{2}\lambda_j^{mm'}$; this will be summed over j with another λ_j term which comes from the wiggle diagram decomposition (shown later). We therefore label the vertex by j. Also, the non-spontaneous cross vertex differs in that it carries an extra factor of 1/N.

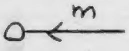

: 1

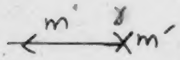

: $\frac{1}{N}\,\delta_{mm'}$

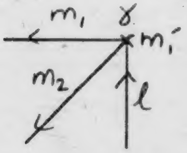

: $$\left[-\left(1-\frac{1}{N}\right)\delta_{m_1m_1'}\delta_{m_2\ell}+\frac{1}{2}\sum_j \lambda_j^{m_1m_1'}\lambda_j^{m_2\ell}\right]\varepsilon^\gamma \equiv$$

$$\equiv\left[-\left(1-\frac{1}{N}\right)\mathbb{1}\otimes\mathbb{1}+\frac{1}{2}\lambda_j\otimes\lambda_j\right]\varepsilon^\gamma$$

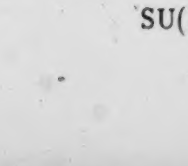

: $\frac{1}{2}\lambda_j^{mm'}$

FIG. 4.16

SU(N) Feynman Rules for Vertices in the $\langle P_1\rangle$ Sector

4.9.3.4 Feynman Rules for the n–Point ξ–Function

Construction of diagrams for the n–point ξ–function proceeds similarly to the non–SU(N) rules. The broken–chain SU(N) rules are presented below, paralleling the non–SU(N) rules of the last section.

1) Define $\Gamma^{\{\alpha\}\{\gamma\}}_{n\{m\}\{m'\}}(\{t\},\{t'\})$ as in eq. (4.123).

2) Draw $\frac{n}{2}$ dots and $\frac{n}{2}$ crosses.

3) Start with the $\langle P_o\rangle$ sector. Draw lines connecting the dots and crosses according to the rules for vertices in FIG. 4.15. As before, there are no restrictions on how many crosses form spontaneous vertices, other than the requirement that at least one cross must remain as a non–spontaneous vertex.

4) As before, S_{ε_f} lines are not allowed to form closed loops.

5) Spin label all lines and crosses as in FIG. 4.7.

6) Keep in mind that each dot and cross is also labelled by thermal index and time.

7) For each line write $S^{\alpha\gamma}_{\varepsilon_f}(t-t')$.

8) For each vertex, use the vertex factors shown in FIG. 4.15.

9) The overall sign of the diagram is determined by the anti–commutation of ξ–operators in the T–product.

10) A completed diagram carries an overall factor of $\langle P_o\rangle$.

11) Now do the $\langle P_1\rangle$ sector. Construct a diagram identical to one which appears in the $\langle P_o\rangle$ sector and label it as before.

12) Suppose there are p non–spontaneous cross vertices, where $1 \leq p \leq \frac{n}{2}$. Unlike the non–SU(N) case, these vertices may remain as is: Or q of them $(2 \leq q \leq p)$ may form a q–wiggle, $\{j_1 j_2 \cdots j_q\}$. Or q_1 of them may form a q_1–wiggle, q_2 of them may form a q_2–wiggle, ... and q_m of

them may form a q_m–wiggle: $\{i_1 i_2 \ldots i_{q_1}\}\ \{j_1 j_2 \ldots j_{q_2}\} \ldots$ $\{k_1 k_2 \ldots k_{q_m}\}$, such that $2 \le \sum_{\ell=1}^{m} q_\ell \le p$.

13) Label the vertices in a q–wiggle $\{j_1 j_2 \cdots j_q\}$ by $j_1, j_2, \cdots j_q$.

14) Unlike the non–SU(N) case, the number of non–spontaneous cross vertices is not limited to 1 or 0. The number may range from 0 to n/2.

15) For each vertex, use the vertex factors shown in FIG. 4.16.

16) A completed diagram with no wiggle vertices carries an overall factor of $\langle P_1 \rangle$.

17) A completed diagram with wiggle vertices carries an overall factor of $\langle P_1 \rangle / f_p(\tilde{\varepsilon}_f - \mu)$, where the value of $\tilde{\varepsilon}_f$ is chosen arbitrarily. $\tilde{\varepsilon}_f$ will be used in the decomposition of wiggle diagrams discussed below.

4.9.3.5 Decomposition of the Wiggle Diagrams

Wiggle line diagrams are decomposed into linear chains of $S_{\tilde{\varepsilon}_f}$ loops, in a manner similar to how it was done in the non–SU(N) case. But there is a number of differences. Firstly, we don't bother with spin labelling, because each $S_{\tilde{\varepsilon}_f}$ line carries a dummy spin which is summed over in the λ_j matrix traces. Instead, we label each cross by j, the index of the λ_j matrix appearing in the X_j–operator.

To facilitate having systematic rules for vertex factors in the decomposition of wiggle lines, it is useful to introduce a direction to the chain. The loop containing the vertex i, which is the starting point of the reduction, will be called the "tip" of the chain, in the same manner that ξ forms the tip of the S_{ε_f} propagator. The opposite end of the chain will be called the "tail". We define a direction going from the tail to the tip, as illustrated in FIG. 4.17. Thus each link vertex will have an "incoming" loop and an "outgoing" loop, (towards "i").

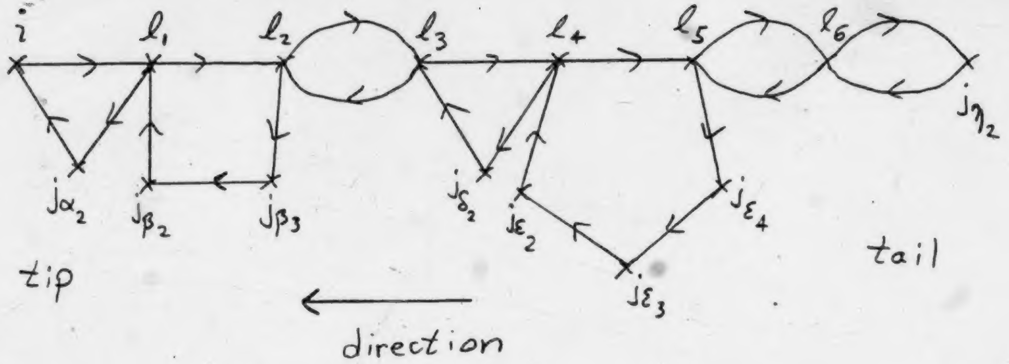

FIG. 4.17

Example: SU(N) Decomposition of a 15–Point Wiggle Diagram

This illustrates a chain in the reduction of a 15–point SU(N) wiggle diagram, $\{j_1 j_2 \ldots j_{15}\}$. Vertex "i" is taken as the starting point of the reduction. The direction of the chain is defined towards i, such that each vertex has in incoming loop and an outgoing loop. A general chain has the structure $G(i\, j_{\alpha_2} j_{\alpha_3} \ldots \ell_1) \times G(\ell_1 j_{\beta_2} j_{\beta_3} \ldots \ell_2) \times G(\ell_2 j_{\gamma_2} j_{\gamma_3} \ldots \ell_3) \ldots$, where $\ell_1, \ell_2, \ldots$ are the link vertices, and $G(j_1 j_2 \ldots j_n)$ is defined in eq. (4.58). The vertices $j_1, j_2, \ldots j_n$ are ordered from right to left in G, following the direction of the arrows on the lines. Note that the link vertex ℓ_n is always the vertex immediately following the last link vertex ℓ_{n-1}. This remains true for all permutations.

4.9.3.6 The Dotted Line

Note from the examples in sect. 4.8.9, that the rules for a two vertex loop, G(ij), differ depending on whether or not G(ij) is at the tail of the chain. To make a diagrammatic distinction between the G(ij) at the tail and not at the tail, the G(ij) at the tail will be represented by an S_{ε_f} loop as usual, but the G(ij) not at the tail will be represented by a dotted line, with an arrow directed towards i. Therefore the 15–point chain of FIG. 4.17 will be redrawn as shown in FIG. 4.18.

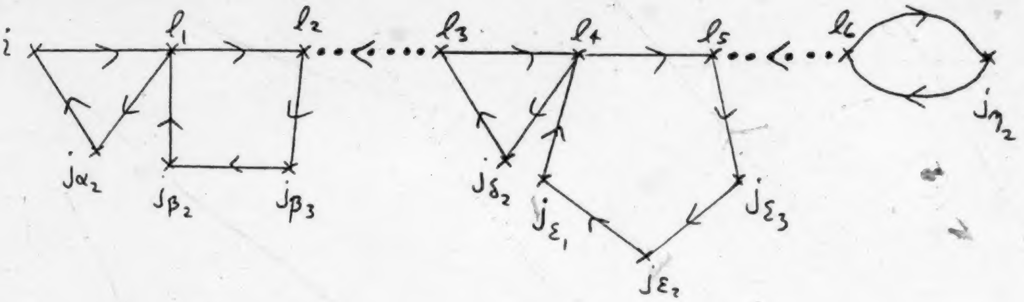
i
l_1
l_2
l_3
l_4
l_5
l_6
j_{α_2}
j_{β_2}
j_{β_3}
j_{δ_2}
j_{ε_1}
j_{ε_2}
j_{ε_3}
j_{η_2}

FIG. 4.18

Dotted Lines in a 15–Point SU(N) Wiggle Diagram

This shows again the 15–point SU(N) wiggle diagram of FIG. 4.17. Two–vertex loops which are not at the tail of the chain have been replaced by a dotted line.

Calculation shows that G(ij) is actually time–independent and given by:

$$G^{\gamma_1\gamma_2}_{\tilde{\varepsilon}_f}(t'_1-t'_2) = f_F(\tilde{\varepsilon}_f-\mu) \ . \tag{4.124}$$

Therefore, each dotted line represents a constant factor, $f_F(\tilde{\varepsilon}_f-\mu)$.

4.9.3.7 Feynman Rules for Wiggle Vertices

There are six different types of vertices one may find inside a wiggle diagram. The Feynman rules for these vertices are illustrated in FIG. 4.19. Note that each vertex may be connected to the tail of an S_{ε_f} line external to the wiggle diagram. For the sake of clarity, these are omitted.

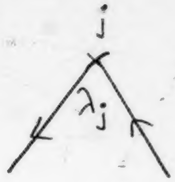

- λ_j at vertex
- ε^γ

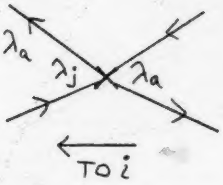

- factor of $\frac{1}{2}$
- λ_a on incoming loop at vertex
- λ_j on outgoing loop at vertex
- λ_a on outgoing line of outgoing loop

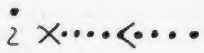

- $d i \sqcup \sqcup$ (2 blanks determined by vertex at tail-end of dotted line.)

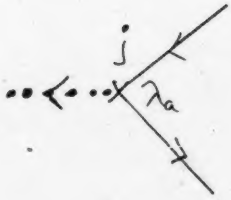

- ε^γ
- λ_a on incoming loop at vertex
- $d \sqcup j a$ (blank determined by vertex at tip-end of dotted line.)

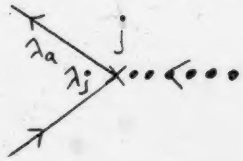

- factor of $\frac{1}{2}$
- ε^γ
- λ_j on outgoing loop at vertex
- λ_a on outgoing line of outgoing loop
- $d a \sqcup \sqcup$ (2 blanks determined by vertex at tail-end of dotted line.)

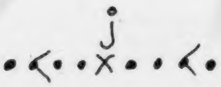

- $d \sqcup j a$ (blank determined by vertex at tip-end of outgoing dotted line.)
- $d a \sqcup \sqcup$ (2 blanks determined by vertex at tail-end of incoming dotted line.)

FIG. 4.19
SU(N) Feynman Rules for Vertices Inside Wiggle Diagrams

For each loop in the chain, one must take Tr($\lambda_{j_1}, \lambda_{j_2}, \ldots$), where the positioning of the λ matrices is determined by the rules in FIG. 4.19, and ordered from right to left inside Tr(...), following the direction of the arrows on the $S_{\tilde{\varepsilon}_f}$ lines of the loop. This is illustrated in FIG. 4.20. Each loop also carries a factor of $\frac{-1}{f_F(-\tilde{\varepsilon}_f+\mu)}$. The chain carries an overall factor of $\frac{1}{N}$.

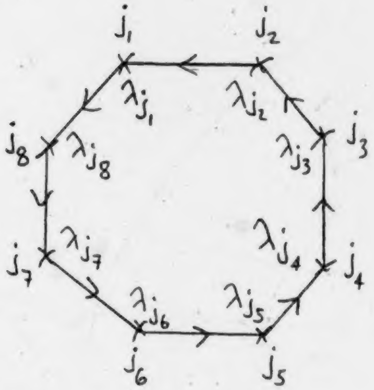
j_1
j_2
j_3
j_4
j_5
j_6
j_7
j_8
λ_{j_1}
λ_{j_2}
λ_{j_3}
λ_{j_4}
λ_{j_5}
λ_{j_6}
λ_{j_7}
λ_{j_8}

$$: \mathrm{Tr}\left(\lambda_{j_1}\lambda_{j_2}\lambda_{j_3}\lambda_{j_4}\lambda_{j_5}\lambda_{j_6}\lambda_{j_7}\lambda_{j_8}\right)$$

FIG. 4.20
The Trace Convention

This shows how the λ matrices are ordered, following the arrows on a loop of a chain in the SU(N) reduction of a wiggle diagram.

4.9.3.8 The 2–Wiggle, 3–Wiggle, 4–Wiggle, and 5–Wiggle

In FIGS. 4.21(a)–(d), the 2–wiggle, 3–wiggle, 4–wiggle and 5–wiggle of eqs. (4.151) – (4.154) are illustrated. Repeated indices (a,b,c ...) should be summed over.

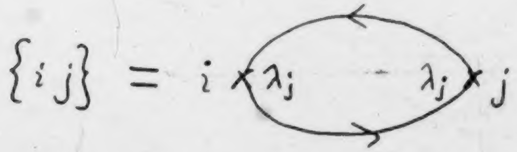
$\{i\,j\} =$
i
λ_j
λ_j
j

FIG. 4.21(a)
The SU(N) 2–Wiggle Decomposition

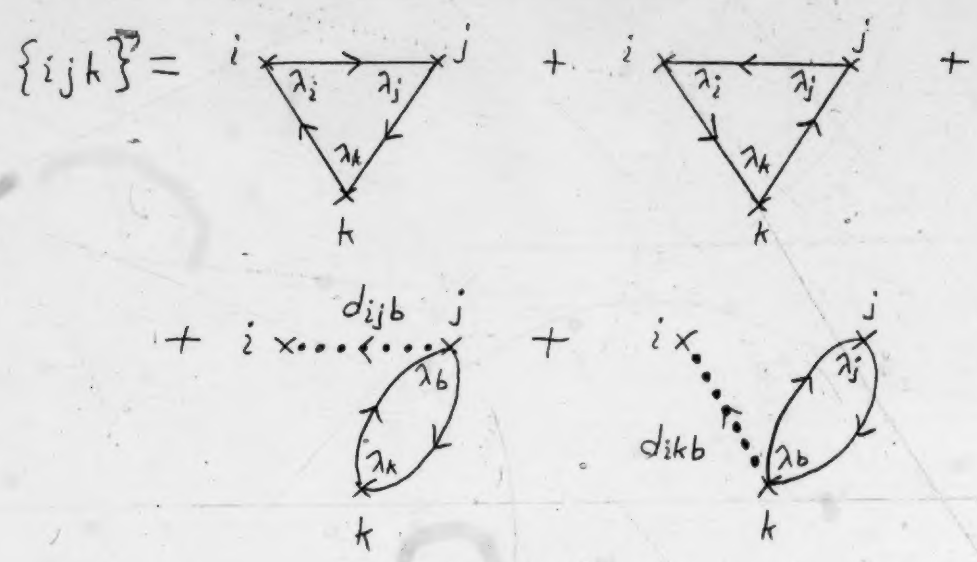
{ijk} =
i
j
k
λ_i
λ_j
λ_k
+
d_{ijb}
λ_b
d_{ikb}

FIG. 4.21(b)
The SU(N) 3–Wiggle Decomposition

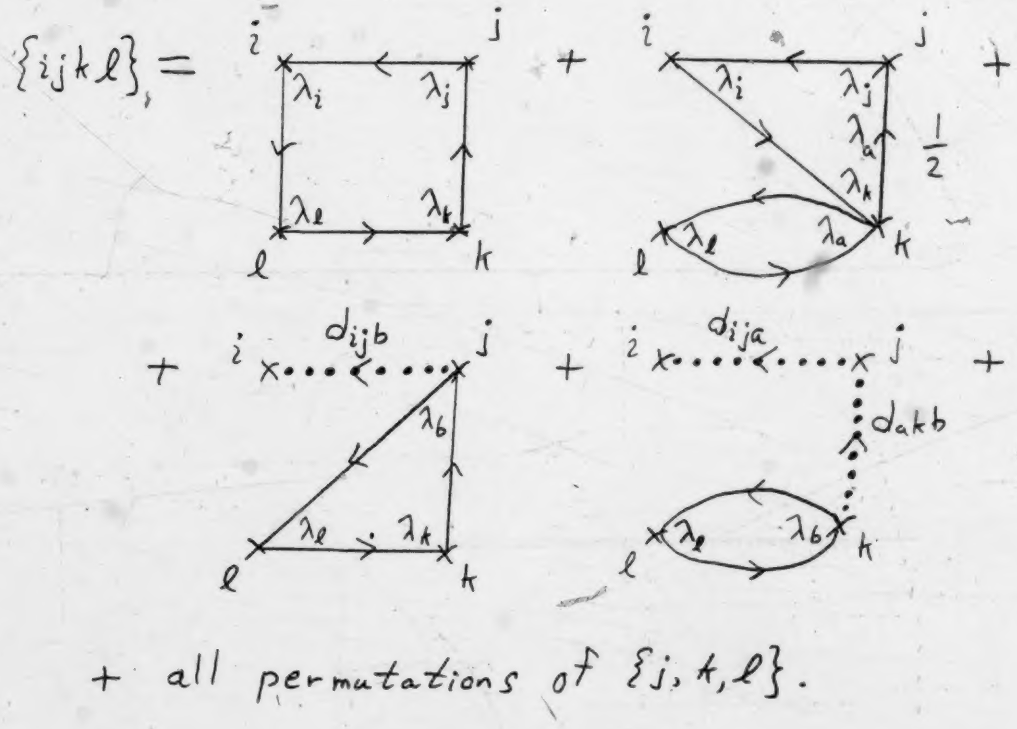
{ijkl} =
i
j
k
l
λ_i
λ_j
λ_k
λ_l
λ_a
$\frac{1}{2}$
+
d_{ijb}
λ_b
d_{ija}
d_{akb}
+ all permutations of {j, k, l}.

FIG. 4.21(c)
The SU(N) 4–Wiggle Decomposition

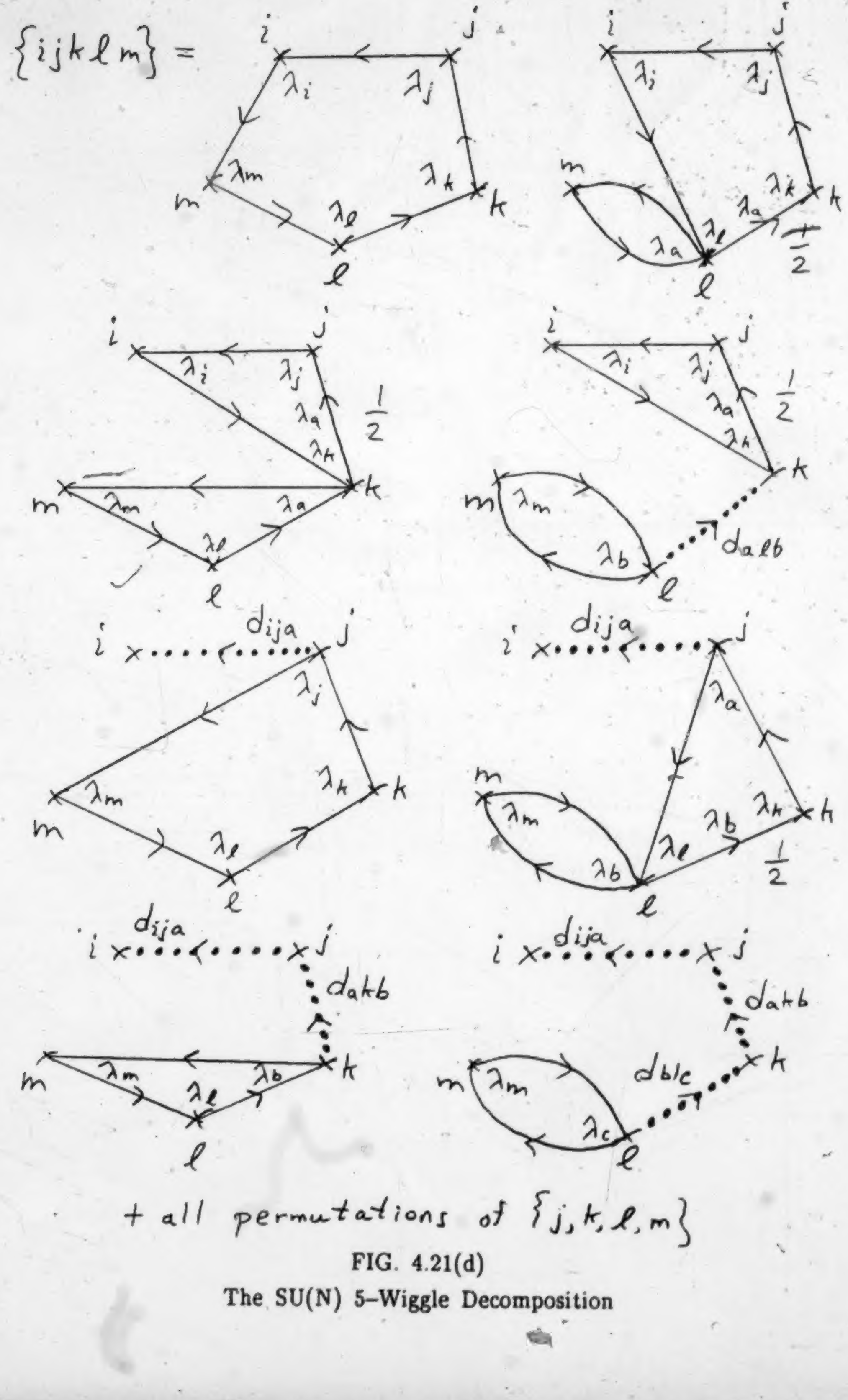
{ijklm} =
i
j
k
l
m
λi
λj
λk
λl
λm
λa
λb
λc
1/2
1/2
1/2
1/2
daℓb
dija
dakb
dblc

+ all permutations of {j, k, l, m}

FIG. 4.21(d)
The SU(N) 5–Wiggle Decomposition

4.9.3.9 Completion of Feynman Rules for the n–Point ξ–Function

We are now ready to complete the SU(N) Feynman rules for the n–point ξ–function:

18) Decompose wiggle diagrams into all possible linear chains of loops choosing a vertex i to be fixed as the starting point of the chain and permuting over all other vertices. The link between two loops must occur at the second vertex of each successive loop. This is illustrated in FIG. 4.17. Define a direction towards i as in FIG. 4.17 as well.

19) The 2–vertex loop is allowed only at the tail of the chain. At all other locations it must replaced with a dotted line, as in FIG. 4.18, with an arrow directed towards i. The dotted line is not allowed at the tail of the chain.

20) For each solid line which forms part of a loop, write $S^{\alpha\gamma}_{\tilde{\varepsilon}_f}(t-t')$, where the value of $\tilde{\varepsilon}_f$ was chosen in step 16.

21) For each dotted line, write $f_F(\tilde{\varepsilon}_f-\mu)$.

22) For each vertex in the chain, use the vertex factors shown in FIG. 4.19.

23) For each loop in the chain, take $\mathrm{Tr}(\lambda_{j_1}\lambda_{j_2}\ldots)$ where the positioning of the λ–matrices is determined in step 22, and ordered from right to left inside $\mathrm{Tr}(\ldots)$ following the direction of the arrows on the $S_{\tilde{\varepsilon}_f}$ lines of the loop. (See FIG. 4.20.)

24) Sum over repeated indices.

25) Each loop carries a factor of $\dfrac{-1}{f_F(-\tilde{\varepsilon}_f+\mu)}$.

26) A complete chain carries an overall factor of $\dfrac{1}{N}$.

4.9.3.10 The 2–Point, 4–Point, and 6–Point ξ–Functions

The application of these Feynman rules to the 2–point, 4–point, and 6–point ξ–functions is similar to that illustrated in FIGS. 4.12–4.14. In fact, the 2–point function with SU(N) rules is identical to the one illustrated in FIG. 4.12 for non–SU(N) rules. Also, the 4–point function in the $\langle P_o \rangle$ sector is the same as the one illustrated in FIG. 4.13(a), except that the δ–function spontaneous vertices are written in terms of λ–matrices. The 4–point function in the $\langle P_1 \rangle$ sector, though, is a little different and is illustrated in FIG. 4.22.

The 6–point ξ–function in the $\langle P_o \rangle$ sector with SU(N) rules is the same as FIG. 4.14(a) for the non–SU(N) rules, except that the δ–function spontaneous vertices are written in terms of λ–matrices. The 6–point function in the $\langle P_1 \rangle$ sector is illustrated below in FIG. 4.23.

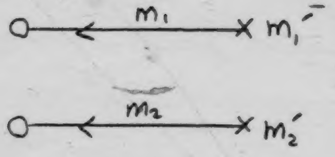

$$= \frac{1}{N^2}\delta_{m_1m_1'}\delta_{m_2m_2'} S_{\varepsilon_f}^{\alpha_1\gamma_1}(t_1-t_1') S_{\varepsilon_f}^{\alpha_2\gamma_2}(t_2-t_2')\langle P_1\rangle$$

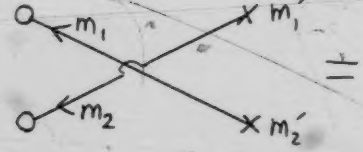

$$= -\frac{1}{N^2}\delta_{m_1m_2'}\delta_{m_2m_1'} S_{\varepsilon_f}^{\alpha_1\gamma_2}(t_1-t_2') S_{\varepsilon_f}^{\alpha_2\gamma_1}(t_2-t_1')\langle P_1\rangle$$

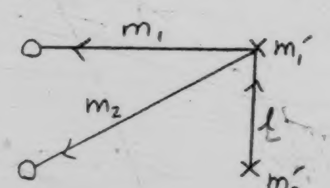

$$= \frac{1}{N}\left[-\left(1-\frac{1}{N}\right)\delta_{m_1m_1'}\delta_{m_2\ell}+\frac{1}{2}\sum_j \lambda_j^{m_1m_1'}\lambda_j^{m_2\ell}\right]\varepsilon^{\gamma_1}\delta_{\ell m_2'}\times$$

$$\times S_{\varepsilon_f}^{\alpha_1\gamma_1}(t_1-t_1') S_{\varepsilon_f}^{\alpha_2\gamma_1}(t_2-t_1') S_{\varepsilon_f}^{\gamma_1\gamma_2}(t_1'-t_2')\langle P_1\rangle$$

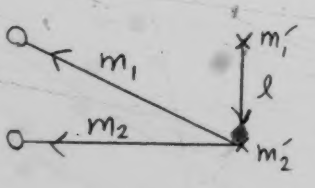

$$= -\frac{1}{N}\left[-\left(1-\frac{1}{N}\right)\delta_{m_1m_2'}\delta_{m_2\ell}+\frac{1}{2}\sum_j \lambda_j^{m_1m_2'}\lambda_j^{m_2\ell}\right]\varepsilon^{\gamma_2}\delta_{\ell m_1'}\times$$

$$\times S_{\varepsilon_f}^{\alpha_1\gamma_2}(t_1-t_2') S_{\varepsilon_f}^{\alpha_2\gamma_2}(t_2-t_2') S_{\varepsilon_f}^{\gamma_2\gamma_1}(t_2'-t_1')\langle P_1\rangle$$

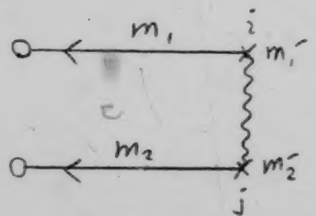

$=$

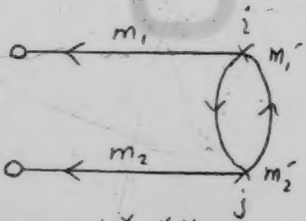

$$= S_{\varepsilon_f}^{\alpha_1\gamma_1}(t_1-t_1') S_{\varepsilon_f}^{\alpha_2\gamma_2}(t_2-t_2')\times$$

$$\times \frac{1}{4}\lambda_i^{m_1m_1'}\lambda_j^{m_2m_2'}\frac{1}{N}\mathrm{Tr}(\lambda_i\lambda_j)(-)\frac{\varepsilon^{\gamma_1}S_{\tilde{\varepsilon}_f}^{\gamma_1\gamma_2}(t_1'-t_2')\varepsilon^{\gamma_2}S_{\tilde{\varepsilon}_f}^{\gamma_2\gamma_1}(t_2'-t_1')}{f_F(-\tilde{\varepsilon}_f+\mu)}\cdot\frac{\langle P_1\rangle}{f_F(\tilde{\varepsilon}_F-\mu)}$$

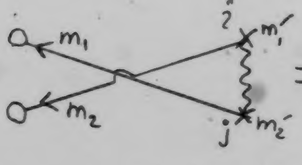

$=$

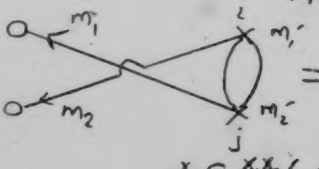

$$= -S_{\varepsilon_f}^{\alpha_1\gamma_2}(t_1-t_2') S_{\varepsilon_f}^{\alpha_2\gamma_1}(t_2-t_1')\times$$

$$\times \frac{1}{4}\lambda_i^{m_2m_1'}\lambda_j^{m_1m_2'}\frac{1}{N}\mathrm{Tr}(\lambda_i\lambda_j)(-)\frac{\varepsilon^{\gamma_1}S_{\tilde{\varepsilon}_F}^{\gamma_1\gamma_2}(t_1'-t_2')\varepsilon^{\gamma_2}S_{\tilde{\varepsilon}_f}^{\gamma_2\gamma_1}(t_2'-t_1')}{f_F(-\tilde{\varepsilon}_F+\mu)}\;\frac{\langle P_1\rangle}{f_F(\tilde{\varepsilon}_f-\mu)}$$

FIG. 4.22

The 4–Point ξ–Function in the $\langle P_1\rangle$ Sector with SU(N) Rules

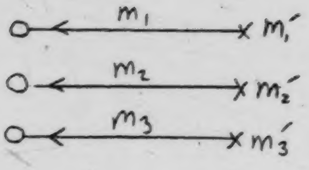

$$= \frac{1}{N^3}\delta_{m_1m_1'}\delta_{m_2m_2'}\delta_{m_3m_3'} S_{\varepsilon_f}^{\alpha_1\gamma_1}(t_1-t_1') \times$$
$$\times S_{\varepsilon_f}^{\alpha_2\gamma_2}(t_2-t_2')\, S_{\varepsilon_f}^{\alpha_3\gamma_3}(t_3-t_3')\, \langle P_1\rangle .$$

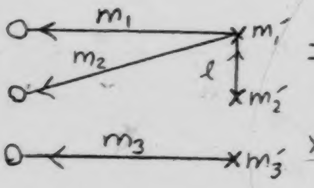

$$= \frac{1}{N^2}\left[-\left(1-\frac{1}{N}\right)\delta_{m_1m_1'}\delta_{m_2\ell} + \frac{1}{2}\sum_j \lambda_j^{m_1m_1'}\lambda_j^{m_2\ell}\right]\delta_{\ell m_2'}\,\delta_{m_3m_3'}\,\varepsilon^{\gamma_1}\times$$
$$\times S_{\varepsilon_f}^{\alpha_1\gamma_1}(t_1-t_1') S_{\varepsilon_f}^{\alpha_2\gamma_1}(t_2-t_1') S_{\varepsilon_f}^{\gamma_1\gamma_2}(t_1'-t_2') S_{\varepsilon_f}^{\alpha_3\gamma_3}(t_3-t_3')\langle P_1\rangle$$

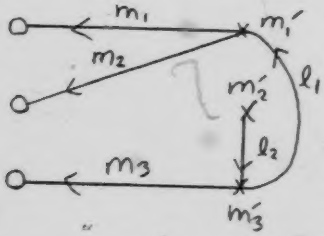

$$= \frac{1}{N}\left[-\left(1-\frac{1}{N}\right)\delta_{m_1m_1'}\delta_{m_2\ell_1} + \frac{1}{2}\sum_j \lambda_j^{m_1m_1'}\lambda_j^{m_2\ell_1}\right]\varepsilon^{\gamma_1}\times$$
$$\times\left[-\left(1-\frac{1}{N}\right)\delta_{m_3m_3'}\delta_{\ell_1\ell_2} + \frac{1}{2}\sum_j \lambda_j^{m_3m_3'}\lambda_j^{\ell_1\ell_2}\right]\varepsilon^{\gamma_3}\delta_{\ell_2m_2'}\times$$
$$\times S_{\varepsilon_f}^{\alpha_1\gamma_1}(t_1-t_1') S_{\varepsilon_f}^{\alpha_2\gamma_1}(t_2-t_1') S_{\varepsilon_f}^{\alpha_3\gamma_3}(t_3-t_3') S_{\varepsilon_f}^{\gamma_3\gamma_2}(t_3'-t_2') S_{\varepsilon_f}^{\gamma_1\gamma_3}(t_1'-t_3')\langle P_1\rangle$$

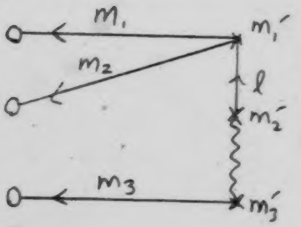

$=$

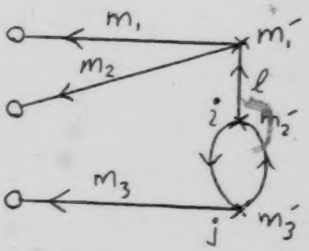

$=$

$$= \left[-\left(1-\frac{1}{N}\right)\delta_{m_1m_1'}\delta_{m_2\ell} + \frac{1}{2}\sum_k \lambda_k^{m_1m_1'}\lambda_k^{m_2\ell}\right]\varepsilon^{\gamma_1}\,\frac{1}{4}\lambda_i^{\ell m_2'}\lambda_j^{m_3m_3'}\times$$
$$\times S_{\varepsilon_f}^{\alpha_1\gamma_1}(t_1-t_1') S_{\varepsilon_f}^{\alpha_2\gamma_1}(t_2-t_1') S_{\varepsilon_f}^{\gamma_1\gamma_2}(t_1'-t_2') S_{\varepsilon_f}^{\alpha_3\gamma_3}(t_3-t_3')\frac{1}{N}\mathrm{Tr}(\lambda_i\lambda_j)\times$$
$$\times(-)\,\frac{\varepsilon^{\gamma_2}S_{\tilde{\varepsilon}_f}^{\gamma_2\gamma_3}(t_2'-t_3')\,\varepsilon^{\gamma_3}S_{\tilde{\varepsilon}_f}^{\gamma_3\gamma_2}(t_3'-t_2')}{f_F(-\tilde{\varepsilon}_f+\mu)}\;\frac{\langle P_1\rangle}{f_F(\tilde{\varepsilon}_f-\mu)}$$

FIG. 4.23

The 6-Point ξ-Function in the $\langle P_1\rangle$ Sector with SU(N) Rules

* This Figure is continued on the next page.

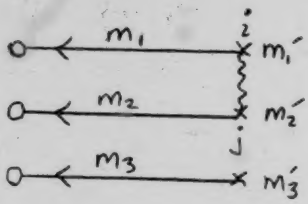

$=$

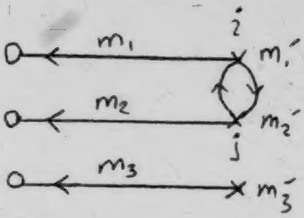

$$= \frac{1}{N}\delta_{m_3 m_3'}\frac{1}{4}\lambda_i^{m_1 m_1'}\lambda_j^{m_2 m_2'} S_{\varepsilon_f}^{\alpha_1\gamma_1}(t_1 - t_1') S_{\varepsilon_f}^{\alpha_2\gamma_2}(t_2 - t_2') S_{\varepsilon_f}^{\alpha_3\gamma_3}(t_3 - t_3') \times$$

$$\times \frac{1}{N}\mathrm{Tr}(\lambda_i\lambda_j)(-)\frac{\varepsilon^{\gamma_1} S_{\tilde{\varepsilon}_f}^{\gamma_1\gamma_2}(t_1' - t_2')\varepsilon^{\gamma_2} S_{\tilde{\varepsilon}_f}^{\gamma_2\gamma_1}(t_2' - t_1')}{f_F(-\tilde{\varepsilon}_f + \mu)}\frac{\langle P_1\rangle}{f_F(\tilde{\varepsilon}_f - \mu)}$$

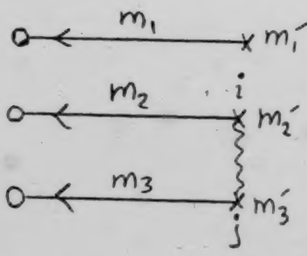

$=$

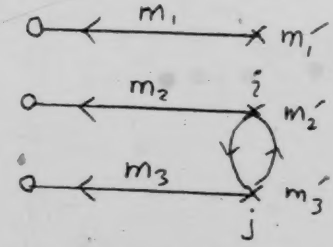

$=$

$$= \frac{1}{N}\delta_{m_1 m_1'}\frac{1}{4}\lambda_i^{m_2 m_2'}\lambda_j^{m_3 m_3'} S_{\varepsilon_f}^{\alpha_1\gamma_1}(t_1 - t_1') S_{\varepsilon_f}^{\alpha_2\gamma_2}(t_2 - t_2') S^{\alpha_3\gamma_3}(t_3 - t_3') \times$$

$$\times \frac{1}{N}\mathrm{Tr}(\lambda_i\lambda_j)(-)\frac{\varepsilon^{\gamma_2} S_{\tilde{\varepsilon}_f}^{\gamma_2\gamma_3}(t_1' - t_3')\varepsilon^{\gamma_3} S_{\tilde{\varepsilon}_f}^{\gamma_3\gamma_2}(t_3' - t_1')}{f_F(-\tilde{\varepsilon}_f + \mu)}\frac{\langle \varphi_1\rangle}{f_F(\tilde{\varepsilon}_f - \mu)}$$

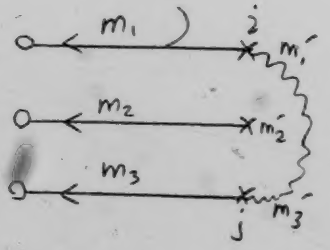

$=$

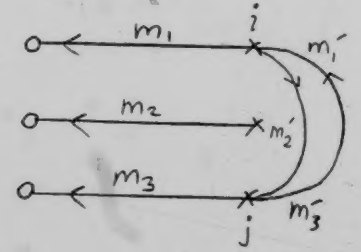

$=$

$$= \frac{1}{N}\delta_{m_2 m_2'}\frac{1}{4}\lambda_i^{m_1 m_1'}\lambda_j^{m_3 m_3'} S_{\varepsilon_f}^{\alpha_1\gamma_1}(t_1 - t_1') S_{\varepsilon_f}^{\alpha_2\gamma_2}(t_2 - t_2') S_{\varepsilon_f}^{\alpha_3\gamma_3}(t_3 - t_3') \times$$

$$\times \frac{1}{N}\mathrm{Tr}(\lambda_i\lambda_j)(-)\frac{\varepsilon^{\gamma_1} S_{\tilde{\varepsilon}_f}^{\gamma_1\gamma_3}(t_1' - t_3')\varepsilon^{\gamma_3} S_{\tilde{\varepsilon}_f}^{\gamma_3\gamma_1}(t_3' - t_1')}{f_F(-\tilde{\varepsilon}_f + \mu)}\frac{\langle P_1\rangle}{f_F(\tilde{\varepsilon}_f - \mu)}$$

FIG. 4.23 Continued

The 6–Point ξ–Function in the $\langle P_1\rangle$ Sector with SU(N) Rules

This Figure is continued from the last page. It is also continued on the next page.

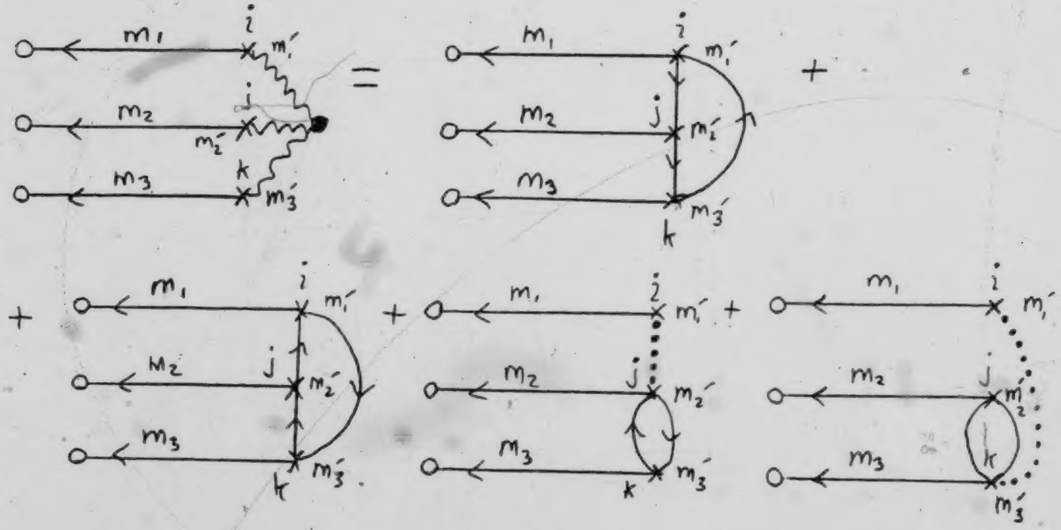

$$= \frac{1}{8N}\lambda_i^{m_1m_1'}\lambda_j^{m_2m_2'}\lambda_k^{m_3m_3'}\, S_{\varepsilon_f}^{\alpha_1\gamma_1}(t_1-t_1')\, S_{\varepsilon_f}^{\alpha_2\gamma_2}(t_2-t_2')\, S_{\varepsilon_f}^{\alpha_3}(t_3-t_3')\times$$

$$\times\Big\{\mathrm{Tr}(\lambda_i\lambda_k\lambda_j)(-)\frac{\varepsilon^{\gamma_1}S_{\tilde\varepsilon_f}^{\gamma_1\gamma_3}(t_1'-t_3')\,\varepsilon^{\gamma_3}S_{\tilde\varepsilon_f}^{\gamma_3\gamma_2}(t_3'-t_2')\,\varepsilon^{\gamma_2}S_{\tilde\varepsilon_f}^{\gamma_2\gamma_1}(t_2'-t_1')}{f_F(-\tilde\varepsilon_f+\mu)}+$$

$$+\,\mathrm{Tr}(\lambda_i\lambda_j\lambda_k)(-)\frac{\varepsilon^{\gamma_1}S_{\tilde\varepsilon_f}^{\gamma_1\gamma_2}(t_1'-t_2')\,\varepsilon^{\gamma_2}S_{\tilde\varepsilon_f}^{\gamma_2\gamma_3}(t_2'-t_3')\,\varepsilon^{\gamma_3}S_{\tilde\varepsilon_f}^{\gamma_3\gamma_1}(t_3'-t_1')}{f_F(-\tilde\varepsilon_f+\mu)}+$$

$$+\,d_{ija}\,\mathrm{Tr}(\lambda_a\lambda_k)\,f_F(\tilde\varepsilon_f-\mu)(-)\frac{\varepsilon^{\gamma_2}S_{\tilde\varepsilon_f}^{\gamma_2\gamma_3}(t_2'-t_3')\,\varepsilon^{\gamma_3}S_{\tilde\varepsilon_f}^{\gamma_3\gamma_2}(t_3'-t_2')}{f_F(-\tilde\varepsilon_f+\mu)}+$$

$$+\,d_{ika}\,\mathrm{Tr}(\lambda_a\lambda_j)\,f_F(\tilde\varepsilon_f-\mu)(-)\frac{\varepsilon^{\gamma_3}S_{\tilde\varepsilon_f}^{\gamma_3\gamma_2}(t_3'-t_2')\,\varepsilon^{\gamma_2}S_{\tilde\varepsilon_f}^{\gamma_2\gamma_3}(t_2'-t_3')}{f_F(-\tilde\varepsilon_f+\mu)}\Big\}\,\frac{\langle P_1\rangle}{f_F(\tilde\varepsilon_f-\mu)}$$

FIG. 4.23 Further Continued
The 6–Point ξ–Function in the $\langle P_1\rangle$ Sector with SU(N) Rules

This Figure is continued from the preceeding two pages.

4.10 CONCLUSION

A "simple" non–interacting quantum algebra was explored in this chapter, and found to be actually very complicated, due to the spontaneous vertices, and non–commuting zero–energy boson eigenoperator T–products. Nevertheless, it was possible to present systematic Feynman rules for calculating n–point X–functions and n–point ξ–functions. The next step is to see how perturbation theory works. This is considered in the next chapter for a very simple interaction.

CHAPTER 5

AN EXACTLY SOLVABLE MODEL: SHIFTING THE ENERGY OF A CONSTRAINED FERMIONIC STATE

5.1 INTRODUCTION

As discussed in section 4.1, the exposition of the generalized Gell–Mann Low formula and non–cancelling vacuum diagrams was deferred to this chapter. The noninteracting quantum algebra of Chapter 4 was found to be very complicated indeed. To introduce an interaction term and do perturbation theory with the generalized Gell–Mann Low formula adds the further complication of non–cancelling vacuum diagrams. In the interest of minimizing this complication, we add a very simple interaction to the model of Chapter 4: a shift of energy. This will serve as a very useful illustration of how the theory works, before considering the real Anderson model in Chapter 6.

5.2 THE MODEL

As a free Hamiltonian, we consider the n–fold degenerate infinite–U Anderson model of eq. (4.7) with the eigenoperator algebra as given by eqs. (4.3)–(4.6), eq. (4.17e), eq. (4.28b), eqs. (4.35)–(4.36), and eq. (4.41). For the sake of convenience, these equations are reproduced below.

The algebra $\mathcal{A}$ consists of the following operators:

$$\left\{ \xi_m , \xi_m^\dagger , P_o , X_{m'm} , P_1 , M_{mm'} , \mathbb{1} \right\} \in \mathcal{A} \ . \tag{5.1}$$

These operators are interrelated as follows:

$$P_o \equiv \xi_m \, \xi_m^\dagger \ , \tag{5.2a}$$

$$X_{m'm} \equiv \xi_{m'}^\dagger \, \xi_m \ , \tag{5.2b}$$

$$P_1 \equiv \sum_m X_{mm} = \sum_m \xi_m^\dagger \, \xi_m \ , \tag{5.2c}$$

$$M_{mm'} \equiv \delta_{mm'} P_o + X_{m'm} \quad , \tag{5.2d}$$

$$\mathbb{1} \equiv P_o + P_1 \quad . \tag{5.2e}$$

Further operator products are given as:

$$P_o^2 = P_o \quad , \quad P_1^2 = P_1 \quad , \quad P_o P_1 = P_1 P_o = 0 \quad , \tag{5.3a}$$

$$P_o X_{m'm} = X_{m'm} P_o = 0 \quad , \quad P_1 X_{m'm} = X_{m'm} P_1 = X_{m'm} \tag{5.3b}$$

$$P_o \xi_m = \xi_m P_1 = \xi_m \quad , \quad \xi_m P_o = P_1 \xi_m = 0 \quad , \tag{5.3c}$$

$$P_o \xi_m^\dagger = \xi_m^\dagger P_1 = 0 \quad , \quad \xi_m^\dagger P_o = P_1 \xi_m^\dagger = \xi_m^\dagger \quad , \tag{5.3d}$$

$$\xi_m \xi_{m'}^\dagger = \delta_{mm'} P_o \quad , \quad \xi_m \xi_{m'} = 0 \quad , \quad \xi_m^\dagger \xi_{m'}^\dagger = 0 \quad , \tag{5.3e}$$

$$\left.\begin{array}{c} \xi_{m''} X_{m'm} = \delta_{m''m'} \xi_m \quad , \quad X_{m'm} \xi_{m''} = \xi_{m''}^\dagger X_{m'm} = 0 \\ X_{m'm} \xi_{m''}^\dagger = \delta_{mm''} \xi_{m'}^\dagger \end{array} \quad , \right\} \tag{5.3f}$$

$$X_{m_1 m_2} X_{m_3 m_4} = \delta_{m_2 m_3} X_{m_1 m_4} \quad , \tag{5.3g}$$

$$\mathbb{1}^2 = \mathbb{1} \quad , \quad \mathbb{1}\, \mathcal{O}p = \mathcal{O}p\, \mathbb{1} \quad ; \quad \mathcal{O}p \in \mathcal{A} \quad , \tag{5.3h}$$

where $\mathcal{O}p$ in eq. (5.3h) is any operator in the algebra $\mathcal{A}$ That is, $\mathbb{1}$ is the identity operator. P_o and P_1 are projection operators of the 0–particle and 1–particle states respectively. They are related to the electron number operator n, and the hole number operator n_h , by:

$$n = P_1 \quad , \tag{5.4a}$$

$$n_h = P_o \quad . \tag{5.4b}$$

Eqs. (5.2) and (5.3) lead to the following commutation relations:

$$\left[\xi_m , P_o \right] = - \xi_m \tag{5.5a}$$

$$\left[\xi_m , P_1 \right] = \xi_m \tag{5.5b}$$

$$\left[\xi_m^\dagger , P_o \right] = \xi_m^\dagger \tag{5.5c}$$

$$\left[\xi_m^\dagger , P_1 \right] = - \xi_m^\dagger \tag{5.5d}$$

$$\left[\xi_{m''} , X_{m'm} \right] = \delta_{m''m'} \xi_m \tag{5.5e}$$

$$\left[\xi_{m''}^\dagger , X_{m'm} \right] = - \delta_{mm''} \xi_{m'}^\dagger \tag{5.5f}$$

$$\left[\, X_{m_1 m_2} \,,\, X_{m_3 m_4} \,\right] = \delta_{m_2 m_3} \, X_{m_1 m_4} - \delta_{m_4 m_1} \, X_{m_3 m_2} \tag{5.5g}$$

$$\left\{\, \xi_m \,,\, \xi^{\dagger}_{m'} \,\right\} = M_{mm'} \tag{5.5h}$$

$$\left[\, \xi_{m''} \,,\, M_{mm'} \,\right] = - \delta_{mm'} \, \xi_{m''} + \delta_{m''m'} \, \xi_m \tag{5.5i}$$

$$\left[\, \xi^{\dagger}_{m''} \,,\, M_{mm'} \,\right] = \delta_{mm'} \, \xi^{\dagger}_{m''} - \delta_{mm''} \, \xi^{\dagger}_{m'} \quad . \tag{5.5j}$$

For the purposes of this chapter, the algebra will be left in the δ–function form and we will use the non–SU(N) Feynman rules.

Operators in $\mathcal{A}$ act on a Fock space $\mathbb{F}_F$ consisting of the following states:

$$\{\ |0\rangle \ ,\ |m\rangle\ \} \in \mathbb{F}_F \quad . \tag{5.6}$$

These operators are faithfully represented as follows:

$$\xi_m = |0\rangle\langle m| \tag{5.7a}$$

$$\xi^{\dagger}_m = |m\rangle\langle 0| \tag{5.7b}$$

$$P_o = |0\rangle\langle 0| \tag{5.7c}$$

$$X_{m'm} = |m'\rangle\langle m| \tag{5.7d}$$

$$P_1 = \sum_m |m\rangle\langle m| \tag{5.7e}$$

$$M_{mm'} = \delta_{mm'} \, |0\rangle\langle 0| + |m'\rangle\langle m| \tag{5.7f}$$

$$\mathbb{1} = |0\rangle\langle 0| + \sum_m |m\rangle\langle m| \quad . \tag{5.7g}$$

The free Hamiltonian is expressed as:

$$H_o = \varepsilon_f \sum_m \xi^{\dagger}_m \, \xi_m = \varepsilon_f \, P_1 = \varepsilon_f \sum_m |m\rangle\langle m| = \varepsilon_f \, n \quad . \tag{5.8}$$

As an interaction, one may consider a simple shift of energy:

$$H_I = \Delta\varepsilon \sum_m \xi^{\dagger}_m \, \xi_m = \Delta\varepsilon \, P_1 = \Delta\varepsilon \sum_m |m\rangle\langle m| = \Delta\varepsilon \, n \quad . \tag{5.9}$$

Obviously, the solution to this system is to take the free solution with $\varepsilon_f \rightarrow \varepsilon_f + \Delta\varepsilon$. Alternatively, one may use the generalized Wick's theorem and solve perturbatively. The two methods should agree; therefore, the exact solution will serve as a check that the generalized perturbation theory is correct.

5.3 THE FULLY RENORMALIZED ξ-PROPAGATOR

The propagator of $\xi(t)$ (time-evolved using the full H), in the full vacuum $|0(\beta)\rangle$, is denoted as follows:

$$\mathscr{S}^{\alpha\gamma}_{\mathfrak{R}mm'}(t,t') \equiv \langle 0(\beta)|\, T\ \xi^{\alpha}_{m}(t)\ \xi^{\dagger\gamma}_{m'}(t')\ |0(\beta)\rangle \quad , \tag{5.10}$$

where "$\mathfrak{R}$" means that $\mathscr{S}^{\alpha\gamma}_{mm'}$ has been fully renormalized. Letting $\varepsilon_f \rightarrow \varepsilon_f + \Delta\epsilon$ in eqs. (4.18)–(4.19), one finds:

$$\boxed{\mathscr{S}^{\alpha\gamma}_{\mathfrak{R}mm'}(t,t') = \delta_{mm'}\ S^{\alpha\gamma}_{\varepsilon_f+\Delta\varepsilon}(t-t')\left[\ \langle P_o\rangle_{\mathfrak{R}} + \frac{1}{N}\ \langle P_1\rangle_{\mathfrak{R}}\ \right] \quad ,} \tag{5.11}$$

where

$$\langle P_o\rangle_{\mathfrak{R}} = \frac{1}{1 + N\ e^{-\beta(\varepsilon_f+\Delta\varepsilon-\mu)}} \quad , \tag{5.12a}$$

$$\langle P_1\rangle_{\mathfrak{R}} = \frac{N\ e^{-\beta(\varepsilon_f+\Delta\varepsilon-\mu)}}{1 + N\ e^{-\beta(\varepsilon_f+\Delta\varepsilon-\mu)}} \quad , \tag{5.12b}$$

and $S^{\alpha\gamma}_{\varepsilon_f}(t-t')$ is given by eqs. (4.16).

To be consistent, this result should agree with what one obtains using perturbation theory.

5.4 PERTURBATIVE CALCULATION OF THE FULL ξ-PROPAGATOR IGNORING THE VACUUM DIAGRAMS

In this section, let us use the Gell–Mann Low formula of eqs. (2.29) to perturbatively calculate the full ξ propagator. This will serve as an example of why one needs the generalized Gell–Mann Low formula of eq. (3.31), which includes non–cancelling vacuum diagrams.

Substituting eqs. (5.9) and (5.10) into eq. (2.29), one obtains:

$$\mathcal{G}^{\alpha\gamma}_{\ell m m'}(t,t') =$$

$$= \frac{\langle 0,\beta|T \exp\left[-i\Delta\varepsilon \sum_{\alpha'} \varepsilon^{\alpha'} \int_{-\infty}^{\infty} dt'' \, n^{\alpha'}(t'') \right] \xi^{\alpha}_{m}(t) \, \xi^{\dagger\gamma}_{m'}(t') \, |0,\beta\rangle}{\langle 0,\beta|T \exp\left[-i\Delta\varepsilon \sum_{\alpha'} \varepsilon^{\alpha'} \int_{-\infty}^{\infty} dt'' \, n^{\alpha'}(t'') \right] |0,\beta\rangle} , \tag{5.13}$$

where ε^{γ} is defined in eq. (4.32).

First, one notes that the vacuum diagrams do not contribute for the following reason. All vacuum diagrams (v.d.) have the form

$$\text{v.d.} \propto \langle 0,\beta|T \, [n(t_1)-\tilde{n}(t_1)] \, [n(t_2)-\tilde{n}(t_2)] \, \ldots \, [n(t_j)-\tilde{n}(t_j)] \, |0,\beta\rangle . \tag{5.14}$$

Noting that $n(t)$ actually is time-independent, and using the thermal state condition eq. (2.15), one has $\tilde{n}|0,\beta\rangle = n|0,\beta\rangle$. Thus eq. (5.14) vanishes, making it sufficient to consider only the connected diagrams in eq. (5.13). These are denoted by the subscript "c" as follows:

$$\mathcal{G}^{\alpha\gamma}_{\ell m m'}(t,t') =$$

$$= \langle 0,\beta|T \exp\left[-i\Delta\varepsilon \sum_{\alpha'} \varepsilon^{\alpha'} \int_{-\infty}^{\infty} dt'' \, n^{\alpha'}(t'') \right] \xi^{\alpha}_{m}(t) \, \xi^{\dagger\gamma}_{m'}(t') \, |0,\beta\rangle_c . \tag{5.15}$$

Expanding the exponential in the above equation, one obtains:

$$\mathcal{G}^{\alpha\gamma}_{\ell m m'}(t,t') = \sum_{n=0}^{\infty} \frac{(-i\Delta\varepsilon)^n}{n!} \sum_{\{\alpha_\ell\}} \int_{-\infty}^{\infty} \{dt_\ell\} \, \varepsilon^{\alpha_1} \ldots \varepsilon^{\alpha_n} \times$$

$$\times \langle 0,\beta|T \, \xi^{\alpha}_{m}(t) \, \xi^{\dagger\gamma}_{m'}(t') \, n^{\alpha_1}(t_1) \ldots n^{\alpha_n}(t_n) \, |0,\beta\rangle_c . \tag{5.16}$$

Let us consider the first few terms, using the generalized Wick's theorem of eq. (3.13) with the algebra of eqs. (5.5b) and (5.5h). One obtains:

$$\langle 0,\beta|T \, \xi^{\alpha}_{m}(t) \, \xi^{\dagger\gamma}_{m'}(t') \, |0,\beta\rangle_c = S^{\alpha\gamma}_{\varepsilon_f}(t-t') \, \langle 0,\beta| M^{\gamma}_{mm'}(t') |0,\beta\rangle \tag{5.17}$$

$$\langle 0,\beta|\, T\, \xi^{\alpha}_{m}(t)\, \xi^{\dagger\gamma}_{m'}(t')\, n^{\alpha_1}(t_1)\, |0,\beta\rangle_c =$$

$$= S^{\alpha\alpha_1}_{\varepsilon_f}(t-t_1)\ \varepsilon^{\alpha_1}\ S^{\alpha_1\gamma}_{\varepsilon_f}(t_1-t')\ \langle 0,\beta|\, M^{\gamma}_{mm'}(t')\,|0,\beta\rangle \quad , \tag{5.18}$$

$$\langle 0,\beta|\, T\, \xi^{\alpha}_{m}(t)\, \xi^{\dagger\gamma}_{m'}(t')\, n^{\alpha_1}(t_1)\, n^{\alpha_2}(t_2)\, |0,\beta\rangle_c =$$

$$= S^{\alpha\alpha_1}_{\varepsilon_f}(t-t_1)\ \varepsilon^{\alpha_1}\ S^{\alpha_1\alpha_2}_{\varepsilon_f}(t_1-t_2)\ \varepsilon^{\alpha_2}\ S^{\alpha_2\gamma}_{\varepsilon_f}(t_2-t')\ \langle 0,\beta|\, M^{\gamma}_{mm'}(t')\,|0,\beta\rangle \ +$$

$$+ S^{\alpha\alpha_2}_{\varepsilon_f}(t-t_2)\ \varepsilon^{\alpha_2}\ S^{\alpha_2\alpha_1}_{\varepsilon_f}(t_2-t_1)\ \varepsilon^{\alpha_1}\ S^{\alpha_1\gamma}_{\varepsilon_f}(t_1-t')\ \langle 0,\beta|\, M^{\gamma}_{mm'}(t')\,|0,\beta\rangle \quad , \tag{5.19}$$

etc.

Summing up the series using the Fourier representation of eqs. (4.16) along with $U_F U_F^{\dagger} = 1$ (eq. (A.6)), and applying eq. (4.17a), one finds

$$\mathcal{S}^{\alpha\gamma}_{Rmm'}(t,t') = \delta_{mm'}\ S^{\alpha\gamma}_{\varepsilon_f+\Delta\varepsilon}(t-t')\ \left[\ \langle P_o\rangle + \frac{1}{N}\,\langle P_1\rangle\ \right] \quad . \tag{5.20}$$

Compare this to the exact result, eq. (5.11). The energy has been renormalized properly in $S^{\alpha\gamma}$, but the projection operators $\langle P_o\rangle$ and $\langle P_1\rangle$ remain unrenormalized. Hence the perturbation theory of eq. (2.29) is incomplete and one ***must*** use eq. (3.31).

5.5 PERTURBATIVE CALCULATION OF THE FULL ξ-PROPAGATOR USING THE GENERALIZED GELL-MANN LOW FORMULA

In this section we repeat the calculation of the last section, using the generalized Gell-Mann Low formula of eq. (3.31). Because the U terms at $\mathcal{R}e\, t = \pm\infty$ do not contract with the other terms, the connected diagram expansion of eqs. (5.17) to (5.19) is still valid, yielding:

$$\mathcal{S}^{\alpha\gamma}_{Rmm'}(t,t') = S^{\alpha\gamma}_{\varepsilon_f+\Delta\varepsilon}(t-t')\ \times$$

$$\times\ \frac{\langle 0,\beta|\ U(\infty - \frac{i\beta}{2},\ \infty)\, M^{\gamma}_{mm'}\ U(-\infty\ ,\ -\infty + \frac{i\beta}{2})\ |0,\beta\rangle}{\langle 0,\beta|\ U(\infty - \frac{i\beta}{2}\ ,\ \infty\ )\ \ U(-\infty\ ,\ -\infty + \frac{i\beta}{2})\ |0,\beta\rangle} \quad . \tag{5.21}$$

(Compare this to eq. (3.36).)

Let us write the U terms explicitly:

$$U(\infty-\tfrac{i\beta}{2},\infty) = T_\tau \exp\left[-i\Delta\varepsilon \int_{\infty}^{\infty-i\beta/2} d\tau\, n(\tau) \right] , \tag{5.22a}$$

$$U(-\infty,-\infty+\tfrac{i\beta}{2}) = T_\tau \exp\left[-i\Delta\varepsilon \int_{-\infty+i\beta/2}^{-\infty} d\tau\, n(\tau) \right] . \tag{5.22b}$$

Noting that n actually has no time dependence, one finds

$$U(\infty-\tfrac{i\beta}{2},\infty) = \exp\left[-\frac{\beta\Delta\varepsilon}{2}\, n \right] , \tag{5.23a}$$

$$U(-\infty,-\infty+\tfrac{i\beta}{2}) = \exp\left[-\frac{\beta\Delta\varepsilon}{2}\, n \right] . \tag{5.23b}$$

Note also that $[M^\gamma, n] = 0$ so one may commute M^γ to the vacuum, and use the thermal state condition (eq. (2.15)) to state $M^\gamma_{mm'}|0,\beta\rangle = M_{mm'}|0,\beta\rangle$. Thus eq. (5.21) becomes:

$$\mathcal{S}^{\alpha\gamma}_{\ell mm'}(t,t') = S^{\alpha\gamma}_{\varepsilon_f+\Delta\varepsilon}(t-t')\, \frac{\langle 0,\beta|\, e^{-\beta\Delta\varepsilon n}\, M_{mm'}\, |0,\beta\rangle}{\langle 0,\beta|\, e^{-\beta\Delta\varepsilon n}\, |0,\beta\rangle} . \tag{5.24}$$

Using eq. (5.7f) for $M_{mm'}$ one sees that only the diagonal components will contribute to eq. (5.24), so one may write $M_{mm'} = \delta_{mm'}\left[P_0 + \frac{1}{N} P_1 \right]$. Substituting this into the numerator of eq. (5.24) and inserting $\mathbb{1} \equiv P_0 + P_1$ into the denominator, one has:

$$\mathcal{S}^{\alpha\gamma}_{\ell mm'}(t,t') = \delta_{mm'}\, S^{\alpha\gamma}_{\varepsilon_f+\Delta\varepsilon}(t-t')\, \frac{\langle 0,\beta|\, e^{-\beta\Delta\varepsilon n} \left[P_0 + \frac{1}{N} P_1 \right] |0,\beta\rangle}{\langle 0,\beta|\, e^{-\beta\Delta\varepsilon n}\, [P_0 + P_1]\, |0,\beta\rangle} . \tag{5.25}$$

This expression is further simplified when one uses the algebra of eqs. (5.4a) and (5.3a) for the projection operators, resulting in:

$$\mathcal{S}^{\alpha\gamma}_{\ell mm'}(t,t') = \delta_{mm'}\, S^{\alpha\gamma}_{\varepsilon_f+\Delta\varepsilon}(t-t')\, \frac{\langle P_0\rangle + \frac{1}{N} e^{-\beta\Delta\varepsilon} \langle P_1\rangle}{\langle P_0\rangle + e^{-\beta\Delta\varepsilon} \langle P_1\rangle} . \tag{5.26}$$

Making use of eqs. (4.18) and (5.12), one finds

$$\frac{\langle P_0\rangle}{\langle P_0\rangle + e^{-\beta\Delta\varepsilon} \langle P_1\rangle} = \langle P_0\rangle_\ell , \tag{5.27a}$$

$$\frac{e^{-\beta\Delta\varepsilon}\langle P_1\rangle}{\langle P_0\rangle + e^{-\beta\Delta\varepsilon}\langle P_1\rangle} = \langle P_1\rangle_R \ , \tag{5.27b}$$

and thus eq. (5.26) is in agreement with the exact result, eq. (5.11).

To summarize, it is necessary to use the generalized Gell–Mann Low formula (eq. (3.31)) in the case of a quantum algebra. This introduces non–cancelling vacuum diagrams, the purpose of which is to renormalize the sector structure.

This example was very straightforward to calculate, for two reasons: 1) the zero energy boson operators are mutually commuting, and 2) H_I commutes with H_o and thus $\mathcal{H}_I(t)$ has no time–dependence. In fact, all of the examples considered in ref. [60], (the original paper which introduces non–cancelling vacuum diagrams in TFD), are of this simple form. In the real model we wish to consider, both conditions 1 and 2 are broken, making the situation much more complicated.

Before taking the plunge into the real model, let us consider the renormalization of the 4–point function.

5.6 THE FULLY RENORMALIZED 4-POINT ξ-FUNCTION

The fully renormalized 4–point ξ–function is obviously given by eq. (4.63) with $\varepsilon_f \to \varepsilon_f + \Delta\varepsilon$ in the S_{ε_f} propagators, in the G loops, in f_F , and in $\langle P_o\rangle$ and $\langle P_1\rangle$. But we note from the examples in sect. 4.7 that the G–loop chains divided by f_F are actually independent of ε_f . Thus it does not matter if one uses $\varepsilon_f \to \varepsilon_f + \Delta\varepsilon$ or just ε_f in f_F and G. We will use an arbitrary $\tilde{\varepsilon}_f$ in f_F and G. The fully renormalized 4–point ξ–function (Γ_{4R}) is hence given by:

$$
\begin{aligned}
&\Gamma^{\alpha_1\alpha_2\gamma_1\gamma_2}_{4\mathrm{R}m_1m_2m_1'm_2'}(t_1,t_2,t_1',t_2') = \\
&= S^{\alpha_1\gamma_1}_{\varepsilon_f+\Delta\varepsilon}(t_1-t_1')\, S^{\alpha_2\gamma_2}_{\varepsilon_f+\Delta\varepsilon}(t_2-t_2')\, \delta_{m_1m_1'}\, \delta_{m_2m_2'}\, \langle P_o\rangle_{\mathrm{R}} + \\
&- S^{\alpha_1\gamma_2}_{\varepsilon_f+\Delta\varepsilon}(t_1-t_2')\, S^{\alpha_2\gamma_1}_{\varepsilon_f+\Delta\varepsilon}(t_2-t_1')\, \delta_{m_1m_2'}\, \delta_{m_2m_1'}\, \langle P_o\rangle_{\mathrm{R}} + \\
&+ S^{\alpha_1\gamma_1}_{\varepsilon_f+\Delta\varepsilon}(t_1-t_1')\, S^{\alpha_2\gamma_2}_{\varepsilon_f+\Delta\varepsilon}(t_2-t_2')\, \delta_{m_1m_2'}\, \delta_{m_2m_1'}\, G^{\gamma_1\gamma_2}_{\tilde{\varepsilon}_f}(t_1',t_2')\, \frac{\langle P_1\rangle_{\mathrm{R}}}{N\, f_F(\tilde{\varepsilon}_f-\mu)} \\
&- S^{\alpha_1\gamma_2}_{\varepsilon_f+\Delta\varepsilon}(t_1-t_2')\, S^{\alpha_2\gamma_1}_{\varepsilon_f+\Delta\varepsilon}(t_2-t_1')\, \delta_{m_1m_1'}\, \delta_{m_2m_2'}\, G^{\gamma_1\gamma_2}_{\tilde{\varepsilon}_f}(t_1',t_2')\, \frac{\langle P_1\rangle_{\mathrm{R}}}{N\, f_F(\tilde{\varepsilon}_f-\mu)} \\
&+ S^{\alpha_1\gamma_1}_{\varepsilon_f+\Delta\varepsilon}(t_1-t_1')\, S^{\alpha_2\gamma_1}_{\varepsilon_f+\Delta\varepsilon}(t_2-t_1')\, \varepsilon^{\gamma_1}\, S^{\gamma_1\gamma_2}_{\varepsilon_f+\Delta\varepsilon}(t_1'-t_2') \times \\
&\times \left[-\delta_{m_1m_1'}\, \delta_{m_2m_2'} + \delta_{m_1m_2'}\, \delta_{m_2m_1'}\right] \left[\langle P_o\rangle_{\mathrm{R}} + \frac{1}{N}\langle P_1\rangle_{\mathrm{R}}\right] + \\
&- S^{\alpha_1\gamma_2}_{\varepsilon_f+\Delta\varepsilon}(t_1-t_2')\, S^{\alpha_2\gamma_2}_{\varepsilon_f+\Delta\varepsilon}(t_2-t_2')\, \varepsilon^{\gamma_2}\, S^{\gamma_2\gamma_1}_{\varepsilon_f+\Delta\varepsilon}(t_2'-t_1') \times \\
&\times \left[-\delta_{m_1m_2'}\, \delta_{m_2m_1'} + \delta_{m_1m_1'}\, \delta_{m_2m_2'}\right] \left[\langle P_o\rangle_{\mathrm{R}} + \frac{1}{N}\langle P_1\rangle_{\mathrm{R}}\right] . \qquad (5.28)
\end{aligned}
$$

5.7 PERTURBATIVE CALCULATION OF THE FULL 4-POINT ξ-FUNCTION IGNORING VACUUM DIAGRAMS

As was done in sect. 5.4 for the propagator, we will use the Gell–Mann Low formula of eq. (2.29) to perturbatively calculate the 4–point function. Comparing this to the exact result will again show the necessity of using the generalized Gell–Mann Low formula of eq. (3.31).

Following the steps leading to eq. (5.16) in sect. 5.4, one obtains the following expression for the renormalized 4–point function, $\Gamma_{4\mathrm{R}}$:

$$\Gamma^{\alpha_1\alpha_2\gamma_1\gamma_2}_{4\ell m_1 m_2 m_1' m_2'}(t_1,t_2,t_1',t_2') = -\sum_{n=0}^{\infty}\frac{(-i\Delta\varepsilon)^n}{n!}\sum_{\{\bar\alpha_\ell\}}\int_{-\infty}^{\infty}\{d\bar t_\ell\}\;\varepsilon^{\bar\alpha_1}\ldots\varepsilon^{\bar\alpha_n}\,\times$$

$$\times\;\langle 0,\beta|\,T\,\xi^{\alpha_1}_{m_1}(t_1)\,\xi^{\alpha_2}_{m_2}(t_2)\,\xi^{\dagger\gamma_1}_{m_1'}(t_1')\,\xi^{\dagger\gamma_2}_{m_2'}(t_2')\,n^{\bar\alpha_1}(\bar t_1)\ldots n^{\bar\alpha_n}(\bar t_n)\,|0,\beta\rangle\,. \tag{5.29}$$

Examples of the various types of contractions obtained using the generalized Wick's theorem (eq. (3.13)) are presented below.

E.g. 1:

$$\underbrace{\underbrace{\xi^{\alpha_1}_{m_1}(t_1)\;\mathrlap{\overbrace{\phantom{\xi^{\alpha_2}_{m_2}(t_2)\;n^{\alpha}(t)\;\xi^{\dagger\gamma_1}_{m_1'}(t_1')\;\xi^{\dagger\gamma_2}_{m_2'}(t_2')}}^{\mathbf{M}^{\gamma_2}_{m_2m_2'}(t_2')}}\xi^{\alpha_2}_{m_2}(t_2)\;n^{\alpha}(t)}_{\xi^{\alpha}_{m_1}(t)}\;\xi^{\dagger\gamma_1}_{m_1'}(t_1')}_{\mathbf{M}^{\gamma_1}_{m_1m_1'}(t_1')}\;\xi^{\dagger\gamma_2}_{m_2'}(t_2')$$

This type of contraction renormalizes the $S^{\alpha_1\gamma_1}_{\varepsilon_f}(t_1-t_1')$ propagator in the 1st and 3rd terms of eq. (4.63).

E.g. 2:

$$\mathrlap{\overbrace{\phantom{\xi^{\alpha_1}_{m_1}(t_1)\;\xi^{\alpha_2}_{m_2}(t_2)\;n^{\alpha}(t)\;\xi^{\dagger\gamma_1}_{m_1'}(t_1')}}^{\mathbf{M}^{\gamma_1}_{m_1m_1'}(t_1')}}\xi^{\alpha_1}_{m_1}(t_1)\;\underbrace{\underbrace{\xi^{\alpha_2}_{m_2}(t_2)\;n^{\alpha}(t)}_{\xi^{\alpha}_{m_2}(t)}\;\xi^{\dagger\gamma_1}_{m_1'}(t_1')\;\xi^{\dagger\gamma_2}_{m_2'}(t_2')}_{\mathbf{M}^{\gamma_2}_{m_2m_2'}(t_2')}$$

This type of contraction renormalizes the $S^{\alpha_2\gamma_2}_{\varepsilon_f}(t_2-t_2')$ propagator in the 1st and 3rd terms of eq. (4.63). Similarly, one may renormalize the S_{ε_f} propagators in the 2nd and 4th terms of eq. (4.63).

E.g. 3:

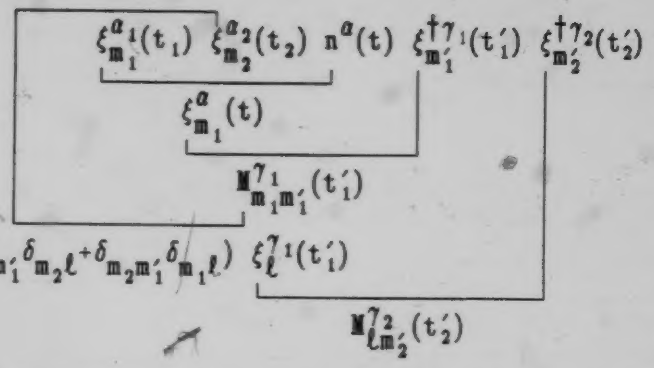

$$\xi^{\alpha_1}_{m_1}(t_1)\,\xi^{\alpha_2}_{m_2}(t_2)\,n^{\alpha}(t)\,\xi^{\dagger\gamma_1}_{m_1'}(t_1')\,\xi^{\dagger\gamma_2}_{m_2'}(t_2')$$

$$\xi^{\alpha}_{m_1}(t)$$

$$M^{\gamma_1}_{m_1m_1'}(t_1')$$

$$(-\delta_{m_1m_1'}\delta_{m_2\ell}+\delta_{m_2m_1'}\delta_{m_1\ell})\,\xi^{\gamma_1}_{\ell}(t_1')$$

$$M^{\gamma_2}_{\ell m_2'}(t_2')$$

This type of contraction renormalizes the $S^{\alpha_1\gamma_1}_{\varepsilon_f}(t_1-t_1')$ propagator in the 5th term of eq. (4.63).

E.g. 4:

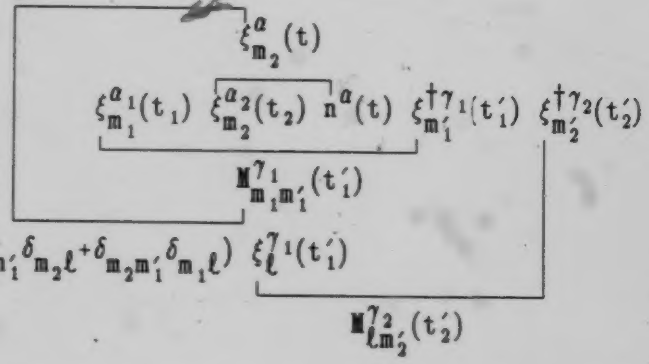

$$\xi^{\alpha}_{m_2}(t)$$

$$\xi^{\alpha_1}_{m_1}(t_1)\,\xi^{\alpha_2}_{m_2}(t_2)\,n^{\alpha}(t)\,\xi^{\dagger\gamma_1}_{m_1'}(t_1')\,\xi^{\dagger\gamma_2}_{m_2'}(t_2')$$

$$M^{\gamma_1}_{m_1m_1'}(t_1')$$

$$(-\delta_{m_1m_1'}\delta_{m_2\ell}+\delta_{m_2m_1'}\delta_{m_1\ell})\,\xi^{\gamma_1}_{\ell}(t_1')$$

$$M^{\gamma_2}_{\ell m_2'}(t_2')$$

This type of contraction renormalizes the $S^{\alpha_2\gamma_1}_{\varepsilon_f}(t_2-t_1')$ propagator in the 5th term of eq. (4.63).

E.g. 5:

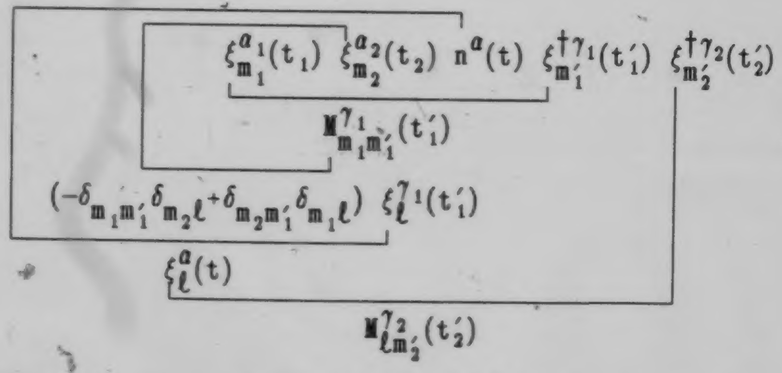

$$\xi^{\alpha_1}_{m_1}(t_1)\,\xi^{\alpha_2}_{m_2}(t_2)\,n^{\alpha}(t)\,\xi^{\dagger\gamma_1}_{m_1'}(t_1')\,\xi^{\dagger\gamma_2}_{m_2'}(t_2')$$

$$M^{\gamma_1}_{m_1m_1'}(t_1')$$

$$(-\delta_{m_1m_1'}\delta_{m_2\ell}+\delta_{m_2m_1'}\delta_{m_1\ell})\,\xi^{\gamma_1}_{\ell}(t_1')$$

$$\xi^{\alpha}_{\ell}(t)$$

$$M^{\gamma_2}_{\ell m_2'}(t_2')$$

This type of contraction renormalizes the $S^{\gamma_1\gamma_2}_{\varepsilon_f}(t_1'-t_2')$ propagator in the 5th term of eq. (4.63). Similarly, one may renormalize the S_{ε_f} propagators in the 6th term of eq. (4.63).

By extending the above examples to include multiple n–contractions as in sect. 5.4, and summing all the terms, one finds that all the S_{ε_f} terms in eq. (4.63) are renormalized to $S_{\varepsilon_f+\Delta\varepsilon}$.

What about the G's? They should be renormalized by the following type of expression:

E.g. 6: $$\varepsilon^{\alpha}\; n^{\alpha}(t)\; X^{\gamma_1}_{m_1' m_1}(t_1')\; X^{\gamma_2}_{m_2' m_2}(t_2')$$

But $n^{\alpha}(t)$ is actually t–independent and furthermore it commutes with the X's. Thus we may always bring it to the vacuum, where we have $(n-\tilde{n})|0,\beta\rangle = 0$ by the thermal state condition (eq. (2.15)). Thus the G's remain unrenormalized by eq. (5.29). This does not matter, as shown by the exact result, eq. (5.28).

The renormalized 4–point ξ–function, as calculated perturbatively using the Gell–Mann Low formula of eq. (2.29), is therefore given as follows:

$$\Gamma^{\alpha_1\alpha_2\gamma_1\gamma_2}_{4R\,m_1 m_2 m_1' m_2'}(t_1,t_2,t_1',t_2') =$$

$$\begin{aligned}
&= S^{\alpha_1\gamma_1}_{\varepsilon_f+\Delta\varepsilon}(t_1-t_1')\; S^{\alpha_2\gamma_2}_{\varepsilon_f+\Delta\varepsilon}(t_2-t_2')\; \delta_{m_1m_1'}\; \delta_{m_2m_2'}\; \langle P_o\rangle \;+\\
&- S^{\alpha_1\gamma_2}_{\varepsilon_f+\Delta\varepsilon}(t_1-t_2')\; S^{\alpha_2\gamma_1}_{\varepsilon_f+\Delta\varepsilon}(t_2-t_1')\; \delta_{m_1m_2'}\; \delta_{m_2m_1'}\; \langle P_o\rangle \;+\\
&+ S^{\alpha_1\gamma_1}_{\varepsilon_f+\Delta\varepsilon}(t_1-t_1')\; S^{\alpha_2\gamma_2}_{\varepsilon_f+\Delta\varepsilon}(t_2-t_2')\; \delta_{m_1m_2'}\; \delta_{m_2m_1'}\; G^{\gamma_1\gamma_2}_{\varepsilon_f}(t_1',t_2')\; \frac{\langle P_1\rangle}{N\, f_F(\varepsilon_f-\mu)}\\
&- S^{\alpha_1\gamma_2}_{\varepsilon_f+\Delta\varepsilon}(t_1-t_2')\; S^{\alpha_2\gamma_1}_{\varepsilon_f+\Delta\varepsilon}(t_2-t_1')\; \delta_{m_1m_1'}\; \delta_{m_2m_2'}\; G^{\gamma_1\gamma_2}_{\varepsilon_f}(t_1',t_2')\; \frac{\langle P_1\rangle}{N\, f_F(\varepsilon_f-\mu)}\\
&+ S^{\alpha_1\gamma_1}_{\varepsilon_f+\Delta\varepsilon}(t_1-t_1')\; S^{\alpha_2\gamma_1}_{\varepsilon_f+\Delta\varepsilon}(t_2-t_1')\; \varepsilon^{\gamma_1}\; S^{\gamma_1\gamma_2}_{\varepsilon_f+\Delta\varepsilon}(t_1'-t_2') \;\times\\
&\times \left[-\delta_{m_1m_1'}\; \delta_{m_2m_2'} + \delta_{m_1m_2'}\; \delta_{m_2m_1'}\right] \left[\langle P_o\rangle + \frac{1}{N}\langle P_1\rangle\right] +\\
&- S^{\alpha_1\gamma_2}_{\varepsilon_f+\Delta\varepsilon}(t_1-t_2')\; S^{\alpha_2\gamma_2}_{\varepsilon_f+\Delta\varepsilon}(t_2-t_2')\; \varepsilon^{\gamma_2}\; S^{\gamma_2\gamma_1}_{\varepsilon_f+\Delta\varepsilon}(t_2'-t_1') \;\times\\
&\times \left[-\delta_{m_1m_2'}\; \delta_{m_2m_1'} + \delta_{m_1m_1'}\; \delta_{m_2m_2'}\right] \left[\langle P_o\rangle + \frac{1}{N}\langle P_1\rangle\right] .
\end{aligned} \tag{5.30}$$

Comparing this to the exact result, eq. (5.28), one finds that $\langle P_o \rangle$ and $\langle P_1 \rangle$ should be renormalized and they are not. Thus the renormalization of Γ_4 using eq. (2.29) is incomplete, again demonstrating the need for the generalized Gell–Mann Low formula of eq. (3.31).

5.8 PERTURBATIVE CALCULATION OF THE FULL 4-POINT ε-FUNCTION USING THE GENERALIZED GELL–MANN LOW FORMULA

Let us repeat the calculation of the last section, using the generalized Gell–Mann Low formula of eq. (3.31).

The arguments presented in sect. 5.5 for the propagator extend directly to the case of the 4–point function. Firstly, the U terms at $\mathcal{Re}\, t = \pm\infty$ contribute only to the 0–energy boson T–product. Secondly, their effect is simply multiplication by 1 in the P_o subspace and multiplication by $e^{-\beta\Delta\varepsilon}$ in the P_1 subspace. Thirdly, this has the effect of transforming $\langle P_o \rangle$ into $\langle P_o \rangle_R$ and $\langle P_1 \rangle$ into $\langle P_1 \rangle_R$. Therefore, the fully renormalized 4–point function as calculated perturbatively using the generalized Gell–Mann Low formula of eq. (3.31) is:

$$
\begin{aligned}
&\Gamma^{\alpha_1\alpha_2\gamma_1\gamma_2}_{4\mathbf{R}m_1m_2m_1'm_2'}(t_1,t_2,t_1',t_2') = \\
&= S^{\alpha_1\gamma_1}_{\varepsilon_f+\Delta\varepsilon}(t_1-t_1')\, S^{\alpha_2\gamma_2}_{\varepsilon_f+\Delta\varepsilon}(t_2-t_2')\, \delta_{m_1m_1'}\, \delta_{m_2m_2'}\, \langle P_o\rangle_{\mathbf{R}} + \\
&- S^{\alpha_1\gamma_2}_{\varepsilon_f+\Delta\varepsilon}(t_1-t_2')\, S^{\alpha_2\gamma_1}_{\varepsilon_f+\Delta\varepsilon}(t_2-t_1')\, \delta_{m_1m_2'}\, \delta_{m_2m_1'}\, \langle P_o\rangle_{\mathbf{R}} + \\
&+ S^{\alpha_1\gamma_1}_{\varepsilon_f+\Delta\varepsilon}(t_1-t_1')\, S^{\alpha_2\gamma_2}_{\varepsilon_f+\Delta\varepsilon}(t_2-t_2')\, \delta_{m_1m_2'}\, \delta_{m_2m_1'}\, G^{\gamma_1\gamma_2}_{\varepsilon_f}(t_1',t_2')\, \frac{\langle P_1\rangle_{\mathbf{R}}}{N\, f_F(\varepsilon_f-\mu)} \\
&- S^{\alpha_1\gamma_2}_{\varepsilon_f+\Delta\varepsilon}(t_1-t_2')\, S^{\alpha_2\gamma_1}_{\varepsilon_f+\Delta\varepsilon}(t_2-t_1')\, \delta_{m_1m_1'}\, \delta_{m_2m_2'}\, G^{\gamma_1\gamma_2}_{\varepsilon_f}(t_1',t_2')\, \frac{\langle P_1\rangle_{\mathbf{R}}}{N\, f_F(\varepsilon_f-\mu)} \\
&+ S^{\alpha_1\gamma_1}_{\varepsilon_f+\Delta\varepsilon}(t_1-t_1')\, S^{\alpha_2\gamma_1}_{\varepsilon_f+\Delta\varepsilon}(t_2-t_1')\, \varepsilon^{\gamma_1}\, S^{\gamma_1\gamma_2}_{\varepsilon_f+\Delta\varepsilon}(t_1'-t_2') \times \\
&\times \left[-\delta_{m_1m_1'}\, \delta_{m_2m_2'} + \delta_{m_1m_2'}\, \delta_{m_2m_1'}\right] \left[\langle P_o\rangle_{\mathbf{R}} + \frac{1}{N}\, \langle P_1\rangle_{\mathbf{R}}\right] + \\
&- S^{\alpha_1\gamma_2}_{\varepsilon_f+\Delta\varepsilon}(t_1-t_2')\, S^{\alpha_2\gamma_2}_{\varepsilon_f+\Delta\varepsilon}(t_2-t_2')\, \varepsilon^{\gamma_2}\, S^{\gamma_2\gamma_1}_{\varepsilon_f+\Delta\varepsilon}(t_2'-t_1') \times \\
&\times \left[-\delta_{m_1m_2'}\, \delta_{m_2m_1'} + \delta_{m_1m_1'}\, \delta_{m_2m_2'}\right] \left[\langle P_o\rangle_{\mathbf{R}} + \frac{1}{N}\, \langle P_1\rangle_{\mathbf{R}}\right] \quad . \qquad (5.31)
\end{aligned}
$$

S_{ε_f} has been renormalized to $S_{\varepsilon_f+\Delta\varepsilon}$, $\langle P_o\rangle$ has been renormalized to $\langle P_o\rangle_{\mathbf{R}}$, and $\langle P_1\rangle$ has been renormalized to $\langle P_1\rangle_{\mathbf{R}}$, but $G_{\varepsilon_f}/f_F(\varepsilon_f-\mu)$ has not been renormalized. Although this agrees with the exact result of eq. (5.28), it still requires some explanation.

The 3rd and 4th terms of eq. (5.31) have the following form:

$$
\text{term 3} = S_{\varepsilon_f+\Delta\varepsilon}\, S_{\varepsilon_f+\Delta\varepsilon} \times
$$

$$
\times \frac{\langle 0,\beta|\ U(\infty-\frac{i\beta}{2},\infty)\ T\left[\, X^{\gamma_1}_{m_1'm_1}(t_1')\ X^{\gamma_2}_{m_2'm_2}(t_2')\,\right] U(-\infty,-\infty+\frac{i\beta}{2})\ |0,\beta\rangle}{\langle P_o\rangle + e^{-\beta\Delta\varepsilon}\ \langle P_1\rangle} \; .
\qquad (5.32)
$$

As before (e.g. 6 of sect. 5.7) the $\hat{U}$ terms have no effect on the X–operator T–product; they have been dropped from eq. (5.32). Noting that the X–operator T–product acts only in the P_1 subspace, and that the U's at $\mathcal{Re}\, t = \pm\infty$ contribute $e^{-\beta\Delta\varepsilon/2}$ in the P_1 subspace, one finds:

$$\text{term 3} = S_{\varepsilon_f+\Delta\varepsilon}\, S_{\varepsilon_f+\Delta\varepsilon}\, \times$$

$$\times\ \frac{e^{-\beta\Delta\varepsilon}\ \langle 0,\beta|\ T\left[\ X^{\gamma_1}_{m_1'm_1}(t_1')\ X^{\gamma_2}_{m_2'm_2}(t_2')\ \right] |0,\beta\rangle}{\langle P_o\rangle + e^{-\beta\Delta\varepsilon}\ \langle P_1\rangle}\ . \tag{5.33}$$

Applying eq. (4.59) to the above yields the result quoted in eq. (5.31).

One must be especially cautious here. The effect of the U's at $\mathcal{R}e\, t = \pm\infty$ was determined before the time–splitting was performed. Suppose one keeps the U's at $\mathcal{R}e\, t = \pm\infty$ in the T–product of eq. (5.32), and then performs the time–splitting. If one argues as before that the ξ contractions with the U's at $\mathcal{R}e\, t = \pm\infty$ are damped out, then one finds:

$$\text{term 3} = S_{\varepsilon_f+\Delta\varepsilon}\, S_{\varepsilon_f+\Delta\varepsilon}\, G_{\varepsilon_f}(t_1',t_2')\ \delta_{m_1m_2'}\ \delta_{m_2m_1'}\ \times$$

$$\times\ \frac{\langle 0,\beta|\ U(\infty-\frac{i\beta}{2},\infty)\ T\left[\ P_o + \frac{1}{N}\ P_1\ \right] U(-\infty,-\infty+\frac{i\beta}{2})\ |0,\beta\rangle}{\langle P_o\rangle + e^{-\beta\Delta\varepsilon}\ \langle P_1\rangle} =$$

$$= S_{\varepsilon_f+\Delta\varepsilon}\, S_{\varepsilon_f+\Delta\varepsilon}\, G_{\varepsilon_f}(t_1',t_2')\ \delta_{m_1m_2'}\ \delta_{m_2m_1'}\left[\langle P_o\rangle_R + \frac{1}{N}\ \langle P_1\rangle_R\right] =$$

$$= S_{\varepsilon_f+\Delta\varepsilon}\, S_{\varepsilon_f+\Delta\varepsilon}\, G_{\varepsilon_f}(t_1',t_2')\ \delta_{m_1m_2'}\ \delta_{m_2m_1'}\ \frac{\langle P_1\rangle_R}{N\ f_F(\varepsilon_f+\Delta\varepsilon-\mu)}\ . \tag{5.34}$$

This does not agree with the previous result, because $f_F(\varepsilon_f-\mu)$ has been renormalized to $f_F(\varepsilon_f + \Delta\varepsilon - \mu)$ in eq. (5.34). The reason is that the damping argument is no longer valid. As shown in sect. 5.9 below, there are times when one must include contractions of ξ with operators at $\mathcal{R}e\, t = \pm\infty$. To avoid this, one should determine the effect of the U's at $\mathcal{R}e\, t = \pm\infty$ before performing the time–splitting.

Therefore, the generalized Gell–Mann Low formula of eq. (3.31) gives the correct answer for the renormalized 4–point ξ–function, if applied correctly.

5.9 CONTRACTIONS WHICH DO NOT DAMP AT $\mathcal{R}e\, t = \pm\infty$

In sect. 3.3.2, it was argued that the contraction of $\xi_a(t)$ $(E_a \neq 0)$ with a U term at $\mathcal{R}e\, t = \pm\infty$ will be damped, and hence the U terms at $\mathcal{R}e\, t = \pm\infty$ contribute only vacuum diagrams. In this section, a counter–example is presented.

It is obvious from eqs. (5.7d) and (4.13) that:

$$\langle 0,\beta |\, X_{mm'}(t)\, | 0,\beta \rangle = \frac{1}{N} \langle P_1 \rangle\, \delta_{mm'} \quad , \tag{5.35}$$

where $\langle P_1 \rangle$ is given by eq. (4.18b). From the relation $P_1 = n$, (eq. (5.4a)), one deduces that

$$\langle 0,\beta |\, X_{mm'}(t)\, n(t^{\bullet})\, | 0,\beta \rangle = \frac{1}{N} \langle P_1 \rangle\, \delta_{mm'} \quad , \tag{5.36}$$

as well. This is because the X–operator acts only in the P_1 subspace and $P_1^2 = P_1$.

Suppose we now calculate this using the time–splitting technique of sect. 4.5. From the generalized reduction formula of eq. (3.13), one obtains:

$$\begin{aligned}
\langle 0,\beta | T\, X^{\gamma\alpha}_{m'm}(t',t)\, n(t^{\bullet})\, | 0,\beta \rangle &= -\, \varepsilon^{\alpha} \langle 0,\beta | T\, \xi^{\alpha}_{m}(t)\, \xi^{\dagger\gamma}_{m'}(t')\, n(t^{\bullet})\, | 0,\beta \rangle = \\
&= -\, \varepsilon^{\alpha} \Big[S^{\alpha\gamma}_{\varepsilon_f}(t-t')\, \langle 0,\beta | T\, M^{\gamma}_{mm'}(t')\, n(t^{\bullet})\, | 0,\beta \rangle + \\
&\quad - S^{\alpha 1}_{\varepsilon_f}(t-t^{\bullet})\, \langle 0,\beta | T\, \xi^{\dagger\gamma}_{m'}(t')\, \xi_m(t^{\bullet})\, | 0,\beta \rangle \Big] = \\
&= -\, \varepsilon^{\alpha} \delta_{mm'} \left\{ S^{\alpha\gamma}_{\varepsilon_f}(t-t')\, \frac{\langle P_1 \rangle}{N} + S^{\alpha 1}_{\varepsilon_f}(t-t^{\bullet})\, S^{1\gamma}_{\varepsilon_f}(t^{\bullet}-t') \left[\langle P_o \rangle + \frac{1}{N} \langle P_1 \rangle \right] \right\} ,
\end{aligned} \tag{5.37}$$

where $X^{\gamma\alpha}_{m'm}(t',t)$ is defined in eq. (4.40a). Letting $\alpha = \gamma$ and $t' = t + \varepsilon^{\gamma}\delta$, and using eq. (4.40b), one obtains:

$$\begin{aligned}
&\langle 0,\beta | T\, X^{\gamma}_{m'm}(t)\, n(t^{\bullet})\, | 0,\beta \rangle = \\
&= -\, \varepsilon^{\gamma}\, \delta_{mm'} \left\{ S^{\gamma\gamma}_{\varepsilon_f}(-\varepsilon^{\gamma}\delta)\, \frac{\langle P_1 \rangle}{N} + S^{\gamma 1}_{\varepsilon_f}(t-t^{\bullet})\, S^{1\gamma}_{\varepsilon_f}(t^{\bullet}-t) \left[\langle P_o \rangle + \frac{1}{N} \langle P_1 \rangle \right] \right\} .
\end{aligned} \tag{5.38}$$

Using eqs. (4.45) and (4.58) in the above yields:

$$\langle 0,\beta|\mathrm{T}\ X^{\gamma}_{m',m}(t)\ n(t')\ |0,\beta\rangle =$$

$$= \delta_{mm'} \left\{ f_F(\varepsilon_f-\mu)\ \frac{\langle P_1\rangle}{N} + f_F(-\varepsilon_f+\mu)\ G^{\gamma 1}_{\varepsilon_f}(t,t')\ \left[\langle P_o\rangle + \frac{1}{N}\ \langle P_1\rangle\right]\right\} . \tag{5.39}$$

With eq. (4.49a), this becomes

$$\langle 0,\beta|\mathrm{T}\ X^{\gamma}_{m',m}(t)\ n(t')\ |0,\beta\rangle =$$

$$= \delta_{mm'} \left\{ f_F(\varepsilon_f-\mu)\ \frac{\langle P_1\rangle}{N} + G^{\gamma 1}_{\varepsilon_f}(t,t')\ \langle P_o\rangle \right\} . \tag{5.40}$$

Using eq. (4.124) for $G_{\varepsilon_f}(t,t')$ along with eq. (4.49b), one finds that eq. (5.40) reduces to eq. (5.36). Therefore the time–splitting method is consistent with the result of direct evaluation.

Suppose now that we let $t' = -\infty$. If one now argues that the $\xi(t)$ contraction with $n(-\infty)$ is damped out, then one keeps only the first term in eq. (5.37). This leaves only the first term of eq. (5.40), which is in obvious contradiction with eq. (5.36). Therefore it is ***absolutely necessary*** that one doesn't assume that the contraction of $\xi(t)$ with $n(-\infty)$ is damped out!

Does this invalidate the argument of sect. 3.3.2 that the U terms at $\mathcal{R}e\, t = \pm\infty$ contribute only vacuum diagrams? Not if one is careful. The non–damping problem only arises when attempting to do the time–splitting with operators at $\mathcal{R}e\, t = \pm\infty$ present. It is imperative that one determines the effect of the U–operators at $\mathcal{R}e\, t = \pm\infty$, and removes them from the operator product before performing the time–splitting, as was demonstrated in sect. 5.8.

5.10 CONCLUSION

Perturbation theory in the context of an exactly soluable quantum algebra was presented. It was found that the generalized Gell–Mann Low formula and its non–cancelling vacuum diagrams are necessary in order to obtain the correct answer. Some important lessons were learned. Firstly, the effect of the U terms at $\mathcal{R}e\, t = \pm\infty$ should be determined before the time-splitting is performed. Secondly, if this is possible, then the U terms at $\mathcal{R}e\, t = \pm\infty$ contribute vacuum diagrams, whose purpose is to renormalize the projection operators, and hence the sector structure. Thirdly, if it is not possible to determine the effect of the U terms at $\mathcal{R}e\, t = \pm\infty$ before performing the time-splitting, then these U terms must be contracted with the other terms when performing the time-splitting. This would have the effect of connecting the so called "vacuum diagrams" to the main diagram.

As will be seen in the next chapter, it is this third point which causes problems when considering the ~~real~~ Anderson Model.

CHAPTER 6

THE SINGLE IMPURITY INFINITE-U ANDERSON MODEL

6.1 THE MODEL

6.1.1 THE HAMILTONIAN

Having developed and extensively discussed a finite temperature quantum field theoretic methodology, for dealing with a localized f-electron state having restricted occupancy, we now let this state interact with a conduction electron gas. This is the single-site Anderson model, which was presented in section 1.5 and reviewed in section 1.7.

As a model, we will use the Hamiltonian of eq. (1.15), in which the infinite Coulomb term has been removed by restricting the Fock space of the f-electrons. This yields the following Hamiltonian:

$$H = H_o + H_I \ , \tag{6.1a}$$

$$H_o = \sum_m \int d^3x \, c_m^\dagger(\vec{x}) \, \varepsilon(-i\vec{\nabla}) \, c_m(\vec{x}) + \varepsilon_f \sum_m \xi_m^\dagger \xi_m \ , \tag{6.1b}$$

$$H_I = \sqrt{\frac{2}{N}} \, V \sum_m \left[c_{om}^\dagger \xi_m + \xi_m^\dagger c_{om} \right] . \tag{6.1c}$$

The properties of the ξ_m-operators, and other related operators in the algebra, are summarized in eqs. (5.1) to (5.7g). As in eq. (1.8), the single-site conduction electron operator c_{om} is given by:

$$c_{om} \equiv \sqrt{\Omega} \, c_m(\vec{x} = 0) \ , \tag{6.2}$$

where Ω is the volume of a unit cell of the metal. This ensures the following anti-commutation relations:

$$\left\{ c_m(\vec{x}) , c_{m'}^\dagger(\vec{x}') \right\} = \delta_{mm'} \, \delta^3(\vec{x} - \vec{x}') \ , \tag{6.3a}$$

$$\left\{ c_{om} , c_{om'}^\dagger \right\} = \delta_{mm'} \ , \tag{6.3b}$$

noting eqs. (1.10a) and (1.10b) for the Dirac delta functions.

6.1.2 CHEMICAL POTENTIALS AND THE ENERGY SCALE

As was set out in chapter 2, TFD was designed to match the results of a grand canonical ensemble. (See eq. (2.1).) In a grand canonical ensemble, one uses H-μN, which is why the chemical potential μ appears in the explicit construction of the thermal vacuum (eq. (2.4)), and also appears in the thermal state condition (eq. (2.15)). This means that the thermal Bogoliubov transformation matrix of simple creation/annihilation operators (eq. (2.21b)) contains μ. And, for general Fermi/Bose fields, the propagators (eqs. (2.22b) – (2.22c)) are also μ-dependent, μ being carried by the thermal U-matrices. When dealing with a quantum algebra, the μ-dependent nature also appears in the thermal U-matrices, as seen in the generalized Wick's theorem of section 3.2.3.

In the Anderson model, one is dealing with two fermion fields, which means there are two chemical potentials:

$$\mu N \to \mu_c n_c + \mu_f n_f = \mu_c \sum_m \int d^3x \; c_m^\dagger(\vec{x})\, c_m(\vec{x}) + \mu_f \sum_m \xi_m^\dagger \xi_m \quad . \tag{6.4}$$

The purpose of μ_c is obvious: At T=0, it is the Fermi level of the conduction electron gas. As T increases, μ_c must be modified in order to keep the number of conduction electrons constant.

The purpose of μ_f is less obvious. In chapters 4 and 5, μ_f was kept explicit, in a finite temperature quantum field theoretic description of a localized f–state. Upon reflection, this is totally meaningless. How can one talk about "temperature" and "chemical potential", when there is only one f–state, whose spectrum is a delta function? Temperature manifests itself as a distribution of occupied and unoccupied states. Here, there is only one state, and it is always occupied; there is no place for the electron to go to.

One may think of the models of chapters 4 and 5 as having infinite chemical potential; when $\mu_f = \infty$, the state is ***always*** occupied, regardless of the value of β. This corresponds to $V = 0$ in the Anderson model.

The moment a $V \neq 0$ exists, one would expect an infinite renormalization of μ_f, because now the f–electrons would have some place to go to. Specifically, they could hop into the conduction bands. If $\epsilon_f > \mu_c$, one would expect the f–state to empty out into the conduction band. On the other hand, if $\epsilon_f < \mu_c$, conduction levels at this energy are already filled, and one would expect the f–state to remain occupied. Thus $\mu_f \rightarrow \mu_c$ when the interaction is switched on.

Rather than use the bare $\mu_f = \infty$, we will use the renormalized $\mu_f^{\mathbf{R}} = \mu_c^{\mathbf{R}}$. Note that μ_c also carries the "**R**" (≡ "**Renormalized**") superscript, because μ_c itself will be renormalized due to conduction states being occupied by the displaced f–electrons. This is significant in the lattice Anderson model, but may be ignored in the single–site case as a $1/N_c$ effect. (N_c is the number of unit cells in the crystal.)

Strictly speaking, this thesis will define the zero–point of the energy scale to be $\mu_c(V{=}0\,, T{=}0) = 0$. That is, all energies will be measured relative to the unrenormalized conduction electron chemical potential at T=0. As there is really only one chemical potential, this thesis will define $\mu(T) \equiv \mu_f^{\mathbf{R}} = \mu_c^{\mathbf{R}}$. Therefore $\mu(T) \rightarrow 0$ as $T \rightarrow 0$ and $V \rightarrow 0$. One may expect $\mu(T) \simeq 0$ in the single–site case, because the effect of V is $O(1/N_c)$, and the effect of T is $O((T/T_F)^2)$. (Here T_F is the Fermi temperature, which is roughly $10^4 - 10^5$ K.) Nevertheless, for the sake of generality, μ will be kept explicit in the calculations.

6.1.3 THE PROPAGATORS AND THEIR SPECTRAL FUNCTIONS

The bare c–electron propagator $C(\vec{x}-\vec{x}',t-t')$, the bare site–localized c–electron propagator $C_o(t-t')$, and the bare f–electron propagator $\mathcal{F}(t-t')$ are defined as follows:

$$\delta_{mm'}\, C^{\alpha\gamma}(\mathbf{x}-\mathbf{x}',t-t') \equiv \langle 0,\beta|\, T\, c^{\alpha}_{m}(\mathbf{x},t)\, c^{\dagger\gamma}_{m'}(\mathbf{x}',t')\, |0,\beta\rangle \;, \tag{6.5a}$$

$$\delta_{mm'}\, C^{\alpha\gamma}_{o}(t-t') \equiv \langle 0,\beta|\, T\, c^{\alpha}_{om}(t)\, c^{\dagger\gamma}_{om'}(t')\, |0,\beta\rangle \;, \tag{6.5b}$$

$$\delta_{mm'}\, \mathcal{S}^{\alpha\gamma}(t-t') = \langle 0,\beta|\, T\, \xi^{\alpha}_{m}(t)\, \xi^{\dagger\gamma}_{m'}(t')\, |0,\beta\rangle \;. \tag{6.5c}$$

Here $|0,\beta\rangle$ is the thermal vacuum of the free Hamiltonian, and is given by:

$$|0,\beta\rangle \equiv |0,\beta\rangle_{f} \otimes |0,\beta\rangle_{c} \;, \tag{6.6}$$

where $|0,\beta\rangle_{f}$ is the free thermal vacuum of the f–electrons, and $|0,\beta\rangle_{c}$ is the free thermal vacuum of the c–electrons. An explicit construction of $|0,\beta\rangle_{f}$ is given in eqs. (4.13). Similarly, $|0,\beta\rangle_{c}$ may be explicitly constructed as in eqs. (2.4) – (2.5).

The fully renormalized c–electron propagator $C_{R}(\mathbf{x},\mathbf{x}'\,;t-t')$, the fully renormalized site–localized c–electron propagator $C_{oR}(t-t')$, and the fully renormalized f–electron propagator $\mathcal{S}_{R}(t-t')$, are defined in terms of $|0(\beta)\rangle$, the thermal vacuum of the *full* Hamiltonian, as follows:

$$C^{\alpha\gamma}_{Rmm'}(\mathbf{x},\mathbf{x}'\,;t-t') \equiv \langle 0(\beta)|\, T\, c^{\alpha}_{m}(\mathbf{x},t)\, c^{\dagger\gamma}_{m'}(\mathbf{x}',t')\, |0(\beta)\rangle \;, \tag{6.7a}$$

$$C^{\alpha\gamma}_{oRmm'}(t-t') \equiv \langle 0(\beta)|\, T\, c^{\alpha}_{om}(t)\, c^{\dagger\gamma}_{om'}(t')\, |0(\beta)\rangle \;, \tag{6.7b}$$

$$\mathcal{S}^{\alpha\gamma}_{Rmm'}(t-t') \equiv \langle 0(\beta)|\, T\, \xi^{\alpha}_{m}(t)\, \xi^{\dagger\gamma}_{m'}(t')\, |0(\beta)\rangle \;, \tag{6.7c}$$

where the operators are time–evolved under the full Hamiltonian.

As in eq. (4.19), the bare f–electron propagator is given by:

$$\mathcal{S}^{\alpha\gamma}(t-t') = S^{\alpha\gamma}_{\varepsilon_f}(t-t') \left[\langle P_o\rangle + \frac{1}{N}\langle P_1\rangle \right] \tag{6.8}$$

Here $S_{\varepsilon_f}(t-t')$ is given by eqs. (4.16a) – (4.16c). $\langle P_o\rangle$ and $\langle P_1\rangle$ are the bare thermal vacuum expectation values of the 0–particle and 1–particle projection operators, as given in eqs. (4.17b) – (4.17e). The evaluation of $\langle P_o\rangle$ and $\langle P_1\rangle$ is given by eqs. (4.18a) – (4.18b).

One may also define the fully renormalized projection operator expectation values in terms of $|0(\beta)\rangle$, as follows::

$$\langle P_o\rangle_R \equiv \langle 0(\beta)|P_o|0(\beta)\rangle \ , \tag{6.9a}$$

$$\langle P_l\rangle_R \equiv \langle 0(\beta)|P_l|0(\beta)\rangle \ , \tag{6.9b}$$

$$\langle P_l^{(m)}\rangle_R \equiv \langle 0(\beta)|P_l^{(m)}|0(\beta)\rangle \ , \tag{6.9c}$$

where $P_l = \sum_m P_l^{(m)}$ and $P_l^{(m)} \equiv |m\rangle\langle m|$, the spin-m projection operator.

The conduction electron operators obey the usual anti–commutation relations. Thus, the bare c–electron propagator has the standard form of eqs. (2.22a) – (2.24), with a spectral function of:

$$\sigma_c(\kappa,\vec{k}) = \delta(\kappa-\varepsilon_{\vec{k}}) \ , \tag{6.10a}$$

$$\varepsilon_{\vec{k}} = \frac{|\vec{k}|^2}{2m_e} - E_F \ , \tag{6.10b}$$

where m_e is the mass of the bare electron, and E_F is the Fermi energy (as measured from the bottom of the band). Note that $\varepsilon_k(k=k_F) = 0$, (where k_F is the Fermi momentum), conforming with the zero–point of the energy scale defined in sect. 6.1.2.

From eq. (2.24), the (1,1)-component of the "barred" c-electron propagator is given by:

$$\bar{C}^{11}(\omega,\vec{k}) = \frac{1}{\omega - \varepsilon_k + i\delta} \tag{6.11}$$

From eqs. (6.5a), (6.5b), and (6.2), one finds the site–localized c–electron propagator to be given by:

$$C_o^{\alpha\gamma}(t-t') = \Omega\ C^{\alpha\gamma}(\vec{x}-\vec{x}'=0\,,\,t-t') \ . \tag{6.12}$$

Using this in conjunction with the Fourier transform defined in eq. (2.22a), and dropping the thermal matrices, one finds the (1,1)-component of the "barred", site–localized, c–electron propagator to be given by:

$$\bar{C}_o^{11}(\omega) = \Omega \int_{\Omega_B} \frac{d^3k}{(2\pi)^3}\, \frac{1}{\omega - \varepsilon_k + i\delta} \ , \tag{6.13}$$

where the domain of integration Ω_B is the Brillouin zone.

As a rough approximation, we may assume that the band is spherically symmetric, with $\epsilon_k \to E_{BZ}$ $\left[\equiv \frac{k_{BZ}^2}{2m_e} - E_F\right]$ when $k \to k_{BZ}$, the Brillouin zone edge. Then:

$$\int_{\Omega_B} d^3k = 4\pi \int_0^{k_{BZ}} k^2\, dk = 2\pi \int_0^{k_{BZ}} k\, dk^2 = 2\pi (2m_e)^{\frac{1}{2}} \int_0^{k_{BZ}^2/2m_e} \sqrt{\epsilon}\, d\epsilon =$$

$$= 2\pi (2m_e)^{\frac{1}{2}} \int_{-E_F}^{E_{BZ}} \sqrt{\epsilon_k + E_F}\, d\epsilon_k = 2\pi (2m_e)^{\frac{1}{2}} \sqrt{E_F} \int_{-E_F}^{E_{BZ}} \sqrt{1 + \frac{\epsilon_k}{E_F}}\, d\epsilon_k . \tag{6.14}$$

Noting $\Omega/(2\pi)^3 = 1/\Omega_B$, and $\Omega_B = \frac{4}{3}\pi k_{BZ}^3 = \frac{4}{3}\pi (2m_e)^{\frac{3}{2}} (E_{BZ}+E_F)^{\frac{3}{2}}$, eq. (6.14) becomes:

$$\Omega \int_{\Omega_B} \frac{d^3k}{(2\pi)^3} = \frac{1}{\Omega_B} \int_{\Omega_B} d^3k = \frac{3/2}{E_F \left[1 + \frac{E_{BZ}}{E_F}\right]^{3/2}} \int_{-E_F}^{E_{BZ}} \sqrt{1 + \frac{\epsilon_k}{E_F}}\, d\epsilon_k . \tag{6.15}$$

Let us make the following definition:

$$N(\epsilon_k) \equiv \frac{3}{2} \frac{1}{E_F} \left[1 + \frac{E_{BZ}}{E_F}\right]^{-3/2} \sqrt{1 + \frac{\epsilon_k}{E_F}} . \tag{6.16}$$

Here $N(\epsilon_k)$ is the number of momentum states per unit energy per unit cell, at energy ϵ_k. This may be written as::

$$N(\epsilon_k) = N(0) \sqrt{1 + \frac{\epsilon_k}{E_F}} , \tag{6.17}$$

where $N(0)$ is the density of states at the Fermi surface (ϵ_k=0).

With the use of eqs. (6.15) to (6.17), eq. (6.13) becomes:

$$\tilde{C}_o^{11}(\omega) = N(0) \int_{-E_F}^{E_{BZ}} d\epsilon_k \sqrt{1 + \frac{\epsilon_k}{E_F}}\ \frac{1}{\omega - \epsilon_k + i\delta} . \tag{6.18}$$

Using eq. (2.28) to find the spectral function of $C_o^{\alpha\gamma}(\omega;\mu)$, one obtains:

$$\sigma_{c_o}(\omega) = N(0)\sqrt{1+\frac{\omega}{E_F}}\left[\theta(E_{BZ}-\omega) - \theta(-E_F-\omega)\right] . \qquad (6.19)$$

The density of states of the bare, site–localized c-electron propagator, therefore, has the shape of the upper half of a sideways parabola straddling the ω–axis. The zero–point of the parabola is at $\omega = -E_F$; it rises from there until $\omega = E_{BZ}$, at which point there is a cut–off. This is illustrated in FIG. 6.1.

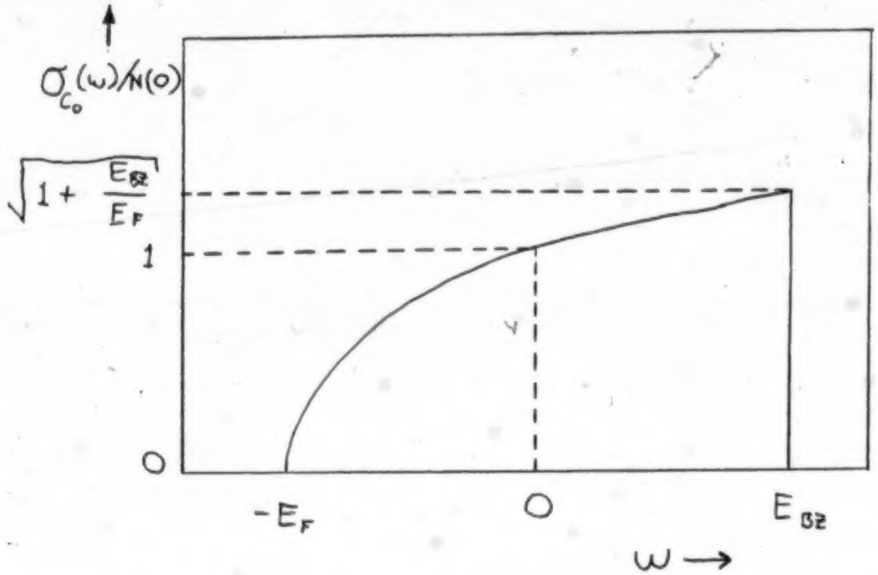

FIG. 6.1

The Free Conduction Electron Density of States

The free conduction electron density of states is plotted as a function of energy. At T=0, these states will be fully occupied up to ω=0, and unoccupied above this energy. Here E_F is the Fermi energy and E_{BZ} is the energy at the Brillouin zone edge.

As stated in sect. 2.4.3, the spectral function gives only the density of states; nothing is said about the occupation of these states. Their occupation is determined by the thermal U–matrices, which carry μ. As T → 0, $\mu \rightarrow 0$, and therefore all the states from $\omega = -E_F$ to $\omega = 0$ of FIG. 6.1 will be occupied, and all the states from $\omega = 0$ to $\omega = E_{BZ}$ will be unoccupied. If n_o is the number of conduction electrons per unit cell, then at finite T one should find:

$$n_o = N\int d\omega\, \sigma_{C_o}(\omega)\, f_F(\omega-\mu) = N(0)\, N\int_{-E_F}^{E_{BZ}} d\omega \sqrt{1+\frac{\omega}{E_F}}\; f_F(\omega-\mu) \quad , \tag{6.20}$$

where the factor of N is because there are N spin states for each momentum state.

Noting that n_o is a fixed number, this will be the equation that determines $\mu(T)$.

6.1.4 STATEMENT OF THE PROBLEM

In sect. 6.1.3, the structure of the bare f–electron and bare c–electron propagators was discussed, and the renormalized f– and c–electron propagators were introduced. The problem is to calculate $\mathcal{G}_R$ and C_R , and obtain their spectral functions. This will show the density of states as a function of temperature, and should exhibit the Kondo resonance peak appearing at the Kondo temperature, as discussed in Chapter 1.

6.1.5 THE FLAT BAND (D – CUTOFF) APPROXIMATION

It was noted in sect. 1.7.2 that, due to the degenerate nature of the electron gas, the c–states relevant to the transport properties of a metal are those near the Fermi surface ($|\omega| << E_F$). We also assume that ϵ_f is fairly close to the Fermi surface ($|\epsilon_f| << E_F$), such that the dominant contributions of relevant integrals come from ω near the Fermi surface. One may then assume the conduction band to be flat, having a constant density of states, N(0). This is what most authors do, as presented in sects. 1.4 and 1.7.2.

Under this approximation, eqs. (6.15), (6.18), and (6.19) become:

$$\Omega\int_{\Omega_B} \frac{d^3k}{(2\pi)^3} = N(0)\int_{-D_-}^{D_+} d\epsilon_k \quad , \tag{6.21}$$

$$\tilde{C}_o^{11}(\omega) = N(0)\int_{-D_-}^{D_+} d\varepsilon \, \frac{1}{\omega - \varepsilon + i\delta} \quad , \tag{6.22}$$

$$\sigma_{C_o}(\omega) = N(0)[\,\theta(D_+ - \omega) - \theta(-D_- - \omega)\,] \quad , \tag{6.23}$$

with:

$$[\,D_+ + D_-\,]\,N(0) = 1 \quad . \tag{6.24}$$

Note that the square root term has been dropped, and, to compensate for this, the cutoffs have been changed to D_+ and $-D_-$. These roughly correspond to E_{BZ} and $-E_F$. Note from eq. (6.24) that the c–band is normalized to one momentum state per unit cell, as was the case in eq. (6.15).

The actual number of c–electrons per unit cell may be anywhere from 0 to N, depending on the occupation of these states. In keeping with previous approximations, we assume that the Fermi surface is roughly in the middle of the c–band, such that n_o is close to N/2. Using eq. (6.20) at T=0 (and therefore μ=0), along with eqs. (6.23) and (6.24), one finds:

$$n_o = N\,N(0)\,D_- = N\,\frac{D_-}{D_+ + D_-} = \frac{N}{1 + D_+/D_-} \quad . \tag{6.25}$$

That is, n_o determines the ratio of D_+ to D_-, such that n_o=N/2 corresponds to D_+=D_-. Once these parameters are set at T=0, one must adjust μ at finite temperature via:

$$n_o = N\,N(0)\int_{-D_-}^{D_+} d\omega\, f_F(\omega - \mu) \quad , \tag{6.26}$$

Having roughly N/2 c–electrons per unit cell is not very physical. It is a consequence of considering the approximate Hamiltonian of eqs. (6.1), in which a full angular momentum treatment is neglected. As compensation, the interaction term of eq. (6.1c) is multiplied by $\sqrt{\frac{2}{N}}$, thereby reducing the effective coupling of each electron by a factor of 2/N. The net result should be roughly equivalent to having one electron per unit cell.

Let us obtain an explicit expression for $\tilde{C}_o^{11}(\omega)$. Performing the integral in eq. (6.22), one obtains:

$$\check{C}_o^{11}(\omega) = N(0)\,\ell n\left[\frac{-D_- - \omega - i\delta}{D_+ - \omega - i\delta}\right] =$$

$$= N(0)\left\{\ell n\left|\frac{D_- + \omega}{D_+ - \omega}\right| - i\pi\left[\theta(D_+ - \omega) - \theta(-D_- - \omega)\right]\right\} \qquad (6.27)$$

Because $\check{C}_o$ will be used in contour integrals, it is desirable to analytically extend $\check{C}_o^{11}(\omega)$ to $\check{C}_o^{11}(\kappa)$, where κ is complex. Performing the extension on eq. (6.27), one obtains:

$$\check{C}_o^{11}(\kappa) = N(0)\left\{\frac{1}{2}\ell n\left[\frac{(D_- + \mathcal{R}e\kappa)^2 + (\mathcal{I}m\kappa + \delta)^2}{(D_+ - \mathcal{R}e\kappa)^2 + (\mathcal{I}m\kappa + \delta)^2}\right] + \right.$$

$$- i\pi\left[\operatorname{sgn}(\mathcal{I}m\kappa + \delta)\left[\theta(D_+ - \mathcal{R}e\kappa) - \theta(-D_- - \mathcal{R}e\kappa)\right] + \right.$$

$$\left.\left. - \frac{1}{\pi}\tan^{-1}\left[\frac{\mathcal{I}m\kappa + \delta}{D_- + \mathcal{R}e\kappa}\right] - \frac{1}{\pi}\tan^{-1}\left[\frac{\mathcal{I}m\kappa + \delta}{D_+ - \mathcal{R}e\kappa}\right]\right]\right\} \quad . \qquad (6.28)$$

where sgn(x) is the sign of x.

Note that the above form has a branch cut at $\mathcal{I}m\kappa = -\delta$, as one expects from the analytic nature of propagators discussed in sect. 2.4.2. In particular, eq. (6.28) satisfies eq. (2.25), showing that $\check{C}_o^{11}$ is defined on the two half sheets 1U and 1L. To form the smooth propagator $\check{C}^{11}_{o1U/2L}$, which has no branch cut, one simply drops the sgn($\mathcal{I}m\kappa + \delta$) from eq. (6.28), leaving:

$$\check{C}^{11}_{o1U/2L}(\kappa) = N(0)\left\{\frac{1}{2}\ell n\left[\frac{(D_- + \mathcal{R}e\kappa)^2 + (\mathcal{I}m\kappa + \delta)^2}{(D_+ - \mathcal{R}e\kappa)^2 + (\mathcal{I}m\kappa + \delta)^2}\right] + \right.$$

$$- i\pi\left[\left[\theta(D_+ - \mathcal{R}e\kappa) - \theta(-D_- - \mathcal{R}e\kappa)\right] + \right.$$

$$\left.\left. - \frac{1}{\pi}\tan^{-1}\left[\frac{\mathcal{I}m\kappa + \delta}{D_- + \mathcal{R}e\kappa}\right] - \frac{1}{\pi}\tan^{-1}\left[\frac{\mathcal{I}m\kappa + \delta}{D_+ - \mathcal{R}e\kappa}\right]\right]\right\} \qquad (6.29)$$

It should not be necessary to use this equation in its full grandeur. Usually, the integrals converge long before the cutoffs are reached; in these cases the following form should suffice:

$$\bar{C}^{\alpha\gamma}_{\circ\,1U/2L}(\kappa) \simeq -i\pi\, N(0)\, \tau^{\alpha\gamma} . \tag{6.30}$$

Even when the integrals do not converge, the following form is usually okay:

$$\bar{C}^{\alpha\gamma}_{\circ\,1U/2L}(\kappa) \simeq -i\pi\, N(0)\, \tau^{\alpha\gamma}\,[\theta(D_+ - \mathcal{R}e\,\kappa) - \theta(-D_- - \mathcal{R}e\,\kappa)] . \tag{6.31}$$

One should be careful, though, because the *ln* term of eq. (6.29) diverges when $\kappa = D_+ - i\delta$ and $\kappa = -D_- - i\delta$.

6.2 THE PARTICLE/HOLE SUM RULE

6.2.1 DERIVATION OF THE PARTICLE/HOLE SUM RULE

The unit operator on the Fock space of f–electrons was presented in eq. (4.3) and reiterated in section 5.2. It is given by:

$$\mathbb{1} = P_0 + P_1 . \tag{6.32}$$

Of course, $\langle 0,\beta|\, \mathbb{1}\, |0,\beta\rangle = 1$, because of eq. (6.6). That is, ${}_c\langle 0,\beta|0,\beta\rangle_c = 1$, leaving behind only ${}_f\langle 0,\beta|\, \mathbb{1}\, |0,\beta\rangle_f$, which is obviously equal to 1.

What happens when one takes the expectation value of $\mathbb{1}$ in the *full* thermal vacuum, $|0(\beta)\rangle$? One may expect the f–states to be mixed with the c–states, and eq. (6.6) will no longer be valid. But the f–space is finite, and that being so, all representations of this space are unitarily equivalent. Therefore, $\mathbb{1}$ will still be the unit operator on the f–part of $|0(\beta)\rangle$. Even if the c–part of $|0(\beta)\rangle$ is composed of states from a space orthogonal to $|0,\beta\rangle_c$, one would expect that $\mathbb{1}$ does not affect these states. All things considered, the relation $\mathbb{1}\,|0(\beta)\rangle = |0(\beta)\rangle$ must be true, yielding:

$$\langle 0(\beta)|\, \mathbb{1}\, |0(\beta)\rangle = 1 . \tag{6.33}$$

Using the renormalized projection operators defined in eqs. (6.9), one obtains:

$$\langle P_o \rangle_\ell + \langle P_1 \rangle_\ell = 1 . \tag{6.34}$$

From the explicit representations of P_o and P_1 given in eqs. (5.7c) and (5.7e), it can be seen that P_1 counts the number of f–electrons occupying the impurity state, and P_o counts the number of holes, (or the "non–occupation"), in the impurity state. Making the following definitions:

$$n_h \equiv \langle P_o \rangle_\ell \quad , \tag{6.35a}$$

$$n_f \equiv \langle P_1 \rangle_\ell \quad , \tag{6.35b}$$

the relation of eq. (6.34) becomes:

$$n_f + n_h = 1 . \tag{6.36}$$

This is called the "particle/hole sum rule".

6.2.2 EFFECT OF THE PARTICLE/HOLE SUM RULE ON THE f–ELECTRON SPECTRAL FUNCTION

Taking eq. (5.2c) for P_1 , and eq. (5.2a) for P_o , and using them with $\mathcal{G}_\ell$ of eq. (6.7c), results in:

$$n_f = - \lim_{\delta \to 0^+} \sum_m \mathcal{G}^{11}_{\ell mm}(t-(t+\delta)) = \sum_m \langle 0(\beta) | m \rangle \langle m | 0(\beta) \rangle \ , \tag{6.37a}$$

$$n_h = \lim_{\delta \to 0^+} \mathcal{G}^{11}_{\ell mm}(t-(t-\delta)) = \langle 0(\beta) | 0 \rangle \langle 0 | 0(\beta) \rangle \tag{6.37b}$$

(Note that there is no sum over m in the second equation.) Using the Fourier transform defined in eq. (2.22a) yields:

$$n_f = -i \sum_m \int_+ \frac{d\omega}{2\pi} \mathcal{G}^{11}_{\ell mm}(\omega ;\mu) \ , \tag{6.38a}$$

$$n_h = i \int_- \frac{d\omega}{2\pi} \mathcal{G}^{11}_{\ell mm}(\omega ;\mu) \ , \tag{6.38b}$$

where the "+" ("-") means "close the contour in the upper (lower) half of the complex ω–plane". Let us now use the spectral representation, eq. (2.24), for a general propagator, yielding:

$$n_f = -\sum_m \int d\kappa \; \sigma^R_{\mathcal{G}_{mm}}(\kappa) \; i\int_+ \frac{d\omega}{2\pi} \left[\frac{1 - f_F(\kappa-\mu)}{\omega - \kappa + i\delta} + \frac{f_F(\kappa-\mu)}{\omega - \kappa - i\delta} \right] , \tag{6.39a}$$

$$n_h = \int d\kappa \; \sigma^R_{\mathcal{G}_{mm}}(\kappa) \; i\int \frac{d\omega}{2\pi} \left[\frac{1 - f_F(\kappa-\mu)}{\omega - \kappa + i\delta} + \frac{f_F(\kappa-\mu)}{\omega - \kappa - i\delta} \right] , \tag{6.39b}$$

where $\sigma^R_{\mathcal{G}_{mm}}(\kappa)$ is the spectral function of $\mathcal{G}^{\alpha\gamma}_{Rmm}(t-t')$, and f_F is the Fermi function:

$$f_F(\omega) \equiv \frac{1}{e^{\beta\omega} + 1} . \tag{6.40}$$

Performing the integrals yields:

$$n_f = \sum_m \int d\kappa \; \sigma^R_{\mathcal{G}_{mm}}(\kappa) \; f_F(\kappa-\mu) , \tag{6.41a}$$

$$n_h = \int d\kappa \; \sigma^R_{\mathcal{G}_{mm}}(\kappa) \; [\, 1 - f_F(\kappa-\mu) \,] . \tag{6.41b}$$

This is an explicit example of what was stated in sect. 2.4.3, namely, the spectral function describes the density of states, and the U–matrices determine their occupation. Eq. (6.41a) counts the occupied states and eq. (6.41b) counts the unoccupied states.

Assuming the full propagator $\mathcal{G}_{Rmm}$ to be m–independent, the sum over m becomes a factor of N, yielding eqs. (1.25) – (1.26) presented in chapter 1.

Using eqs. (6.41a) – (6.41b) in eq. (6.36) yields:

$$\int d\kappa \left[1 + f_F(\kappa-\mu) \left[-1 + \sum_m \right] \right] \sigma^R_{\mathcal{G}_{mm}}(\kappa) = 1 . \tag{6.42}$$

The particle/hole sum rule thereby dictates a condition on the f–electron spectral function, which *must* be satisfied if the perturbation expansion is to be physically meaningful.

The non-interacting f-electron spectral function also obeys this sum rule, as can be seen in sect. 4.3.4.

6.2.3 THE PARTICLE/HOLE SUM RULE WITH A MAGNETIC INTERACTION: A PARADOX?

The particle/hole sum rule was derived from fundamental principles, independent of the nature of the interaction. In particular, the above equations will also be valid when the Hamiltonian contains an external magnetic field, such that each spin state, m, carries a different energy, ϵ_{f_m}. At first this may seem paradoxical, because $\sigma^{\ell}_{\mathscr{d}_{mm}}$ will be m–dependent, whereas n_h, which is obtained from $\sigma^{\ell}_{\mathscr{d}_{mm}}$ via eq. (6.41b), must be m–independent. Nevertheless, eq. (6.41b) is true.

It is not the intent of this thesis to fully deal with a magnetic interaction in the Anderson model. But the above "paradox" should be addressed, therefore this section will deal with a very simple magnetic model.

Let us take the non–interacting model of chapter 4, and make the substitution $\epsilon_f \rightarrow \epsilon_{f_m}$ in the Hamiltonian. The explicit construction of the thermal vacuum, eq. (4.13a), then becomes:

$$|0,\beta\rangle = \frac{1}{\sqrt{Z}}\left[\,|0\,\tilde{0}\rangle + \sum_m e^{-\beta(\epsilon_{f_m}-\mu)/2}\,|m\,\tilde{m}\rangle\right] , \tag{6.43a}$$

$$Z = 1 + \sum_m e^{-\beta(\epsilon_{f_m}-\mu)} , \tag{6.43b}$$

and the projection operators, eqs. (4.18), become:

$$\langle P_o\rangle = 1/Z , \tag{6.44a}$$

$$\langle P_1^{(m)}\rangle = \frac{1}{Z}\, e^{-\beta(\epsilon_{f_m}-\mu)} \tag{6.44b}$$

One also finds the propagator to be:

$$\mathscr{d}^{\alpha\gamma}_{mm'}(t-t') = \delta_{mm'}\, S^{\alpha\gamma}_{\epsilon_{f_m}}(t-t')\left[\,\langle P_o\rangle + \langle P_1^{(m)}\rangle\right] \tag{6.45}$$

such that the spectral function is:

$$\sigma_{\mathscr{d}_{mm}}(\kappa) = \delta(\kappa-\epsilon_{f_m})\left[\,\langle P_o\rangle + \langle P_1^{(m)}\rangle\,\right] \tag{6.46}$$

Using the above spectral function in the particle/hole sum rule of eqs. (6.41a) – (6.41b), one finds:

$$n_f = \sum_m f_F(\varepsilon_{f_m}-\mu)\left[\langle P_o\rangle + \langle P_1^{(m)}\rangle\right] , \qquad (6.47a)$$

$$n_h = \left[1 - f_F(\varepsilon_{f_m}-\mu)\right]\left[\langle P_o\rangle + \langle P_1^{(m)}\rangle\right] . \qquad (6.47b)$$

Now, n_h appears to be m–dependent. But, one may use eqs. (6.43b) to (6.44b), to obtain:

$$f_F(\varepsilon_{f_m}-\mu)\left[\langle P_o\rangle + \langle P_1^{(m)}\rangle\right] = \langle P_1^{(m)}\rangle , \qquad (6.48a)$$

$$\left[1 - f_F(\varepsilon_{f_m}-\mu)\right]\left[\langle P_o\rangle + \langle P_1^{(m)}\rangle\right] = \langle P_o\rangle , \qquad (6.48b)$$

and therefore:

$$n_f = \sum_m \langle P_1^{(m)}\rangle , \qquad (6.49a)$$

$$n_h = \langle P_o\rangle . \qquad (6.49b)$$

Thus n_h , which appears m–dependent in eq. (6.47b), is actually m–independent, as shown by eqs. (6.48b) and (6.49b).

When the hybridization interaction is included in this model, a check on the correctness of the perturbation expansion will be that n_h , as calculated by eq. (6.41b), should be m–independent.

6.3 THE HEISENBERG EQUATIONS AND THE RESULTING BETHE–SALPETER EQUATIONS

6.3.1 DERIVATION OF THE HEISENBERG EQUATIONS

The time evolution of a thermal doublet field $A^\alpha(t)$, is governed by the Hamiltonian $\hat{H} = H - \tilde{H}$ (see chapter 2), as follows:

$$i\frac{\partial A^\alpha(t)}{\partial t} = -\left[\hat{H} , A^\alpha(t)\right] . \qquad (6.50)$$

This is called the Heisenberg equation. It is easy to derive the Heisenberg equations of the non–tilde fields, using the explicit representation of the non–tilde fields given in sect. 5.2. The results are quoted below. An extension of this to the thermal doublet is straightforward, using the tilde conjugation rules (eqs. (2.14)).

$$\left[i\frac{\partial}{\partial t} - \epsilon_f \right] \xi_m(t) = \sqrt{\frac{2}{N}}\, V \sum_{m'} M_{mm'}(t)\, c_{om'}(t) \tag{6.51}$$

$$\left[-i\frac{\partial}{\partial t} - \epsilon_f \right] \xi^\dagger_m(t) = \sqrt{\frac{2}{N}}\, V \sum_{m'} c^\dagger_{om'}(t)\, M_{m'm}(t) \tag{6.52}$$

$$\left[i\frac{\partial}{\partial t} - \epsilon(-i\vec{\nabla}) \right] c_m(x) = \sqrt{\frac{2}{N}}\, V\sqrt{\Omega}\; \delta^3(\ell)\, \xi_m(t) \tag{6.53}$$

$$\left[-i\frac{\partial}{\partial t} - \epsilon(i\vec{\nabla}) \right] c^\dagger_m(x) = \sqrt{\frac{2}{N}}\, V\sqrt{\Omega}\; \delta^3(\ell)\, \xi^\dagger_m(t) \tag{6.54}$$

$$i\frac{\partial}{\partial t} P_o(t) = \sqrt{\frac{2}{N}}\, V \sum_m \left[c^\dagger_{om}(t)\, \xi_m(t) - \xi^\dagger_m(t)\, c_{om}(t) \right] \tag{6.55}$$

$$i\frac{\partial}{\partial t} X_{mm'}(t) = \sqrt{\frac{2}{N}}\, V \left[\xi^\dagger_m(t)\, c_{om'}(t) - c^\dagger_{om}(t)\, \xi_{m'}(t) \right] \tag{6.56}$$

$$i\frac{\partial}{\partial t} P_1(t) = \sqrt{\frac{2}{N}}\, V \sum_m \left[\xi^\dagger_m(t)\, c_{om}(t) - c^\dagger_{om}(t)\, \xi_m(t) \right] \tag{6.57}$$

$$\begin{aligned} i\frac{\partial}{\partial t} M_{mm'}(t) = \sqrt{\frac{2}{N}}\, V \Big\{ \delta_{mm'} \sum_{m''} \left[c^\dagger_{om''}(t)\, \xi_{m''}(t) - \xi^\dagger_{m''}(t)\, c_{om''}(t) \right] + \\ + \left[\xi^\dagger_{m'}(t)\, c_{om}(t) - c^\dagger_{om'}(t)\, \xi_m(t) \right] \Big\} \end{aligned} \tag{6.58}$$

6.3.2 THE BETHE–SALPETER EQUATION
FOR THE $\tilde{c}$–ELECTRON PROPAGATOR

Let us start by considering the fully renormalized conduction electron propagator defined in eq. (6.7a). Using eq. (6.53), one obtains

$$\begin{aligned} \left[i\frac{\partial}{\partial t} - \epsilon(-i\vec{\nabla}) \right] C^{\alpha\gamma}_{\ell mm'}(\ell,\ell',t-t') = i\delta(t-t')\, \delta^3(\ell-\ell')\, \delta_{mm'}\, \delta^{\alpha\gamma} + \\ + \sqrt{\frac{2}{N}}\, V\sqrt{\Omega}\; \delta^3(\ell)\, \langle 0(\beta)|\, T\, \xi^\alpha_m(t)\, c^{\dagger\gamma}_{m'}(\ell',t')\, |0(\beta)\rangle \end{aligned} \tag{6.59}$$

Now, using eq. (6.54) on the above, one ends up with

$$\left[i\frac{\partial}{\partial t} - \varepsilon(-i\vec{\nabla}) \right] C^{\alpha\gamma}_{\mathrm{R}mm'}(\vec{x},\vec{x}';t-t') \left[-i\frac{\overleftarrow{\partial}}{\partial t'} - \varepsilon(i\overleftarrow{\nabla}') \right] =$$

$$= i\delta(t-t')\,\delta^3(\vec{x}-\vec{x}')\,\delta_{mm'}\,\delta^{\alpha\gamma} \left[-i\frac{\overleftarrow{\partial}}{\partial t'} - \varepsilon(i\overleftarrow{\nabla}') \right] +$$

$$+ \frac{2}{N} V^2 \Omega\, \delta^3(\vec{x})\, \delta^3(\vec{x}')\, \mathcal{S}^{\alpha\gamma}_{\mathrm{R}mm'}(t-t') \ . \tag{6.60}$$

Thus, the fully renormalized c–propagator is related to the fully renormalized f–propagator.

To make eq. (6.60) more explicit, let us consider the Fourier representation (of eqs. (2.22)), as follows:

$$C^{\alpha\gamma}_{\mathrm{R}mm'}(\vec{x},\vec{x}';t-t') = i\int\frac{d\omega}{2\pi}\int_{\Omega_B}\frac{d^3k}{(2\pi)^3}\int_{\Omega_B}\frac{d^3q}{(2\pi)^3}\, e^{-i\omega(t-t')}\, e^{i(\vec{k}\cdot\vec{x} - \vec{q}\cdot\vec{x}')} \times$$

$$\times \left[U_F(\omega-\mu)\, \bar{C}_{\mathrm{R}mm'}(\omega;\vec{k},\vec{q})\, U^\dagger_F(\omega-\mu) \right]^{\alpha\gamma} . \tag{6.61}$$

$$\mathcal{S}^{\alpha\gamma}_{\mathrm{R}mm'}(t-t') = i\int\frac{d\omega}{2\pi} e^{-i\omega(t-t')} \left[U_F(\omega-\mu)\, \bar{\mathcal{S}}_{\mathrm{R}mm'}(\omega)\, U^\dagger_F(\omega-\mu) \right]^{\alpha\gamma} . \tag{6.62}$$

In this representation, eq. (6.60) becomes:

$$\bar{C}^{11}_{\mathrm{R}mm'}(\omega;\vec{k},\vec{q}) = (2\pi)^3\,\delta_{mm'}\,\delta^3(\vec{k}-\vec{q})\,\frac{1}{\omega - \varepsilon_k + i\delta} +$$

$$+ \frac{2}{N} V^2 \Omega \frac{1}{\omega - \varepsilon_k + i\delta}\, \bar{\mathcal{S}}^{11}_{\mathrm{R}mm'}(\omega)\, \frac{1}{\omega - \varepsilon_q + i\delta} \ . \tag{6.63}$$

Using eq. (6.11) for the bare conduction electron propagator, one ends up with:

$$\bar{C}_{\mathrm{R}mm'}(\omega;\vec{k},\vec{q}) = (2\pi)^3\,\delta_{mm'}\,\delta^3(\vec{k}-\vec{q})\,\bar{C}(\omega,\vec{k}) + \frac{2}{N} V^2 \Omega\, \bar{C}(\omega,\vec{k})\, \bar{\mathcal{S}}_{\mathrm{R}mm'}(\omega)\, \bar{C}(\omega,\vec{q}) \ . \tag{6.64}$$

This Bethe–Salpeter equation is very simple, and cuts the problem, as stated in sect. 6.1.4, in half. It is only necessary to calculate $\mathcal{S}_{\mathrm{R}}$. From this, C_{R} may be obtained via eq. (6.64). There is a straight–through term, representing free propagation, plus a scattering term.

$C_{o\mathrm{R}mm'}(\omega)$ may be obtained from $C_{\mathrm{R}mm'}(\omega;\vec{k},\vec{q})$, by multiplying by Ω and performing the integrals over k and q. Noting eq. (6.13), this yields:

$$\bar{C}_{o\ell mm'}(\omega) = \delta_{mm'}\,\bar{C}_o(\omega) + \frac{2}{N}V^2\,\bar{C}_o(\omega)\,\bar{\mathscr{S}}_{\ell mm'}(\omega)\,\bar{C}_o(\omega)\ . \tag{6.65}$$

6.3.3 THE UNITARY LIMIT

Inserting eq. (6.31) for $\bar{C}_o(\omega)$ into eq. (6.65) for $\bar{C}_{o\ell}(\omega)$, one obtains:

$$\bar{C}^{11}_{o\ell mm'}(\omega) = N(0)\,[\,\theta(D_+-\omega) - \theta(-D_--\omega)\,]\left\{-i\pi\delta_{mm'} - \frac{2}{N}\pi\Delta\,\bar{\mathscr{S}}^{11}_{\ell mm'}(\omega)\right\}, \tag{6.66}$$

where:

$$\Delta \equiv \pi V^2 N(0)\ . \tag{6.67}$$

Using eq. (2.28), to obtain the spectral function of this propagator, yields the following:

$$\sigma^{\ell}_{C_{o_{mm'}}}(\omega) = N(0)\,[\,\theta(D_+-\omega) - \theta(-D_--\omega)\,]\left\{\delta_{mm'} - \frac{2}{N}\pi\Delta\,\sigma^{\ell}_{\mathscr{S}_{mm'}}(\omega)\right\}. \tag{6.68}$$

One of the most important properties of physical spectral functions is that they are non–negative. This property is very significant when considering eq. (6.68). Firstly, it means that $C_{\ell mm'}$ and $\mathscr{S}_{\ell mm'}$ are proportional to $\delta_{mm'}$. We may then write:

$$\sigma^{\ell}_{C_{o_{mm'}}}(\omega) = \delta_{mm'}\,N(0)\,[\,\theta(D_+-\omega) - \theta(-D_--\omega)\,]\left\{1 - \frac{2}{N}\pi\Delta\,\sigma^{\ell}_{\mathscr{S}_{mm}}(\omega)\right\}. \tag{6.69}$$

Secondly,

$$\sigma^{\ell}_{\mathscr{S}_{mm}}(\omega) \le \frac{N}{2\pi\Delta}\ , \tag{6.70}$$

otherwise $\sigma^{\ell}_{C_o}(\omega)$ becomes negative. This is the unitary limit. If $\sigma^{\ell}_{\mathscr{S}}(\omega)$ reaches its maximum of $N/2\pi\Delta$, then there is scattering at the unitary limit. If $\sigma^{\ell}_{\mathscr{S}}(\omega)$ exceeds this limit, then the calculation is in error because unitarity has been broken, resulting in a negative state density.

6.3.4 BETHE–SALPETER EQUATIONS FOR THE f–ELECTRON PROPAGATOR

Let us now consider the fully renormalized f–electron propagator defined in eq. (6.7c). Using eq. (6.51), one obtains:

$$\left[i\frac{\partial}{\partial t} - \varepsilon_f \right] \mathcal{G}^{\alpha\gamma}_{\mathrm{R}mm'}(t-t') = i\,\delta(t-t')\,\delta^{\alpha\gamma}\,\langle 0(\beta)|\,M_{mm'}\,|0(\beta)\rangle \; +$$

$$+ \sqrt{\frac{2}{N}}\,V \sum_{\bar{m}} \langle 0(\beta)|\,T\, M^{\alpha}_{m\bar{m}}(t)\, c^{\alpha}_{o\bar{m}}(t)\, \xi^{\dagger\gamma}_{m'}(t')\,|0(\beta)\rangle \; . \tag{6.71}$$

The expectation value of $M_{mm'}$ is evaluated simply by using eq. (5.7f) along with definitions (6.9a) and (6.9b). One obtains:

$$\langle 0(\beta)|\, M_{mm'}\,|0(\beta)\rangle = \delta_{mm'} \left[\langle P_o\rangle_{\mathrm{R}} + \langle P^{(m)}_1\rangle_{\mathrm{R}} \right] . \tag{6.72}$$

Now, using this in eq. (6.71), along with eq. (6.52), one has:

$$\left[i\frac{\partial}{\partial t} - \varepsilon_f \right] \mathcal{G}^{\alpha\gamma}_{\mathrm{R}mm'}(t-t') \left[-i\frac{\overleftarrow{\partial}}{\partial t'} - \varepsilon_f \right] =$$

$$= i\,\delta(t-t')\,\delta^{\alpha\gamma}\,\delta_{mm'} \left[\langle P_o\rangle_{\mathrm{R}} + \langle P^{(m)}_1\rangle_{\mathrm{R}} \right] \left[-i\frac{\overleftarrow{\partial}}{\partial t'} - \varepsilon_f \right] +$$

$$+ \frac{2}{N}V^2 \sum_{\bar{m}\bar{m}'} \langle 0(\beta)|\,T\; M^{\alpha}_{m\bar{m}}(t)\, c^{\alpha}_{o\bar{m}}(t)\, c^{\dagger\gamma}_{o\bar{m}'}(t')\, M^{\gamma}_{\bar{m}'m'}(t')\,|0(\beta)\rangle \; +$$

$$+ \; i\,\delta(t-t')\,\delta^{\alpha\gamma} \sqrt{\frac{2}{N}}\,V\,\varepsilon^{\alpha} \times$$

$$\times \left[\delta_{mm'} \sum_{\bar{m}} \langle 0(\beta)|\, c^{\alpha}_{o\bar{m}}\, \xi^{\dagger\alpha}_{\bar{m}}\,|0(\beta)\rangle - \langle 0(\beta)|\, c^{\alpha}_{om}\, \xi^{\dagger\alpha}_{m'}\,|0(\beta)\rangle \right] . \tag{6.73}$$

The last term comes from differentiating the θ–functions in the last term of eq. (6.71).

The Bethe–Salpeter equation of eq. (6.73) is quite complicated, due to the quantum algebra of the ξ and M eigenoperators. Perhaps its most notable feature is that the projection operators are renormalized in the first term. This is a valuable clue, indicating that the projection operators must be renormalized, as they were in the example of Chapter 5.

In the last section, it was determined that $\mathcal{S}_{\mathrm{Rmm}'}$ is proportional to $\delta_{\mathrm{mm}'}$. Let us use this result in eq. (6.73). We also assume that spin rotational invariance is not broken, (there is no external magnetic field nor spontaneous magnetization), such that:

$$\langle \mathrm{P}_1^{(\mathrm{m})} \rangle_{\mathrm{R}} = \frac{1}{\mathrm{N}} \langle \mathrm{P}_l \rangle_{\mathrm{R}} \, . \tag{6.74}$$

In the last terms of eq. (6.73), the sum over $\bar{\mathrm{m}}$ will simply yield a factor of N. One then obtains:

$$\begin{aligned} &\left[i\frac{\partial}{\partial \mathrm{t}} - \varepsilon_{\mathrm{f}} \right] \mathcal{S}^{\alpha\gamma}_{\mathrm{Rmm}'}(\mathrm{t}-\mathrm{t}') \left[-i\frac{\overleftarrow{\partial}}{\partial \mathrm{t}'} - \varepsilon_{\mathrm{f}} \right] = \\ &= i\,\delta(\mathrm{t}-\mathrm{t}')\, \delta^{\alpha\gamma}\, \delta_{\mathrm{mm}'} \left[\langle \mathrm{P}_{\mathrm{o}} \rangle_{\mathrm{R}} + \frac{1}{\mathrm{N}} \langle \mathrm{P}_l \rangle_{\mathrm{R}} \right] \left[-i\frac{\overleftarrow{\partial}}{\partial \mathrm{t}'} - \varepsilon_{\mathrm{f}} \right] + \\ &+ i\,\delta(\mathrm{t}-\mathrm{t}')\, \delta^{\alpha\gamma}\, \delta_{\mathrm{mm}'} \frac{2}{\mathrm{N}} \mathrm{V}^2 (\mathrm{N}-1)\, \mathrm{J}^{\alpha}_{\mathrm{o}} + \frac{2}{\mathrm{N}} \mathrm{V}^2\, \delta_{\mathrm{mm}'}\, \mathrm{J}^{\alpha\gamma}_{4}(\mathrm{t}-\mathrm{t}') \quad , \end{aligned} \tag{6.75}$$

where:

$$\sqrt{\frac{2}{\mathrm{N}}}\, \mathrm{V}\, \mathrm{J}^{\alpha}_{\mathrm{o}} \equiv \varepsilon^{\alpha} \langle 0(\beta)|\, \mathrm{c}^{\alpha}_{\mathrm{om}}\, \xi^{\dagger\alpha}_{\mathrm{m}}\, |0(\beta)\rangle \ , \tag{6.76}$$

$$\mathrm{J}^{\alpha\gamma}_{4}(\mathrm{t}-\mathrm{t}') \equiv \sum_{\bar{\mathrm{m}}\bar{\mathrm{m}}'} \langle 0(\beta)|\mathrm{T}\ \mathrm{M}^{\alpha}_{\mathrm{m}\bar{\mathrm{m}}}(\mathrm{t})\, \mathrm{c}^{\alpha}_{\mathrm{o}\bar{\mathrm{m}}}(\mathrm{t})\, \mathrm{c}^{\dagger\gamma}_{\mathrm{o}\bar{\mathrm{m}}'}(\mathrm{t}')\, \mathrm{M}^{\gamma}_{\bar{\mathrm{m}}'\mathrm{m}}(\mathrm{t}')\, |0(\beta)\rangle \ . \tag{6.77}$$

(Note that there is ***no*** implied summation over m in eq. (6.76).)

Eq. (6.76) is actually α-independent, as can be seen when applying the tilde conjugation rules, as follows:

$$\begin{aligned} \sqrt{\frac{2}{\mathrm{N}}}\, \mathrm{V}\, \mathrm{J}^{(2)}_{\mathrm{o}} &= -\langle 0(\beta)|\, \mathrm{c}^{(2)}_{\mathrm{om}}\, \xi^{\dagger(2)}_{\mathrm{m}}\, |0(\beta)\rangle = -\langle 0(\beta)|\, \tilde{\mathrm{c}}^{\dagger}_{\mathrm{om}}\, \tilde{\xi}_{\mathrm{m}}\, |0(\beta)\rangle = \\ &= \langle 0(\beta)|\, (\xi_{\mathrm{m}}\, \mathrm{c}^{\dagger}_{\mathrm{om}})^{\sim}\, |0(\beta)\rangle = \langle 0(\beta)|\, (\mathrm{c}_{\mathrm{om}}\, \xi^{\dagger}_{\mathrm{m}})^{\dagger\sim}\, |0(\beta)\rangle = \\ &= \langle 0(\beta)|\, \mathrm{c}_{\mathrm{om}}\, \xi^{\dagger}_{\mathrm{m}}\, |0(\beta)\rangle = \sqrt{\frac{2}{\mathrm{N}}}\, \mathrm{V}\, \mathrm{J}^{(1)}_{\mathrm{o}} \ . \end{aligned} \tag{6.78}$$

We therefore find:

$$\sqrt{\frac{2}{\mathrm{N}}}\, \mathrm{V}\, \mathrm{J}^{\alpha}_{\mathrm{o}} = \sqrt{\frac{2}{\mathrm{N}}}\, \mathrm{V}\, \mathrm{J}_{\mathrm{o}} \equiv \langle 0(\beta)|\, \mathrm{c}_{\mathrm{om}}\, \xi^{\dagger}_{\mathrm{m}}\, |0(\beta)\rangle \ . \tag{6.79}$$

Using the Fourier representation of eqs. (2.22) on the above eq. (6.75) yields:

$$\bar{\mathcal{J}}^{\alpha\gamma}_{\mathfrak{R}mm'}(\omega) = \delta_{mm'}\,\bar{S}^{\alpha\gamma}_{\varepsilon_f}(\omega)\left[\langle P_o\rangle_{\mathfrak{R}} + \frac{1}{N}\langle P_1\rangle_{\mathfrak{R}}\right] +$$

$$+ \frac{2}{N}V^2\,\delta_{mm'}\,\bar{S}^{\alpha\gamma}_{\varepsilon_f}(\omega)\left[(N-1)\,J_o + \bar{J}^{\alpha\gamma}_4(\omega)\right]\bar{S}^{\alpha\gamma}_{\varepsilon_f}(\omega)\;. \tag{6.80}$$

* Another useful 2–point function to consider is defined as follows:

$$\sqrt{\frac{2}{N}}\,V\,J^{\alpha\gamma}_2(t-t') \equiv \langle 0(\beta)|\,T\,c^{\alpha}_{om}(t)\,\xi^{\dagger\,\gamma}_{m}(t')\,|0(\beta)\rangle\;. \tag{6.81}$$

(Note that there is ***no*** implied summation over m in this equation.) Using eq. (6.52) on this, one obtains:

$$\sqrt{\frac{2}{N}}\,V\,J^{\alpha\gamma}_2(t-t')\left[-i\frac{\overleftarrow{\partial}}{\partial t'} - \varepsilon_f\right] =$$

$$= \sqrt{\frac{2}{N}}\,V\sum_{\bar{m}}\langle 0(\beta)|\,T\;c^{\alpha}_{om}(t)\,c^{\dagger\,\gamma}_{o\bar{m}}(t')\,M^{\gamma}_{\bar{m}m}(t')\,|0(\beta)\rangle\;. \tag{6.82}$$

If we make the following definition:

$$J^{\alpha\gamma}_3(t-t') \equiv \sum_{\bar{m}}\langle 0(\beta)|\,T\;c^{\alpha}_{om}(t)\,c^{\dagger\,\gamma}_{o\bar{m}}(t')\,M^{\gamma}_{\bar{m}m}(t')\,|0(\beta)\rangle\;, \tag{6.83}$$

then eq. (6.82) becomes:

$$J^{\alpha\gamma}_2(t-t')\left[-i\frac{\overleftarrow{\partial}}{\partial t'} - \varepsilon_f\right] = J^{\alpha\gamma}_3(t-t')\;, \tag{6.84}$$

and in the Fourier representation:

$$\bar{J}^{\alpha\gamma}_2(\omega) = \bar{S}^{\alpha\gamma}_{\varepsilon_f}(\omega)\,\bar{J}^{\alpha\gamma}_3(\omega)\;. \tag{6.85}$$

Now, from eqs. (6.76) and (6.81), one finds the following relation:

$$J^{\alpha}_o = \varepsilon^{\alpha}\,J^{\alpha\alpha}_2(t-(t-\delta))\;. \tag{6.86a}$$

In the Fourier representation of eqs. (2.22), this becomes:

$$J^{\alpha}_o = \varepsilon^{\alpha}\,i\int_{-}\frac{d\omega}{2\pi}\left[U_F(\omega-\mu)\,\bar{J}_2(\omega)\,U^{\dagger}_F(\omega-\mu)\right]^{\alpha\alpha}\;, \tag{6.86b}$$

where "-" means to close the contour in the lower half of the complex ω–plane. Using the spectral representation defined in eq. (2.24), one finds:

$$J^{(1)}_o = \int d\kappa\,\sigma_{J_2}(\kappa)\,i\int_{-}\frac{d\omega}{2\pi}\left[\frac{1 - f_F(\kappa-\mu)}{\omega - \kappa + i\delta} + \frac{f_F(\kappa-\mu)}{\omega - \kappa - i\delta}\right]\;, \tag{6.87a}$$

$$J^{(2)}_o = -\int d\kappa\,\sigma_{J_2}(\kappa)\,i\int_{-}\frac{d\omega}{2\pi}\left[\frac{f_F(\kappa-\mu)}{\omega - \kappa + i\delta} + \frac{1 - f_F(\kappa-\mu)}{\omega - \kappa - i\delta}\right]\;. \tag{6.87b}$$

Performing the integrals yields:

$$J_o^{(1)} = \int d\kappa\, \sigma_{J_2}(\kappa)\,[\,1 - f_F(\kappa-\mu)\,]\ , \tag{6.88a}$$

$$J_o^{(2)} = -\int d\kappa\, \sigma_{J_2}(\kappa)\, f_F(\kappa-\mu)\ . \tag{6.88b}$$

At first there seems to be a contradiction. From eq. (6.79) one has $J_o^{(1)} = J_o^{(2)}$. The only way this can be consistent with eqs. (6.88) is to have:

$$\int d\kappa\, \sigma_{J_2}(\kappa) = 0\ . \tag{6.89}$$

Then one may write:

$$J_o = -\int d\kappa\, \sigma_{J_2}(\kappa)\, f_F(\kappa-\mu)\ . \tag{6.90}$$

Eq. (6.89) implies that $\sigma_{J_2}(\kappa)$ is negative in some domain of κ. Although this appears to contradict the positive definiteness of spectral functions (as described in sect. 2.4.3), this is okay because J_2 is not a physical particle propagator. It is the spectral functions of C_{oR} and $\mathscr{S}_R$ which one expects to be positive definite.

In summary, the Bethe–Salpeter equation for the f–electron propagator is given by eq. (6.80), which expresses $\mathscr{S}_R$ in terms of the bare S_{ε_f} , J_o , J_4 , and the renormalized projection operators. J_o may be obtained via eq. (6.90), which involves J_2 . J_2 may in turn be obtained from eq. (6.85) which involves J_3 . This leaves us with two unknowns: J_3 and J_4 , which were defined in eqs. (6.83) and (6.77). To evaluate them, they must be expanded using perturbation theory.

Perturbation theory apparently cannot be avoided. Thus, the B–S equations for the f–electron propagator are not as useful as the B–S equation for the c–electron propagator was.

6.4 THE FEYNMAN RULES, IGNORING VACUUM DIAGRAMS

6.4.1 WHY IGNORE THE VACUUM DIAGRAMS?

Vacuum diagrams are very important to the renormalization process. (This was discovered in Chapter 5.) Why, then, does the heading of section 6.4 indicate that the vacuum diagrams are to be ignored? It is because the determination of vacuum diagram effects requires very involved diagrammatic analysis. This is deferred until the basic Feynman rules have been introduced.

6.4.2. THE c–ELECTRON PROPAGATOR

The interaction Hamiltonian of eq. (6.1c) is very straightforward: a c–electron can turn into an f–electron and vice–versa. Furthermore, the c–electron has no spontaneous vertex structure, nor other quantum algebra effects, which are inherent to the f–electrons. Thus $C_o^{\alpha\gamma}(t-t')$ may be written very compactly as a dot at t′ followed by a cross at t connected to the dot by a very short line. This is illustrated in FIG. 6.2.

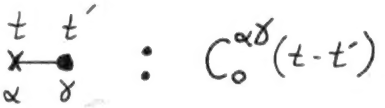

FIG. 6.2
Diagrammatic Representation of the C_o Propagator

6.4.3 THE NON–SU(N) RULES

The non–SU(N) Feynman rules for decomposing n–point ξ–functions, and the corresponding X–operator functions, were presented in section 4.9.2. The extension of these rules to include a hybridization interaction with the C_o propagator is easy; the C_o propagator was designed so that its dot will connect to the dot of a ξ–function, and likewise its cross will connect to the cross of a ξ–function. It is not even necessary to spin–label the C_o propagator; it will carry the same spin as the incoming ξ–propagator.

The interaction vertices in the $\langle P_o \rangle$ sector are illustrated in FIG. 6.3. They are a direct extension of the no–interaction vertices presented in FIG. 4.8. Similarly the interaction vertices in the $\langle P_l \rangle$ sector are illustrated in FIG. 6.4. They are a direct extension of the no–interaction vertices presented in FIGS. 4.9 and 4.11.

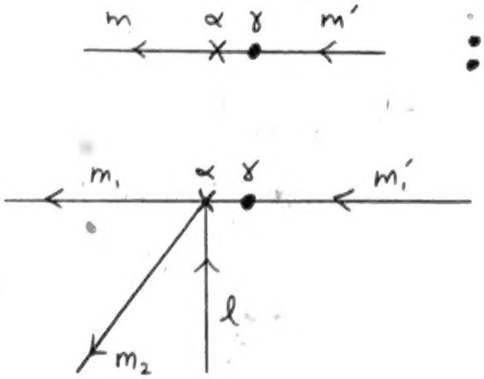

$$: \quad \frac{2}{N} V^2 C_o^{\alpha\gamma}(t-t')\,\delta_{mm'}$$

$$: \quad \frac{2}{N} V^2 \varepsilon^{\alpha} C_o^{\alpha\gamma}(t-t') \times$$

$$\times\left[-\delta_{m_1 m_1'}\delta_{m_2 l}+\delta_{m_1 l}\delta_{m_2 m_1'}\right]$$

FIG. 6.3

Non–SU(N) Feynman Rules for Interaction Vertices in the $\langle P_o \rangle$ Sector

Compare this to the noninteracting Feynman rules given in FIG. 4.8. The interaction simply adds an incoming line to the cross vertex. This incoming line must encounter a "dot" (change into a c–electron) before entering the cross vertex.

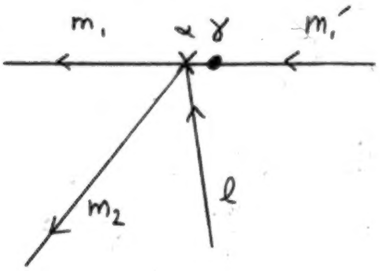
m_1
$\alpha\gamma$
m_1'
m_2
l

$$: \frac{2}{N} V^2 \varepsilon^{\alpha} C_0^{\alpha\gamma}(t-t') \times$$
$$\times \left[-\delta_{m_1 m_1'} \delta_{m_2 l} + \delta_{m_1 l} \delta_{m_2 m_1'} \right]$$

If

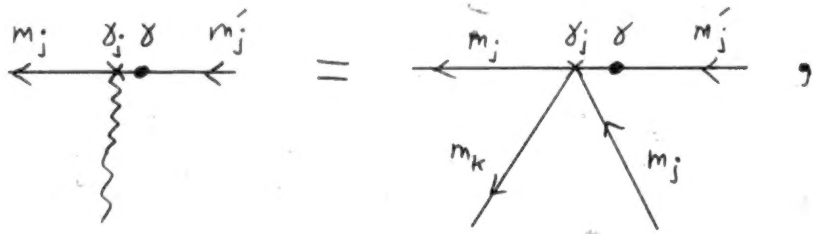
m_j
$\gamma_j\ \gamma$
m_j'
=
m_j
$\gamma_j\ \gamma$
m_j'
m_k
m_j
,

then $\frac{2}{N} V^2 \varepsilon^{\gamma_j} C_0^{\gamma_j\gamma}(t_j-t') \delta_{m_k m_j'}$

If

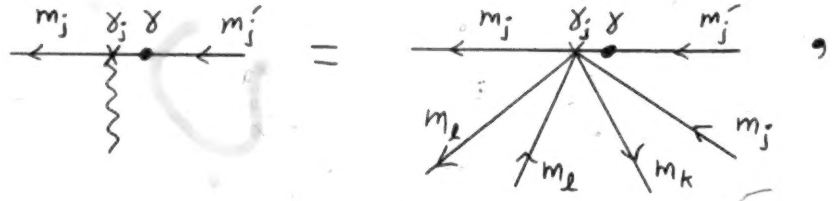
m_j
$\gamma_j\ \gamma$
m_j'
=
m_j
$\gamma_j\ \gamma$
m_j'
m_l
m_l
m_k
m_j
,

then $\frac{2}{N} V^2 C_0^{\gamma_j\gamma}(t_j-t') \delta_{m_k m_j'}$

FIG. 6.4

Non–SU(N) Feynman Rules for Interaction Vertices in the $\langle P_1 \rangle$ Sector

Compare this to the noninteracting Feynman rules given in FIGS. 4.9 and 4.11. As before, the interaction simply adds an incoming line to the cross vertex, which must encounter a "dot" (change into a c–electron) before entering the cross vertex.

In this manner, a c–electron hybridization appears as a "dot" on an incoming ξ–line.

Using these vertices, the non–SU(N) Feynman rules are essentially the same as rules 1 to 21 given in sections 4.9.2.6 and 4.9.2.9. Note that rule 4 should be modified slightly, as follows:

4′) S_{ε_f} lines outside of a wiggle diagram are not allowed to form closed loops ***unless the loop contains at least one dot.***

Another rule which should be added is:

4.5) All ξ–lines may be renormalized by a dot, with the exception of ξ–lines contained in the decomposition of a wiggle diagram.

A useful tool when calculating these diagrams is to diagrammatically point–split a cross vertex into two (or three) cross vertices, separated by a very short zigzag line. The purpose of this is to show the flow of spin; the zigzag lines transmit energy but not spin. With this notation, the spin delta–functions may be dropped, and every loop gives a factor of N, due to the spin trace. This tool is illustrated in FIG. 6.5.

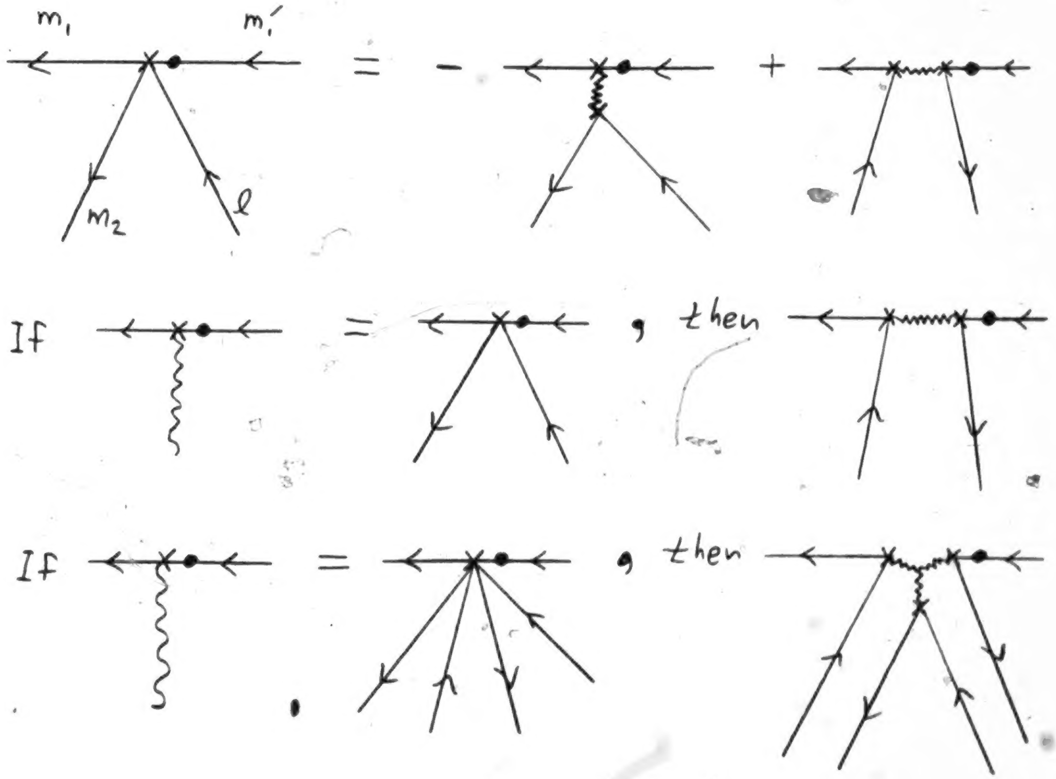

FIG. 6.5

Point–Splitting of the Cross–Vertex, Showing the Flow of Spin

Spin–labelling is no longer necessary when the Feynman diagrams of FIG. 6.4 are point–split as shown here. The zigzag lines carry only energy and no spin, allowing the flow of spin to be traced by following the f–electron lines.

6.4.4 THE BROKEN–CHAIN SU(N) RULES

The broken–chain SU(N) Feynman rules for decomposing n–point ξ-functions, and the corresponding X_i-operator functions, were presented in section 4.9.3. As in the non–SU(N) case, the extension of these rules to include a hybridization interaction with the C_o propagator is easy. The interaction vertices in the $\langle P_o \rangle$ sector are illustrated in FIG. 6.6. They are a direct extension of the no–interaction vertices presented in FIG. 4.15. Similarly, the interaction vertices in the $\langle P_1 \rangle$ sector are illustrated in FIG. 6.7. They are a direct extension of the no–interaction vertices presented in FIG. 4.16. As before, a c–electron hybridization appears as a “dot” on an incoming ξ–line.

Using these vertices, the broken–chain SU(N) Feynman rules are essentially the same as rules 1 to 26 given in sections 4.9.3.4 and 4.9.3.9. As before, rule 4 should be changed to rule 4′ above, and rule 4.5 should be added.

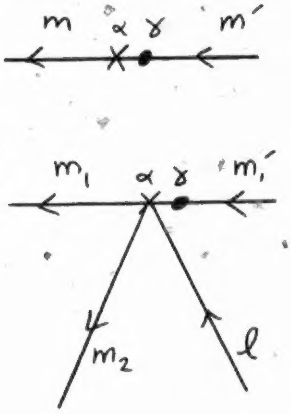

$$: \quad \frac{2}{N} V^2 C_o^{\alpha\gamma}(t-t')\, \delta_{mm'}$$

$$: \quad \frac{2}{N} V^2 \varepsilon^{\alpha} C_o^{\alpha\gamma}(t-t') \times$$

$$\times \left[-\left(1-\frac{1}{N}\right) \delta_{m_1 m_1'} \delta_{m_2 \ell} + \frac{1}{2} \sum_j \lambda_j^{m_1 m_1'} \lambda_j^{m_2 \ell} \right]$$

FIG. 6.6

SU(N) Feynman Rules for Interaction Vertices in the $\langle P_o \rangle$ Sector

Compare this to the noninteracting Feynman rules given in FIG. 4.15. As before, the interaction simply adds an incoming line to the cross vertex, which must encounter a "dot" (change into a c–electron) before entering the cross vertex.

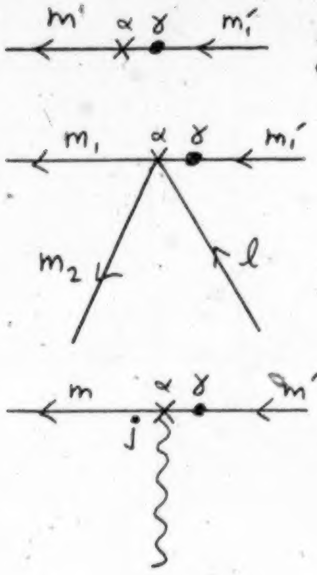

$$: \frac{2}{N} V^2 C_0^{\alpha\gamma}(t-t') \frac{1}{N} \delta_{mm'}$$

$$: \frac{2}{N} V^2 \varepsilon^{\alpha} C_0^{\alpha\gamma}(t-t') \times$$

$$\times \left[-\left(1-\frac{1}{N}\right) \delta_{m_1 m_1'} \delta_{m_2 \ell} + \frac{1}{2} \sum_j \lambda_j^{m_1 m_1'} \lambda_j^{m_2 \ell} \right]$$

$$: \frac{2}{N} V^2 C_0^{\alpha\gamma}(t-t') \frac{1}{2} \lambda_j^{mm'}$$

FIG. 6.7

SU(N) Feynman Rules for Interaction Vertices in the $\langle P_1 \rangle$ Sector

Compare this to the noninteracting Feynman rules given in FIG. 4.16. As before, the interaction simply adds an incoming line to the cross vertex, which must encounter a "dot" (change into a c–electron) before entering the cross vertex.

6.5 "VACUUM DIAGRAMS" AND THEIR EFFECTS

6.5.1 ARE THEY *REALLY* VACUUM DIAGRAMS?

Now it is time to address one of the most formidable problems with this approach to the Anderson model, namely, that of the "vacuum diagrams". These two words are enclosed in quotation marks, because it is not clear that these "vacuum diagrams" actually disconnect from the main diagrams. Let us explore this predicament further.

Vacuum diagrams, in the context of the quantum algebra approach, were introduced in sect. 3.3. Suppose that one wishes to calculate the full ξ–propagator, $\mathcal{G}_{\xi}$, via the generalized Gell–Mann Low formula of eq. (3.31).

Following the arguments of sect. 3.3.2, and using the generalized Wick's theorem of eq. (3.13) to contract ξ, $\xi^\dagger$, and the $\hat{U}$ terms, one will be left with an expression like eq. (3.36). That is:

$$\mathcal{G}^{\alpha_2\alpha_1}_{\ell m_2 m_1}(t_2-t_1) =$$

$$= \frac{1}{D_v}\sum_{wc}\int d\{t'\}\, F^{\alpha_2\alpha_1\{\alpha'\}}_{wc_{m_2 m_1\{m',\bar{m}'\}}}\left[S_{\varepsilon_f}, C_o\, ; t_2-t_1, \{t'\}\right]\, N^{\{\alpha'\}}_{wc_{\{m',\bar{m}'\}}}(\{t'\}) \, , \tag{6.91a}$$

where:

$$D_v = \sum_{vwc}\int d\{t''\} F^{\{\alpha''\}}_{vwc_{\{m'',\bar{m}''\}}}\left[S_{\varepsilon_f}, C_o\, ; \{t''\}\right]\, N^{\{\alpha''\}}_{vwc_{\{m'',\bar{m}''\}}}(\{t''\}) \, , \tag{6.91b}$$

$$N^{\{\alpha'\}}_{wc_{\{m',\bar{m}'\}}}(\{t'\}) =$$

$$= \langle 0,\beta|\, U(\infty-\tfrac{i\beta}{2},\infty)\, T\left[M^{\alpha'_1}_{m'_1\bar{m}'_1}(t'_1) \,\ldots\, M^{\alpha'_j}_{m'_j\bar{m}'_j}(t'_j)\right]_{wc} U(-\infty,-\infty+\tfrac{i\beta}{2})\, |0,\beta\rangle \, , \tag{6.91c}$$

$$N^{\{\alpha''\}}_{vwc_{\{m'',\bar{m}''\}}}(\{t''\}) =$$

$$= \langle 0,\beta|\, U(\infty-\tfrac{i\beta}{2},\infty)\, T\left[M^{\alpha''_1}_{m''_1\bar{m}''_1}(t''_1) \,\ldots\, M^{\alpha''_j}_{m''_j\bar{m}''_j}(t''_j)\right]_{vwc} U(-\infty,-\infty+\tfrac{i\beta}{2})\, |0,\beta\rangle \, . \tag{6.91d}$$

As in eq. (3.36), "wc" represents all possible sets of Wick contractions using eq. (3.13), and "vwc" represents all possible sets of Wick contractions which lead to vacuum diagrams. F_{wc} includes all connected and disconnected Feynman diagrams formed from S_{ε_f} and C_o lines. Similarly, F_{vwc} contains all vacuum diagrams formed from S_{ε_f} and C_o lines.

In the numerator, and in the denominator, one is left with a sum of terms, each one being a tangled web of S_{ε_f} and C_o lines, multiplied by the vacuum expectation value of a T-product of M-operators, sandwiched between the U–operators at $\mathcal{R}e\, t = \pm\infty$. If one ignores the U–operators at $\mathcal{R}e\, t = \pm\infty$, and performs the time–splitting described in chapter 4, one ends up with the Feynman rules presented in sections 6.4.3 and 6.4.4. These rules are wrong. The effects of the U–operators at $\mathcal{R}e\, t = \pm\infty$ are essential, as was demonstrated in Chapter 5.

How does one determine the effects of these U–operators? One should keep in mind the important lessons learned in sections 5.8 and 5.9, namely: 1) one must determine the effects of the U–operators before the time–splitting is performed on the M–operators, or 2) when performing the time–splitting on the M–operators, with the U–operators present, one must contract with the operators at $\mathcal{R}e\, t = \pm\infty$ contained in U. We will use a combination of points 1 and 2.

Firstly, let us use the generalized Wick's theorem of eq. (3.13) on the U–operators at $\mathcal{R}e\, t = \pm\infty$, following point 1. This generates "disconnected" diagrams composed of S_{ϵ_f} and C_0 propagators, and leaves behind a T–product of M–operators at $\mathcal{R}e\, t = \pm\infty$. One does not have to worry about contracting ξ–operators contained in U with M–operators contained in the finite–time T–product; in this case the damping argument is still valid. The result~~s~~ of this process are as follows:

$$N^{\{\alpha\}}_{wc_{\{m,\bar{m}\}}}(\{t\}) = \sum_{\substack{wc+\\ wc-}} \int d\{\tau\}\, d\{\tau'\}\, V_{wc+_{\{m',\bar{m}'\}}}\left[S_{\epsilon_f}, C_o\, ;\{\tau\}\right] \times$$

$$\times\, N^{\{\alpha\}}_{wc\pm_{\{m',\bar{m}',m,\bar{m},m'',\bar{m}''\}}}(\{\tau,t,\tau'\})\; V_{wc-_{\{m'',\bar{m}''\}}}\left[S_{\epsilon_f}, C_o\, ;\{\tau'\}\right] , \tag{6.92a}$$

$$N^{\{\alpha\}}_{\mathrm{vwc}_{\{m,\bar{m}\}}}(\{t\}) = \sum_{\substack{\mathrm{wc+} \\ \mathrm{wc-}}} \int d\{\tau\}\, d\{\tau'\}\, V_{\mathrm{wc+}_{\{m',\bar{m}'\}}}\left[S_{\varepsilon_f}, C_o\,;\{\tau\}\right] \times$$

$$\times\, N^{\{\alpha\}}_{\mathrm{vwc}\pm_{\{m',\bar{m}',m,\bar{m},m'',\bar{m}''\}}}(\{\tau,t,\tau'\})\; V_{\mathrm{wc-}_{\{m'',\bar{m}''\}}}\left[S_{\varepsilon_f}, C_o\,;\{\tau'\}\right] , \tag{6.92b}$$

where:

$$N^{\{\alpha\}}_{\mathrm{wc}\pm_{\{m',\bar{m}',m,\bar{m},m'',\bar{m}''\}}}(\{\tau,t,\tau'\}) =$$

$$= \langle 0,\beta|\, T_\tau \left[M_{m_1'\bar{m}_1'}\left[\infty - \frac{i\tau_1}{2}\right] \ldots M_{m_j'\bar{m}_j'}\left[\infty - \frac{i\tau_j}{2}\right] \right]_{\mathrm{wc+}} \times$$

$$\times\, T\left[M^{\alpha_1}_{m_1\bar{m}_1}(t_1) \ldots M^{\alpha_k}_{m_k\bar{m}_k}(t_k) \right]_{\mathrm{wc}} \times$$

$$\times\, T^{-1}_{\tau'} \left[M_{m_1''\bar{m}_1''}\left[-\infty + \frac{i\tau_1'}{2}\right] \ldots M_{m_\ell''\bar{m}_\ell''}\left[-\infty + \frac{i\tau_\ell'}{2}\right] \right]_{\mathrm{wc-}} |0,\beta\rangle \;, \tag{6.93a}$$

$$N^{\{\alpha\}}_{\mathrm{vwc}\pm_{\{m',\bar{m}',m,\bar{m},m'',\bar{m}''\}}}(\{\tau,t,\tau'\}) =$$

$$= \langle 0,\beta|\, T_\tau \left[M_{m_1'\bar{m}_1'}\left[\infty - \frac{i\tau_1}{2}\right] \ldots M_{m_j'\bar{m}_j'}\left[\infty - \frac{i\tau_j}{2}\right] \right]_{\mathrm{wc+}} \times$$

$$\times\, T\left[M^{\alpha_1}_{m_1\bar{m}_1}(t_1) \ldots M^{\alpha_k}_{m_k\bar{m}_k}(t_k) \right]_{\mathrm{vwc}} \times$$

$$\times\, T^{-1}_{\tau'} \left[M_{m_1''\bar{m}_1''}\left[-\infty + \frac{i\tau_1'}{2}\right] \ldots M_{m_\ell''\bar{m}_\ell''}\left[-\infty + \frac{i\tau_\ell'}{2}\right] \right]_{\mathrm{wc-}} |0,\beta\rangle \tag{6.93b}$$

Here “wc+” refers to Wick contractions of U–terms at $\mathcal{R}e\, t = +\infty$, which lead to “disconnected” diagrams composed of S_{ε_f} and C_o propagators. These diagrams are represented by “$V_{\mathrm{wc+}}$”. Likewise, “wc-” refers to Wick contractions of U–terms at $\mathcal{R}e\, t = -\infty$, which also lead to “disconnected” diagrams composed of S_{ε_f} and C_o propagators. These diagrams are represented by “$V_{\mathrm{wc-}}$”.

Left behind, in the vacuum expectation values, are T–products of

M–operators coming from the original Wick contractions in eqs. (6.91), multiplied by T_τ-products of M–operators coming from the "wc+" contractions, and $T^{-1}_{\tau'}$-products of M–operators coming from the "wc-" contractions. These vacuum expectation values are represented by $N_{wc\pm}$ in the numerator, and by $N_{vwc\pm}$ in the denominator. (Note that one uses $T^{-1}_{\tau'}$ rather than $T_{\tau'}$, because τ' is decreasing rather than increasing.)

What are the consequences of this analysis? In the $\langle P_o\rangle$ sector, there is no problem: All of the $M_{m\bar{m}}$ operators become $\delta_{m\bar{m}}\, P_o$, consequently the entire vacuum expectation value becomes a product of δ–functions multiplied by $\langle P_o\rangle$. Using eq. (4.56b), one finds:

$$
\begin{aligned}
N^{\{\alpha\}}_{wc\pm\,\{m',\bar{m}',m,\bar{m},m'',\bar{m}''\}}(\{\tau,t,\tau'\}) = {} & \prod_{\{j,k,\ell\}_{wc\pm}} \delta_{m'_j\bar{m}'_j}\;\delta_{m_k\bar{m}_k}\;\delta_{m''_\ell\bar{m}''_\ell}\;\langle P_o\rangle \;+ \\
& + \langle 0,\beta|\; T_\tau\left[X_{\bar{m}'_1 m'_1}\!\left[\infty - \frac{i\tau_1}{2}\right] \cdots X_{\bar{m}'_j m'_j}\!\left[\infty - \frac{i\tau_j}{2}\right]\right]_{wc+} \times \\
& \times T\left[X^{\alpha_1}_{\bar{m}_1 m_1}(t_1) \cdots X^{\alpha_k}_{\bar{m}_k m_k}(t_k)\right]_{wc} \times \\
& \times T^{-1}_{\tau'}\left[X_{\bar{m}''_1 m''_1}\!\left[-\infty + \frac{i\tau'_1}{2}\right] \cdots X_{\bar{m}''_\ell m''_\ell}\!\left[-\infty + \frac{i\tau'_\ell}{2}\right]\right]_{wc-} |0,\beta\rangle ,
\end{aligned}
\tag{6.94}
$$

with a similar result for $N_{vwc\pm}$. Thus, the vacuum diagrams V_{wc+} and V_{wc-} truly do disconnect in the $\langle P_o\rangle$ sector. As evidenced in chapter 5, it is expected that these vacuum diagrams will renormalize $\langle P_o\rangle$ so that it becomes $\langle P_o\rangle_R$. Further confirmation of this may be obtained from the Bethe–Salpeter equation of eq. (6.80), in which the first term explicitly contains $\langle P_o\rangle_R$.

But it's a different story in the $\langle P_1\rangle$ sector, as can be seen from eq. (6.94). Now we must use point 2 above. Namely, we cannot perform the time–splitting on the finite–time X–operator T–product *alone*; we must include contractions with ***all*** X–operators, even those at $\mathcal{R}e\, t = \pm\infty$. The damping argument no longer holds, because all these operators are zero–energy boson eigenoperators.

Suppose one uses the non–SU(N) rules of chapter 4 to reduce the X–operator function in eq. (6.94). One must connect all the vertices, $\tau_1 \ldots \tau_j$, $t_1 \ldots t_k$, and $\tau_1' \ldots \tau_\ell'$, by one gigantic $(j+k+\ell)$–wiggle. This means that the "vacuum diagrams" in the $\langle P_1 \rangle$ sector are actually connected to the main diagram via wiggle lines. ***The "vacuum diagrams" are no longer disconnected!***

Even if one uses the broken–chain SU(N) rules of chapter 4 to reduce the X–operator function, one must include terms which connect the "vacuum diagrams" to the main diagrams. The predicament seems unavoidable.

6.5.2 DISCONNECTION OF THE VACUUM DIAGRAMS

6.5.2.1 The Hypothesis of Disconnection

Vacuum diagrams were found to renormalize $\langle P_0 \rangle$ and $\langle P_1 \rangle$ in chapter 5. It was hoped that vacuum diagrams in the Anderson model would perform the same function. Unfortunately, "vacuum diagrams" in the $\langle P_1 \rangle$ sector remain connected to the main diagrams via wiggle diagrams. Not only that, but the reduction is written in terms of $\langle P_1 \rangle$, the ***bare*** projection operator, rather than $\langle P_1 \rangle_R$. There ***must*** be some way in which to disconnect the vacuum diagrams, such that they renormalize the projection operator, and that the reduction may be written in terms of $\langle P_1 \rangle_R$. The purpose of this subsection is to explore such a hypothesis.

6.5.2.2 Diagrammatic Representation of the Hypothesis

Let us diagrammatically represent $F_{wc}\left[S_{\epsilon_f}, C_e \right]$, in eq. (6.91a), by a blob with a line emanating from it, as in FIG. 6.8. The blob represents all diagrams, connected or disconnected, one–particle–irreducible or not, which can be formed from the S_{ε_f} and C_o lines, using the interaction vertices and the Feynman rules. This includes cases where the starting cross of the propagator forms a spontaneous vertex, which explains why the blob includes this cross. Note that the dot end of the propagator never forms a spontaneous vertex, which is why it stands alone, outside the blob.

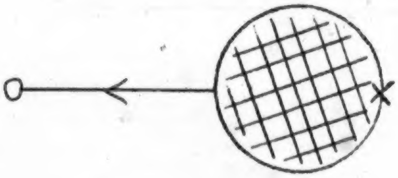

FIG. 6.8

Diagrammatic Representation of $F_{wc}\left[S_{\varepsilon_f}, C_o\right]$

The blob represents the sum of all possible Feynman diagrams before the zero–energy boson reduction is performed. The cross is included in the blob because it may form a spontaneous vertex.

In a similar manner, let us diagrammatically represent $V_{wc+}\left[S_{\varepsilon_f}, C_o\right]$ and $V_{wc-}\left[S_{\varepsilon_f}, C_o\right]$ as shown in FIG. 6.9. Again, the blob represents all diagrams composed of the S_{ε_f} and C_o lines using the interaction vertices. Here, a c–electron propagator connects to the dot end of the ξ–propagator, and brings it back to the cross end.

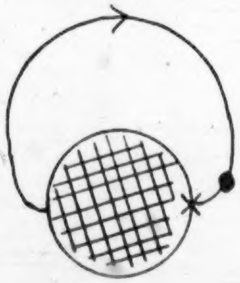

FIG. 6.9

Diagrammatic Representation of $V_{wc+}\left[S_{\varepsilon_f}, C_o\right]$ and $V_{wc-}\left[S_{\varepsilon_f}, C_o\right]$

The blob represents the sum of all possible Feynman diagrams at $\mathcal{R}e\, t = \pm\infty$, before the zero energy boson reduction is performed.

The hypothesis of disconnection is expressed diagrammatically in FIGS. 6.10 and 6.11. FIG. 6.10 shows that the main diagram is connected to the "vacuum diagrams" via wiggle lines. It is hypothesized that the wiggle diagrams will split apart into three separate pieces, as in FIG. 6.11, such that the vacuum diagrams disconnect, and each disconnected object will be separately renormalized by the wiggle lines.

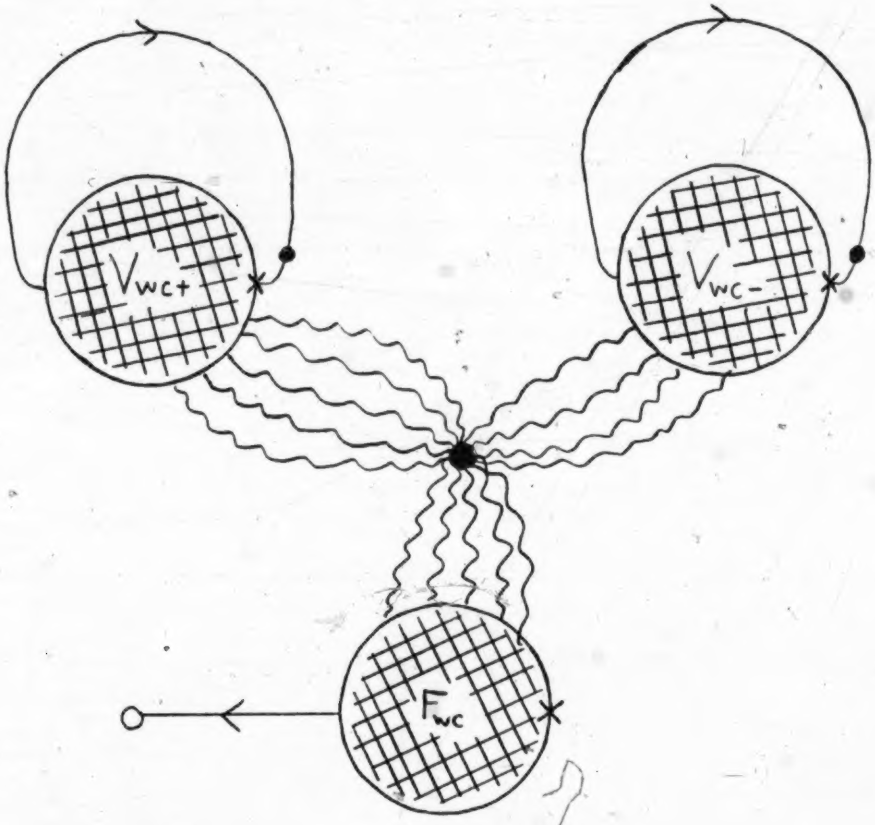

FIG. 6.10

Connection of the "Vacuum Diagrams" to the Main Diagram

After the zero–energy boson reduction is performed, one finds that wiggle lines connect the "vacuum diagrams" at $\mathcal{R}e\, t = \pm\infty$ with the main diagrams.

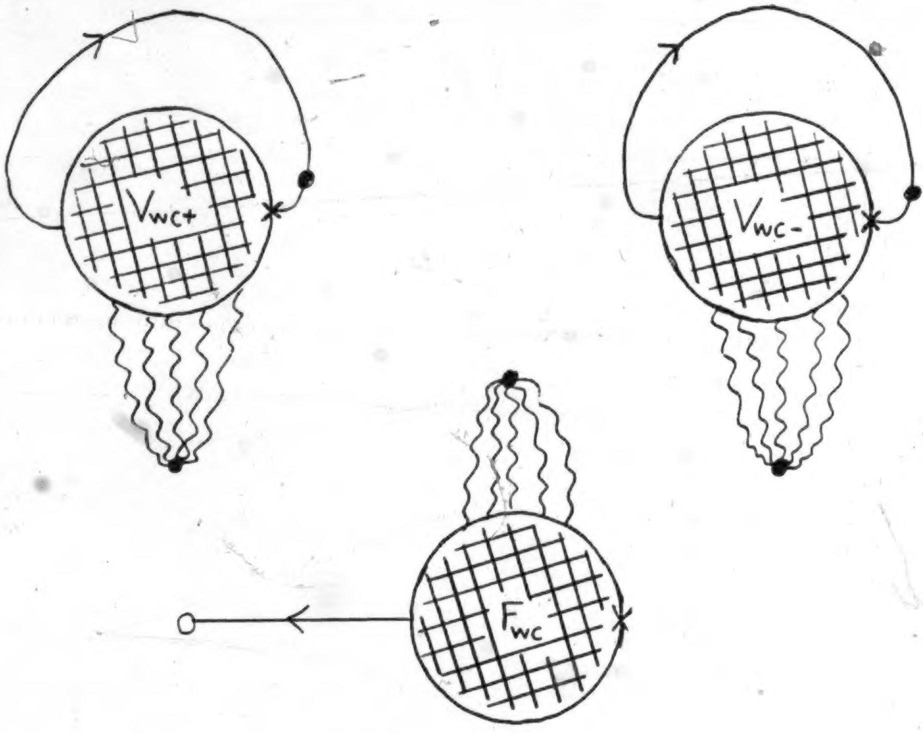

FIG. 6.11

How the Vacuum Diagrams Might Disconnect from the Main Diagrams

This shows how the wiggle diagram of FIG. 6.10 may split apart into three disconnected pieces, such that the "vacuum diagrams" disconnect and become true vacuum diagrams.

6.5.2.3 A Direct Non–Feynman Evaluation of the X–Operator T–Product

The Feynman rules for reducing a T–product of X–operators were given in chapter 4. Both the SU(N) rules and the non–SU(N) rules are so complicated, that it is hopeless to use them in an attempt at proving disconnection. The only viable method is to forget about Feynman diagrams, and directly evaluate the X–functions in terms of spin delta–functions and time θ–functions.

From eq. (4.64), one has the following relation for *any* T–product of X–operators, (including complex times, because it is only the *ordering* of the X–operators which depends on time):

$$\begin{aligned}\langle 1\,2\ldots \ell\rangle &\equiv \langle 0,\beta|\,\mathrm{T}\,X^{\gamma_1}_{m'_1m_1}(t_1)\ldots X^{\gamma_j}_{m'_jm_j}(t_j)\,|0,\beta\rangle = \\ &=\sum_{mm'}\langle \tilde{m}\,m|\,\mathrm{T}\,X^{\gamma_1}_{m'_1m_1}(t_1)\ldots X^{\gamma_j}_{m'_jm_j}(t_j)\,|m'\,\tilde{m}'\rangle\,\frac{1}{N}\,\langle P_1\rangle = \\ &\equiv W^{\{\gamma\}}_{\{m',m\}}(\{t\})\,\frac{1}{N}\,\langle P_1\rangle\ .\end{aligned} \tag{6.95}$$

Because operators commute with their tilde conjugate, let us put all the non–tilde operators on the left and all the tilde operators on the right:

$$\begin{aligned}W^{\{\gamma\}}_{\{m',m\}}(\{t\}) &= \sum_{\{a\}\{b\}}\delta_{\gamma_{a_1}1}\,\delta_{\gamma_{a_2}1}\cdots\delta_{\gamma_{a_n}1}\,\delta_{\gamma_{b_1}2}\,\delta_{\gamma_{b_2}2}\cdots\delta_{\gamma_{b_p}2}\ \times \\ &\times\sum_{mm'}\langle\tilde{m}\,m|\,\mathrm{T}\left[X_{m'_{a_1}m_{a_1}}(t_{a_1})\,X_{m'_{a_2}m_{a_2}}(t_{a_2})\ldots X_{m'_{a_n}m_{a_n}}(t_{a_n})\right]\times \\ &\times\ \mathrm{T}\left[\tilde{X}^{\dagger}_{m'_{b_1}m_{b_1}}(t_{b_1})\,\tilde{X}^{\dagger}_{m'_{b_2}m_{b_2}}(t_{b_2})\ldots\tilde{X}^{\dagger}_{m'_{b_p}m_{b_p}}(t_{b_p})\right]|m'\,\tilde{m}'\rangle\ .\end{aligned} \tag{6.96}$$

Here $\{a\}$ and $\{b\}$ represent all distinct sets, whose elements satisfy the following conditions: $1 \le a \le j$, $1 \le b \le j$, $a \ne b$, $a_1 < a_2 < \ldots < a_n$, $b_1 < b_2 < \ldots < b_p$, and $n + p = j$.

Let us further explicate W by pulling out the time θ–functions, as follows:

$$\begin{aligned}W^{\{\gamma\}}_{\{m',m\}}(\{t\}) &= \sum_{\{a\}\{b\}}\delta_{\gamma_{a_1}1}\,\delta_{\gamma_{a_2}1}\cdots\delta_{\gamma_{a_n}1}\,\delta_{\gamma_{b_1}2}\,\delta_{\gamma_{b_2}2}\cdots\delta_{\gamma_{b_p}2}\ \times \\ &\sum_{\{P_i\}\{P_k\}}\theta(t_{a_{i_1}}-t_{a_{i_2}})\ldots\theta(t_{a_{i_{n-1}}}-t_{a_{i_n}})\,\theta(t_{b_{k_1}}-t_{b_{k_2}})\ldots\theta(t_{b_{k_{p-1}}}-t_{b_{k_p}})\times \\ &\times\sum_{mm'}\langle\tilde{m}\,m|\,X_{m'_{a_{i_1}}m_{a_{i_1}}}\,X_{m'_{a_{i_2}}m_{a_{i_2}}}\ldots X_{m'_{a_{i_n}}m_{a_{i_n}}}\ \times \\ &\times\ \tilde{X}^{\dagger}_{m'_{b_{k_1}}m_{b_{k_1}}}\,\tilde{X}^{\dagger}_{m'_{b_{k_2}}m_{b_{k_2}}}\ldots\tilde{X}^{\dagger}_{m'_{b_{k_p}}m_{b_{k_p}}}\,|m'\,\tilde{m}'\rangle\ ,\end{aligned} \tag{6.97}$$

where $\{P_i\}$ represents all permutations on elements of the set $\{a\}$, and $\{P_k\}$ represents all permutations on the set $\{b\}$.

It is trivial to show that the following relation is true:

$$\sum_{m} \tilde{X}^{\dagger}_{m_i' m_i} |m\, \tilde{m}\rangle = \sum_{m} X_{m_i' m_i} |m\, \tilde{m}\rangle \tag{6.98}$$

(Just use the representation for X given in eq. (5.7d).) Using this relation in eq. (6.97), one may turn the rightmost $\tilde{X}^{\dagger}$ into X. Then, noting that the tilde operators commute past the non–tilde operators, one may bring this X to the left of all the $\tilde{X}^{\dagger}$'s. Iterating this process changes all the $\tilde{X}^{\dagger}$'s into X's, and reverses their order. That is:

$$\begin{aligned}
&\sum_{mm'} \langle \tilde{m}\, m|\, X_{m'_{a_{i_1}} m_{a_{i_1}}} X_{m'_{a_{i_2}} m_{a_{i_2}}} \cdots X_{m'_{a_{i_n}} m_{a_{i_n}}} \times \\
&\times\ \tilde{X}^{\dagger}_{m'_{b_{k_1}} m_{b_{k_1}}} \tilde{X}^{\dagger}_{m'_{b_{k_2}} m_{b_{k_2}}} \cdots \tilde{X}^{\dagger}_{m'_{b_{k_p}} m_{b_{k_p}}} |m'\, \tilde{m}'\rangle = \\
&= \sum_{mm'} \langle \tilde{m}\, m|\, X_{m'_{a_{i_1}} m_{a_{i_1}}} X_{m'_{a_{i_2}} m_{a_{i_2}}} \cdots X_{m'_{a_{i_n}} m_{a_{i_n}}} \times \\
&\times\ X_{m'_{b_{k_p}} m_{b_{k_p}}} X_{m'_{b_{k_{p-1}}} m_{b_{k_{p-1}}}} \cdots X_{m'_{b_{k_1}} m_{b_{k_1}}} |m'\, \tilde{m}'\rangle\ .
\end{aligned} \tag{6.99}$$

Because there are no tilde operators left on the right–hand side of eq. (6.99), the tilde states give $\delta_{mm'}$, such that the sum over m becomes a trace. Using the representation $X_{mm'} = |m\rangle\langle m'|$, one is left with a product of spin delta–functions. The result is that eq. (6.97) becomes:

$$\boxed{\begin{aligned}
W^{\{\gamma\}}_{\{m',m\}}(\{t\}) = &\sum_{\{a\}\{b\}} \delta_{\gamma_{a_1} 1}\, \delta_{\gamma_{a_2} 1} \cdots \delta_{\gamma_{a_n} 1}\, \delta_{\gamma_{b_1} 2}\, \delta_{\gamma_{b_2} 2} \cdots \delta_{\gamma_{b_p} 2} \times \\
&\times \sum_{\{P_i\}\{P_k\}} \theta(t_{a_{i_1}} - t_{a_{i_2}}) \cdots \theta(t_{a_{i_{n-1}}} - t_{a_{i_n}})\, \theta(t_{b_{k_1}} - t_{b_{k_2}}) \cdots \times \\
&\times\ \theta(t_{b_{k_{p-1}}} - t_{b_{k_p}})\, \delta_{m_{a_{i_1}} m'_{a_{i_2}}}\, \delta_{m_{a_{i_2}} m'_{a_{i_3}}} \cdots \delta_{m_{a_{i_{n-1}}} m'_{a_{i_n}}} \times \\
&\times\ \delta_{m_{a_{i_n}} m'_{b_{k_p}}}\, \delta_{m_{b_{k_p}} m'_{b_{k_{p-1}}}} \cdots \delta_{m_{b_{k_2}} m'_{b_{k_1}}}\, \delta_{m_{b_{k_1}} m'_{a_{i_1}}}
\end{aligned}} \tag{6.100}$$

6.5.2.4 Direct Evaluation of the X–Operator T–Product Which Results When Vacuum Diagrams are Present

Let us apply the above method to eq. (6.94). To facilitate this application, we define:

$$W^{\{\alpha\}}_{wc\pm\{m',\bar{m}',m,\bar{m},m'',\bar{m}''\}}(\{\tau,t,\tau'\})\,\frac{1}{N}\langle P_1\rangle \equiv$$

$$\equiv \langle 0,\beta|\, T_\tau\left[X_{\bar{m}'_1 m'_1}\left[\infty-\frac{i\tau_1}{2}\right]\,\ldots\,X_{\bar{m}'_j m'_j}\left[\infty-\frac{i\tau_j}{2}\right]\right]_{wc+}\times$$

$$\times\, T\left[X^{\alpha_1}_{\bar{m}_1 m_1}(t_1)\,\ldots\,X^{\alpha_k}_{\bar{m}_k m_k}(t_k)\right]_{wc}\times$$

$$\times\, T^{-1}_{\tau'}\left[X_{\bar{m}''_1 m''_1}\left[-\infty+\frac{i\tau'_1}{2}\right]\,\ldots\,X_{\bar{m}''_\ell m''_\ell}\left[-\infty+\frac{i\tau'_\ell}{2}\right]\right]_{wc-}|0,\beta\rangle\ . \qquad (6.101)$$

As in eq. (6.96), let us put all the tilde operators on the right. Note that these exist only in the finite–time T–product; the X–operators at $\mathcal{Re}\, t = \pm\infty$ are all non–tilde operators. The result is:

$$W^{\{\alpha\}}_{wc\pm\{m',\bar{m}',m,\bar{m},m'',\bar{m}''\}}(\{\tau,t,\tau'\}) =$$

$$= \sum_{\{a\}\{b\}} \delta_{\alpha_{a_1}1}\,\delta_{\alpha_{a_2}1}\cdots\delta_{\alpha_{a_n}1}\,\delta_{\alpha_{b_1}2}\,\delta_{\alpha_{b_2}2}\cdots\delta_{\alpha_{b_p}2}\times$$

$$\times \sum_{mm'}\langle\tilde{m}\,m|\,T_\tau\left[X_{\bar{m}'_1 m'_1}\left[\infty-\frac{i\tau_1}{2}\right]\,\ldots\,X_{\bar{m}'_j m'_j}\left[\infty-\frac{i\tau_j}{2}\right]\right]_{wc+}\times$$

$$\times\, T\left[X_{\bar{m}_{a_1} m_{a_1}}(t_{a_1})\,X_{\bar{m}_{a_2} m_{a_2}}(t_{a_2})\ldots X_{\bar{m}_{a_n} m_{a_n}}(t_{a_n})\right]_{wc}\times$$

$$\times\, T^{-1}_{\tau'}\left[X_{\bar{m}''_1 m''_1}\left[-\infty+\frac{i\tau'_1}{2}\right]\,\ldots\,X_{\bar{m}''_\ell m''_\ell}\left[-\infty+\frac{i\tau'_\ell}{2}\right]\right]_{wc-}\times$$

$$\times\, T\left[\tilde{X}^\dagger_{\bar{m}_{b_1} m_{b_1}}(t_{b_1})\,\tilde{X}^\dagger_{\bar{m}_{b_2} m_{b_2}}(t_{b_2})\ldots\tilde{X}^\dagger_{\bar{m}_{b_p} m_{b_p}}(t_{b_p})\right]_{wc}|m'\,\tilde{m}'\rangle\ , \qquad (6.102)$$

where {a} and {b} represent all distinct sets, whose elements satisfy the following conditions: $1 \le a \le k$, $1 \le b \le k$, $a \neq b$, $a_1 < a_2 < \ldots < a_n$, $b_1 < b_2 < \ldots < b_p$, and $n + p = k$.

As in eq. (6.97), we now pull out the time θ-functions, yielding:

$$\begin{aligned}
&W^{\{\alpha\}}_{wc\pm\{m',\bar{m}',m,\bar{m},m'',\bar{m}''\}}(\{\tau,t,\tau'\}) = \\
&= \sum_{\{a\}\{b\}} \delta_{\alpha_{a_1}1}\,\delta_{\alpha_{a_2}1}\cdots\delta_{\alpha_{a_n}1}\,\delta_{\alpha_{b_1}2}\,\delta_{\alpha_{b_2}2}\cdots\delta_{\alpha_{b_p}2}\;\times \\
&\times \sum_{\substack{\{P_q\}\{P_r\}\\ \{P_s\}\{P_u\}}} \theta(\tau_{q_1}-\tau_{q_2})\ldots\theta(\tau_{q_{j-1}}-\tau_{q_j})\,\theta(t_{a_{r_1}}-t_{a_{r_2}})\ldots\theta(t_{a_{r_{n-1}}}-t_{a_{r_n}})\;\times \\
&\times\,\theta(\tau'_{s_1}-\tau'_{s_2})\ldots\theta(\tau'_{s_{\ell-1}}-\tau'_{s_\ell})\,\theta(t_{b_{u_1}}-t_{b_{u_2}})\ldots\theta(t_{b_{u_{p-1}}}-t_{b_{u_p}})\;\times \\
&\times \sum_{mm'} \langle \tilde{m}\, m|\, X_{\bar{m}'_{q_1}m'_{q_1}}\, X_{\bar{m}'_{q_2}m'_{q_2}}\ldots X_{\bar{m}'_{q_j}m'_{q_j}}\;\times \\
&\times\; X_{\bar{m}_{a_{r_1}}m_{a_{r_1}}}\, X_{\bar{m}_{a_{r_2}}m_{a_{r_2}}}\ldots X_{\bar{m}_{a_{r_n}}m_{a_{r_n}}}\;\times \\
&\times\; X_{\bar{m}''_{s_\ell}m''_{s_\ell}}\, X_{\bar{m}''_{s_{\ell-1}}m''_{s_{\ell-1}}}\ldots X_{\bar{m}''_{s_1}m''_{s_1}}\;\times \\
&\times\; \tilde{X}^{\dagger}_{\bar{m}_{b_{u_1}}m_{b_{u_1}}}\, \tilde{X}^{\dagger}_{\bar{m}_{b_{u_2}}m_{b_{u_2}}}\ldots \tilde{X}^{\dagger}_{\bar{m}_{b_{u_p}}m_{b_{u_p}}}\,|m'\,\tilde{m}'\rangle\;,
\end{aligned} \tag{6.103}$$

where $\{P_r\}$ and $\{P_u\}$ represent all permutations on elements of the sets $\{a\}$ and $\{b\}$ respectively, and $\{P_q\}$ and $\{P_s\}$ represent all permutations on the indices of the operators at $\mathcal{Re}\, t = \infty$ and $\mathcal{Re}\, t = -\infty$, respectively.

Now, using eq. (6.99), one may turn the $\tilde{X}^{\dagger}$'s into X's and reverse their order. The expectation value of the X's then becomes a product of delta functions, as in eq. (6.100). The net result is as follows:

$$
\boxed{\begin{aligned}
& W^{\{\alpha\}}_{wc\pm\{m',\bar{m}',m,\bar{m},m'',\bar{m}''\}}(\{\tau,t,\tau'\}) = \\
&= \sum_{\{a\}\{b\}} \delta_{\alpha_{a_1}1}\,\delta_{\alpha_{a_2}1}\cdots\delta_{\alpha_{a_n}1}\,\delta_{\alpha_{b_1}2}\,\delta_{\alpha_{b_2}2}\cdots\delta_{\alpha_{b_p}2}\times \\
&\quad\times \sum_{\substack{\{P_q\}\{P_r\}\\ \{P_s\}\{P_u\}}} \theta(\tau_{q_1}-\tau_{q_2})\ldots\theta(\tau_{q_{j-1}}-\tau_{q_j})\times \\
&\quad\times\ \theta(t_{a_{r_1}}-t_{a_{r_2}})\ldots\theta(t_{a_{r_{n-1}}}-t_{a_{r_n}})\times \\
&\quad\times\ \theta(\tau'_{s_1}-\tau'_{s_2})\ldots\theta(\tau'_{s_{\ell-1}}-\tau'_{s_\ell})\,\theta(t_{b_{u_1}}-t_{b_{u_2}})\ldots\theta(t_{b_{u_{p-1}}}-t_{b_{u_p}})\times \\
&\quad\times\ \delta_{m'_{q_1}\bar{m}'_{q_2}}\,\delta_{m'_{q_2}\bar{m}'_{q_3}}\cdots\delta_{m'_{q_{j-1}}\bar{m}'_{q_j}}\,\delta_{m'_{q_j}\bar{m}_{a_{r_1}}}\,\delta_{m_{a_{r_1}}\bar{m}_{a_{r_2}}}\,\delta_{m_{a_{r_2}}\bar{m}_{a_{r_3}}}\times \\
&\quad\times\cdots\delta_{m_{a_{r_{n-1}}}\bar{m}_{a_{r_n}}}\,\delta_{m_{a_{r_n}}\bar{m}''_{s_\ell}}\,\delta_{m''_{s_\ell}\bar{m}''_{s_{\ell-1}}}\,\delta_{m''_{s_{\ell-1}}\bar{m}''_{s_{\ell-2}}}\cdots\delta_{m''_{s_2}\bar{m}''_{s_1}}\times \\
&\quad\times\ \delta_{m''_{s_1}\bar{m}_{b_{u_p}}}\,\delta_{m_{b_{u_p}}\bar{m}_{b_{u_{p-1}}}}\cdots\delta_{m_{b_{u_2}}\bar{m}_{b_{u_1}}}\,\delta_{m_{b_{u_1}}\bar{m}'_{q_1}}\ .
\end{aligned}}
\tag{6.104}
$$

Manifest in the above expression is the disconnection of θ–functions; all that connects the “vacuum diagrams” to the main diagrams are the spin delta–functions, specifically: $\delta_{m'_{q_j}\bar{m}_{a_{r_1}}}$, $\delta_{m_{a_{r_n}}\bar{m}''_{s_\ell}}$, $\delta_{m''_{s_1}\bar{m}_{b_{u_p}}}$, and $\delta_{m_{b_{u_1}}\bar{m}'_{q_1}}$. An illustration of this is given in FIG. 6.12, where S_{ε_f} lines are used to carry the spin. This is in accordance with the Feynman rules for wiggle–line decomposition, given in sections 4.9.2.7 to 4.9.2.9 .

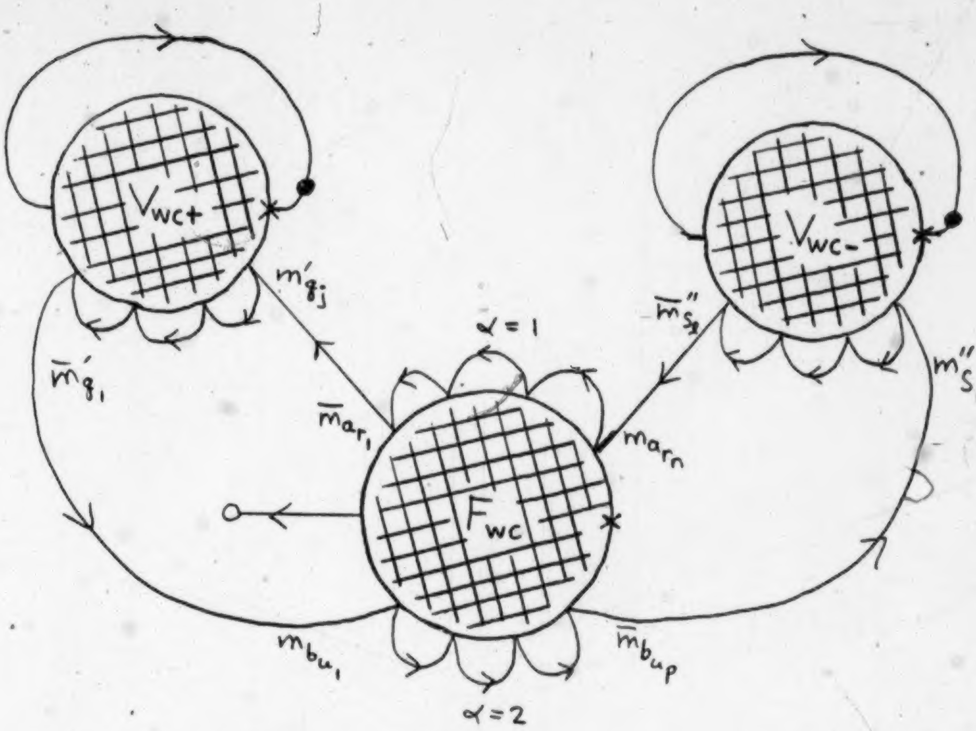

FIG. 6.12

A Decomposition of FIG. 6.10 Using Equation (6.104)

This shows, explicitly, how the vacuum diagrams at $\mathcal{R}e\, t = \pm\infty$ connect to the main diagram.

6.5.2.5 Proof of Disconnection; Confirmation of the Hypothesis

Disconnection is now very easy to prove, by making use of spin conservation. That is, there are no sources nor sinks of spin. Therefore, what goes into a vacuum diagram must come back out. Looking at FIG. 6.12, one finds $\bar{m}_{b_{u_p}}$ going into V_{wc-} and $\bar{m}''_{s_\ell}$ coming back out; this implies $\bar{m}_{b_{u_p}} = \bar{m}''_{s_\ell}$. Paralleling this, one finds $\bar{m}_{a_{r_1}}$ going into V_{wc+} and $\bar{m}'_{q_1}$ coming back out; this implies $\bar{m}_{a_{r_1}} = \bar{m}'_{q_1}$.

One may prove these two relations much more formally, by considering the following two conservation rules:

$$\sum_{m'_q} = \sum_{\bar{m}'_q} \;, \qquad (6.105a)$$

$$\sum_{m''_s} = \sum_{\bar{m}''_s} \;. \qquad (6.105b)$$

These rules are simply a statement that the spin into a vacuum diagram must equal the spin out of a vacuum diagram. Noting the δ–functions in eq. (6.104), one finds:

$$\sum_{m'_q} = m'_{q_1} + m'_{q_2} + \ldots + m'_{q_j} =$$

$$= \bar{m}'_{q_2} + \bar{m}'_{q_3} + \ldots + \bar{m}'_{q_j} + \bar{m}_{a_{r_1}} \;, \qquad (6.106a)$$

$$\sum_{m''_s} = m''_{s_\ell} + m''_{s_{\ell-1}} + \ldots + m''_{s_1} =$$

$$= \bar{m}''_{s_{\ell-1}} + \bar{m}''_{s_{\ell-2}} + \ldots + \bar{m}''_{s_1} + \bar{m}_{b_{u_p}} \;. \qquad (6.106b)$$

Using eqs. (6.106) with eqs. (6.105) proves:

$$\bar{m}'_{q_1} = \bar{m}_{a_{r_1}} \;, \qquad (6.107a)$$

$$\bar{m}''_{s_\ell} = \bar{m}_{b_{u_p}} \;, \qquad (6.107b)$$

as desired.

Utilizing eqs. (6.107) in eq. (6.104), generates the following result:

$$W^{\{\alpha\}}_{wc\pm_{\{m',\bar{m}',m,\bar{m},m'',\bar{m}''\}}}(\{\tau,t,\tau'\}) =$$

$$= W^{\{\alpha\}}_{wc_{\{m,\bar{m}\}}}(\{t\})\, W_{wc+_{\{m',\bar{m}'\}}}(\{\tau\})\, W_{wc-_{\{m'',\bar{m}''\}}}(\{\tau'\}) \times$$

$$\times\; \delta_{m'_{q_j}\bar{m}_{a_{r_1}}}\, \delta_{m_{a_{r_n}}\bar{m}''_{s_\ell}}\, \delta_{m''_{s_1}\bar{m}_{b_{u_p}}}\, \delta_{m_{b_{u_1}}\bar{m}'_{q_1}} \;, \qquad (6.108a)$$

where

$$W_{wc+_{\{m',\bar{m}'\}}}(\{\tau\}) \equiv \sum_{\{P_q\}} \theta(\tau_{q_1} - \tau_{q_2}) \ldots \theta(\tau_{q_{j-1}} - \tau_{q_j}) \times$$

$$\times\; \delta_{m'_{q_1}\bar{m}'_{q_2}}\, \delta_{m'_{q_2}\bar{m}'_{q_3}} \cdots \delta_{m'_{q_{j-1}}\bar{m}'_{q_j}}\, \delta_{m'_{q_j}\bar{m}'_{q_1}} \;, \qquad (6.108b)$$

$$W_{wc-_{\{m',\bar{m}'\}}}(\{\tau'\}) \equiv \sum_{\{P_s\}} \theta(\tau'_{s_1} - \tau'_{s_2}) \ldots \theta(\tau'_{s_{\ell-1}} - \tau'_{s_\ell}) \times$$
$$\times \, \delta_{m'_{s_\ell}\bar{m}'_{s_{\ell-1}}} \delta_{m'_{s_{\ell-1}}\bar{m}'_{s_{\ell-2}}} \cdots \delta_{m'_{s_2}\bar{m}'_{s_1}} \delta_{m'_{s_1}\bar{m}'_{s_\ell}} , \qquad (6.108c)$$

and W_{wc} was given in eq. (6.100).

Without the extra δ–functions in eq. (6.108a), there would be complete disconnection of the vacuum diagrams from the main diagrams. W_{wc} is simply the bare T–product of X–operators considered in Chapter 4 (with the factor of $\langle P_1\rangle/N$ removed), and it may be decomposed in terms of the Feynman rules given in sections 4.9.2.7 – 4.9.2.9. Similarly, W_{wc+} and W_{wc-} will obey the same Feynman rules, with the exception that the thermal index γ is always equal to 1. (Note also that there is only one overall factor of $\langle P_1\rangle/N$ for the product of the three wiggle diagrams.) Thus, ignoring the extra δ–functions, there are three independent wiggle diagrams; the picture of FIG. 6.12 becomes the picture of FIG. 6.13.

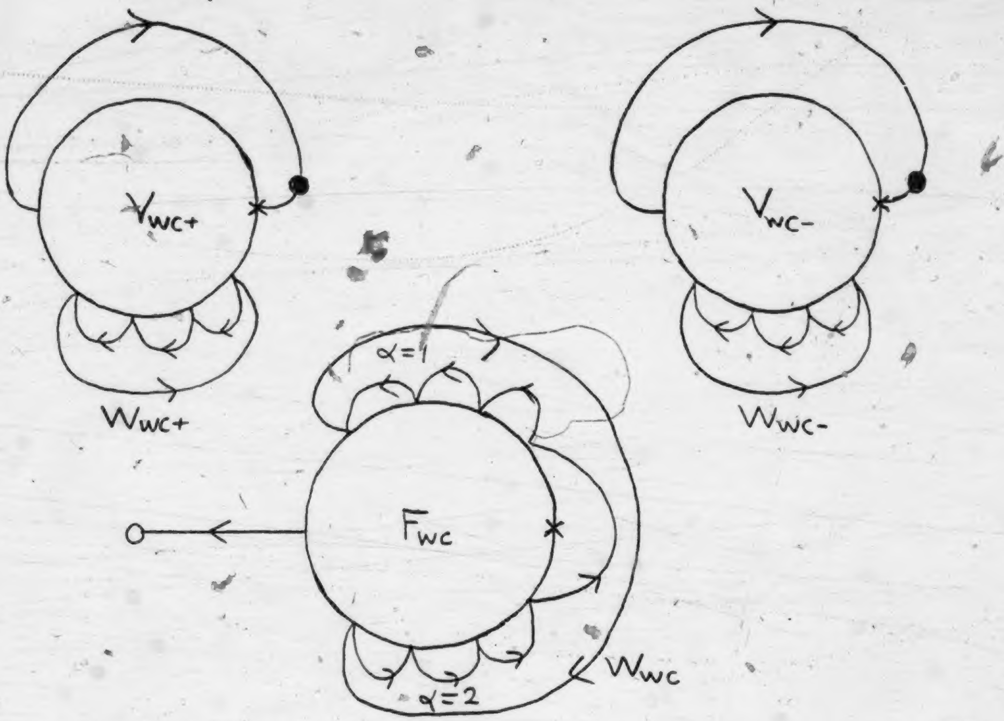

FIG. 6.13

How FIG. 6.12 Disconnects, Confirming the Hypothesis of FIG. 6.11

The vacuum diagrams at $\mathcal{R}e\, t = \pm\infty$ in FIG. 6.12 can be made to disconnect as shown. This will induce two extra spin loops, and therefore an extra factor of N^2 will appear.

Of course, one cannot ignore the extra delta functions. The three wiggle diagrams are not really independent, because the delta functions put a constraint on the spin traces. By considering how FIG. 6.12 becomes FIG. 6.13, the effect of the δ–functions on the spin traces is easy to determine. In FIG. 6.12, there are two spin loops of interest – the $\bar{m}_{b_{u_p}} = m'_{s_1} = \bar{m}'_{s_\ell} = m_{a_{r_n}}$ spin loop, and the $\bar{m}_{a_{r_1}} = m'_{q_j} = \bar{m}'_{q_1} = m_{b_{u_1}}$ spin loop. These two loops will carry a certain total spin trace, say N^c, where c is a non–negative integer. (c depends on whether the loops are open or closed, and how they connect.) Now look at FIG. 6.13. The main diagram $F_{wc}\, W_{wc}$ carries these same two spin loops. It does not matter that the loops no longer pass through the vacuum diagrams; the total spin trace contribution of these two loops is still N^c. But, closing the $m'_{q_j} = \bar{m}'_{q_1}$ spin loop on V_{wc+}, and closing the $m''_{s_1} = \bar{m}''_{s_\ell}$ spin loop on V_{wc-} introduces two ***additional*** closed loops. Thus FIG. 6.13 carries a factor of N^2 more than FIG. 6.12. To equate these two diagrams, one must multiply FIG. 6.13 by a factor of $1/N^2$. Therefore, eq. (6.108a) becomes:

$$\boxed{\begin{aligned} & W^{\{\alpha\}}_{wc\pm_{\{m',\bar{m}',m,\bar{m},m'',\bar{m}''\}}}(\{\tau,t,\tau'\}) = \\ & = \frac{1}{N^2}\, W^{\{\alpha\}}_{wc_{\{m,\bar{m}\}}}(\{t\})\, W_{wc+_{\{m',\bar{m}'\}}}(\{\tau\})\, W_{wc-_{\{m'',\bar{m}''\}}}(\{\tau'\})\ . \end{aligned}} \tag{6.109}$$

This confirms the hypothesis of disconnection posed in FIG. 6.11.

6.5.2.6 The Vacuum–Disconnected Perturbation Expansion

Applying the generalized Wick's theorem to $\mathscr{S}_{\mathbb{R}}$ led to eqs. (6.91). Using eqs. (6.92), (6.94), (6.101), and (6.109) in eq. (6.91) leads to the vacuum–disconnected perturbation expansion for $\mathscr{S}_{\mathbb{R}}$. It is given as follows:

$$\boxed{\begin{aligned} \mathscr{S}^{\alpha_2\alpha_1}_{\mathbb{R}m_2m_1}(t_2-t_1) &= \frac{1}{D_{\underset{\sim}{V}}}\sum_{wc}\int d\{t'\}\, F^{\alpha_2\alpha_1\{\alpha'\}}_{wc_{m_2m_1\{m,\bar{m}\}}}\left[S_{\varepsilon_f},C_o\,;t_2-t_1\,,\{t'\}\right] \times \\ & \times\sum_{\substack{wc+\\ wc-}}\int d\{\tau\}d\{\tau'\}\, V_{wc+_{\{m',\bar{m}'\}}}\left[S_{\varepsilon_f},C_o\,;\{\tau\}\right] V_{wc-_{\{m'',\bar{m}''\}}}\left[S_{\varepsilon_f},C_o\,;\{\tau'\}\right] \times \\ & \qquad \times\left\{\prod_{\{j,k,\ell\}_{wc\pm}}\delta_{m'_j\bar{m}'_j}\ \delta_{m_k\bar{m}_k}\ \delta_{m''_\ell\bar{m}''_\ell}\ \langle P_o\rangle\ + \right. \\ & \left. +\ W^{\{\alpha'\}}_{wc_{\{m,\bar{m}\}}}(\{t'\})\, W_{wc+_{\{m',\bar{m}'\}}}(\{\tau\})\, W_{wc-_{\{m'',\bar{m}''\}}}(\{\tau'\})\,\frac{\langle P_1\rangle}{N^3}\right\}, \end{aligned}} \tag{6.110a}$$

where:

$$\boxed{\begin{aligned} D_v \equiv \sum_{vwc} \int d\{t'\}\, F^{\{\alpha'\}}_{vwc_{\{m,\bar{m}\}}}\left[S_{\varepsilon_f}, C_o\, ; \{t'\}\right] \times \\ \times \sum_{\substack{wc+\\ wc-}} \int d\{\tau\} d\{\tau'\}\, V_{wc+_{\{m',\bar{m}'\}}}\left[S_{\varepsilon_f}, C_o\, ;\{\tau\}\right] V_{wc-_{\{m'',\bar{m}''\}}}\left[S_{\varepsilon_f}, C_o\, ;\{\tau'\}\right] \times \\ \times \left\{ \prod_{\{j,k,\ell\}_{vwc\pm}} \delta_{m_j'\bar{m}_j'}\ \delta_{m_k\bar{m}_k}\ \delta_{m_\ell''\bar{m}_\ell''}\ \langle P_o \rangle \, + \right. \\ \left. + \ W^{\{\alpha'\}}_{vwc_{\{m,\bar{m}\}}}(\{t'\})\, W_{wc+_{\{m',\bar{m}'\}}}(\{\tau\})\, W_{wc-_{\{m'',\bar{m}''\}}}(\{\tau'\}) \frac{\langle P_1 \rangle}{N^3} \right\} , \end{aligned}}$$

(6.110b)

6.5.2.7 Modifications of the Feynman Rules

From eqs. (6.110), (6.109), (6.108b), (6.108c), (6.100), (6.101), (6.95), and (6.94), it is evident that the Feynman rules need little modification. The non–SU(N) rules set out in sections 4.9.2.6 – 4.9.2.9 are still valid, with the following provisos: 1) One must construct the $\mathcal{R}e\, t = \pm\infty$ vacuum diagrams as well as the main diagrams. 2) Suppose there are j non–spontaneous cross vertices in the vacuum diagram at $\mathcal{R}e\, t = \infty$, k non–spontaneous cross vertices in the main diagram, and ℓ non–spontaneous cross vertices in the vacuum diagram at $\mathcal{R}e\, t = -\infty$. Then, the j–vertices must be connected by a j–point wiggle diagram, the k–vertices must be connected by a k–point wiggle diagram, and the ℓ–vertices must be connected by an ℓ–point wiggle diagram. 3) These wiggle diagrams each carry an overall factor of $1/[N\, f_F(\tilde{\varepsilon}_f - \mu)]$, rather than $\langle P_1 \rangle / [N\, f_F(\tilde{\varepsilon}_f - \mu)]$. 4) There is only one factor of $\langle P_1 \rangle$, which multiplies the product of these three wiggle diagrams.

6.5.2.8 Examples of Vacuum Diagram Disconnection

In order to clarify how the disconnection of eqs. (6.109) works, let us consider a few simple examples, which demonstrate that the spin traces do indeed differ by only a factor of N^2. These examples are illustrated in FIGS. 6.14 to 6.19, using the tool of point-splitting the cross vertex (illustrated in FIG. 6.5).

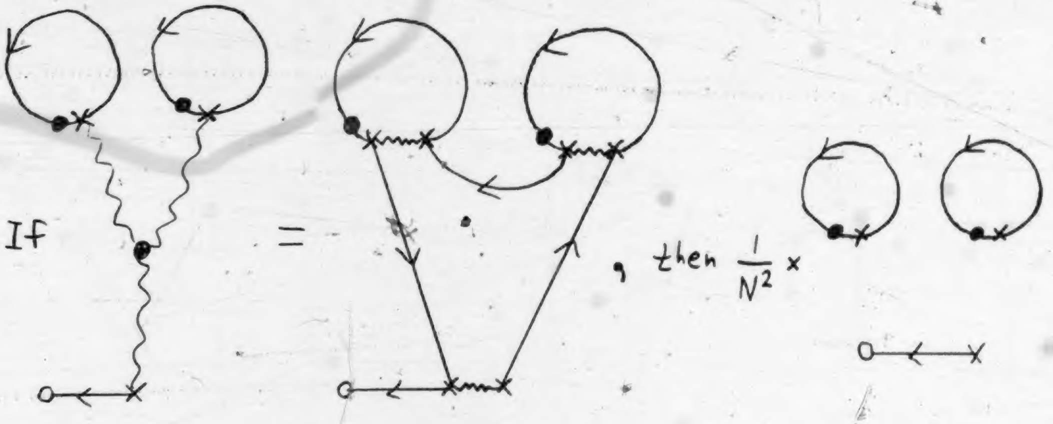

FIG. 6.14

Splitting the 3-Wiggle

This shows a particular diagram in the decomposition of a 3-wiggle, namely, a 1-link chain. This 1-link chain may be split as shown. Before the disconnection, there are no spin loops. Disconnection induces two spin loops, thereby giving an extra factor of N^2.

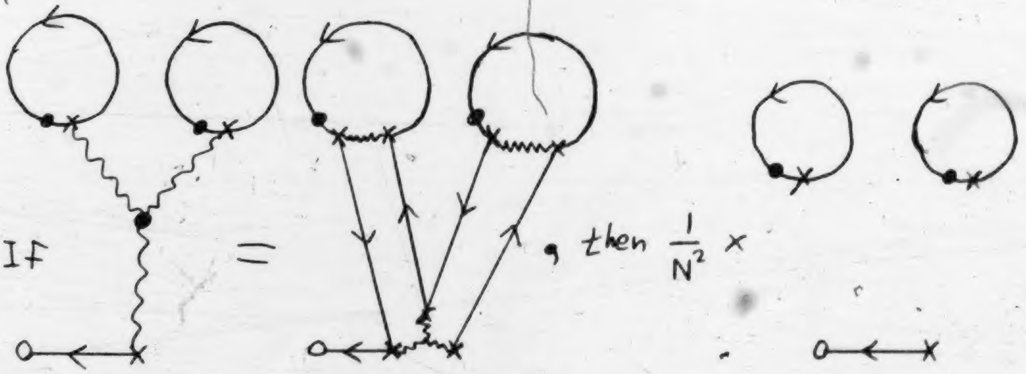

FIG. 6.15

Another Splitting of the 3-Wiggle

This shows another diagram in the decomposition of a 3-wiggle, namely, a 2-link chain. This 2-link chain may also be split, as shown. As before, there are no spin loops before the disconnection, and two spin loops after the disconnection. Therefore an extra factor of N^2 also arises here.

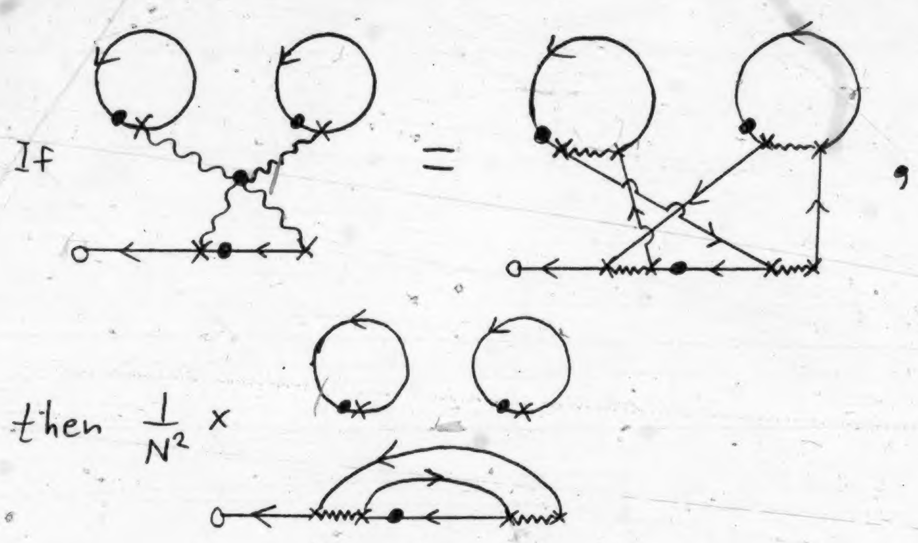

FIG. 6.16

Splitting the 4–Wiggle

This shows a particular diagram in the decomposition of a 4–wiggle, namely, a 1–link chain. This 1–link chain may be split as shown. Before disconnection, there is one spin loop, and therefore a factor of N. After disconnection, there are three spin loops, and therefore a factor of N^3. As before, one finds an extra factor of N^2.

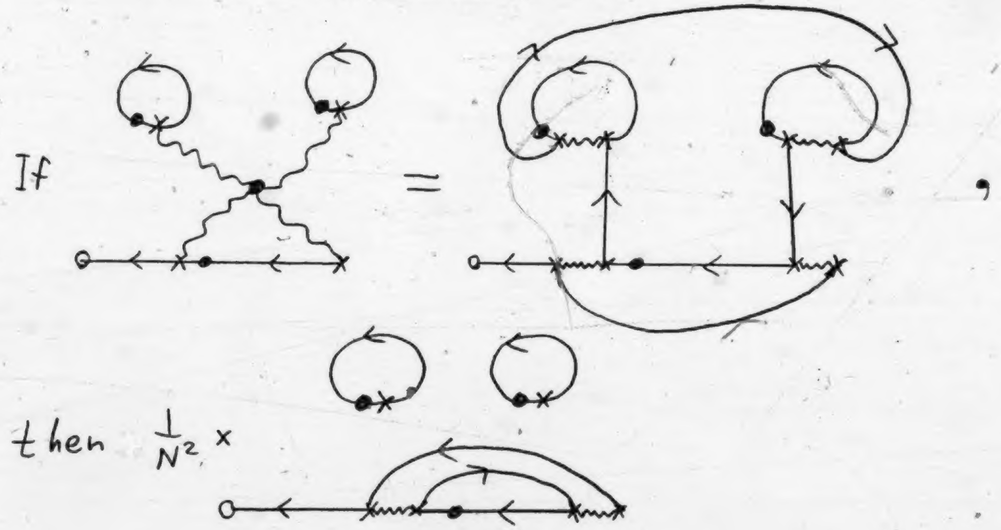

FIG. 6.17

Another Splitting of the 4–Wiggle

This shows another diagram in the decomposition of a 4–wiggle. This is also a 1–link chain, but the ordering of the vertices is different. As before, there is one spin loop before disconnection, and there are three spin loops after disconnection, confirming yet again the extra factor of N^2.

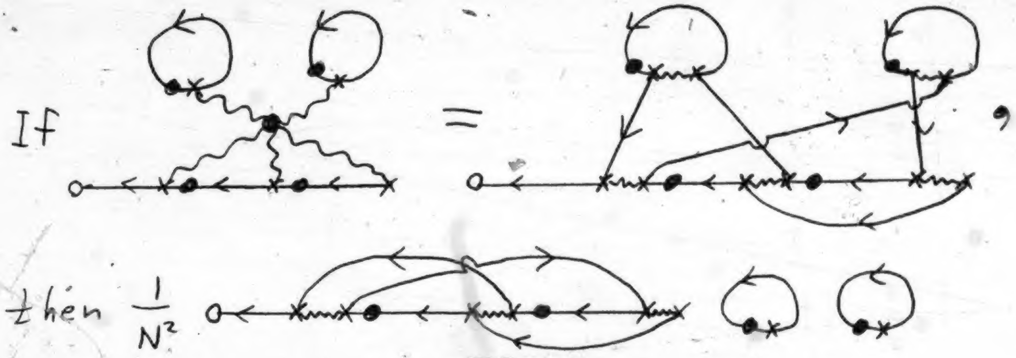

FIG. 6.18

Splitting the 5–Wiggle

This shows a particular diagram in the decomposition of a 5–wiggle, namely, a 1–link chain. This 1–link chain may be split as shown. Before the disconnection, there are no spin loops. Disconnection induces two spin loops, thereby giving the ubiquitous extra factor of N^2.

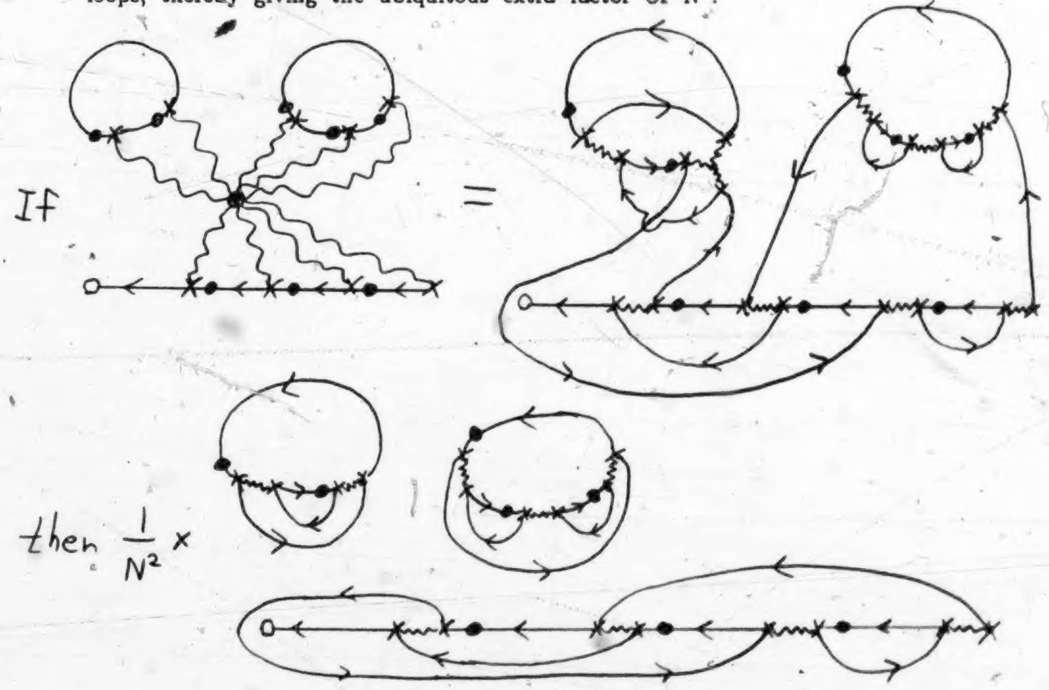

FIG. 6.19

Splitting the 9–Wiggle

The previous examples have been very simple, because there were no wiggle diagrams left attached to the vacuum diagrams after disconnection. This shows a more general example in which there are wiggle diagrams left attached to all three objects after disconnection (namely, the main diagram and the vacuum diagrams at $\mathcal{R}e\, t = \pm\infty$). Illustrated is a 9–wiggle which has been decomposed into a 2–link chain (2 vertices in one link and 8 vertices in the other link). Before disconnection, there are 4 spin loops, giving a factor of N^4. After disconnection, there are 6 spin loops, giving a factor of N^6. Here again, one finds an extra factor of N^2.

6.5.3 RENORMALIZATION OF THE PROJECTION OPERATORS

In section 6.5.2, it was proven that the "vacuum diagrams" at $\mathcal{R}e\, t = \pm\infty$ disconnect, and modified Feynman rules were discussed in section 6.5.2.7. Of course, it would be extremely tedious to actually use these rules, which involve an explicit calculation of the vacuum diagrams. It would be far more convenient if one could prove that these vacuum diagrams have the effect of renormalizing the projection operators, as in Chapter 5. Armed with this proof, one would be able to ignore the vacuum diagrams, and simply replace $\langle P_o \rangle$ and $\langle P_1 \rangle$ in the Feynman rules by $\langle P_o \rangle_R$ and $\langle P_1 \rangle_R$. The perturbational calculation of $\mathcal{S}_R$ would then be an explicit function of two unknowns: $\langle P_o \rangle_R$ and $\langle P_1 \rangle_R$. Using the sum rules (eqs. (6.41a) and (6.41b)), one would then be able to self-consistently solve for $\langle P_o \rangle_R$ and $\langle P_1 \rangle_R$.

Let us examine the perturbation expansions for $\langle P_o \rangle_R$ and $\langle P_1 \rangle_R$. Following a procedure analogous to that used to obtain the perturbation expansion of $\mathcal{S}_R$ in eqs. (6.110) one finds:

$$\boxed{\begin{aligned} \langle P_o \rangle_R = \frac{1}{D_V} \sum_{VWC} \int d\{t'\}\, F^{\{\alpha'\}}_{VWC_{\{m,\bar{m}\}}} \left[S_{\varepsilon_f}, C_o ; \{t'\} \right] \times \\ \times \sum_{\substack{WC+ \\ WC-}} \int d\{\tau\} d\{\tau'\}\, V_{WC+_{\{m',\bar{m}'\}}} \left[S_{\varepsilon_f}, C_o ; \{\tau\} \right] V_{WC-_{\{m'',\bar{m}''\}}} \left[S_{\varepsilon_f}, C_o ; \{\tau'\} \right] \times \\ \times \prod_{\{j,k,\ell\}_{VWC\pm}} \delta_{m_j' \bar{m}_j'}\, \delta_{m_k \bar{m}_k}\, \delta_{m_\ell'' \bar{m}_\ell''}\, \langle P_o \rangle \,, \end{aligned}} \tag{6.111a}$$

$$\boxed{\begin{aligned} \langle P_1\rangle_R = \frac{1}{D_v}\sum_{vwc}\int d\{t'\}\, F^{\{\alpha'\}}_{vwc_{\{m,\bar{m}\}}}\left[S_{\varepsilon_f}, C_o\,;\{t'\}\right] \times \\ \times \sum_{\substack{wc+\\ wc-}}\int d\{\tau\}d\{\tau'\}\, V_{wc+_{\{m',\bar{m}'\}}}\left[S_{\varepsilon_f}, C_o\,;\{\tau\}\right] V_{wc-_{\{m'',\bar{m}''\}}}\left[S_{\varepsilon_f}, C_o\,;\{\tau'\}\right] \times \\ \times\, W^{\{\alpha'\}}_{vwc_{\{m,\bar{m}\}}}(\{t'\})\, W_{wc+_{\{m',\bar{m}'\}}}(\{\tau\})\, W_{wc-_{\{m'',\bar{m}''\}}}(\{\tau'\})\,\frac{\langle P_1\rangle}{N^3}, \end{aligned}} \tag{6.111b}$$

where D_v is given by eq. (6.110b).

Compare these two equations to eqs. (6.110) for $\mathcal{S}_R$. Before we can pull out $\langle P_o\rangle_R$ and $\langle P_1\rangle_R$ from $\mathcal{S}_R$, we must separate the vacuum diagrams F_{vwc} from F_{wc}. These vacuum diagrams are the "regular" vacuum diagrams, ***not*** the special ones which are at $\mathcal{R}e\, t = \pm\infty$. These "regular" vacuum diagrams are considered in the next section.

6.6 "REGULAR" VACUUM DIAGRAMS

6.6.1 DO THE REGULAR VACUUM DIAGRAMS CONTRIBUTE?

It has been stated [63, 64] that the regular vacuum diagrams in thermo field dynamics are zero. This is no longer true in the quantum algebra case, as evidenced in the $\langle P_1\rangle$ sector, where the vacuum diagrams are all strung-up with wiggle lines connecting to the main diagram.

It is instructive to consider the SU(N) rules. It is easy to show, using the trace rules for λ-matrices in appendix A, that diagrams such as those illustrated in FIG. 6.20 are equal to zero. But the diagram illustrated in FIG. 6.21 does not vanish. Therefore we have a simple example of a regular vacuum diagram which, in the $\langle P_1\rangle$ sector, is no longer a vacuum diagram, and is non-zero.

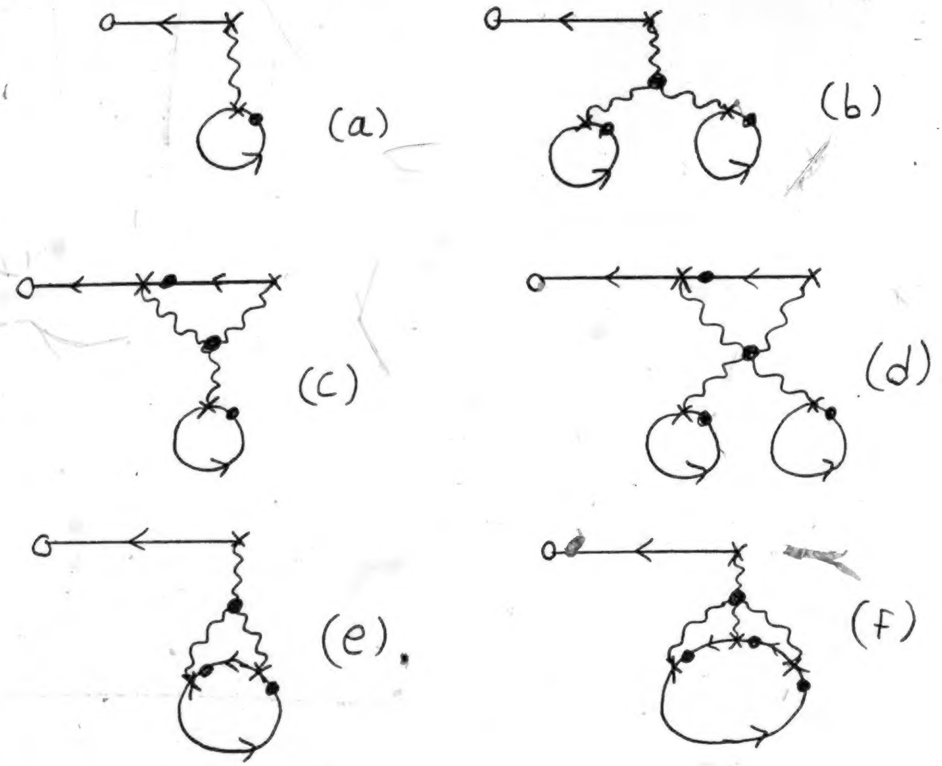

FIG. 6.20

Regular Vacuum Diagrams Which Vanish Using the SU(N) Trace Rules

(a), (b), (c), and (d) all vanish because $\mathrm{Tr}(\lambda_j) = 0$. (e) and (f) may also be shown to vanish by using the SU(N) Feynman rules of sect. 4.9.3.7 along with the identities in Appendix A.

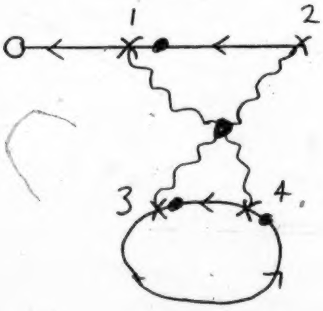

FIG. 6.21

A Regular Vacuum Diagram Which Does Not Vanish

This diagram does not vanish when using the SU(N) rules. Not only that, but this "vacuum diagram" cannot be disconnected. We thus have an example of a regular vacuum diagram which is no longer a vacuum diagram in the $\langle P_1 \rangle$ sector.

6.6.2 DISCONNECTION OF THE REGULAR VACUUM DIAGRAMS

6.6.2.1 An Attempt, Using the Non–SU(N) Rules

Having established that the regular vacuum diagrams contribute, the next step is to try to disconnect them. It is not as easy as it was for the vacuum diagrams at $\mathcal{R}e\, t = \pm\infty$ (if one may call this "easy"), because they share the same time domain as the main diagrams. That is, the θ–functions in the decomposition of the X–operator T–products are all mixed together. (See eq. (6.100).) The approach of section 6.5.2.5 will not work.

To illustrate, let us consider the diagram of FIG. 6.21. We will start by assuming $\gamma_1 = \gamma_2 = \gamma_3 = \gamma_4 = 1$, and $t_1 > t_3 > t_4 > t_2$. Using the non–SU(N) rules and the direct X–reduction of eq. (6.100), one finds that the spin delta functions are $\delta_{m_1m'_3}\,\delta_{m_3m'_4}\,\delta_{m_4m'_2}\,\delta_{m_2m'_1}$. This is multiplied by $\delta_{m_3m'_4}\,\delta_{m_4m'_3}$ from the vacuum loop. An illustration of this is given in FIG. 6.22(a), where S_{ε_f} lines are used to carry the spin. This is in accordance with the non–SU(N) Feynman rules for wiggle–line decomposition, given in sections 4.9.2.7 to 4.9.2.9. For sake of clarity, the diagram has been point–split, in accordance with sect. 6.4.3.

Now, it is obvious that $(\delta_{m_1m'_3}\,\delta_{m_3m'_4}\,\delta_{m_4m'_2}\,\delta_{m_2m'_1})\,\delta_{m_3m'_4}\,\delta_{m_4m'_3} =$ $= (\delta_{m_1m'_2}\,\delta_{m_2m'_1}\,\delta_{m_3m'_4}\,\delta_{m_4m'_3})\,\delta_{m_4m'_2}$. The expression in parenthesis is the set of δ–functions which would come from splitting the 4–wiggle into two 2–wiggles. If we drop the final $\delta_{m_4m'_2}$, there is an extra spin trace induced, so one must multiply the resulting diagram by $1/N$. This is shown in FIG. 6.22(b), and is reminiscent of the vacuum disconnections illustrated in FIGS. 6.14 – 6.19. Therefore, it appears that the 4–wiggle can be split into two 2–wiggles multiplied by $1/N$.

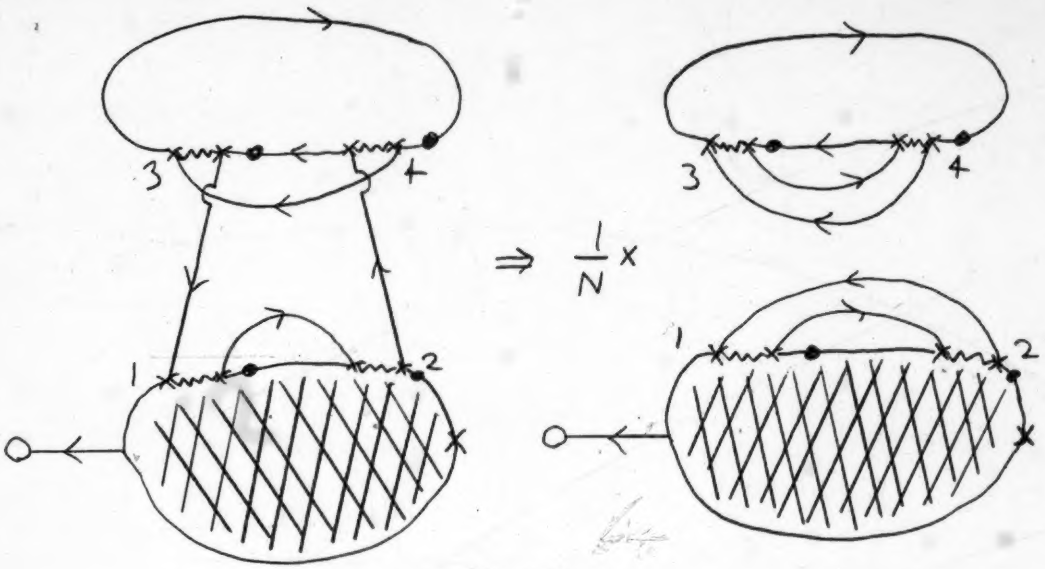

FIG. 6.22

Splitting the 4–Wiggle Into Two 2–Wiggles When $t_1 > t_3 > t_4 > t_2$ and $\gamma_1 = \gamma_2 = \gamma_3 = \gamma_4 = 1$

An attempt is made to disconnect the regular vacuum diagram from the main diagram. This is done using non–SU(N) rules and is illustrated with the tool of point–splitting (see sect. 6.4.3). It is valid only for this particular time ordering.

Of course, this is valid only for the given time ordering. Now let's see what happens for $\gamma_1 = \gamma_2 = \gamma_3 = \gamma_4 = 1$, and $t_1 > t_3 > t_2 > t_4$. Using the non–SU(N) rules and the direct X–reduction of eq. (6.100), one finds that the spin delta functions are $\delta_{m_1m_3'}\,\delta_{m_3m_2'}\,\delta_{m_2m_4'}\,\delta_{m_4m_1'}$. As before, ~~this is~~ multiplied by $\delta_{m_3m_4'}\,\delta_{m_4m_3'}$ from the vacuum loop. An illustration of this is given in FIG. 6.23(a).

Now, it is obvious that $(\delta_{m_1m_3'}\,\delta_{m_3m_2'}\,\delta_{m_2m_4'}\,\delta_{m_4m_1'})\,\delta_{m_3m_4'}\,\delta_{m_4m_3'} =$ $= (\delta_{m_1m_1'}\,\delta_{m_2m_2'}\,\delta_{m_3m_4'}\,\delta_{m_4m_3'})\,\delta_{m_1m_3'}\,\delta_{m_2m_4'}$. The expression in brackets is the set of δ–functions which would come from completely disconnecting the 4–wiggle from the main diagram, leaving only a 2–wiggle on the vacuum diagram. If we drop the final $\delta_{m_1m_3'}\,\delta_{m_2m_4'}$, there are two extra spin traces induced, so one must multiply the resulting diagram by $1/N^2$. This is shown in FIG. 6.23(b).

Sadly, this approach has failed. The wiggle diagrams cannot be consistently split, because the result depends upon the time ordering. If we are to disconnect the regular vacuum diagrams, another method must be found.

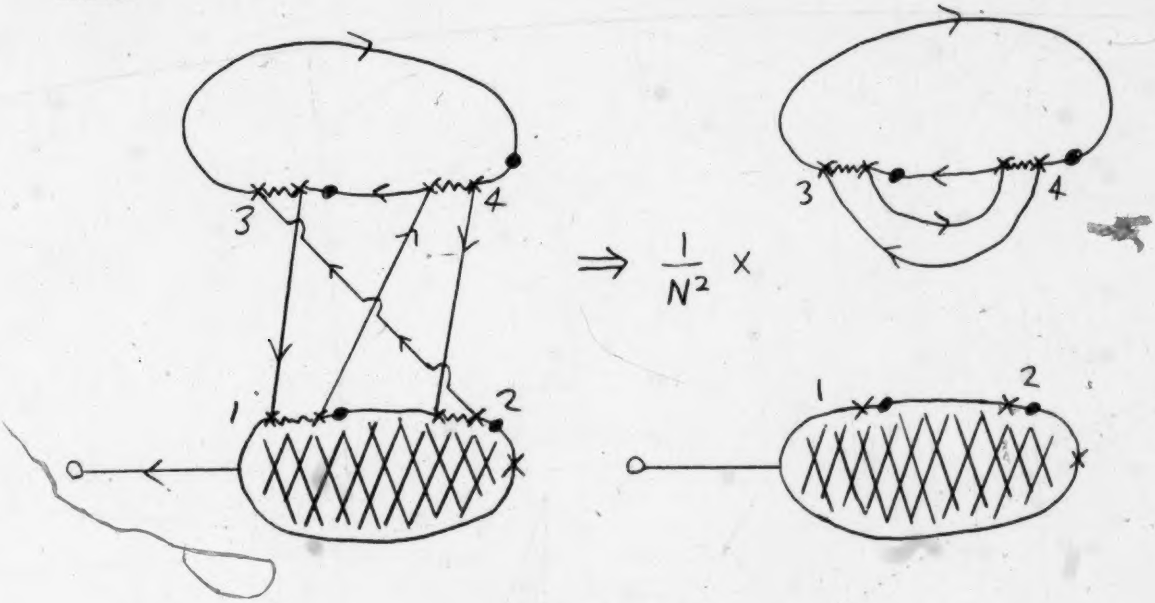

FIG. 6.23

Reducing the 4–Wiggle When $t_1 > t_3 > t_2 > t_4$ and $\gamma_1 = \gamma_2 = \gamma_3 = \gamma_4 = 1$

An attempt is made to disconnect the regular vacuum diagram from the main diagram.. This is done using non–SU(N) rules and is illustrated with the tool of point–splitting (see sect. 6.4.3). It is valid only for this particular time ordering, and differs from FIG. 6.22 which uses a different time ordering.

6.6.2.2 Partial Disconnection Using the Broken–Chain SU(N) Rules

The broken–chain SU(N) rules are very useful (see sect. 4.9.3), because the non–spontaneous cross vertices are not all connected together via wiggle diagrams (see rule 12 of sect. 4.9.3.4). Thus, some of the regular vacuum diagrams are naturally disconnected. Others will still be connected to the main diagram. Let us test the value of this "partial" disconnection by considering the diagrammatics of $\langle P_1\rangle_{\mathfrak{R}}$ and $\mathcal{A}_{\mathfrak{R}}$.

Firstly, consider $\langle P_1\rangle_{\mathfrak{R}}$, as given by eq. (6.111b). The vacuum diagrams at $\mathcal{R}e\, t = \pm\infty$ are already taken care of. Let us therefore consider only F_{vwc} the regular vacuum diagrams, and W_{vwc} the X–operator T–product which connects to these vacuum diagrams. These are diagrammatically decomposed in FIG. 6.24.

$$\sum_{wc}\int d\{t'\}\, F_{vwc}(\{t'\})\,\frac{1}{N}\,W_{vwc}(\{t'\}) = 1 + \dots$$

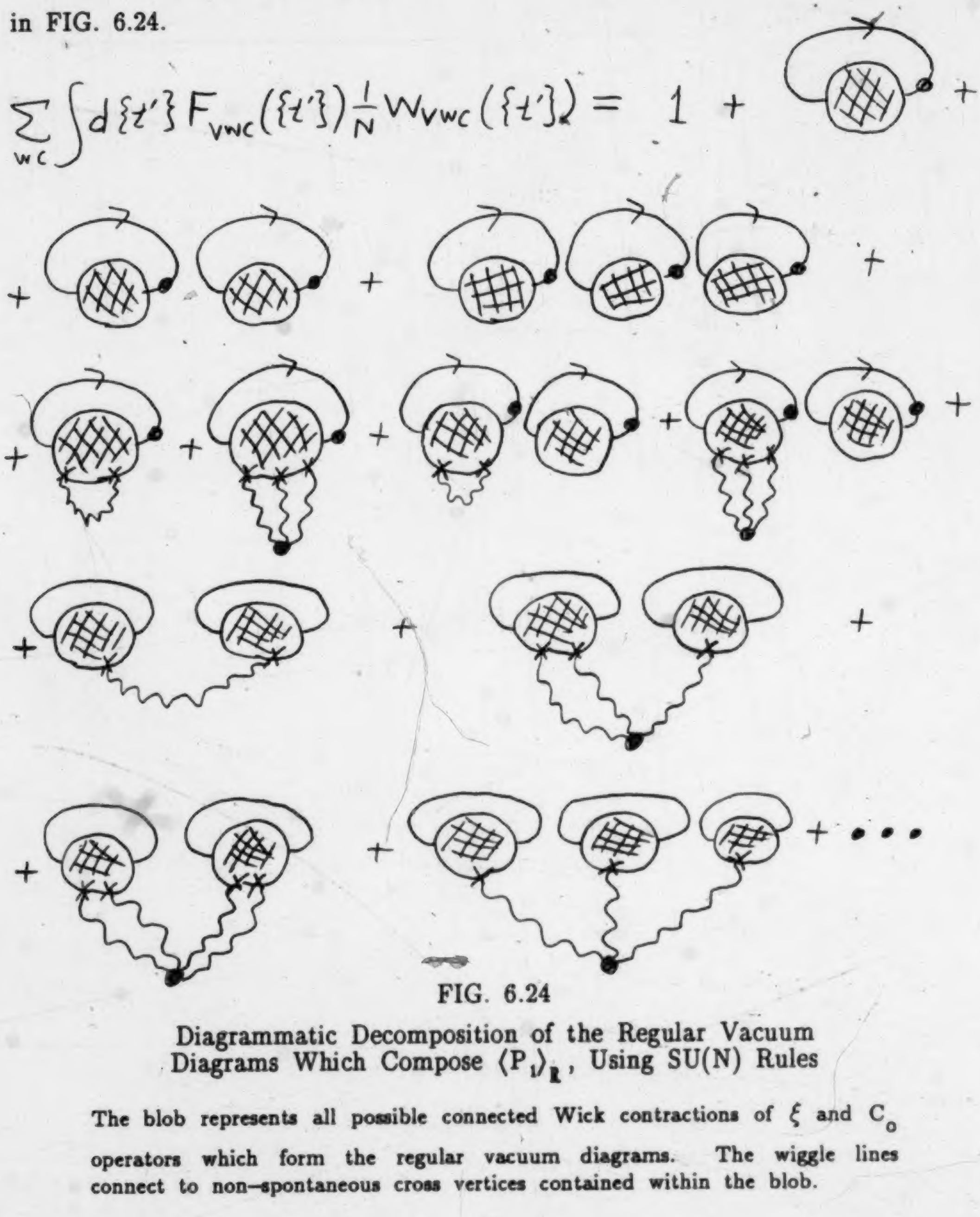

FIG. 6.24

Diagrammatic Decomposition of the Regular Vacuum Diagrams Which Compose $\langle P_1\rangle_{\mathfrak{R}}$, Using SU(N) Rules

The blob represents all possible connected Wick contractions of ξ and C_0 operators which form the regular vacuum diagrams. The wiggle lines connect to non–spontaneous cross vertices contained within the blob.

Now let us consider $\mathscr{A}_R$, as given by eq. (6.110a). It is obvious that one may write:

$$F_{wc}(\{t'\}) = F_{cwc}(\{t_c'\})\, F_{vwc}(\{t_v'\}) \,, \tag{6.112}$$

where F_{cwc} are the connected Wick contractions of ξ and C_o, ie. the ones which connect to the external lines, and F_{vwc} are the vacuum Wick contractions of ξ and C_o. ($\{t_c'\}$ are the time vertices of the connected diagrams and $\{t_v'\}$ are the time vertices of the vacuum diagrams.) What is not so obvious is what happens with W_{wc}, the X–operator T–product. Let us diagrammatically expand $\int d\{t_c'\}d\{t_v'\}\, F_{cwc}(\{t_c'\})\, F_{vwc}(\{t_v'\}) \times$ $\times\, W_{wc}(\{t_c'\},\{t_v'\})$. The results are shown in FIG. 6.25.

By visually inspecting FIG. 6.25, one can speculate that the diagrams of FIG. 6.24 factorize out. Such a proposal is illustrated in FIG. 6.26.

$$\sum_{wc}{}' \int d\{t_c'\}\, d\{t_v'\}\, F_{cwc}(\{t_c'\})\, F_{vwc}(\{t_v'\})\, \frac{1}{N} W_{wc}(\{t_c'\},\{t_v'\}) =$$

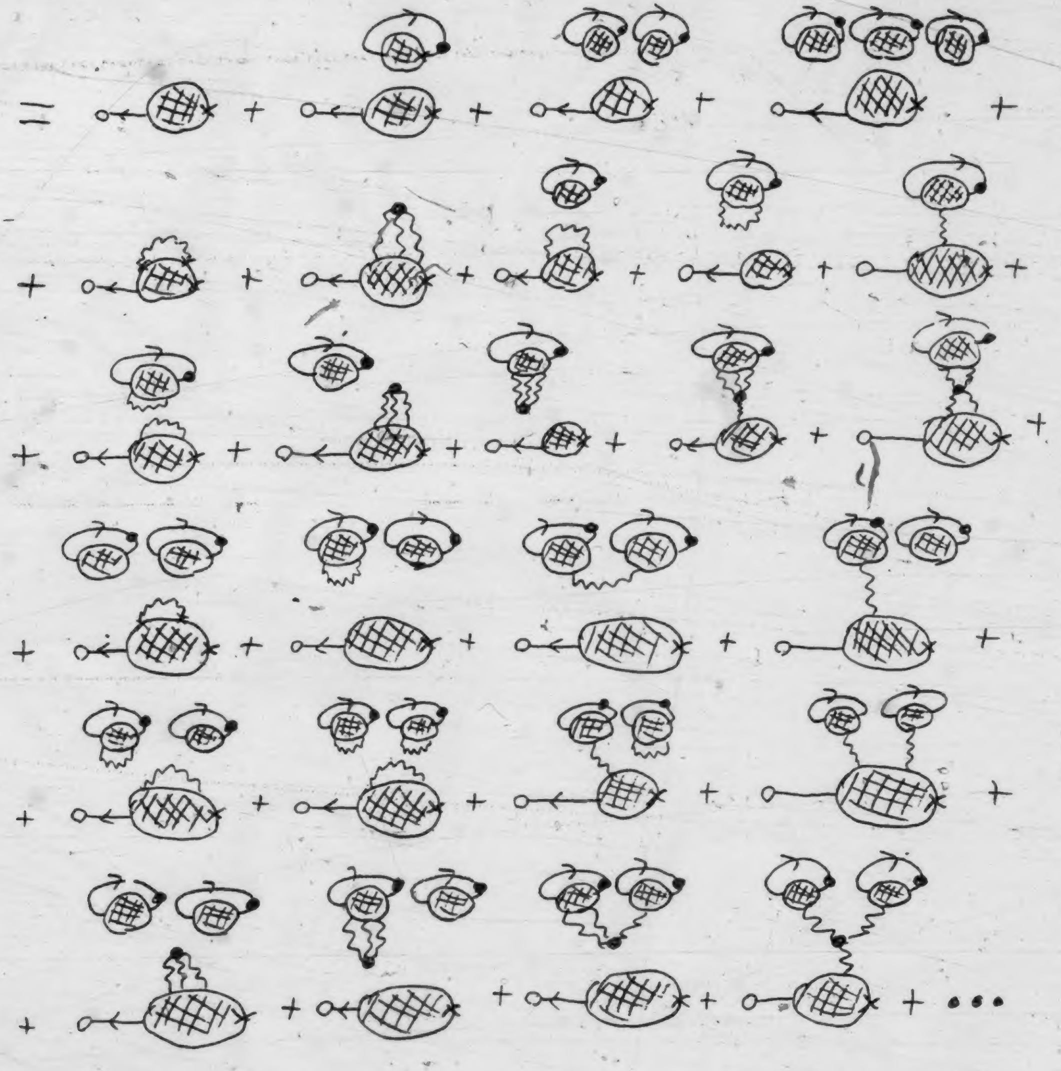

FIG. 6.25

Decomposition of $\mathcal{S}_R$ in the $\langle P_1 \rangle$ Sector, Using SU(N) Rules and Ignoring Vacuum Diagrams at $\mathcal{R}e\, t = \pm\infty$.

The blobs represent all possible connected Wick contractions of ξ and C_0 operators, which form the regular vacuum diagrams and the externally connected diagrams. The wiggle lines connect to non-spontaneous cross vertices contained within the blobs, using the SU(N) rules.

$$\sum_{wc}\int d\{t_c'\}\,d\{t_v'\}\,F_{cwc}(\{t_c'\})\,F_{vwc}(\{t_v'\})\,\frac{1}{N}\,W_{wc}(\{t_c'\},\{t_v'\}) =$$

$$\overset{?}{=}\sum_{vwc}\int d\{t_v'\}\,F_{vwc}\{t_v'\}\times\frac{1}{N}\,W_{vwc}(\{t_v'\})\times$$

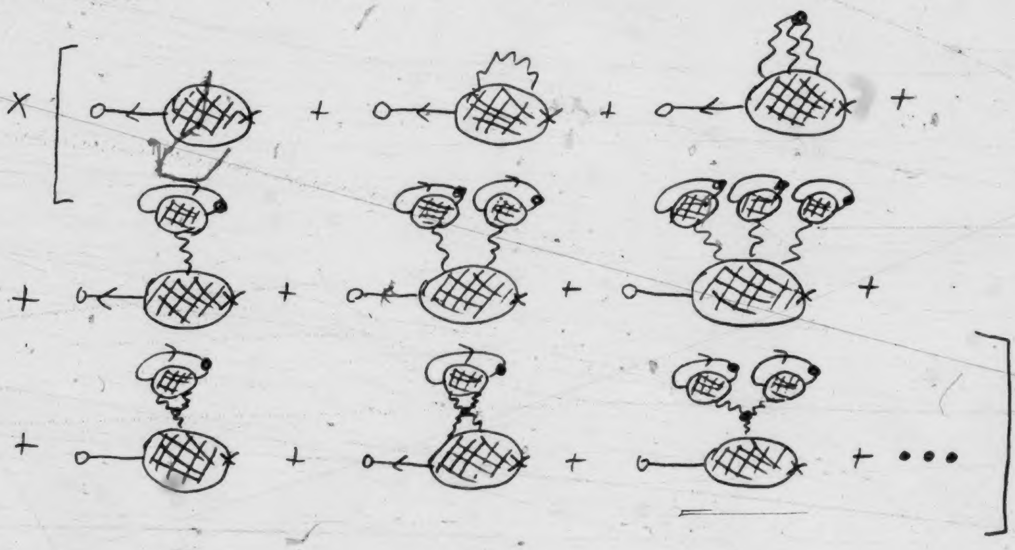

$$\equiv\sum_{vwc}\int d\{t_v'\}\,F_{vwc}(\{t_v'\})\,\frac{1}{N}\,W_{vwc}(\{t_v'\})\times$$

$$\times\sum_{wc}\int d\{t_c'\}\,d\{t_v''\}\,F_{cwc}(\{t_c'\})\,F_{vwc}(\{t_v''\})\,\Xi_{wc}(\{t_c'\},\{t_v''\})$$

FIG. 6.26

An Attempt at Factorizing the Diagrams Which Renormalize $\langle P_1\rangle$

It appears that $\int F_{vwc} W_{vwc}$ may factorize out from FIG. 6.25. This diagram illustrates the proposed factorization. Ξ_{wc} represents only those SU(N) wiggle diagrams which connect regular vacuum diagrams to the main diagram. Many of these are zero, but some are non–zero (eg. FIG. 6.21).

This factorization depends, of course, on the series being infinite. I must point out that this is not a mathematically rigorous proof; it is merely a speculation which seems reasonable. Let us take it as a working assumption and go with it:

$$\sum_{wc}\int d\{t_c'\}\, d\{t_v'\}\, F_{cwc}(\{t_c'\})\, F_{vwc}(\{t_v'\})\, \frac{1}{N}\, W_{wc}(\{t_c'\},\{t_v'\}) =$$

$$= \sum_{vwc}\int d\{t_v'\}\, F_{vwc}(\{t_v'\})\, \frac{1}{N}\, W_{vwc}(\{t_v'\}) \times$$

$$\times \sum_{wc}\int d\{t_c'\}\, d\{t_v''\}\, F_{cwc}(\{t_c'\})\, F_{vwc}(\{t_v''\})\, \Xi_{wc}(\{t_c'\},\{t_v''\}) \tag{6.113}$$

Here Ξ_{wc} represents only those SU(N) wiggle diagrams which connect regular vacuum diagrams to the main diagrams, when these vacuum diagrams exist. They cannot be split apart. Ξ_{wc} also includes the usual wiggle diagrams when no regular vacuum diagrams are present (as illustrated in FIG. 6.26).

We are now committed to the SU(N) rules, because the non–SU(N) wiggle diagrams may be split apart by going to the SU(N) rules. Therefore, we cannot use a non–SU(N) wiggle in Ξ_{wc} ; this would imply that Ξ_{wc} could be split apart.

6.7 THE RENORMALIZED PERTURBATION EXPANSION FOR $\mathscr{L}_R$

6.7.1 $\mathscr{L}_R$ IN TERMS OF THE RENORMALIZED PROJECTION OPERATORS

Using eqs. (6.110) for $\mathscr{L}_R$, with eqs. (6.111) for $\langle P_0\rangle_R$ and $\langle P_1\rangle_R$, and using eqs. (6.112) and (6.113) for partially disconnecting the regular vacuum diagrams, one finds:

$$\boxed{\begin{aligned} &\mathscr{S}^{a_2a_1}_{\mathbf{R}m_2m_1}(t_2-t_1) = \\ &= \sum_{cwc} \int d\{t_c'\}\, F^{\alpha_2\alpha_1}_{cwc_{m_2m_1\{m',\bar{m}'\}}}\left[S_{\varepsilon_f}, C_o\, ; t_2-t_1, \{t_c'\}\right] \prod_{\{k\}_{cwc}} \delta_{m_k'\bar{m}_k'}\, \langle P_o\rangle_{\mathbf{R}} + \\ &\quad + \sum_{wc} \int d\{t_c'\} d\{t_v''\}\, F^{\alpha_2\alpha_1\{\alpha'\}}_{cwc_{m_2m_1\{m',\bar{m}'\}}}\left[S_{\varepsilon_f}, C_o\, ; t_2-t_1, \{t_c'\}\right] \times \\ &\times F^{\{\alpha''\}}_{vwc_{\{m'',\bar{m}''\}}}\left[S_{\varepsilon_f}, C_o\, ; \{t_v''\}\right] \Xi^{\{\alpha',\alpha''\}}_{wc_{\{m',\bar{m}',m'',\bar{m}''\}}}\left[\{t_c'\},\{t_v''\}\right] \langle P_1\rangle_{\mathbf{R}}\, . \end{aligned}} \tag{6.114}$$

Eureka! The renormalized ξ–propagator has now been re–expressed in terms of the renormalized projection operators. Let us define the following:

$$\begin{aligned} &\mathscr{S}^{a_2a_1}_{\mathbf{R}m_2m_1}(t_2-t_1\, ; \ell=0) \equiv \\ &\equiv \sum_{cwc} \int d\{t_c'\}\, F^{\alpha_2\alpha_1}_{cwc_{m_2m_1\{m',\bar{m}'\}}}\left[S_{\varepsilon_f}, C_o\, ; t_2-t_1, \{t_c'\}\right] \prod_{\{k\}_{cwc}} \delta_{m_k'\bar{m}_k'}\ , \end{aligned} \tag{6.115a}$$

$$\begin{aligned} &\mathscr{S}^{a_2a_1}_{\mathbf{R}m_2m_1}(t_2-t_1\, ; \ell=1) \equiv \\ &\equiv \sum_{wc} \int d\{t_c'\} d\{t_v''\}\, F^{\alpha_2\alpha_1\{\alpha'\}}_{cwc_{m_2m_1\{m',\bar{m}'\}}}\left[S_{\varepsilon_f}, C_o\, ; t_2-t_1, \{t_c'\}\right] \times \\ &\times F^{\{\alpha''\}}_{vwc_{\{m'',\bar{m}''\}}}\left[S_{\varepsilon_f}, C_o\, ; \{t_v''\}\right] \Xi^{\{\alpha',\alpha''\}}_{wc_{\{m',\bar{m}',m'',\bar{m}''\}}}\left[\{t_c'\},\{t_v''\}\right] . \end{aligned} \tag{6.115b}$$

Then eq. (6.114) may be simply expressed as:

$$\boxed{\mathscr{S}^{a_2a_1}_{\mathbf{R}m_2m_1}(t_2-t_1) = \sum_{\ell=0}^{1} \mathscr{S}^{a_2a_1}_{\mathbf{R}m_2m_1}(t_2-t_1\, ; \ell)\, \langle P_\ell\rangle_{\mathbf{R}}} \tag{6.116}$$

6.7.2 THE RENORMALIZED FEYNMAN RULES

The renormalized Feynman rules are essentially the same as those presented in section 6.4, with the following modifications:

- Replace all $\langle P_o\rangle$'s by $\langle P_o\rangle_R$ and all $\langle P_1\rangle$'s by $\langle P_1\rangle_R$.
- Ignore all vacuum diagrams in the $\langle P_o\rangle$ sector.
- Ignore all vacuum diagrams in the $\langle P_1\rangle$ sector, with the exception of vacuum diagrams connected to the main diagram via an unbroken SU(N) wiggle chain. These are illustrated in FIG. 6.26.

6.7.3 THE SELF–CONSISTENT CALCULATION

The Feynman rules may be used to obtain $\mathscr{S}_R$ in terms of two unknowns: $\langle P_o\rangle_R$ and $\langle P_1\rangle_R$. $\langle P_o\rangle_R$ and $\langle P_1\rangle_R$ may then be self–consistently evaluated via the particle/hole sum rule of eqs. (6.41). One obtains:

$$\langle P_1\rangle_R = N\int d\kappa\, f_F(\kappa-\mu)\left[\sigma^R_{\mathscr{S}}(\kappa;\ell=0)\,\langle P_o\rangle_R + \sigma^R_{\mathscr{S}}(\kappa;\ell=1)\,\langle P_1\rangle_R\right], \tag{6.117a}$$

$$\langle P_o\rangle_R = \int d\kappa\left[1-f_F(\kappa-\mu)\right]\left[\sigma^R_{\mathscr{S}}(\kappa;\ell=0)\,\langle P_o\rangle_R + \sigma^R_{\mathscr{S}}(\kappa;\ell=1)\,\langle P_1\rangle_R\right]. \tag{6.117b}$$

Using eq. (6.117a) with $P_o + P_1 = 1$, one finds:

$$\boxed{\langle P_1\rangle_R = \frac{N\int d\kappa\; f_F(\kappa-\mu)\,\sigma^R_{\mathscr{S}}(\kappa;\ell=0)}{1 + N\int d\kappa\; f_F(\kappa-\mu)\,[\sigma^R_{\mathscr{S}}(\kappa;\ell=0) - \sigma^R_{\mathscr{S}}(\kappa;\ell=1)]}} \tag{6.118}$$

$$\boxed{\langle P_o\rangle_R = \frac{1 - N\int d\kappa\; f_F(\kappa-\mu)\,\sigma^R_{\mathscr{S}}(\kappa;\ell=1)}{1 + N\int d\kappa\; f_F(\kappa-\mu)\,[\sigma^R_{\mathscr{S}}(\kappa;\ell=0) - \sigma^R_{\mathscr{S}}(\kappa;\ell=1)]}} \tag{6.119}$$

Using eq. (6.117b) gives the following sum rule:

$$\boxed{\frac{1 - N\int d\kappa\ f_F(\text{[illegible]}-\mu)\ \sigma^R_{\mathcal{S}}(\kappa;\ell=1)}{N\int d\kappa\ f_F(\kappa-\mu)\ \sigma^R_{\mathcal{S}}(\kappa;\ell=0)} = \frac{\int d\kappa\ [1-f_F(\kappa-\mu)]\ \sigma^R_{\mathcal{S}}(\kappa;\ell=1)}{1 - \int d\kappa\,[1-f_F(\kappa-\mu)]\ \sigma^R_{\mathcal{S}}(\kappa;\ell=0)}} \tag{6.120}$$

6.8 CONCLUSION

Vacuum diagram effects were found to be incredibly complex in the real Anderson model, because the interaction Hamiltonian no longer commutes with the unperturbed Hamiltonian. A clue as to how these vacuum diagrams may renormalize the expectation values of the projection operators was found by considering the Bethe–Salpeter equations. To actually prove this projection operator renormalization involved very convoluted and subtle reasoning. After much effort, the multiply–connected vacuum diagrams at $\mathcal{R}e\, t = \pm\infty$ were found to disconnect from the main diagrams. The regular finite–t vacuum diagrams were also found to have a contribution. Disconnection of these finite–t diagrams was harder to prove, and it was found that some of these vacuum diagrams actually remain connected to the main diagram, via unbroken SU(N) wiggle chains. Through arguments not entirely rigorous, we managed to factorize the diagrams which renormalize $\langle P_1 \rangle$, yielding a renormalized perturbation expression which could be self–consistently solved for $\langle P_0 \rangle_R$ and $\langle P_1 \rangle_R$. A sum rule was obtained.

A very careful and thorough exposition of thermo field dynamics of a quantum algebra, as applied to the Anderson model, has now been given. Systematic, but incredibly complicated, Feynman rules have been derived. Let us now see if these have any practical use. The results are presented in Chapter 7.

CHAPTER 7
RESULTS

7.1 THE $\langle P_0 \rangle$ SECTOR

7.1.1 THE RENORMALIZED PROPAGATORS, THE SELF-ENERGIES, AND THE STARTING-POINT FUNCTION

Using the Feynman rules of sect. 6.7.2, one may analyze the structure of $\mathcal{S}_R(\omega;\ell=0)$. (This is the Fourier transform of $\mathcal{S}_R(t-t';\ell=0)$, defined in eq. (6.115a).) The results of such an analysis are shown in FIG. 7.1.

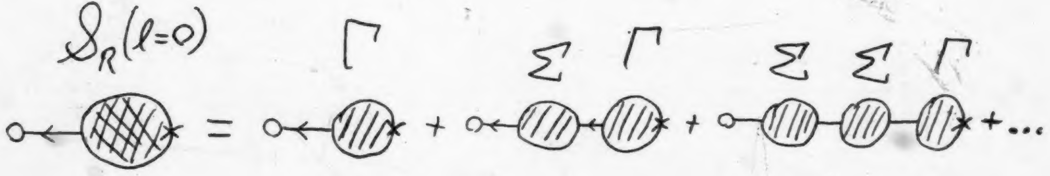

FIG. 7.1

The Self-Energy Expansion of $\mathcal{S}_R$ in the $\langle P_0 \rangle$ Sector

$\mathcal{S}_R(\ell=0)$ may be decomposed as shown. Σ is the self-energy, and Γ is the "starting-point function".

$\Sigma(\omega;\ell=0)$ contains all one-particle-irreducible diagrams not attached to the tail-end of the propagator; let us call this the "self-energy". $\Gamma(\omega;\ell=0)$ contains all 1-particle-irreducible diagrams attached to the tail-end of the propagator; let us call this the "starting-point function".

We define:

$$\mathcal{S}_R(\omega;\ell=0) \equiv S_R(\omega;\ell=0)\,\Gamma(\omega;\ell=0)\ , \tag{7.1a}$$

where

$$\bar{S}_R^{11}(\omega;\ell=0) = \frac{1}{\omega - \epsilon_f - \Sigma^{11}(\omega;\ell=0)}\ . \tag{7.1b}$$

(As before, the bar means that the thermal U_P matrices have been removed.) At lowest order $S_\ell = S_{\epsilon_f}$, where S_{ϵ_f} is the bare ξ–propagator which was defined in eqs. (4.16).

The self–energy and starting–point function may be reduced into two components: tadpole parts (T), which carry no energy, and non–tadpole parts (N), which do carry energy.

$$\bar\Sigma(\omega;\ell=0) = \bar\Sigma_N(\omega;\ell=0) + \Sigma_T(\ell=0) \qquad (7.2a)$$

$$\bar\Gamma(\omega;\ell=0) = \bar\Gamma_N(\omega;\ell=0) + \Gamma_T(\ell=0) \qquad (7.2b)$$

The non–tadpole self–energy may be further decomposed into two pieces:

$$\bar\Sigma_N(\omega;\ell=0) = \bar\Sigma_{ff}(\omega;\ell=0) + \bar\Sigma_{fc}(\omega;\ell=0) \ , \qquad (7.3a)$$

where $\Sigma_{ff}(\omega;\ell=0) =$ 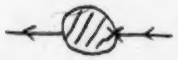 , (7.3b)

and $\Sigma_{fc}(\omega;\ell=0) =$ 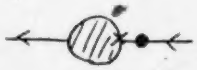 . (7.3c)

That is, Σ_{ff} is composed of all non–tadpole one–particle–irreducible diagrams, in which the external f–line goes straight into a vertex without encountering a dot, and Σ_{fc} is composed of all one–particle–irreducible diagrams, in which the f–line encounters a dot before the vertex (ie. it changes into a c–electron).

A simple diagrammatic analysis shows that Σ_{fc} is related to the starting–point function in the following manner:

$$\bar\Sigma_{fc}(\omega;\ell=0) = \frac{2}{N} V^2 \,\bar\Gamma(\omega;\ell=0)\, \bar C_o(\omega) \ . \qquad (7.4a)$$

Using eq. (6.30) for $\bar C_o(\omega)$, along with the definition (eq. (6.67)) of the interaction strength Δ, one finds:

$$\bar\Sigma^{11}_{fc}(\omega;\ell=0) = -i\frac{2}{N}\Delta\, \bar\Gamma^{11}(\omega;\ell=0) \ . \qquad (7.4b)$$

Note that the C_o used in eq. (7.4a) is the bare (unrenormalized) conduction electron propagator. To use the renormalized conduction electron propagator

$C_{o\boldsymbol{\ell}}$ is unnecessary, and would lead to multiple counting.

Σ_{ff} may be further decomposed into two pieces:

$$\Sigma_{ff}(\omega;\ell=0) = \Sigma_{ff}^{c}(\omega;\ell=0) + \Sigma_{ff}^{nc}(\omega;\ell=0) , \tag{7.5}$$

where Σ_{ff}^{c} is f–connected, and Σ_{ff}^{nc} is non–f–connected; "f–connected" meaning that a pathway through the diagram may be found, in which the f–line does not encounter a dot. The concept of f–connection is illustrated by the examples in FIG. 7.2.

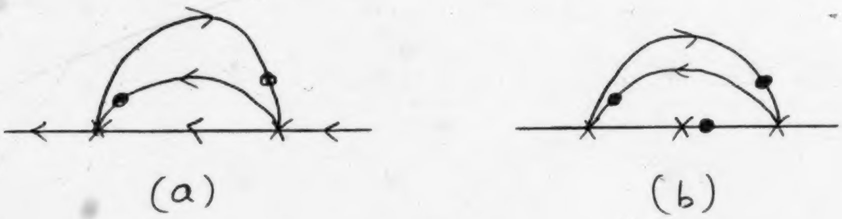

FIG. 7.2

f–Connection

(a) is f–connected, because there exists a pathway through the diagram along which no dots are encountered. (b) is non–f–connected, because such a pathway does not exist.

In terms of the above–defined self–energies, $\bar{S}_{\boldsymbol{\ell}}$ becomes:

$$\bar{S}_{\boldsymbol{\ell}}^{11}(\omega;\ell=0) =$$
$$= \left\{\omega - \varepsilon_f - \Sigma_T(\ell=0) - \bar{\Sigma}_{ff}^{11}(\omega;\ell=0) + i\frac{2}{N}\Delta\left[\Gamma_T(\ell=0) + \bar{\Gamma}_N^{11}(\omega;\ell=0)\right]\right\}^{-1} . \tag{7.6}$$

We may also define an f–connected propagator $S_{\boldsymbol{\ell}}^{C}$, as follows:

$$\bar{S}_{\boldsymbol{\ell}}^{C\,11}(\omega;\ell=0) \equiv \frac{1}{\omega - \varepsilon_f - \Sigma_T(\ell=0) - \Sigma_{ff}^{C\,11}(\omega;\ell=0)} . \tag{7.7}$$

It is possible to travel through this entire propagator on f–lines without once encountering a dot. This is a useful propagator, because connected f–loops are not allowed in the $\langle P_o\rangle$ sector. A loop formed from $S_{\boldsymbol{\ell}}$ contains parts which are disallowed; these illegal parts may be subtracted off by using a loop formed from S_R^C.

Another useful propagator is $\dot{S}_R$, defined as follows:

$$\frac{2}{N}\Delta\,\dot{S}_R(\omega;\ell=0) \equiv \frac{2}{N}V^2\,C_o(\omega)\,S_R(\omega;\ell=0) = -i\frac{2}{N}\Delta\,S_R(\omega;\ell=0)\ . \tag{7.8}$$

These renormalized propagators are represented diagrammatically in FIG. 7.3.

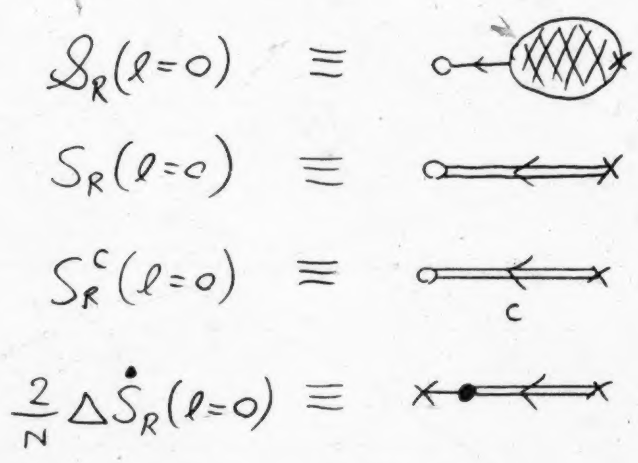
$\mathcal{S}_R(\ell=0) \equiv$
$S_R(\ell=0) \equiv$
$S_R^C(\ell=0) \equiv$
C
$\frac{2}{N}\Delta\dot{S}_R(\ell=0) \equiv$

FIG. 7.3
Diagrammatic Representation of the Renormalized Propagators

7.1.2 DIAGRAMMATICS OF THE ⟨P$_0$⟩ SECTOR TO THREE-LOOP ORDER

Let us consider the diagrammatics of the ⟨P$_o$⟩ sector. For the tadpole diagrams, we may write down an expression valid to all orders of perturbation theory. For the energy-dependent diagrams, we will carry this process only to 3-loop order.

Consider first the tadpole diagrams. They may be expressed as follows:

$\Sigma_T(\ell=0) =$ 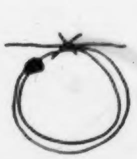 , (7.9)

$\Gamma_T(\ell=0) =$ 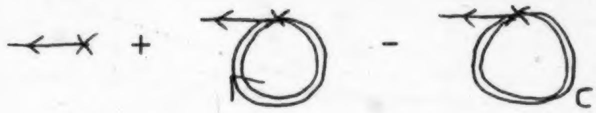

. (7.10)

Note that the f–connected loops had to be subtracted in eq. (7.10) because they are not allowed by the Feynman rules.

The expansion of Σ_{ff} to 3–loop order is given as follows:

$\Sigma_{ff}(\omega;\ell=0) =$ 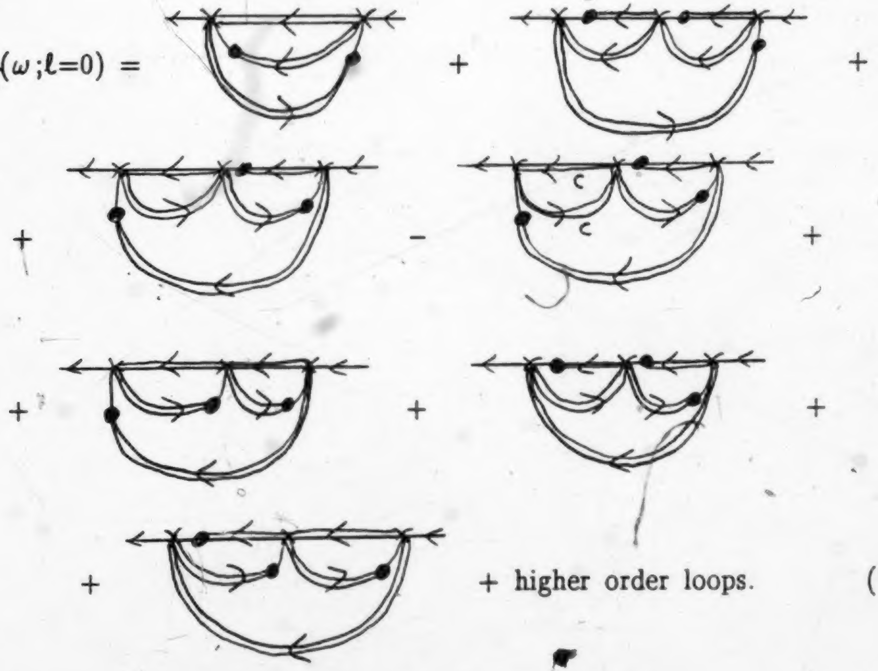

+ higher order loops. (7.11)

The expansion of Γ_N to 3–loop order is given as follows:

$\Gamma_N(\omega;\ell=0) =$ 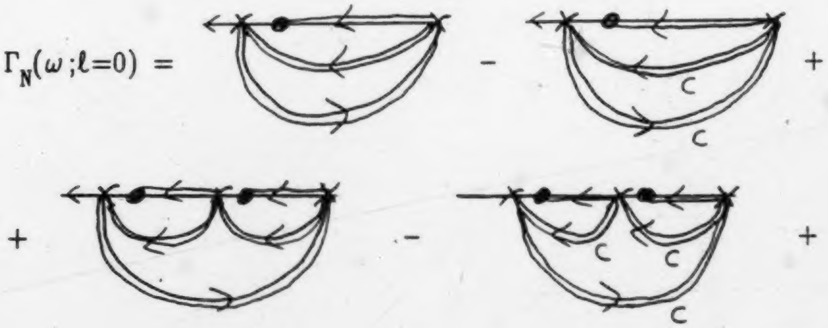

+ 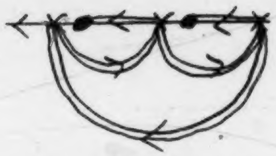 − 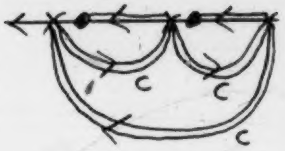

+

+ 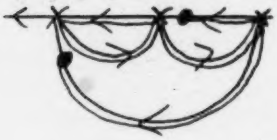 − 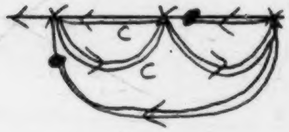

+

+ 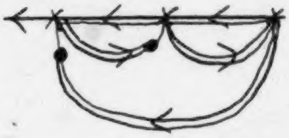 − 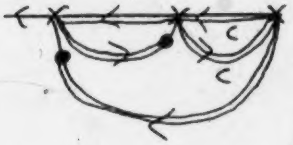

+

+ 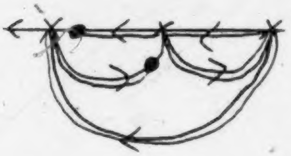 − 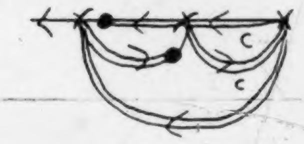

+

+ higher order loops. (7.12)

The expansion of Σ^{c}_{ff} to 3–loop order is given as follows:

$\Sigma^{c}_{ff}(\omega;\ell=0) =$ 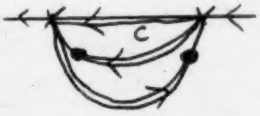

+ 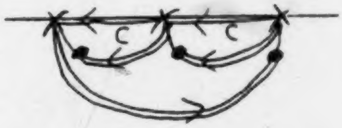

+

+ 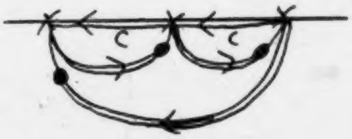

+ 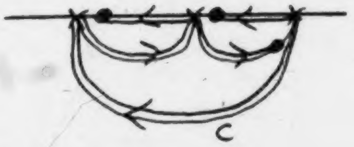

+

+ 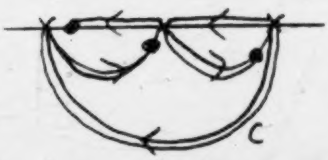

+ higher order loops. (7.13)

Note that the loop expansions presented here are already renormalized. That is, the self–energies, which go into making the renormalized propagators, are expressed in terms of integrals involving the renormalized propagators themselves. This means that the renormalized parameters must be solved for self-consistently. Such a self-consistent calculation is necessary, because we are looking for non-perturbative effects which show up at infinite order. A simple perturbation expansion in terms of bare propagators is bound to fail, as evidenced by the $\ln T$ divergence in the traditional Kondo calculations.

Unfortunately, to solve self-consistently to 3-loop order, or even to 2-loop order, is incredibly complicated and impractical. These 2-loop and 3-loop diagrams are presented only for illustrative purposes. They show that there is a systematic methodology for calculating self-consistently to higher orders, if one had the desire and resources to do so.

Let us stick to a 1-loop self-consistent calculation; primarily because it is easy to do, and secondly because the higher loop order is also a higher order in 1/N. (In keeping with other methods presented in chapter 1, we consider N to be large.)

7.1.3 THE ONE-LOOP SELF-CONSISTENT CALCULATION

General expressions for Σ_T and Γ_T are easy to obtain. Using the Feynman rules on eqs. (7.9) and (7.10) results in the following expressions:

$$\Sigma_T(\ell=0) = 2\left[\frac{N-1}{N}\right] V^2 \sum_\gamma \varepsilon^\gamma i\int\frac{d\omega}{2\pi}\left[S_\ell(\omega;\ell=0)\, C_o(\omega)\right]^{\gamma\gamma} \tag{7.14}$$

$$\Gamma_T(\ell=0) = 1 + (N-1)\sum_\gamma \varepsilon^\gamma i\int\frac{d\omega}{2\pi}\left[S_\ell(\omega;\ell=0) - S^c_\ell(\omega;\ell=0)\right]^{\gamma\gamma} . \tag{7.15}$$

If we use the approximation of eq. (6.30) for $C_o(\omega)$, one finds that the integral in eq. (7.14) diverges. Thus eq. (6.31), which includes the band cutoffs, becomes necessary. Performing the integrals in eq. (7.14), and using the band cutoffs on the divergent parts, one finds:

$$\boxed{\begin{aligned}\Sigma_T(\ell=0) = 2\left[\frac{N-1}{N}\right]\frac{\Delta}{\pi}\Bigg[\ln\left[\frac{\beta(D_- + \mu)}{2\pi}\right] + \\ - \mathcal{R}e\int d\omega\, \sigma_S^{R}(\omega;\ell=0)\,\psi\left[\frac{1}{2}-\frac{i\beta}{2\pi}(\omega-\mu)\right]\Bigg]\end{aligned}}\ ,$$

(7.16)

where σ_S^R is the spectral function of S_R.

Eq. (7.15) is easier to evaluate, because there are no divergences to worry about. Performing the integrals, one finds:

$$\boxed{\Gamma_T(\ell=0) = 1 - (N-1)\int d\omega\, f_F(\omega-\mu)\left[\sigma_S^R(\omega;\ell=0) - \sigma_S^C(\omega;\ell=0)\right]}\ ,$$

(7.17)

where σ_S^C is the spectral function of S_R^C.

Equations (7.16) and (7.17) are general equations for Σ_T and Γ_T, which are ***exact** to all orders of perturbation theory,* assuming we know σ_S^R and σ_S^C. Of course, we don't know σ_S^R and σ_S^C. Let us therefore do a 1–loop self–consistent calculation.

To 1–loop order, the propagators given in eqs. (7.1), (7.6), and (7.7) become:

$$\mathcal{S}_R(\omega;\ell=0) = S_R(\omega;\ell=0)\,\Gamma_T(\ell=0)\ , \tag{7.18a}$$

$$\bar{S}_R^{11}(\omega;\ell=0) = \frac{1}{\omega - \tilde{\varepsilon}_f(\ell=0) + i\tilde{\Delta}(\ell=0)}\ , \tag{7.18b}$$

$$\bar{S}_R^{C11}(\omega;\ell=0) = \frac{1}{\omega - \tilde{\varepsilon}_f(\ell=0) + i\delta}\ , \tag{7.18c}$$

where
$$\tilde{\varepsilon}_f(\ell=0) \equiv \varepsilon_f + \Sigma_T(\ell=0)\ , \tag{7.18d}$$

and
$$\tilde{\Delta}(\ell=0) \equiv \frac{2}{N}\Delta\,\Gamma_T(\ell=0)\ . \tag{7.18e}$$

Using eqs. (7.18) in eqs. (7.16) and (7.17), one obtains the following coupled self–consistent equations for $\tilde{\varepsilon}_f$ and Γ_T:

$$\boxed{\begin{aligned}\tilde{\varepsilon}_f = \varepsilon_f + 2\left[\frac{N-1}{N}\right]\frac{\Delta}{\pi}\Bigg[\ln\left[\frac{\beta(D_-+\mu)}{2\pi}\right] &+ \\ - \mathcal{Re}\,\psi\left[\frac{1}{2}-\frac{i\beta}{2\pi}\left[\tilde{\varepsilon}_f-\mu+i\frac{2}{N}\Delta\,\Gamma_T\right]\right]\Bigg]&\,,\end{aligned}} \tag{7.19}$$

$$\boxed{\Gamma_T = 1 - \frac{(N-1)}{\pi}\,\mathcal{Im}\left[\psi\left[\frac{1}{2}-\frac{i\beta}{2\pi}\left[\tilde{\varepsilon}_f-\mu+i\frac{2}{N}\Delta\,\Gamma_T\right]\right]-\psi\left[\frac{1}{2}-\frac{i\beta}{2\pi}(\tilde{\varepsilon}_f-\mu)\right]\right]\,.} \tag{7.20}$$

These equations may be written compactly, as:

$$\boxed{\begin{aligned}\tilde{z} = \varepsilon_f-\mu+2\left[\frac{N-1}{N}\right]\frac{\Delta}{\pi}\left[\ln\left[\frac{\beta(D_-+\mu)}{2\pi}\right]-\psi\left[\frac{1}{2}-\frac{i\beta}{2\pi}\tilde{z}\right]-i\frac{\pi}{2}\right] &+ \\ + 2i\Delta\left[\frac{1}{N}+\left[\frac{N-1}{N}\right]f_F(\tilde{\varepsilon}_f-\mu)\right]&\,,\end{aligned}} \tag{7.21a}$$

where $$\tilde{z} \equiv \tilde{\varepsilon}_f - \mu + i\tilde{\Delta}\,. \tag{7.21b}$$

7.2 THE $\langle P_1\rangle$ SECTOR

7.2.1 THE BREAKDOWN OF THE SELF–ENERGY EXPANSION IN THE $\langle P_1\rangle$ SECTOR

A systematic, self–consistent method was presented for calculating $\mathcal{S}_R$ in the $\langle P_o\rangle$ sector. Can such a thing be done in the $\langle P_1\rangle$ sector as well?

Let us consider the 1–loop self–consistent calculation of the last section. It is an infinite order non–perturbative calculation. If we decompose this into a diagrammatic expansion, we must include all diagrams in which internal lines are renormalized by sub–internal lines, which are in turn renormalized by sub–sub–internal lines, which are ... etc. An example of one of these diagrams is displayed in FIG. 7.4.

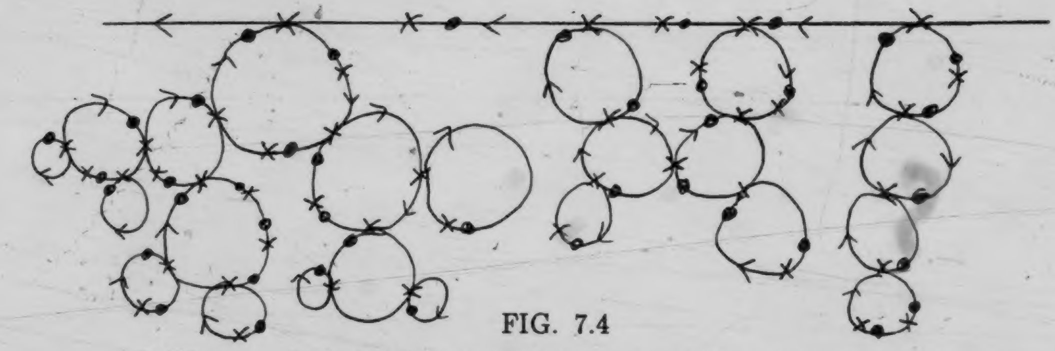

FIG. 7.4

A Diagram Included in the Self–Consistent One–Loop Calculation

This diagram was implicitly included in the self–consistent, 1–loop calculation which was done in the $\langle P_o \rangle$ sector.

The diagram of FIG. 7.4 is multiplied by the vacuum expectation value of a T–product of zero–energy boson operators. In the $\langle P_o \rangle$ sector, all these operators multiply together to give P_o. Conversely, in the $\langle P_1 \rangle$ sector, using non–SU(N) rules, every single non–spontaneous cross vertex (i.e. every single $\leftarrow\!\times\!\bullet\!\leftarrow$) is connected to a wiggle diagram of colossal proportions. Therefore, we don't even have a self–energy expansion; instead we have something virtually impossible to calculate.

What about the SU(N) rules? As shown previously, groups of non–spontaneous cross vertices will be connected by broken–chain diagrams. But these groups have nothing to do with the self–energy expansion. That is even with SU(N) rules, vertices from different self–energy diagrams can be connected together, which will ruin the self–energy expansion.

The only alternative is to independently develop a self–energy expansion in terms of the broken–chain SU(N) diagrams, which has nothing to do with the self–energy expansion which was developed for the $\langle P_o \rangle$ sector. One still expects major problems, because one would be using two different approximation schemes in the two different sectors. Intuitively, one expects that the only way for the particle/hole sum rule to be satisfied is to use the same approximation scheme in both sectors. After all, both sectors are related by the same zero–energy boson T–product.

In spite of these misgivings, let us attempt to develop an independent perturbation scheme for the $\langle P_1 \rangle$ sector. The first thing one might do is consider a self–energy expansion, as was done for the $\langle P_0 \rangle$ sector, and was illustrated in FIG. 7.1. One would have a self–energy $\Sigma(\omega;\ell=1)$, and a starting point function $\Gamma(\omega;\ell=1)$. As before, we could split these into tadpole and non–tadpole parts, and further separate $\Sigma_N(\omega;\ell=1)$ into Σ_{ff} and Σ_{fc} categories.

Carrying the parallel construction still further, we could consider the diagrammatics of these self–energies and the starting–point vertex, renormalized self–consistently to 3–loop order, as was illustrated for the $\langle P_0 \rangle$ sector in sect. 7.1.2. This has been done, but the results are not included in this thesis, because subsequent analysis indicated that this was not a valid perturbation scheme.

The essential point is that we must perform some kind of infinite order self–consistent calculation, in order to obtain the desired non–perturbative results. The question is, "Which infinite set of diagrams can we sum up to give a calculable, yet valid first–order approximation?" In the $\langle P_0 \rangle$ sector, it was easy. The infinite set of renormalized 1–loop diagrams is calculable. Furthermore, the 2–loop and 3–loop diagrams are of a higher order in 1/N.

Such is not the case the $\langle P_1 \rangle$ sector. In fact there is an infinite set of n–loop diagrams, where n is arbitrary, which all contribute at order $1/N^0$. This set of diagrams is illustrated in FIG. 7.5.

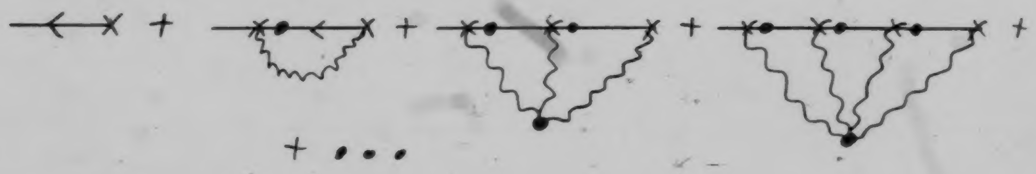

FIG. 7.5
A Set of n–Loop Diagrams Which All Contribute at Order $1/N^0$

The wiggle diagrams in FIG. 7.5 may be decomposed into linear chains of loops using the Feynman rules of chapter 4. Not all the chains which compose a wiggle diagram will contribute at order $1/N^0$. Only the chains having the form illustrated in FIG. 7.6 will contribute. Other ones, such as those illustrated in FIG. 7.7 will not contribute.

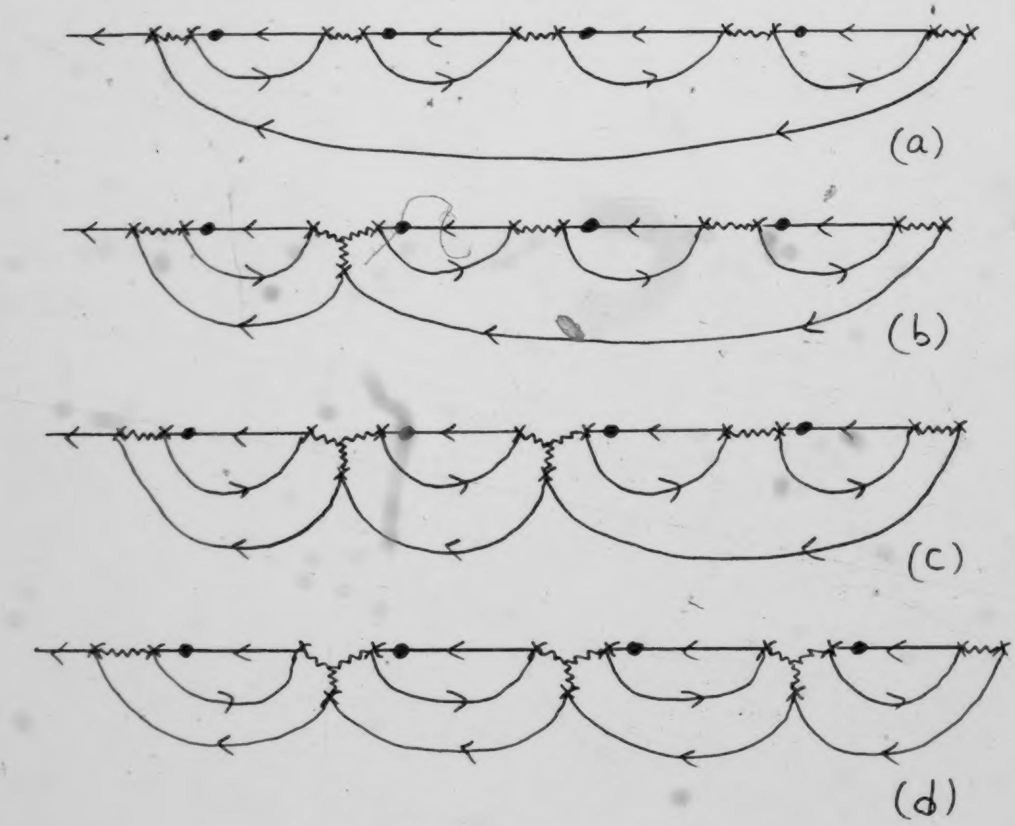

FIG. 7.6

Portions of the 5–Point Wiggle Which Contribute at Order $1/N^0$

Here we use the non–SU(N) Feynman Rules of section 4.9.2 and illustrate with the vertex–splitting tool introduced in section 6.4.3. The order of N is easy to determine with these rules, because there are no complicated λ–matrix traces to perform. We simply note that there are 4 spin loops; this yields a factor of N^4. Each dot carries a factor of $1/N$. There are 4 dots; therefore the net result is a factor of $1/N^0$. (In this we exclude the overall factor $\langle P_l \rangle_R/N$ which multiplies all $\langle P_l \rangle$ sector diagrams.)

(a) shows a simple 1–link chain, (b) shows a 2–link chain, (c) shows a 3–link chain, and (d) shows a 4–link chain, all of which contribute $O(1/N^0)$.

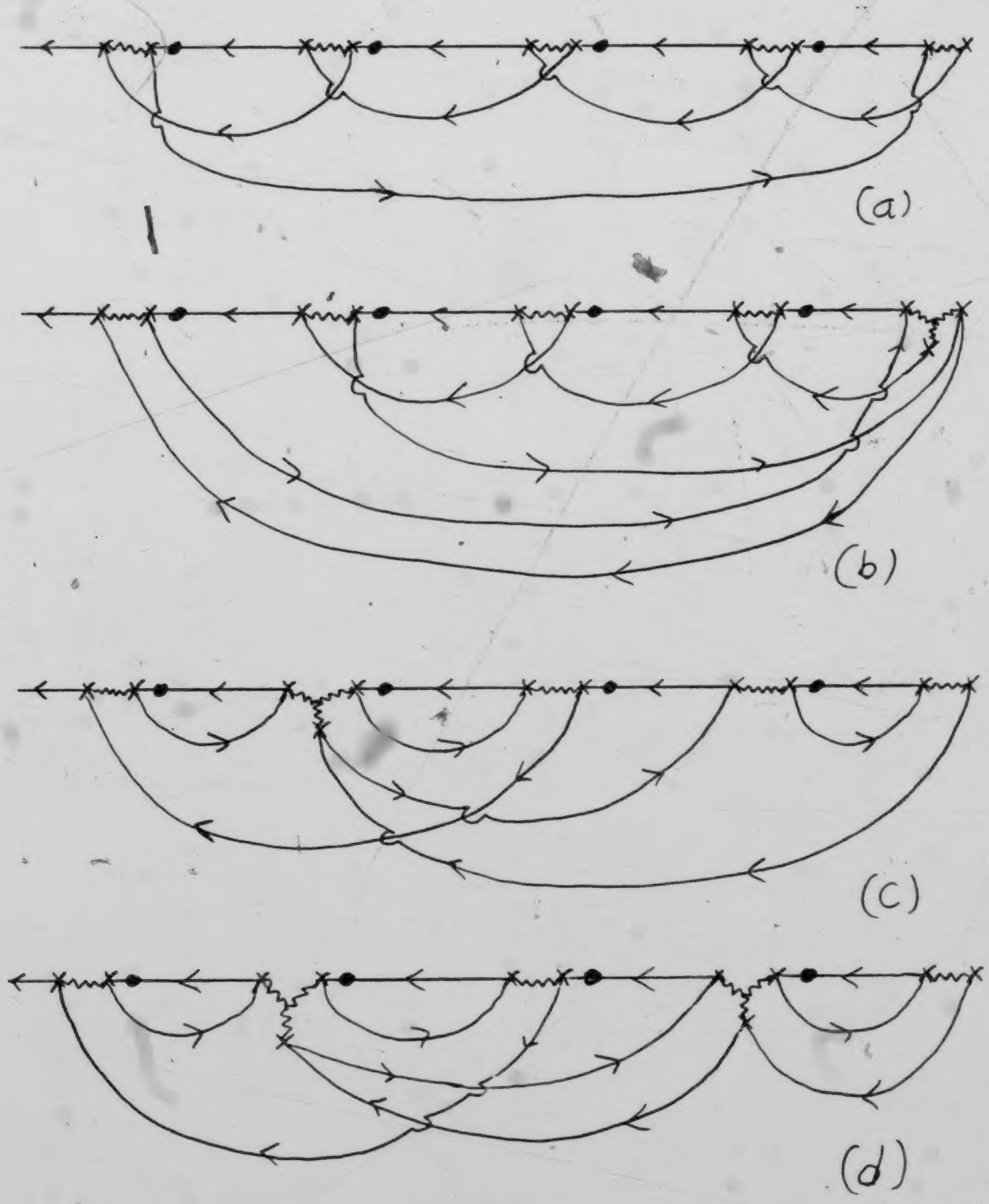

FIG. 7.7

Portions of the 5–Point Wiggle Which Do Not Contribute at $O(1/N^0)$.

As in FIG. 7.6 we use the non–SU(N) rules. (a) shows a 1–link chain which is of $O(1/N^4)$, (b) shows a 2–link chain which is also of $O(1/N^4)$, (c) shows a 2–link chain which is of $O(1/N)$, and (d) shows a 3–link chain which is also of $O(1/N)$. (As before, this order excludes the overall factor of $\langle P_1 \rangle_R / N$ which multiplies all $\langle P_1 \rangle$ sector diagrams.

7.2.2 FINDING A LOWEST–ORDER PERTURBATIVE SCHEME IN THE $\langle P_l \rangle$ SECTOR

It is interesting to note that all the diagrams of FIG. 7.7 have f–electron lines which cross, whereas none of the f–electron lines in FIG. 7.6 cross. This is highly reminiscent of Kuramoto's "non–crossing approximation" which was discussed in sect. 1.7.5.

A reasonable first order approximation, then, seems to be to calculate all non–crossing diagrams such as those illustrated in FIG. 7.6. To be consistent with the approximation scheme used in the $\langle P_0 \rangle$ sector, we should also include the 1–loop tadpole diagrams. This scheme is illustrated in FIG. 7.8.

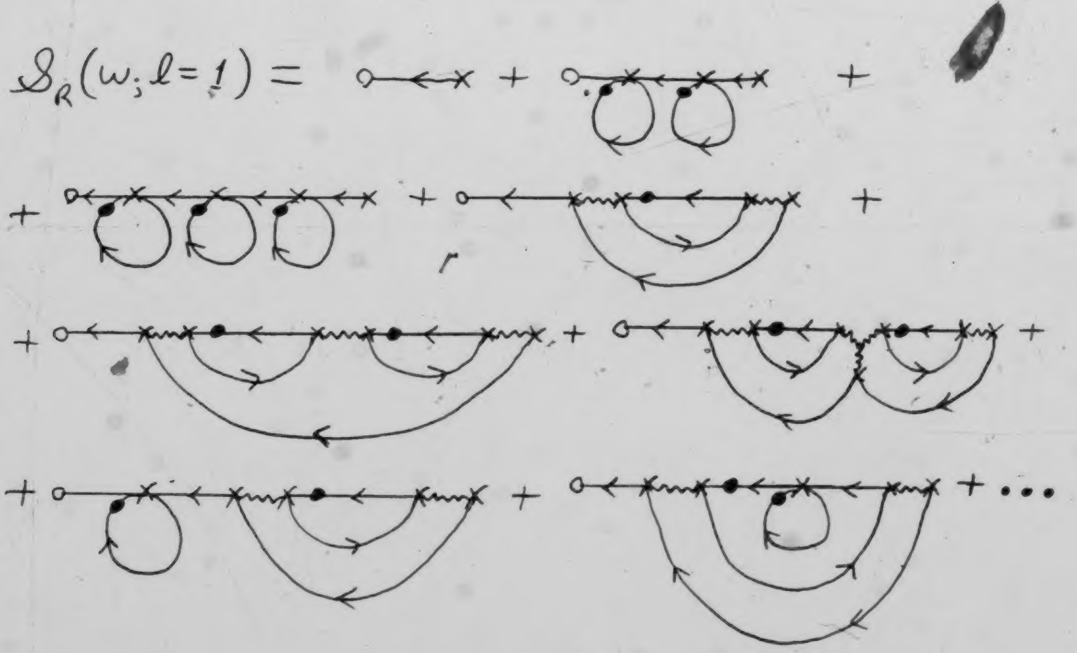

FIG. 7.8

The First Order Approximation for $\mathcal{S}_R$ in the $\langle P_l \rangle$ Sector

All of these diagrams are of order $1/N^0$ (excluding the overall factor of $\langle P_l \rangle_R / N$ which multiplies all $\langle P_l \rangle$ sector diagrams).

There are diagrams with just the 1–loop tadpole corrections, plus diagrams with just the wiggle–line chains, plus diagrams which have both.

Two important features should be noted. Firstly, wiggle line chains which connect to a vertex within a tadpole loop are ignored. An example of one of these diagrams is shown in FIG. 7.9 ; one finds it to be of a higher order in 1/N. Secondly, the regular vacuum diagrams which renormalize the wiggle lines (see section 6.6) have been dropped. An example of one of these diagrams is shown in FIG. 7.10; it too is of a higher order in 1/N.

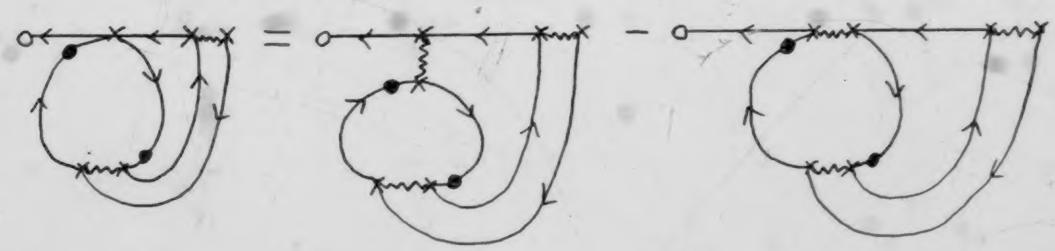

FIG. 7.9

A Wiggle–Line Chain Connected to a Vertex Within a Tadpole Diagram

According to the non–SU(N) Feynman rules, this diagram is composed of two terms, as shown. The first term is of order $1/N^2$, and the second term is of order 1/N. Both of these terms drop out of the order $1/N^0$ approximation shown in FIG. 7.8.

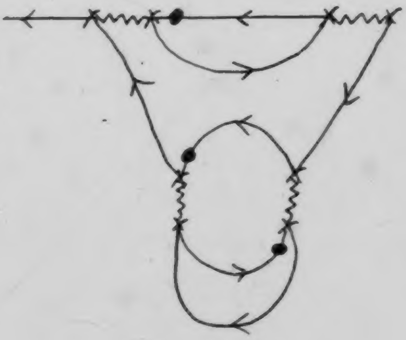

FIG. 7.10

A Regular Vacuum Diagram Which Renormalizes a Wiggle Line Loop

A casual glance at this diagram will reveal that it is of order 1/N. Consequently, this too has been dropped from the order $1/N^0$ approximation shown in FIG. 7.8.

7.2.3 DIAGRAMMATICS OF THE $\langle P_1 \rangle$ SECTOR AT ORDER $1/N^0$

We define:

$$\mathcal{S}_{R}^{(0)}(\omega;\ell=1) \equiv S_{R}^{(0)}(\omega;\ell=1)\,\Gamma^{(0)}(\omega;\ell=1)\ , \tag{7.22}$$

where:

$$\bar{S}_{R}^{11(0)}(\omega;\ell=1) = \frac{1}{\omega - \epsilon_f - \Sigma_T^{(0)}(\ell=1) + i\delta}\ , \tag{7.23}$$

and the superscript "(0)" means that we are considering only the $O(1/N^0)$ approximation. This $S_R^{(0)}(\ell=1)$ propagator will be represented diagrammatically as shown in FIG. 7.11. It differs from $S_R(\ell=0)$ at $O(1/N^0)$ in that there is no $i\bar{\Delta}$ width term. (In fact, $S_R^{(0)}(\ell=1)$ happens to be identical to the 1-loop approximation for $S_R^c(\ell=0)$.)

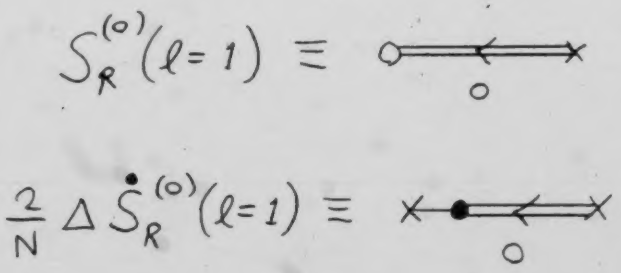

$S_R^{(0)}(\ell=1) \equiv$
0
$\frac{2}{N}\Delta \dot{S}_R^{(0)}(\ell=1) \equiv$
0

FIG. 7.11

Diagrammatic Representation of $S_R^{(0)}(\ell=1)$ and $\dot{S}_R^{(0)}(\ell=1)$

$\Sigma_T^{(0)}(\ell=1)$ may be expressed simply as follows:

$$\Sigma_T^{(0)}(\ell=1) = \quad ; \tag{7.24}$$

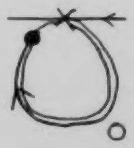

$\Gamma^{(0)}(\omega;\ell=1)$ is not so simple, and involves an infinite sum of loops of arbitrary order. It is given as follows:

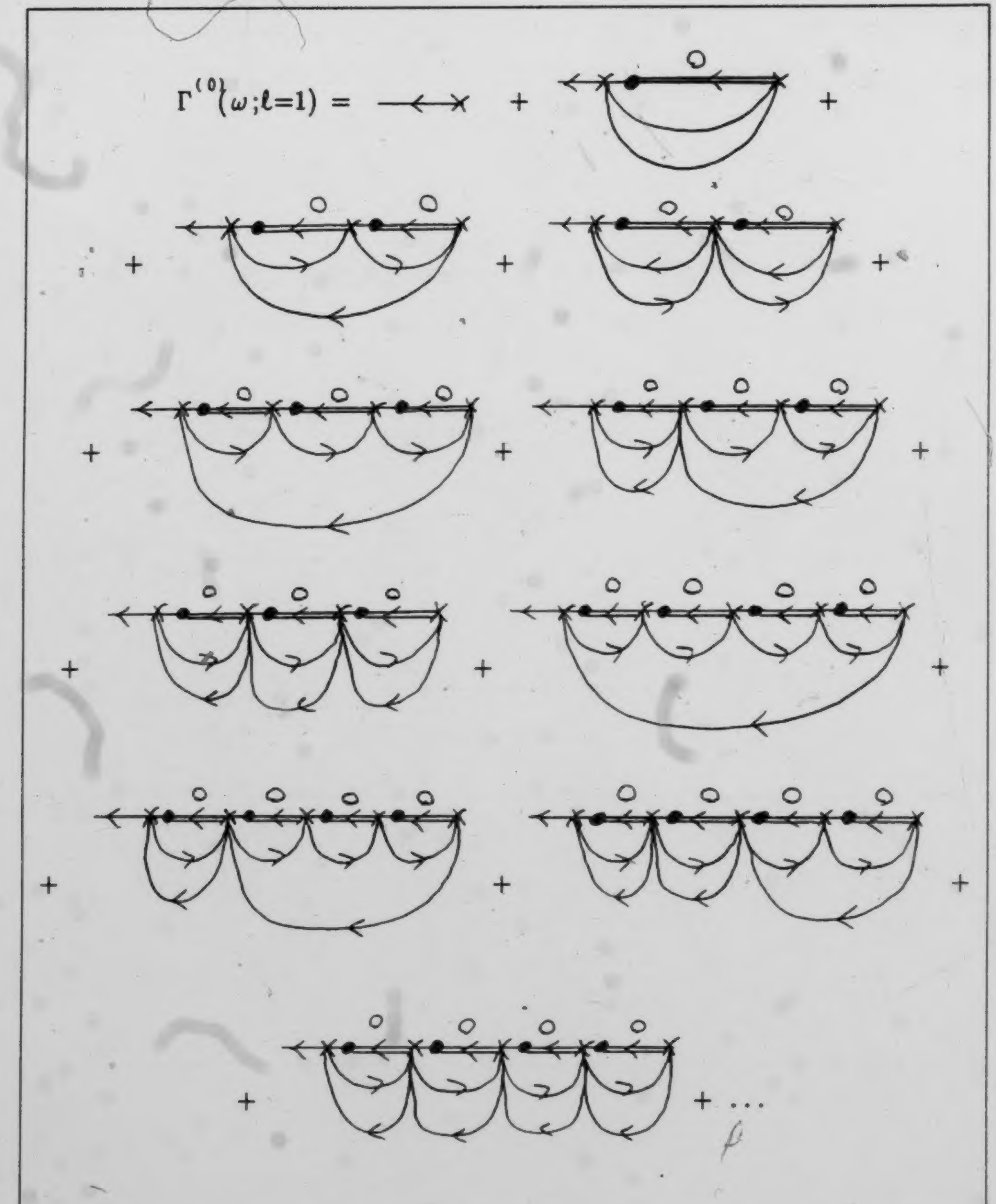

(7.25)

7.2.4 THE $O(1/N^0)$ $\langle P_1 \rangle$ SECTOR CALCULATION

The calculation of $\Sigma_T^{(0)}(\ell=1)$ is similar to the calculation of $\Sigma_T(\ell=0)$, except that the $i\Delta$ term is missing. Let us make the following definitions:

$$\bar{S}_{\mathbf{k}}^{11(0)}(\omega;\ell=1) = \frac{1}{\omega - \tilde{\varepsilon}_f(\ell=1) + i\delta} , \tag{7.26a}$$

where

$$\tilde{\varepsilon}_f(\ell=1) \equiv \varepsilon_f + \Sigma_{\mathrm{T}}^{(0)}(\ell=1) . \tag{7.26b}$$

One obtains the following self-consistent expression for $\tilde{\varepsilon}_f(\ell=1)$:

$$\tilde{\varepsilon}_f(\ell=1) = \varepsilon_f + 2\left[\frac{N-1}{N}\right]\frac{\Delta}{\pi}\left[\ln\left[\frac{\beta(D_- + \mu)}{2\pi}\right] - \mathcal{R}e\,\psi\left[\frac{1}{2} - \frac{i\beta}{2\pi}\left[\tilde{\varepsilon}_f(\ell=1) - \mu\right]\right]\right] \tag{7.27}$$

An analytic expression for $\Gamma^{(0)}(\omega;\ell=1)$ has not been found. One may obtain a very complicated integral expression, which must be integrated numerically. This numerical analysis has not been done. The most we can say at this point is that "something" is happening near $\omega = \tilde{\varepsilon}_f(\ell=1)$, which would show up as some kind of structure in the spectral function of $\mathcal{S}_{\mathbf{k}}(\omega;\ell=1)$.

7.3 THE SINGLE-SITE RESULTS, IGNORING THE $\langle P_1 \rangle$ SECTOR

7.3.1 WHY IGNORE THE $\langle P_1 \rangle$ SECTOR?

We will ignore the $\langle P_1 \rangle$ sector, mainly because the calculations are too complicated. Furthermore, the $\langle P_1 \rangle$ sector may give spectral weight near $\tilde{\varepsilon}_f(\ell=1)$, which may be the renormalized f–level ε_f^* , but this spectral weight evidently does not have a resonance form. Conversely, the $\langle P_o \rangle$ sector propagator does have a nice resonance structure. We may therefore expect that $\tilde{\varepsilon}_f(\ell=0)$ is actually ε_K , the position of the Kondo resonance. The evidence seems to indicate that only the $\langle P_o \rangle$ sector is important to the Kondo effect.

Evidently, the preliminary analysis of section 1.7.8 is wrong. We cannot assume that eq. (1.20) is valid, because the spectral weight at ε_f^* does not have a simple resonance form.

7.3.2 THE $\mathscr{d}_R$ PROPAGATOR AND THE UNITARY LIMIT

Using eqs. (7.18) in eq. (6.116), and ignoring the $\langle P_1\rangle$ sector, one obtains the following propagator:

$$\boxed{\tilde{\mathscr{d}}_R^{11}(\omega) = \frac{\Gamma_T(\ell=0)\ \langle P_o\rangle_R}{\omega - \tilde{\varepsilon}_f(\ell=0) + i\tilde{\Delta}(\ell=0)}\ ,} \tag{7.28}$$

where Γ_T, $\tilde{\varepsilon}_f$, and $\tilde{\Delta}$ are given by eqs. (7.18) – (7.20). Its spectral function is given by:

$$\boxed{\sigma_{\mathscr{d}}^R(\omega) = \frac{1}{\pi}\frac{\tilde{\Delta}(\ell=0)\ \Gamma_T(\ell=0)\ \langle P_o\rangle_R}{[\omega - \tilde{\varepsilon}_f(\ell=0)]^2 + [\tilde{\Delta}(\ell=0)]^2}\ .} \tag{7.29}$$

The maximum value of this spectral function occurs when $\omega = \tilde{\varepsilon}_f(\ell=0)$. It is:

$$\sigma_{\mathscr{d}\,\mathrm{max}}^R = \frac{1}{\pi}\frac{\Gamma_T(\ell=0)\ \langle P_o\rangle_R}{\tilde{\Delta}(\ell=0)} = \frac{N}{2\pi\Delta}\langle P_o\rangle_R\ . \tag{7.30}$$

Noting eq. (6.70) for the unitary limit (ie. $\sigma_{\mathscr{d}}^R \leq \frac{N}{2\pi\Delta}$), and keeping in mind that $\langle P_o\rangle_R \leq 1$, one finds that $\sigma_{\mathscr{d}}^R(\omega)$ satisfies the unitarity condition.

7.3.3 VIOLATION OF THE PARTICLE/HOLE SUM RULE

From eq. (7.29), one may prove the following two identities:

$$\int d\kappa\, \sigma_{\mathscr{d}}^R(\kappa;\ell=0) = \Gamma_T(\ell=0)\ , \tag{7.31}$$

$$\int d\kappa\, f_F(\kappa-\mu)\, \sigma_{\mathscr{d}}^R(\kappa;\ell=0) = \Gamma_T(\ell=0)\left[\frac{1}{2} + \frac{1}{\pi}\mathcal{Im}\ \psi\!\left[\frac{1}{2} - \frac{i\beta}{2\pi}(\tilde{\varepsilon}_f-\mu+i\tilde{\Delta})\right]\right]. \tag{7.32}$$

From eq. (7.20) for Γ_T, one finds another identity:

$$\frac{1}{2} + \frac{1}{\pi}\mathscr{Im}\,\psi\left[\frac{1}{2} - \frac{i\beta}{2\pi}(\tilde{\varepsilon}_f - \mu + i\tilde{\Delta})\right] = \frac{1 - \Gamma_T(\ell=0)}{N-1} + f_F(\tilde{\varepsilon}_f - \mu) \; . \tag{7.33}$$

Inserting eq. (7.33) into eq. (7.32) simplifies the identity, yielding:

$$\int d\kappa\, f_F(\kappa-\mu)\, \sigma^{R}_{\mathscr{B}}(\kappa;\ell=0) = \Gamma_T(\ell=0)\left[\frac{1 - \Gamma_T(\ell=0)}{N-1} + f_F(\tilde{\varepsilon}_f - \mu)\right] . \tag{7.34}$$

Since we are ignoring the $\langle P_1 \rangle$ sector, the particle/hole sum rule of eq. (6.120) becomes:

$$N\int d\kappa\; f_F(\kappa-\mu)\, \sigma^{R}_{\mathscr{B}}(\kappa;\ell=0) = 1 \; . \tag{7.35}$$

Using this with the identity given in eq. (7.34) implies:

$$\left[\frac{N}{N-1}\right] \Gamma_T^2(\ell=0) - \left[\left[\frac{N}{N-1}\right] + N\, f_F(\tilde{\varepsilon}_f - \mu)\right] \Gamma_T(\ell=0) + 1 = 0 \; . \tag{7.36}$$

The solution of this equation is in obvious contradiction to the solution of eq. (7.20). Therefore the particle/hole sum rule is broken.

The fact that the particle/hole sum rule is broken is not too surprising, because we have neglected the $\langle P_1 \rangle$ sector. Although the $\langle P_1 \rangle$ sector may not be important to the Kondo effect, it is definitely important to the spectral weight.

7.3.4 NUMERICAL CALCULATIONS

Equations (7.19) and (7.20) were solved numerically. The results are plotted in FIGS. 7.12 to 7.17. All energies are normalized to $|\varepsilon_f|$ the bare f–electron energy. We take $D\_/|\varepsilon_f| = 8.33$, $\mu = 0$, and input various values of $\Delta/|\varepsilon_f|$.

FIGS. 7.12, 7.14, and 7.16 show plots of $\tilde{\varepsilon}_f$ versus temperature for $N = 4$, $N = 15$, and $N = \infty$, respectively. FIGS. 7.13, 7.15, and 7.17 show the corresponding plots of Γ_T versus temperature, for $N = 4$, $N = 15$, and $N = \infty$, respectively.

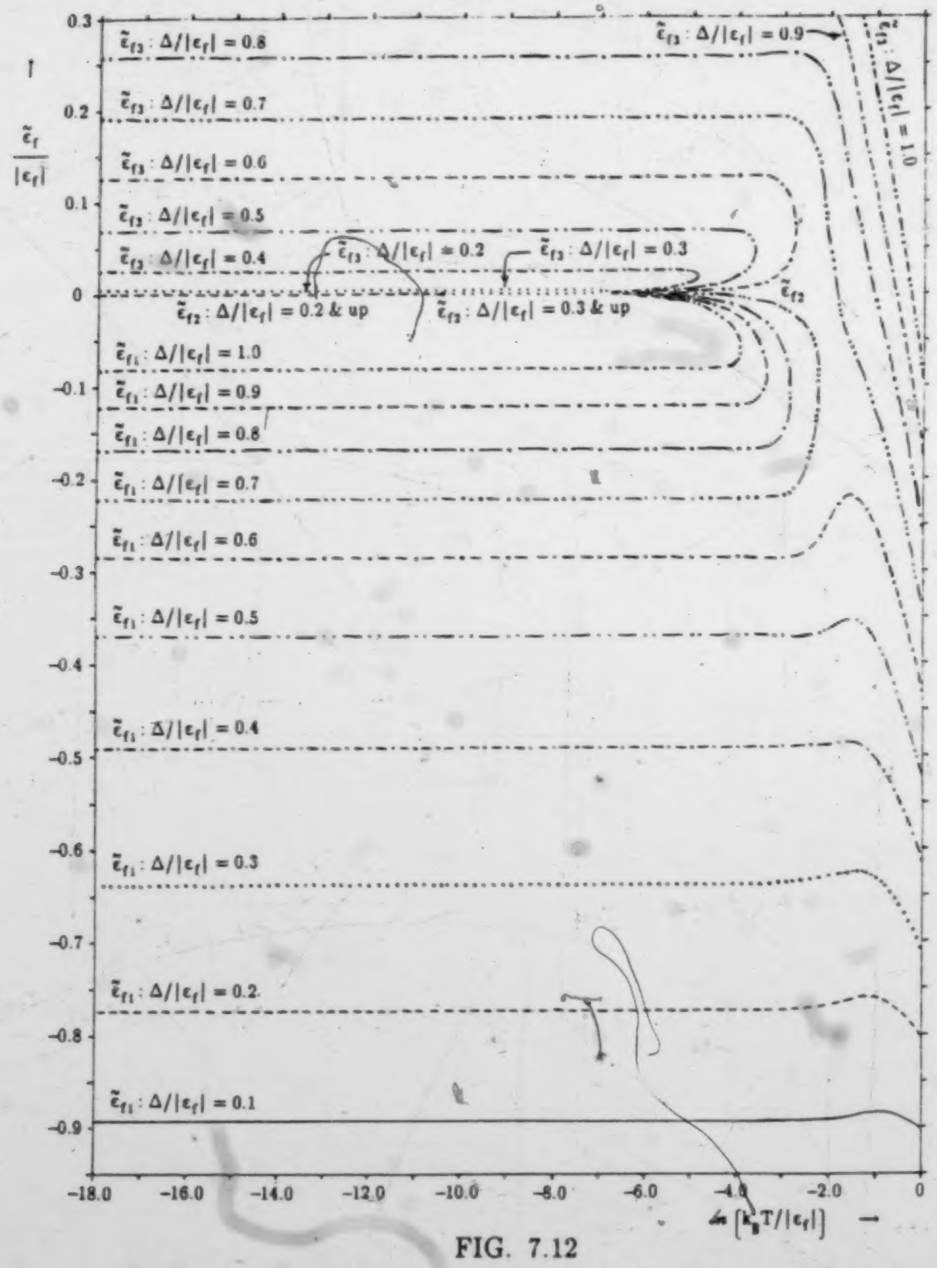

FIG. 7.12

$\tilde{\varepsilon}_f$ Versus $\ell n\,(k_B T/|\varepsilon_f|)$ for D = 8.33, N = 4, and Various Δ

At low temperature, there are three solutions ($\tilde{\varepsilon}_{f1}$, $\tilde{\varepsilon}_{f2}$, and $\tilde{\varepsilon}_{f3}$) for every value of Δ. As the temperature is raised, two of these solutions merge, leaving only one solution. Which solution remains, and at which temperature this happens, depend on the value of Δ. When $\Delta/|\varepsilon_f| = 0.1$, solutions #2 and #3 exist only at temperatures so low that they are off the ℓn T scale of this graph. When $\Delta/|\varepsilon_f| = 0.2$, solutions #2 and #3 exist only below $\ell n\, T/|\varepsilon_f| = -10.45$. They are so close together as to be indistinguishable on the scale of this graph.

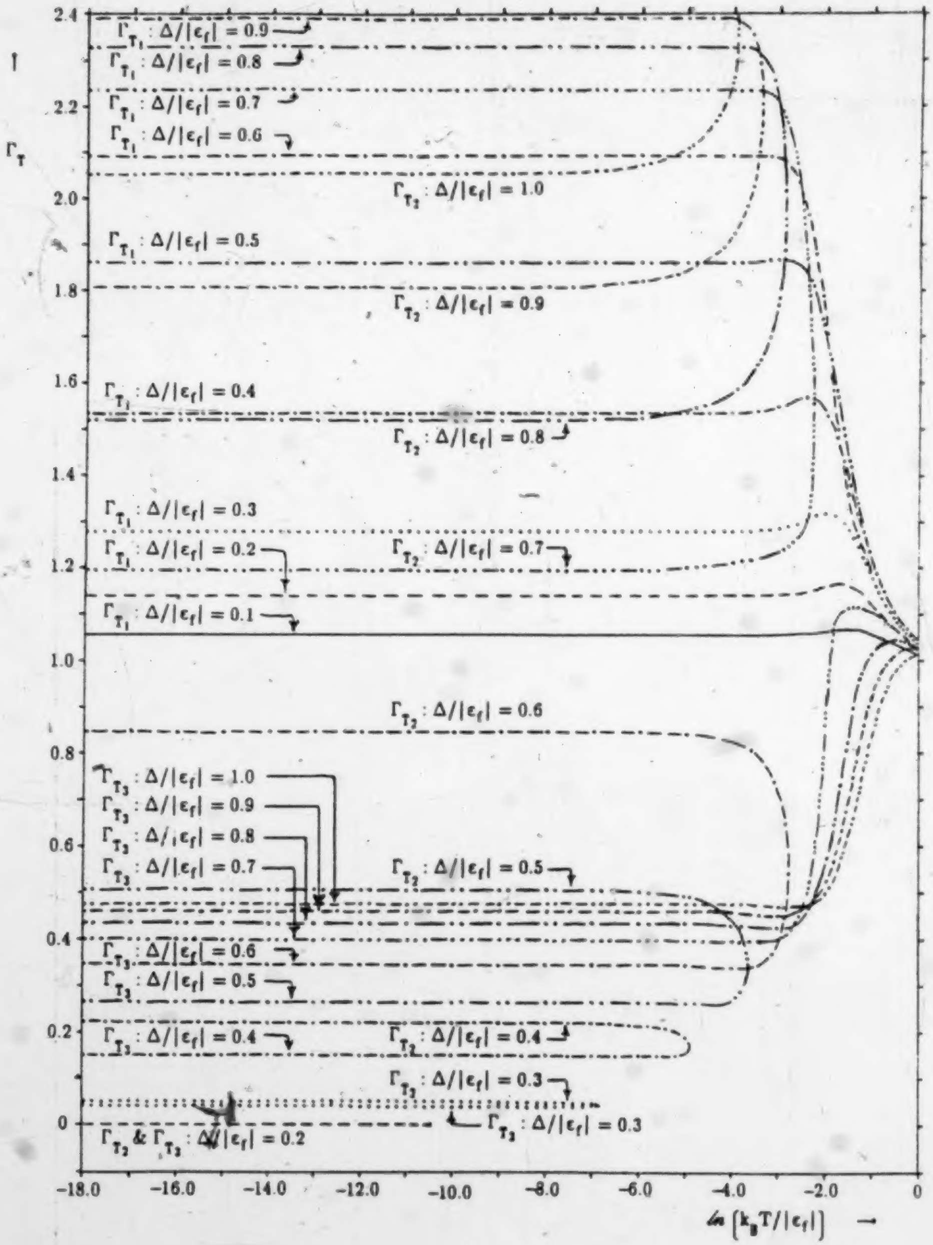

FIG. 7.13

Γ_T Versus $ln(k_B T/|\epsilon_f|)$ for $D = 8.33$, $N = 4$, and Various Δ

Corresponding to the three $\tilde{\epsilon}_f$ solutions in FIG. 7.12, there are also three Γ_T solutions (Γ_{T_1}, Γ_{T_2}, and Γ_{T_3}). As in FIG. 7.12, two of these solutions merge as the temperature is raised. At low temperature, solutions #2 and #3 are quite narrow, but solution #2 broadens rapidly with increasing Δ.

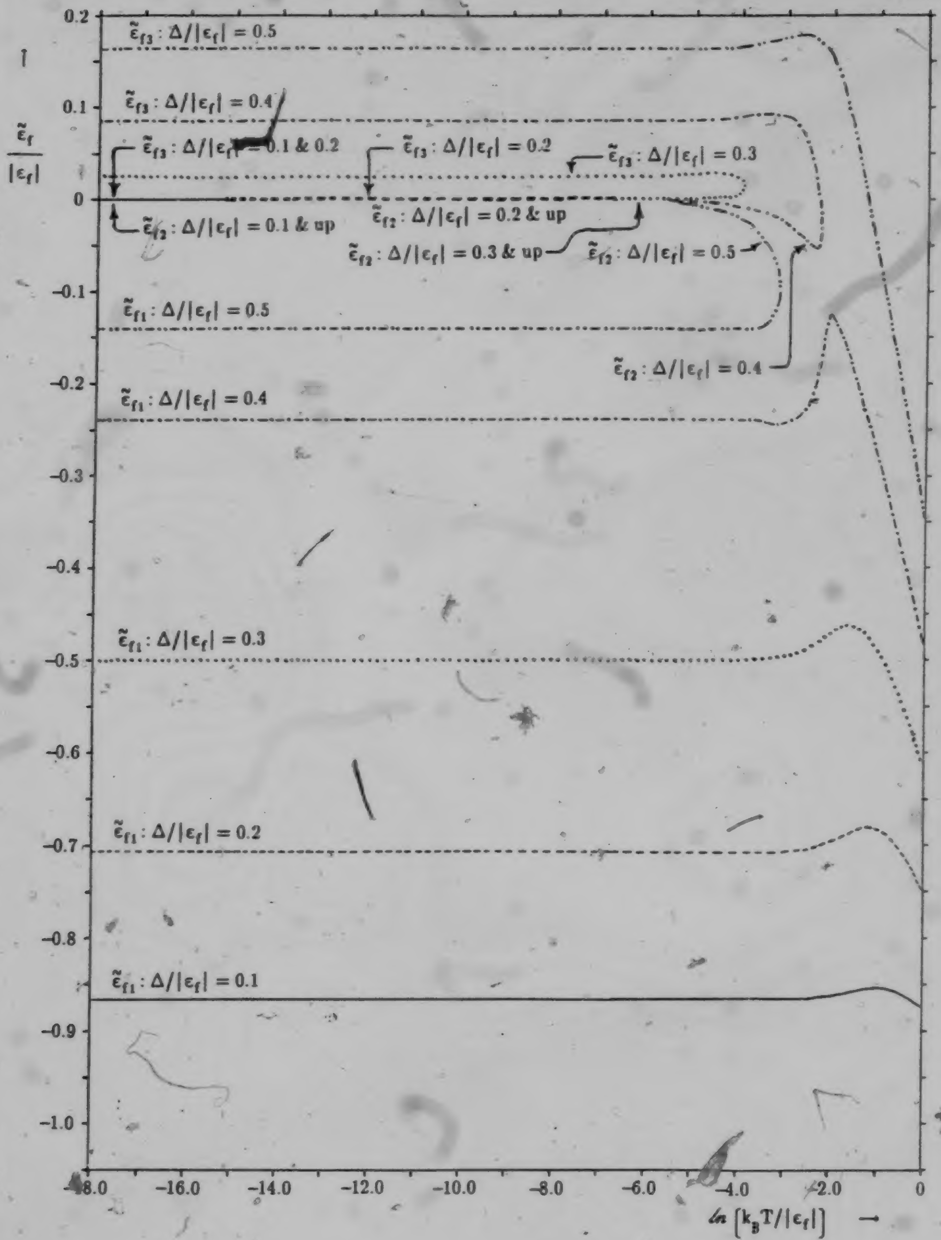

FIG. 7.14

$\tilde{\varepsilon}_f$ Versus $\ln(k_B T/|\varepsilon_f|)$ for $D = 8.33$, $N = 15$, and Various Δ

As in FIG. 7.12, there are three solutions at low temperature. As a function of Δ, these solutions are less dense than for the $N = 4$ case. Solutions #2 and #3, when $\Delta/|\varepsilon_f| = 0.1$, are now within the $\ln$ T scale of the graph (they exist below $\ln T/|\varepsilon_f| = -15.22$). But, they are so close together that they are indistinguishable on the energy scale of this graph, as are these solutions when $\Delta/|\varepsilon_f| = 0.2$.

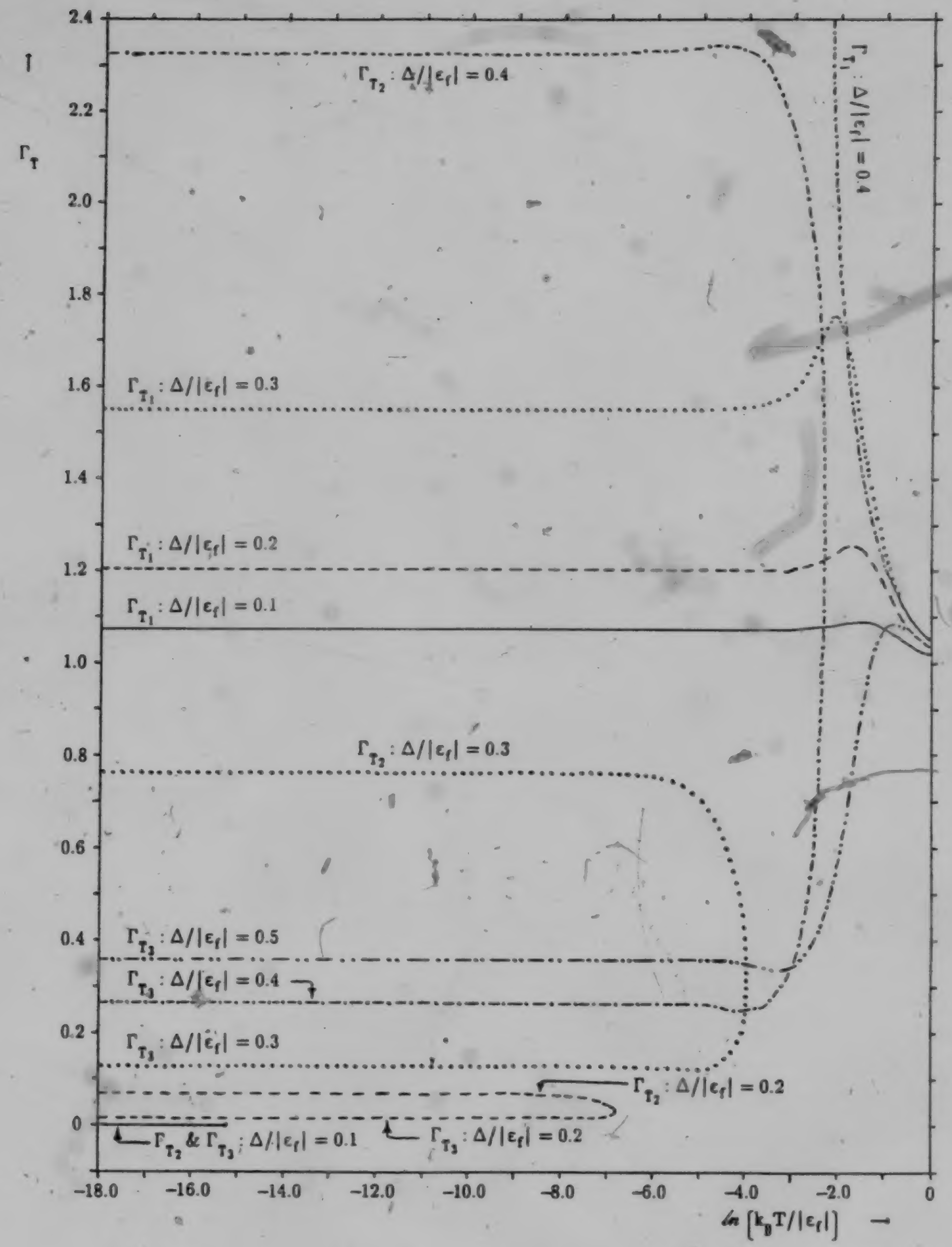

FIG. 7.15

Γ_T Versus ln$(k_B T/|\varepsilon_f|)$ for $D = 8.33$, $N = 15$, and Various Δ

This shows the values of Γ_T corresponding to the three sets of solutions plotted in FIG. 7.14. Solutions #2 and #3 are very narrow for small Δ. As Δ is raised at low temperature, solution #3 remains narrow, but Γ_{T_2} rises quite rapidly, as does Γ_{T_1}, which goes off-scale for $\Delta/|\varepsilon_f| = 0.4$. When $\Delta/|\varepsilon_f| = 0.5$, only Γ_{T_3} remains within the Γ_T scale of this graph.

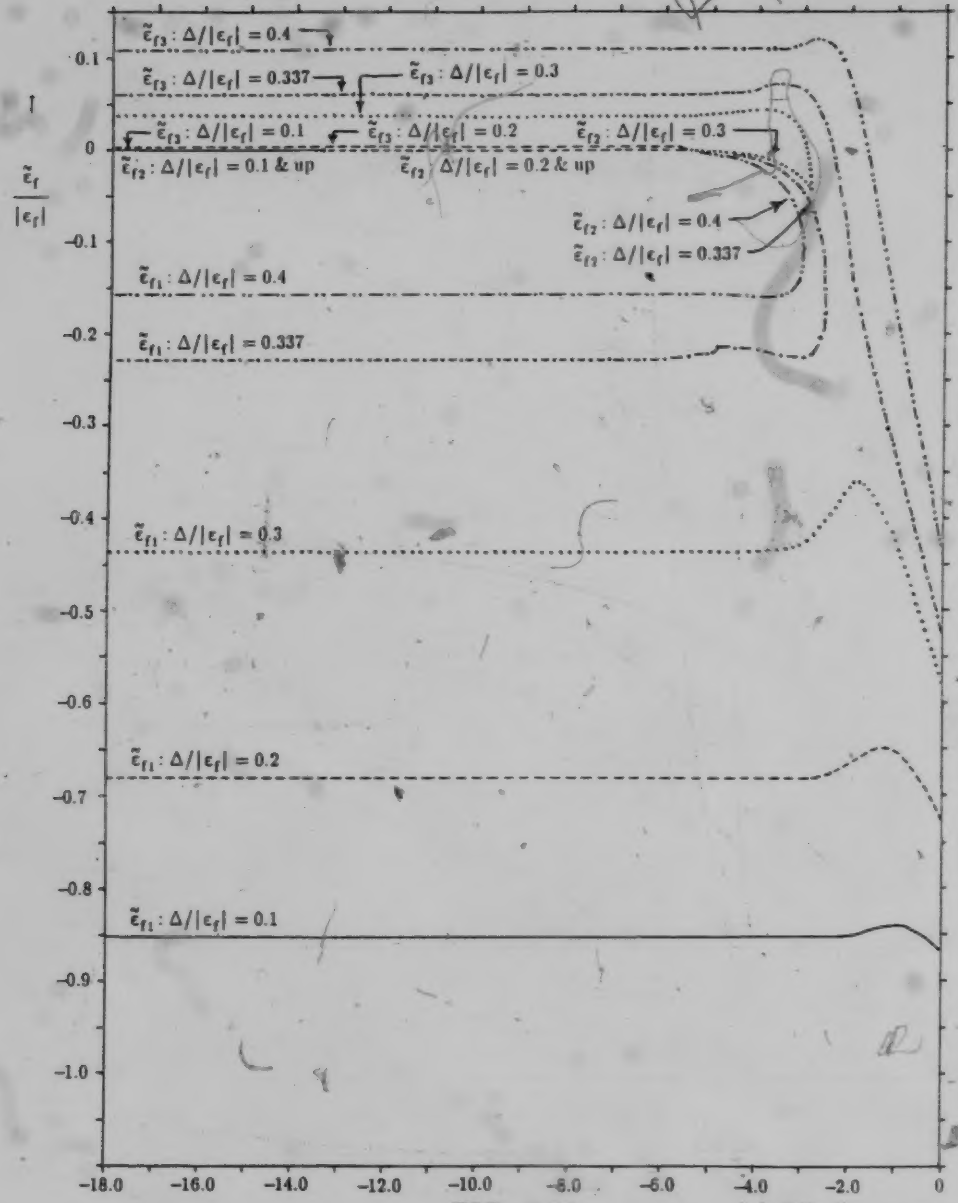

FIG. 7.16

$\tilde{\varepsilon}_f$ Versus $\ln(k_BT/|\varepsilon_f|)$ for $D = 8.33$, $N = \infty$, and Various Δ

These plots are similar to the $N = 15$ ones in FIG. 7.14, with some interesting differences. When $\Delta < 0.337$, solutions #2 and #3 merge as the temperature is raised, but solution #3 has a finite Γ_T and solution #2 has an infinite Γ_T. These plots show a discontinuity in the derivative where the finite joins with the infinite. (See the cusp for $\Delta/|\varepsilon_f| = 0.3$.) For $\Delta/|\varepsilon_f| \geq 0.4$ solution #1 also has an infinite Γ_T. A peculiar thing happens for $\Delta/|\varepsilon_f| = 0.337$; solution #1 has finite Γ_T for $\ln T/|\varepsilon_f| < -4.9$, whereupon it becomes infinite. (There is also a discontinuity in the derivative at this point.)

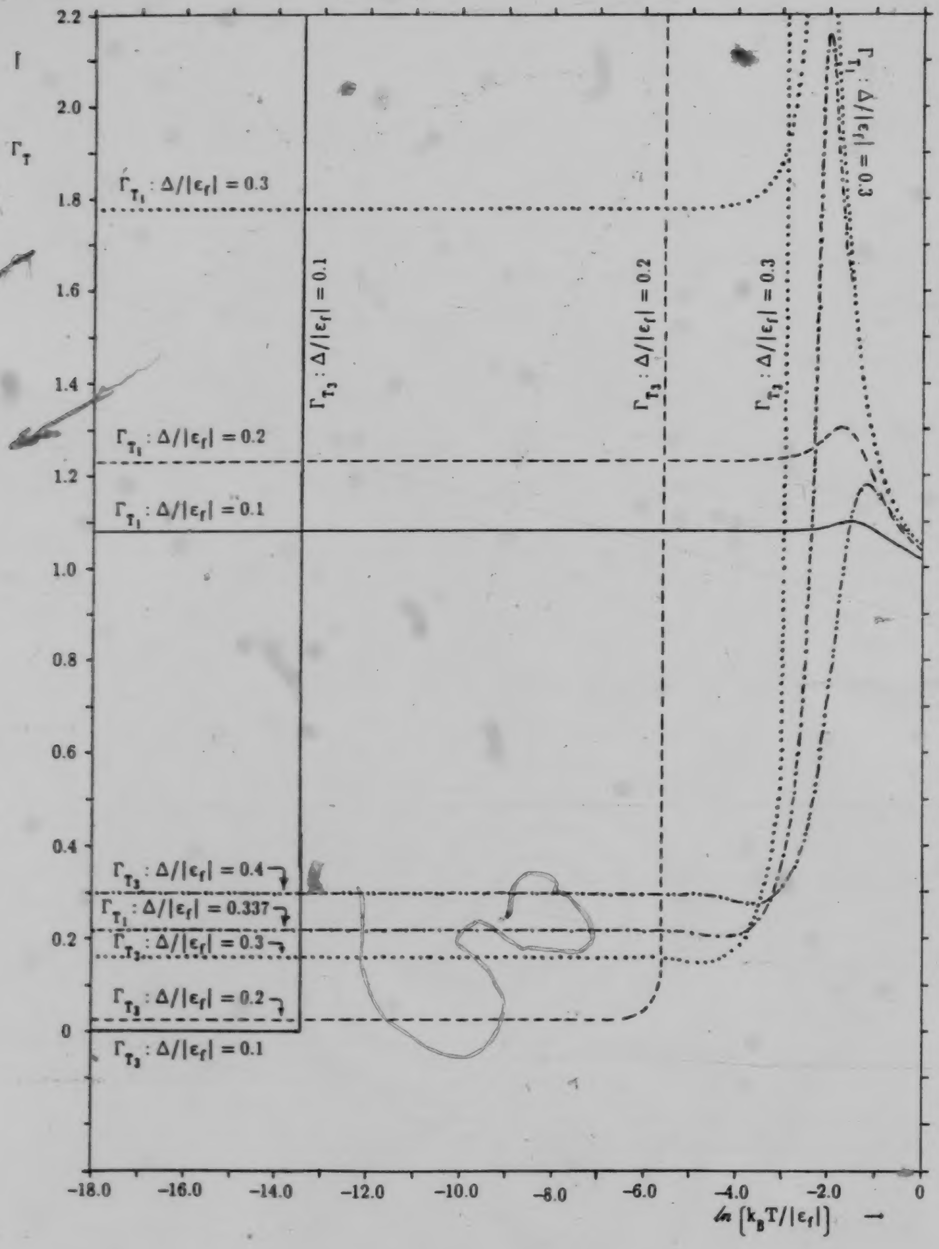

FIG. 7.17

Γ_T Versus $ln(k_B T/|\varepsilon_f|)$ for $D = 8.33$, $N = \infty$, and Various Δ

This shows the values of Γ_T corresponding to the plots in FIG. 7.16. Γ_{T_2} is not shown because it is infinite. When $\Delta/|\varepsilon_f| < 0.337$, Γ_{T_3} rises very sharply, and becomes infinite, at the temperature where this solution merges with solution #2. When $\Delta/|\varepsilon_f| \geq 0.337$, only solution #3 remains within the Γ scale of this graph.

The solutions plotted in FIGS. 7.12 – 7.17 show the following features:

1) There are three solutions: $\tilde{\varepsilon}_{f1} < \tilde{\varepsilon}_{f2} < \tilde{\varepsilon}_{f3}$; $\Gamma_{T_2} > \Gamma_{T_3}$. All three solutions exist as $T \to 0$.

2) As Δ increases at fixed temperature, $\tilde{\varepsilon}_{f1}$, $\tilde{\varepsilon}_{f3}$, Γ_{T_1}, Γ_{T_2}, and Γ_{T_3} all increase, whereas $\tilde{\varepsilon}_{f2}$ decreases.

3) At low temperature, $\tilde{\varepsilon}_{f1}$ is below the Fermi surface, $\tilde{\varepsilon}_{f3}$ is above the Fermi surface, and $\tilde{\varepsilon}_{f2}$ is very close to the Fermi surface.

4) There exists an interaction strength Δ_* which has the following properties:

    4.1) When the temperature is raised for fixed $\Delta < \Delta_*$, there exists a temperature $T_{23}(\Delta)$, at which $\tilde{\varepsilon}_{f2} = \tilde{\varepsilon}_{f3} \equiv \tilde{\varepsilon}_{f23}(\Delta)$ and $\Gamma_{T_2} = \Gamma_{T_3} \equiv \Gamma_{T_{23}}(\Delta)$. For $T > T_{23}(\Delta)$, only solution #1 remains.

    4.2) When the temperature is raised for fixed $\Delta > \Delta_*$, there exists a temperature $T_{12}(\Delta)$, at which $\tilde{\varepsilon}_{f1} = \tilde{\varepsilon}_{f2} \equiv \tilde{\varepsilon}_{f12}(\Delta)$ and $\Gamma_{T_1} = \Gamma_{T_2} \equiv \Gamma_{T_{12}}(\Delta)$. for $T > T_{12}(\Delta)$, only solution #3 remains.

5) $T_{23}(\Delta)$ increases with increasing Δ.

6) $T_{12}(\Delta)$ decreases with increasing Δ.

7) As $\Delta \to \Delta_*$ from above and below, $T_{23} \to T_{12} \to T_*$, where T_* is the maximum temperature at which solution #2 can exist, for *any* interaction strength Δ.

    7.1) When $T > T_*$ and $\Delta < \Delta_*$, only solution #1 exists.

    7.2) When $T > T_*$ and $\Delta > \Delta_*$, only solution #3 exists.

8) As $\Delta \to \Delta_*$ from above and below, at fixed $T > T_*$, one finds $\tilde{\varepsilon}_{f1} \to \tilde{\varepsilon}_{f3} \to \tilde{\varepsilon}_{f31}(T)$ and $\Gamma_{T_1} \to \Gamma_{T_3} \to \Gamma_{T_{31}}(T)$.

9) When $\Delta < \Delta_*$ and $T << T_{23}$ one finds the following properties:

    9.1) Solution #1 is a broad resonance below the Fermi surface.

    9.2) Solution #2 is a narrow resonance overlapping the Fermi surface. It is centred just slightly above the Fermi surface for small N, and just slightly below it for large N.

9.3) Solution #3 is a very narrow resonance above the Fermi surface.

9.4) As $N \to \infty$, the widths of solutions #1 and #3 go to zero. Only the width of solution #2 remains finite.

10) When $\Delta > \Delta_M$ and $T << T_{12}$ one finds the following properties:

10.1) Solution #1 is a very broad resonance centred below the Fermi surface.

10.2) Solution #2 is a narrow resonance overlapping the Fermi surface, and centred just slightly below it.

10.3) Solution #3 is still a relatively narrow resonance, which moves quite high above the Fermi surface for large Δ, but drops below the Fermi surface when $T > T_{12}$.

10.4) As before, when $N \to \infty$, the width of solution #3 goes to zero, and the width of solution #2 remains finite. Solution #1 also appears to have finite width, although the width may suddenly become zero below a certain temperature, as demonstrated when $\Delta/|\varepsilon_f| = 0.337$.

7.3.5 THE KONDO SOLUTION AND A FINITE–T PHASE TRANSITION

Having outlined the properties of these solutions, the question to ask is, "Which solution is the correct one?" Knowing that we are looking for a Kondo resonance, the obvious choice is solution #2. This choice is guided by the fact that the calculation should become more exact as $N \to \infty$. Solution #3 is eliminated because the width of the resonance goes to zero, but its position above the Fermi surface remains finite.

We will assume $\Delta < \Delta_M$. As the temperature is raised past T_{23}, solution #2 ceases to exist. Then we must choose solution #1, which is the renormalized f–level. A finite temperature phase transition therefore appears at T_{23}, where the solution makes a discontinuous jump from #2 to #1. This is an established artifact of an infinite-N calculation, as discussed in sect. 1.7.3.

An approximate expression for T_{23} may be obtained. It is:

$$k_B T_{23} \sim \frac{2e^{\gamma}}{\pi} D\, e^{-\pi|\epsilon_f|/2\Delta} , \tag{7.37}$$

where γ is Euler's constant. This corresponds to the standard expression for the Kondo temperature*, with the exception of the $\frac{2e^{\gamma}}{\pi}$ factor. (This factor is 1.134 which is approximately equal to 1.)

When $T << T_{23}$, and N is large, solution #2 reduces to the following expressions:

$$\tilde{\epsilon}_{f2} \sim -\frac{2D}{\beta\Delta} e^{-\pi|\epsilon_f|/2\Delta} \sim -\frac{2k_B T_K}{\beta\Delta} , \tag{7.38}$$

$$\frac{\Gamma_{T2}}{N} \sim \frac{D}{2\Delta} e^{-\pi|\epsilon_f|/2\Delta} \sim \frac{k_B T_K}{2\Delta} , \tag{7.39}$$

where T_K is the Kondo temperature.

Using these expressions in eqs. (7.28) and (7.29), one finds:

$$\bar{\mathcal{G}}^{11}_{R}(\omega) \sim \frac{\frac{k_B T_K}{2\Delta} N \langle P_o \rangle_R}{\omega + \frac{2k_B T_K}{\beta\Delta} + i\, k_B T_K} , \tag{7.40}$$

$$\sigma^{R}_{\mathcal{G}}(\omega) \sim \frac{1}{\pi} \frac{(k_B T_K)^2}{2\Delta} \frac{N \langle P_o \rangle_R}{\left[\omega + \frac{2k_B T_K}{\beta\Delta} \right]^2 + (k_B T_K)^2} . \tag{7.41}$$

These expressions are only valid for large β and large N.

The renormalized propagator expressed in eq. (7.40) has a couple of positive features. Firstly, there is a resonance at the Fermi surface, whose width is the Kondo temperature. This indicates that we have chosen the correct Kondo solution; solution #3 would have had a width approaching zero for large N. Secondly, in order that the resonance not carry an excessive weight, we must have $\langle P_o \rangle_R \sim O(1/N)$. Then $\langle P_1 \rangle_R \simeq 1$; another indication that we are in the Kondo regime.

---

* See eq. (2.13) of ref. [34]. Here W_o corresponds to our $\frac{2}{N}\frac{\Delta}{\pi}$.

7.3.6 VIOLATION OF THE FRIEDEL SUM RULE

A negative feature, of the renormalized propagator expressed in eq. (7.40), is that it violates the Friedel sum rule. Plugging eq. (7.40) into eq. (1.19), one obtains a phase shift of

$$\eta(\omega) = \tan^{-1}\left[\frac{k_B T_K}{-\frac{2k_B T_K}{\beta\Delta} - \omega}\right] + \pi\,\theta\left[\omega + \frac{2k_B T_K}{\beta\Delta}\right] . \tag{7.42}$$

At the Fermi surface ($\omega = 0$), we have:

$$\eta(0) = \pi - \tan^{-1}\left[\frac{\beta\Delta}{2}\right] \simeq \frac{\pi}{2} . \tag{7.43}$$

Using this in the Friedel sum rule given by eq. (1.18), one finds:

$$n_f \simeq \frac{N}{2} . \tag{7.44}$$

This is a very strong violation, when we consider that $n_f = \langle P_1 \rangle_R \simeq 1$. For some reason, the Kondo resonance calculated by the 1–loop $\langle P_o \rangle$ sector approximation is acting like there are N/2 scattering centres at the impurity site, rather than just one scattering centre. The problem is that the calculated Kondo resonance straddles the Fermi surface. This contradicts the Fermi liquid picture outlined in sect. 1.7.8, where we expected the Kondo resonance to be situated above the Fermi surface, with only a small portion overlapping it.

7.3.7 COMPARISON TO THE SLAVE BOSON RESULTS

Equation (7.21a) is remarkably similar to the results of Coleman's slave boson mean field calculation. In fact eq. (7.21a) becomes identical to eq. (2.19) of ref. [37] and eq. (2.29) of ref. [38], if we make the following identification*:

$$q = \frac{1}{N} + \frac{N-1}{N} f_F(\tilde{\varepsilon}_f - \mu) \ . \qquad (7.45)$$

Here $q \equiv Q/N$, where Q is the maximum occupation of the f–electron state in Coleman's generalized Anderson model. This result is puzzling, because this thesis has been dealing with the standard $Q = 1$ Anderson model. This is, the second term in eq. (7.45) should not be present. Furthermore, it is not a small deviation from Q=1, but in fact it is a very large discrepancy. Using the $\tilde{\varepsilon}_f$ given by eq. (7.38), one finds that eq. (7.45) yields $Q \simeq N/2$. This is consistent with eq. (7.44) for the Friedel sum rule violation.

How could such a thing have happened, when the algebra of the operators is supposed to constrain the f–electron state to be no more than singly occupied? One possible explanation is that diagrams in the $\langle P_1 \rangle$ sector are responsible for ensuring that the f–state can never be occupied by more than one electron at the same time. "At the same time" is a key phrase, because all the θ–functions in the X–operator reduction would ensure that times of occupation would not overlap. By ignoring the $\langle P_1 \rangle$ sector, we may have allowed occupation times to overlap, causing multiple occupation of the f–state, and subverting the whole quantum algebra approach.

A more plausible explanation is that $Q = 1$ is not violated; it may be that just the Friedel sum rule is violated. Calculating the $\langle P_1 \rangle$ sector diagrams given in eq. (7.25) may fix this problem. After all, the slave boson results are not valid for $q = 1/N$. Therefore, it may be reasonable to expect that eq. (7.21a) does not have to match the $q \to 1/N$ limit of Coleman's results.

---

* Note that Coleman normalized the interaction strength to 1/N whereas I normalize it to 2/N. Therefore one must multiply Coleman's Δ's by a factor of 2 to get my results. Furthermore eq. (2.19) of ref. [37] has a misprint, in that a factor of Δ/π is missing in front of the ℓn term, and eq. (2.29) of ref. [38] also has a misprint, in that it should have "ℓn" rather than "Im".

7.4 THE INFINITE-U LATTICE ANDERSON MODEL

7.4.1 THE LATTICE HAMILTONIAN AND THE FEYNMAN RULES

The Hamiltonian for the infinite-U lattice Anderson model is a direct extension of eqs. (6.1) for the single-impurity infinite-U Anderson model; one merely adds a site index "n" to be summed over. That is:

$$H = H_o + H_I \ , \tag{7.46a}$$

$$H_o = \sum_m \int d^3x \, c_m^\dagger(\vec{x}) \, \varepsilon(-i\vec{\nabla}) \, c_m(\vec{x}) + \varepsilon_f \sum_n \sum_m \xi_{nm}^\dagger \, \xi_{nm} \ , \tag{7.46b}$$

$$H_I = \sqrt{\frac{2}{N}} \, V \sum_n \sum_m \left[c_{nm}^\dagger \, \xi_{nm} + \xi_{nm}^\dagger \, c_{nm} \right] \ , \tag{7.46c}$$

where

$$c_{nm} = \sqrt{\Omega} \, c_m(\vec{x} = \vec{x}_n) \ , \tag{7.47}$$

$\vec{x} = \vec{x}_n$ being the location of site "n", and Ω being the volume of a unit cell of the metal.

The ξ_{nm} operators for a given n obey the same quantum algebra as for the single-site case, in order that each impurity site may be no more than singly occupied. But

$$\left\{ \xi_{nm} \, , \, \xi_{n'm'}^\dagger \right\} \propto \delta_{nn'} \ , \tag{7.48}$$

so that the Fock space of each site is disjoint from the Fock spaces of other sites. In other words, the quantum algebra is localized to each site; the lattice does not complicate the quantum algebra.

Feynman rules are the same as those presented for the single-site case, except that we need an intersite c-electron propagator and its vertices. This propagator is represented by a dashed line, as illustrated in FIG. 7.18a. Its vertices are also shown in FIG. 7.18.

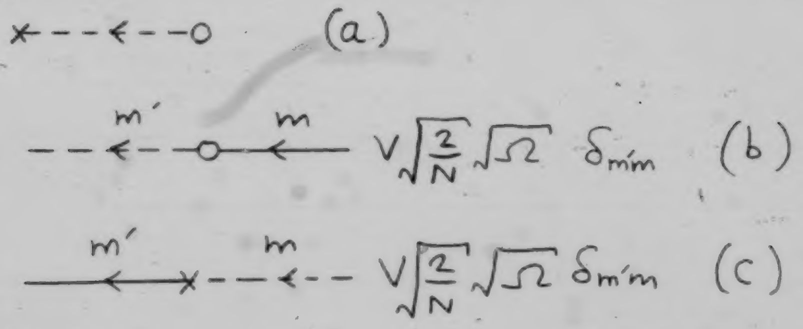
(a)
m′
m
$V\sqrt{\frac{2}{N}}\sqrt{\Omega}\,\delta_{m'm}$
(b)
m′
m
$V\sqrt{\frac{2}{N}}\sqrt{\Omega}\,\delta_{m'm}$
(c)

FIG. 7.18

The Intersite c-Electron Propagator and its Vertices

(a) shows the intersite c-electron propagator. (b) and (c) show its vertices. Basically, the vertex factor is $V\sqrt{2\Omega/N}$ with spin conservation. (The $\sqrt{\Omega}$ comes from eq. (7.47).)

7.4.2 MORE REASON TO IGNORE THE $\langle P_1\rangle$ SECTOR

In the single–site case, the $\langle P_1\rangle$ sector was ignored, for reasons already stated. The lattice case presents still further reason to ignore the $\langle P_1\rangle$ sector, as outlined below.

Due to the fact that the local quantum algebra exists at each lattice site, one finds that the vacuum expectation value of any operator T–product has the following form:

$$\langle 0(\beta)|\, A\, |0(\beta)\rangle = \sum_{\{\ell\}=0}^{1} A(\{\ell\}) \prod_{\ell_j\in\{\ell\}} \langle P_{\ell_j}\rangle_R \,. \qquad (7.49)$$

Suppose we have a self-energy expansion at site "n" in which corrections come from various different sites "n′" in the lattice. Suppose further that a correction line from one part of the self-energy diagram passes through site "j", and that another distinct line *from the same diagram* passes through the *same site* "j", as illustrated in FIG 7.19.

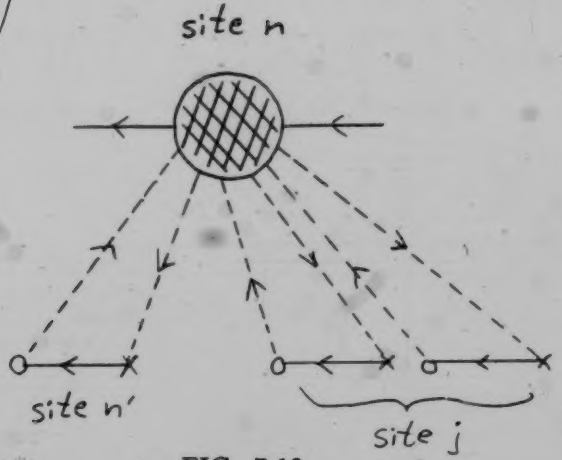

FIG. 7.19

Examples of Lattice Renormalization of a Self–Energy Diagram at Site n

Call one of these lines "a" and the other "b". Although "a" and "b" appear to be two independent loops, they are not really independent, because "a" and "b" must both be in the same sector. That is, one cannot have "a" in the $\langle P_o \rangle$ sector and "b" in the $\langle P_1 \rangle$ sector, because both "a" and "b" exist in the same local subspace. In other words, loops cannot be sector–summed independently.

It therefore becomes necessary to label each site "j" by a sector label "ℓ_j", so that two or more loops which pass through the same site "j" will each carry the "ℓ_j" label, locking them all into the same sector.

A major problem with this approach in that translational symmetry is broken, because each site "n" carries a unique label "ℓ_n", such that

$$\Sigma_n(\ell_1 \ell_2 \ldots) \neq \Sigma_{n'}(\ell_1 \ell_2 \ldots)\ , \tag{7.50}$$

where $\Sigma_n(\ell_1 \ell_2 \ldots)$ is a lattice corrected self–energy diagram at site n. This makes it impossible to perform a Fourier transform over the lattice. Performing the sums over ℓ_j will, of course, restore the translational symmetry. But, performing the sums over ℓ_j makes the self–energy expansion so complicated that a Fourier transform is virtually impossible anyway. The reason for this is that

$$\{\Sigma_n(\ell_1\ell_2\ldots)\Sigma_{n'}(\ell_1\ell_2\ldots)\} \neq \{\Sigma_n(\ell_1\ell_2\ldots)\}\{\Sigma_{n'}(\ell_1\ell_2\ldots)\}\ , \tag{7.51}$$

where { ... } represents the sector summation.

To avoid this unpleasantness, we will ignore the $\langle P_1\rangle$ sector, and consider only the $\langle P_o\rangle$ sector.

7.4.3 THE LATTICE–RENORMALIZED PROPAGATORS, SELF–ENERGIES, AND STARTING–POINT FUNCTION

Define the completely lattice–renormalized c–electron propagators as follows:

$$\delta_{mm'}\, C^{L\alpha\gamma}(t-t';\mathbf{x},\mathbf{x}') \equiv \langle 0(\beta)|\,T\, c^{\alpha}_{m}(\mathbf{x},t)\, c^{\dagger\gamma}_{m'}(\mathbf{x}',t')\,|0(\beta)\rangle\ , \tag{7.52a}$$

$$\delta_{mm'}\, C^{L\alpha\gamma}_{n}(t-t') \equiv \langle 0(\beta)|\,T\, c^{\alpha}_{nm}(t)\, c^{\dagger\gamma}_{nm'}(t')\,|0(\beta)\rangle\ , \tag{7.52b}$$

where $|0(\beta)\rangle$ is the thermal vacuum of the full lattice Hamiltonian.

Similarly, we define the completely lattice–renormalized, single–site f–electron propagator as :

$$\delta_{mm'}\, \mathcal{S}^{L\alpha\gamma}_{n}(t-t') \equiv \langle 0(\beta)|\,T\, \xi^{\alpha}_{nm}(t)\, \xi^{\dagger\gamma}_{nm'}(t')\,|0(\beta)\rangle\ . \tag{7.53}$$

It is convenient to define a renormalized f-electron propagator at site n, $\mathcal{S}^{L}_{nff}(\omega)$, in which self–energies are corrected by lattice effects, but having all of these self–energies entered directly by the f–line, without first changing into a c-electron. That is $\mathcal{S}^{L}_{nff}$ will contain Σ_T and Σ_{ff}, but not Σ_{fc}. (See section 7.1.1.) Note that this is not the same as $\mathcal{S}^{L}_{n}$ the completely lattice–renormalized f–electron propagator at site n.

We define:

$$\mathcal{S}^{L}_{nff}(\omega) \equiv S^{L}_{nff}(\omega)\,\Gamma^{L}_{n}(\omega)\,\langle P_o\rangle_{R}\ , \tag{7.54}$$

where:
$$\bar{S}^{L}_{nff}(\omega) \equiv \frac{1}{\omega - \varepsilon_f - \Sigma^{L}_{nT} - \Sigma^{L}_{nff}(\omega)}\ , \tag{7.55}$$

and
$$\Gamma^L_n(\omega) \equiv \Gamma^L_{nT} + \Gamma^L_{nN}(\omega) \ . \tag{7.56}$$

The self energies and starting-point functions are defined in analogy to the single-site case. That is, Σ^L_{nT}, $\Sigma^L_{nff}(\omega)$, Γ^L_{nT}, and $\Gamma^L_{nN}(\omega)$ are composed of Σ_T, $\Sigma_{ff}(\omega)$, Γ_T, and $\Gamma_N(\omega)$ at site n (see section 7.1.1) with all possible lattice corrections. Some of these lattice corrections are illustrated in FIG. 7.20.

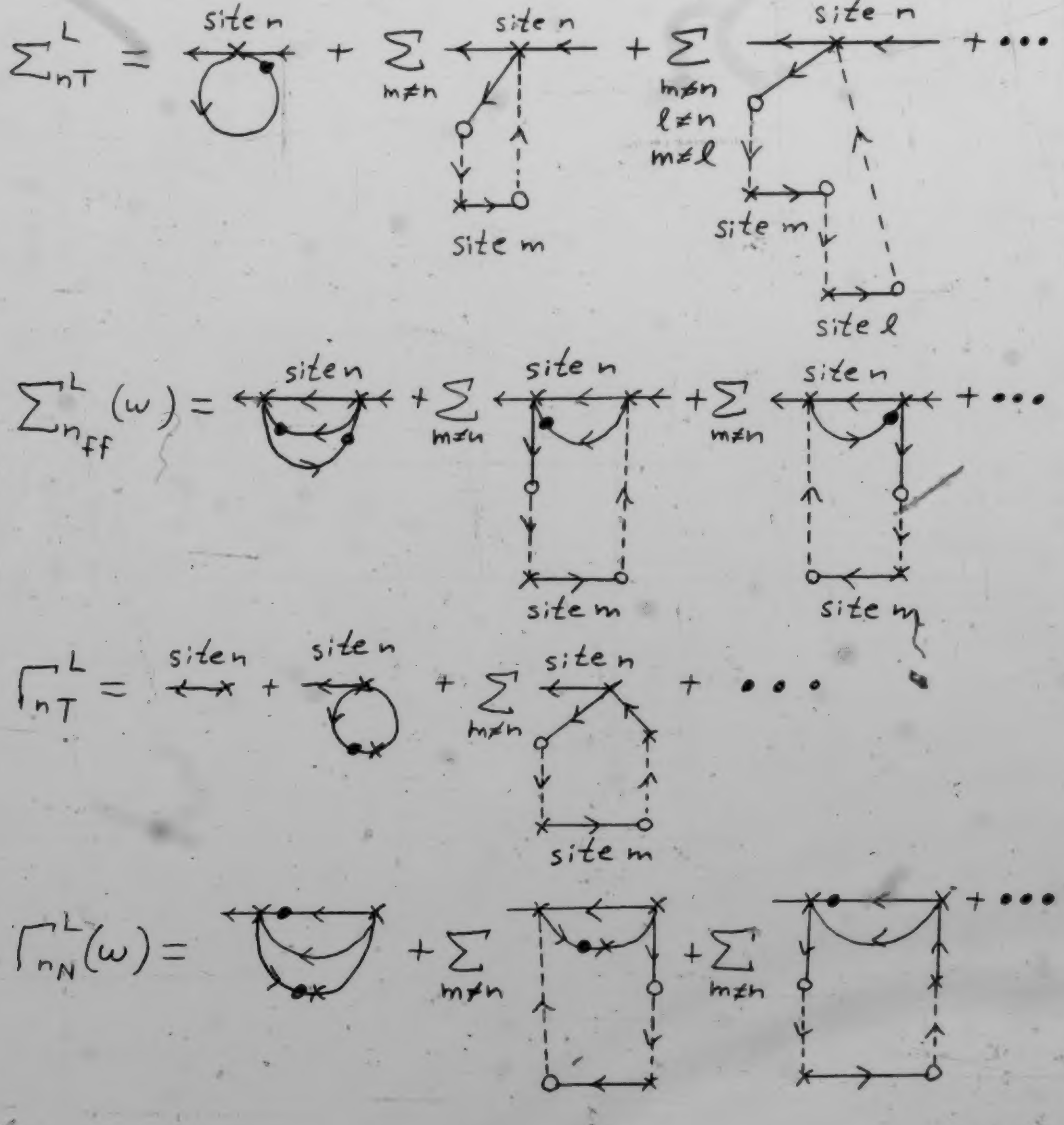
Σ^L_{nT} =
site n
+ Σ m≠n
site n
site m
+ Σ m≠n ℓ≠n m≠ℓ
site n
site m
site ℓ
+ •••
$\Sigma^L_{n_{ff}}(\omega)$ =
site n
+ Σ m≠n
site n
site m
+ Σ m≠n
site n
site m
+ •••
Γ^L_{nT} =
site n
+
site n
+ Σ m≠n
site n
site m
+ •••
$\Gamma^L_{n_N}(\omega)$ =
+ Σ m≠n
+ Σ m≠n
+ •••

FIG. 7.20

Lattice Corrections

This shows some of the lattice corrections to the self-energies and starting-point function. Note the restrictions on the summations.

FIG. 7.20 shows that there are certain summation rules which must be obeyed. For example, consider the third term of Σ^L_{nT}. If $\ell = m$, one has a single-site renormalization of the f-electron propagator at site m. Presumably, this renormalization would be counted as part of the regular single-site renormalization and not the lattice renormalization. Therefore, the sum has been restricted to $\ell \neq m$, in order to avoid double-counting.

As in the single-site case, we also define an f-connected propagator $S^{cL}_n(\omega)$ as follows:

$$S^{cL}_n(\omega) \equiv \frac{1}{\omega - \varepsilon_f - \Sigma^L_{nT} - \Sigma^{cL}_{nff}(\omega)}, \qquad (7.57)$$

where $\Sigma^{cL}_{nff}(\omega)$ is composed of $\Sigma^c_{ff}(\omega)$ at site n (see section 7.1.1), with all possible lattice corrections.

These renormalized propagators are represented diagrammatically in FIG. 7.21.

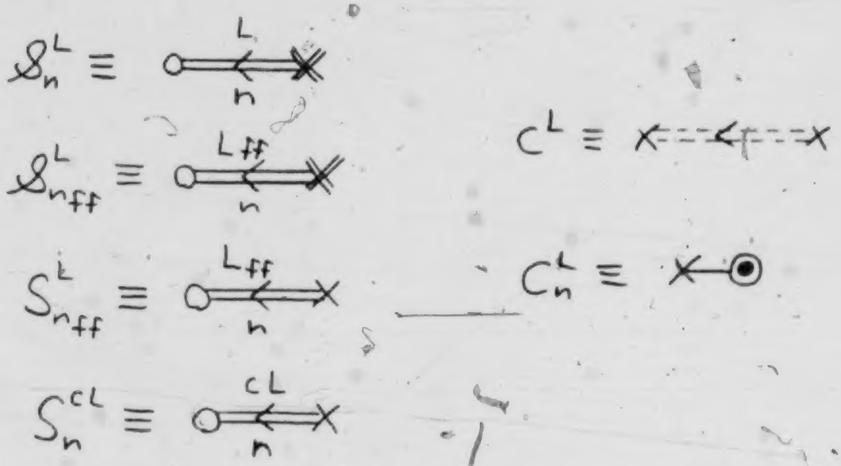

FIG. 7.21
Diagrammatic Representation of the Renormalized Propagators

7.4.4 THE LATTICE DYSON EQUATIONS

The completely lattice renormalized c-electron propagator $C^L(\omega)$ is related to $\mathcal{S}^L_{nff}(\omega)$ via the Dyson equation illustrated in FIG. 7.22.

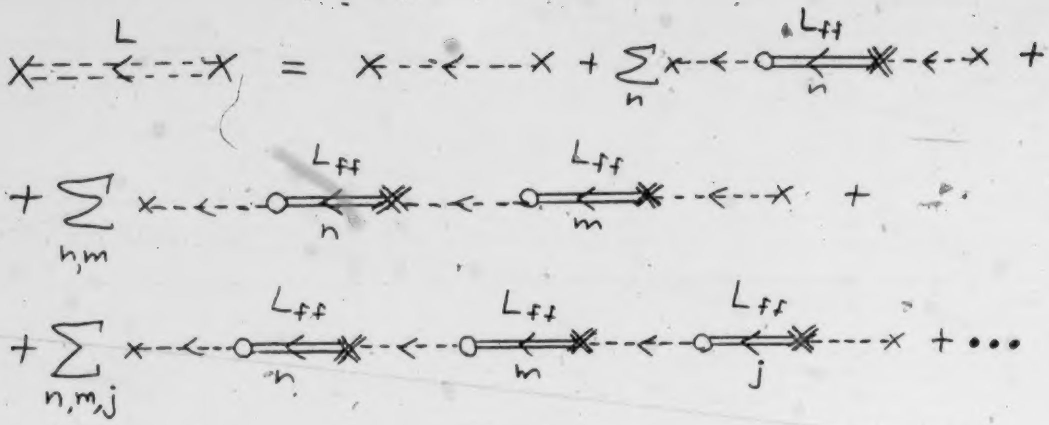

FIG. 7.22

The Dyson Equation for C^L

Note that this is expressed in terms of $\mathscr{S}^L_{nff}$, rather than $\mathscr{S}^L_n$. Note also that there are no restrictions on the summations.

Noteworthy is the absence of summation restrictions in FIG. 7.22. That is, we are summing over all n, m, j ... with no worries about excluding n = m, n = j, m = j, or others. The reason is that these terms will contribute a Σ_{fc} self-energy to the f-electron propagator. Now it becomes clear why $\mathscr{S}^L_{nff}$ was defined, and why C^L is expressed in terms of it, rather than being expressed in terms of $\mathscr{S}^L_n$. *$\mathscr{S}^L_{nff}$ contains no Σ_{fc} terms, and the absence of summation restrictions in* FIG. 7.22 *restores Σ_{fc} terms.* As the number of lattice sites becomes infinite we expect that all Σ_{fc} self-energy diagrams will be accounted for.

Writing the Dyson equation explicitly:

$$C^L(\omega;\vec{x},\vec{y}) = C(\omega,\vec{x}-\vec{y}) + \frac{2}{N}V^2\,\Omega\sum_n C(\omega,\vec{x}-\vec{x}_n)\,\mathscr{S}^L_{nff}(\omega)\,C(\omega,\vec{x}_n-\vec{y}) +$$
$$+ \left[\frac{2}{N}\right]^2 V^4\,\Omega^2\sum_{nn'} C(\omega,\vec{x}-\vec{x}_n)\,\mathscr{S}^L_{nff}(\omega)\,C(\omega,\vec{x}_n-\vec{x}_{n'})\,\mathscr{S}^L_{n'ff}(\omega)\,C(\omega,\vec{x}_{n'}-\vec{y}) +$$
$$+ \cdots \tag{7.58}$$

From this, we may also write the Dyson equation for $C^L_n(\omega)$, as follows:

$$C_n^L(\omega) = C_n(\omega) + \frac{2}{N} V^2 \Omega^2 \sum_{n'} C(\omega, \ell_n - \ell_{n'}) \mathcal{S}^L_{n'ff}(\omega) C(\omega, \ell_{n'} - \ell_n) +$$

$$+ \left[\frac{2}{N}\right]^2 V^4 \Omega^3 \sum_{n'n''} C(\omega, \ell_n - \ell_{n'}) \mathcal{S}^L_{n'ff}(\omega) C(\omega, \ell_{n'} - \ell_{n''}) \mathcal{S}^L_{n''ff}(\omega) C(\omega, \ell_{n''} - \ell_n) +$$

$$+ \ldots \tag{7.59}$$

Diagrammatic analysis shows that the completely lattice–renormalized, single–site f–electron propagator $\mathcal{S}^L_n(\omega)$ is related to $C^L_n(\omega)$ and $\mathcal{S}^L_{nff}(\omega)$ through the following Dyson equation:

$$\mathcal{S}^L_n(\omega) = \mathcal{S}^L_{nff}(\omega) + \frac{2}{N} V^2 S^L_{nff}(\omega) \Gamma^L_n(\omega) C^L_n(\omega) \mathcal{S}^L_{nff}(\omega) . \tag{7.60}$$

There are no more terms; $\mathcal{S}^L_{nff}$ accounts for all possible lattice corrections to Σ_{ff}, and C^L_n accounts for all possible lattice corrections to Σ_{fc}.

When we define:

$$\mathcal{S}^L_n(\omega) \equiv S^L_n(\omega) \Gamma^L_n(\omega) \langle P_o \rangle_\ell , \tag{7.61}$$

eq. (7.60) becomes:

$$S^L_n(\omega) = S^L_{nff}(\omega) + \frac{2}{N} V^2 S^L_{nff}(\omega) \Gamma^L_n(\omega) C^L_n(\omega) S^L_{nff}(\omega) , \tag{7.62}$$

where $S^L_{nff}(\omega)$ is given by eq. (7.55).

We have reduced the problem to a calculation of Σ^L_{nT}, Σ^L_{nff}, Γ^L_{nT}, Γ^L_{nN}, and Σ^{cL}_{nff}. These will give the propagators S^L_{nff}, $\mathcal{S}^L_{nff}$, S^L_n, $\mathcal{S}^L_n$, S^{cL}_n, C^L_n, and, ultimately, C^L, which determines the electrical properties of the metal.

7.4.5 A PROBLEM: HIDDEN SUMMATION RESTRICTIONS

In the Dyson equations, we claim to have removed the sector structure, and the summation rules, rendering the expressions Fourier transformable, and therefore easily calculable. This is not entirely true.

Take, for example, eq. (7.58). When $n = m$ in the second summation, we claim to get a Σ_{fc} renormalization of the f-electron propagator at site n. This is true, but there is an extra factor of $\langle P_o \rangle_\ell$, because $\langle P_o^2 \rangle_\ell \neq \langle P_o \rangle_\ell^2$.

That is, there is a summation restriction which should read, "When $n = m$, divide the expression by $\langle P_o \rangle_\ell$."

There is no easy way around this problem other than to ignore it. We may expect a large error to be induced because this has the effect of saying $\langle P_o \rangle_\ell \simeq 1$, when we know that $\langle P_o \rangle_\ell$ should be of $O(1/N)$ in the Kondo regime. We may expect that this "approximation" will illustrate the itinerant coherence effects while diminishing the localized Kondo effects.

7.4.6 LATTICE DIAGRAMMATICS TO THREE–LOOP ORDER

The tadpole diagrams have the following form:

$\Sigma^L_{nT} =$ 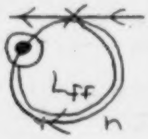 , (7.63)

$\Gamma^L_{nT} =$ 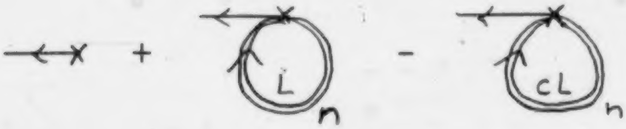 . (7.64)

Eq. (7.63) uses $S^L_{nff}(\omega)$ because the renormalized dot carries all Σ_{fc}'s. But eq. (7.64) uses S^L_n because there is no dot, necessitating the use of the complete propagator. Then we must subtract off the f-connected part S^{cL}_n, because f-connected loops are not allowed by the Feynman rules.

The expansions of of $\Sigma^L_{nff}(\omega)$, $\Gamma^L_{nN}(\omega)$, and $\Sigma^{cL}_{nff}(\omega)$ to three–loop order are similarly given by eqs. (7.11) – (7.13) for $\Sigma_{ff}(\omega)$, $\Gamma_N(\omega)$, and $\Sigma^c_{ff}(\omega)$, using the transformations given in FIG. 7.23.

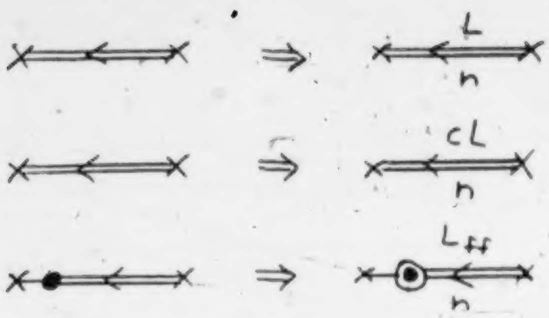

FIG. 7.23

Transformations Which Turn Single-Site Diagrams into Lattice Diagrams

7.4.7 THE ONE-LOOP SELF-CONSISTENT LATTICE CALCULATION

Performing the Fourier transform over the lattice in eq. (7.58), one obtains:

$$\check{C}^{L11}(\omega,\vec{k}) = \frac{1}{\omega - \varepsilon(\vec{k}) - \frac{2}{N} V^2 \mathcal{G}^{L11}_{ff}(\omega) + i\delta} , \qquad (7.65)$$

where $\varepsilon(\vec{k}) = |\vec{k}|^2/2m_e$.

The completely lattice–renormalized single–site c–electron propagator becomes:

$$\check{C}^L_n(\omega) = \Omega \int_{\Omega} \frac{d^3k}{(2\pi)^3} \, \check{C}^L(\omega,\vec{k}) . \qquad (7.66)$$

Using the flat band approximation, as in eq. (6.22), one obtains:

$$\check{C}^L_n(\omega) = N(0) \int_{-D_-}^{D_+} d\varepsilon \; \check{C}^L(\omega,\varepsilon) . \qquad (7.67)$$

The f–electron propagators become:

$$\mathcal{G}^L_{ff}(\omega) = \check{S}^L_{ff}(\omega) \, \Gamma^L_T \langle P_o \rangle_R , \qquad (7.68)$$

$$\check{S}^{L11}_{ff}(\omega) = \check{S}^{cL}(\omega) = \frac{1}{\omega - \tilde{\varepsilon}^L_f + i\delta} , \qquad (7.69)$$

$$\check{S}^{L11}(\omega) = \frac{1}{\omega - \tilde{\varepsilon}^L_f + i\delta} \left[1 + \frac{\frac{2}{N} V^2 \, \Gamma^L_T \, \check{C}^{L11}_o(\omega)}{\omega - \tilde{\varepsilon}^L_f + i\delta} \right] , \qquad (7.70)$$

where:
$$\tilde{\varepsilon}_f^L \equiv \varepsilon_f + \Sigma_T^L . \tag{7.71}$$

Using eqs. (7.68) and (7.69) in eq. (7.65), and separating the poles, one finds:

$$\bar{C}^{L11}(\omega,\varepsilon) = \left\{ \frac{Z_+(\varepsilon)}{\omega - \tilde{\varepsilon}_+(\varepsilon) + i\delta} + \frac{Z_-(\varepsilon)}{\omega - \tilde{\varepsilon}_-(\varepsilon) + i\delta} \right] , \tag{7.72}$$

where:
$$Z_\pm(\varepsilon) \equiv \frac{1}{2}\left[1 \pm \frac{\varepsilon - \tilde{\varepsilon}_f^L}{\sqrt{(\varepsilon - \tilde{\varepsilon}_f^L)^2 + a^2}} \right] , \tag{7.73}$$

$$\tilde{\varepsilon}_\pm(\varepsilon) \equiv \frac{1}{2}\left[(\varepsilon + \tilde{\varepsilon}_f^L) \pm \sqrt{(\varepsilon - \tilde{\varepsilon}_f^L)^2 + a^2} \right] , \tag{7.74}$$

$$a^2 \equiv \frac{8}{N} V^2 \Gamma_T^L \langle P_o \rangle_R \quad ; \quad \Gamma_T^L > 0 . \tag{7.75}$$

This is consistent with the renormalized band structure of Brandow discussed in sect. 1.8.4. Noting that we normalize V^2 by a factor of 2/N, eqs. (7.74) and (7.75) become identical to eqs. (1.36) and (1.37b), with an extra factor of Γ_T^L. This seems to agree with Kuramoto's XNCA discussed in sect. 1.8.5, where the renormalization factor is considerably smaller than $\langle P_o \rangle_R$. (Γ_T^L/N is small but finite, as will be shown below.)

7.4.8 NUMERICAL RESULTS OF THE LATTICE CALCULATION

Let us assume $|\varepsilon_f| << D_\pm$, and $\beta D_\pm >> 1$. If we further assume $a^2 << D_\pm^2$, then we may approximate:

$$\tilde{\varepsilon}_+(-D_-) = \tilde{\varepsilon}_f^L + b_+ \quad ; \quad \tilde{\varepsilon}_-(D_+) = \tilde{\varepsilon}_f^L - b_- \quad ; \tag{7.76}$$

$$b_+ \simeq \frac{a^2}{4D_-} \quad ; \quad b_- \simeq \frac{a^2}{4D_+} . \tag{7.77}$$

If $D_+ = D_- \equiv D$, such that $b_+ = b_- = b$, then:

$$b = \frac{a^2}{4D} = \frac{4\Delta}{\pi N} \Gamma_T^L \langle P_o \rangle_R . \tag{7.78}$$

In any case, we have a band gap of $b_+ + b_-$, which is approximately given by twice eq. (7.78).

With this band gap, the spectral function of C_n^L becomes:

$$\sigma^L_{c_n}(\omega) = N(0)\left\{\left[\theta(D_+ - \omega) - \theta(-D_- - \omega)\right] + \right.$$
$$\left. - \left[\theta(b_+ - (\omega - \tilde{\varepsilon}^L_f)) - \theta(-b_- - (\omega - \tilde{\varepsilon}^L_f))\right]\right\} \qquad (7.79)$$

That is, the site-localized conduction electron spectral function is flat, except for a gap of width $b_+ + b_-$ centred on $\omega = \tilde{\varepsilon}^L_f$.

The spectral function of the f-electron propagator S^L becomes:

$$\sigma^L_S(\omega) = \left[\frac{2}{N}\frac{\Delta}{\pi}\Gamma^L_T\right]\frac{1 - [\,\theta(b_+ - (\omega - \tilde{\varepsilon}^L_f)) - \theta(-b_- - (\omega - \tilde{\varepsilon}^L_f))\,]}{(\omega - \tilde{\varepsilon}^L_f)^2} \qquad (7.80)$$

That is, the f-electron state density has a two-peak structure with a gap of width $b_- + b_+$ centred on $\omega = \tilde{\varepsilon}^L_f$. Again this agrees qualitatively with Brandow's result, discussed in sect. 1.8.4, where he also found a two-peak structure for the f-electron propagator.

Assuming $D_+ = D_- \equiv D$ (so that $b_+ = b_- \equiv b$), and performing the loop integrals, one obtains two coupled self-consistent equations for $\tilde{\varepsilon}^L_f$ and Γ^L_T:

$$\tilde{\varepsilon}^L_f = \varepsilon_f + 2\left[\frac{N-1}{N}\right]\frac{\Delta}{\pi}\left\{ \ln\left[\frac{\beta(D+\mu)}{2\pi}\right] - \mathcal{R}e\,\psi\left[\frac{1}{2} - \frac{i\beta}{2\pi}(\tilde{\varepsilon}^L_f - \mu)\right] + \right.$$
$$\left. - \frac{1}{2}\int_0^{\frac{\beta b}{2}} \frac{d\omega}{\omega}\left[\tanh\left[\omega + \frac{\beta(\tilde{\varepsilon}^L_f - \mu)}{2}\right] + \tanh\left[\omega - \frac{\beta(\tilde{\varepsilon}^L_f - \mu)}{2}\right]\right]\right\}, \qquad (7.81)$$

$$\Gamma^L_T = 1 - 2\left[\frac{N-1}{N}\right]\frac{\Delta}{\pi}\Gamma^L_T\left\{\frac{\beta}{2\pi}\mathcal{I}m\,\psi'\left[\frac{1}{2} - \frac{i\beta}{2\pi}(\tilde{\varepsilon}^L_f - \mu)\right] + \right.$$
$$+ \frac{1}{b}\left[f_F(\tilde{\varepsilon}^L_f - \mu + b) - f_F(\tilde{\varepsilon}^L_f - \mu)\right] - \frac{1}{b}\left[f_F(\tilde{\varepsilon}^L_f - \mu) - f_F(\tilde{\varepsilon}^L_f - \mu - b)\right] +$$
$$\left. + \frac{\beta}{4}\int_0^{\frac{\beta b}{2}} \frac{d\omega}{\omega}\left[\mathrm{sech}^2\left[\omega + \frac{\beta(\tilde{\varepsilon}^L_f - \mu)}{2}\right] - \mathrm{sech}^2\left[\omega - \frac{\beta(\tilde{\varepsilon}^L_f - \mu)}{2}\right]\right]\right\} \qquad (7.82)$$

The numerical calculations have been done, yielding results very similar to the single-site case. For example, there exist three solutions,

$\tilde{\varepsilon}^L_{f1} < \tilde{\varepsilon}^L_{f2} < \tilde{\varepsilon}^L_{f3}$, having very similar properties to $\tilde{\varepsilon}_{f1}$, $\tilde{\varepsilon}_{f2}$, and $\tilde{\varepsilon}_{f3}$. In fact, when $N \rightarrow \infty$ in both the single–site and lattice equations, assuming Γ^L_T and Γ_T remain finite, eqs. (7.81) and (7.82) become identical to eqs. (7.19) and (7.20), yielding identical solutions: $\tilde{\varepsilon}_{f1} = \tilde{\varepsilon}^L_{f1}$ and $\tilde{\varepsilon}_{f3} = \tilde{\varepsilon}^L_{f3}$.

Of course, the solution of interest is #2, for which $\Gamma^L_T \rightarrow \infty$ as $N \rightarrow \infty$ in such a way that Γ^L_T/N remains finite. When $\Delta < \Delta_M$ and $T << T_{23}$ we have the following approximate solutions:

$$b \simeq D e^{-\pi|\varepsilon_f-\mu|/2\Delta} , \tag{7.83}$$

$$\frac{\Gamma^L_{T2}}{N} \simeq \frac{\pi D}{4\Delta} e^{-\pi|\varepsilon_f-\mu|/2\Delta} \langle P_o \rangle_R^{-1} , \tag{7.84}$$

$$\tilde{\varepsilon}^L_{f2} - \mu \simeq -\frac{\pi b}{\Delta\beta} = -\frac{\pi D}{\Delta\beta} e^{-\pi|\varepsilon_f-\mu|/2\Delta} , \tag{7.85}$$

where

$$k_B T_{23} \simeq \frac{2e^{\gamma}}{\pi} D e^{-\pi|\varepsilon_f-\mu|/2\Delta} . \tag{7.86}$$

As in the single–site case, this calculation shows the correct Kondo temperature ($T_{23} \simeq T_K$).

The band renormalization factor a^2 becomes:

$$a^2 = \frac{2\pi V^2}{\Delta} k_B T_K = 4 k_B T_K D . \tag{7.87}$$

Comparing this result to Brandow's result, we find that $\langle P_o \rangle_R$ has been replaced by $\frac{\pi}{2\Delta} k_B T_K$.

7.4.9 THE CHEMICAL POTENTIAL

As was pointed out in sect. 1.8.2, the position of the Fermi surface will be renormalized in the lattice case. This will manifest itself as a renormalization of the chemical potential, as discussed in sect. 6.1.2. Because we do not have the $\langle P_1 \rangle$ sector, and the $\langle P_1 \rangle$ sector is essential to the spectral weight, we cannot actually calculate this renormalization. But, eqs. (7.81) and (7.82) indicate that, whatever the size of μ, $\tilde{\varepsilon}^L_f - \mu$ will be the object calculated. In fact, eq. (7.85) indicates that solution #2 is "locked" onto the Fermi surface, wherever this Fermi surface might be.

7.4.10 THE MASS ENHANCEMENT

Let us assume that $\Delta < \Delta_K$. When $T > T_K$, only solution #1 exists. The f-electron band gap and hybridization effects are well below the Fermi surface, so one may expect the metal to behave normally. When $T < T_K$, we choose solution #2. This means that there will be a phase transition at the Kondo temperature, and the band gap and hybridization effects will suddenly become important.

Eq. (7.85) indicates that $\tilde{\varepsilon}^L_{f2}$ is very close to the Fermi surface, and hence, the band gap is centred on the Fermi surface. Thus, as $T \to 0$, the lower band $\tilde{\varepsilon}_-(\varepsilon)$ is completely filled, and the upper band $\tilde{\varepsilon}_+(\varepsilon)$ is completely empty. It is therefore the electrons at the top of $\tilde{\varepsilon}_-(\varepsilon)$ which are important to the electrical properties of the metal. The effective mass of these electrons is given by:

$$\frac{m^*}{m} = \left[\left. \frac{d\,\tilde{\varepsilon}_-(\varepsilon)}{d\varepsilon} \right|_{\varepsilon = D} \right]^{-1} \tag{7.88}$$

Therefore

$$\frac{m^*}{m} \simeq \frac{4D^2}{a^2} \simeq \frac{D}{k_B T_K} \simeq e^{\pi|\varepsilon_f - \mu|/2\Delta} \tag{7.89}$$

Suppose we use Kuramoto's parameters [34]: $D = 10^4$ K and $\varepsilon_f - \mu = -1200$ K. If we wish to have a Kondo temperature of $T_K = 10$ K, then we must choose $\Delta/|\varepsilon_f - \mu| = 0.223334$, and we find $m^*/m = 1134$. If we wish to have $T_K = 15$ K, then we choose $\Delta/|\varepsilon_f - \mu| = 0.236997$, and we find $m^*/m = 756$. These mass enhancements are the correct size!

In spite of ignoring the $\langle P_1 \rangle$ sector, and violating hidden summation rules, the result turned out surprisingly well. The size of the renormalization factor $a^2/4V^2$ agrees with Kuramoto's a_f, introduced in sect. 1.8.5 (even though the specific form of these factors is different). This is surprising, because Kuramoto's result was derived in the Kondo regime, where $\langle P_o \rangle_R << 1$, whereas our result is valid only when $\langle P_o \rangle_R \simeq 1$, as described in sect. 7.4.5. In fact Kuramoto and Brandow both find $a_f = \langle P_o \rangle_R << 1$ to zeroth order in $1/N$ (see sect. 1.8.5), which is more cause for bemusement.

Like the contradictions appearing in the single-site case, the ultimate source of the problems in the $\langle P_1 \rangle$ sector. We cannot actually calculate $\langle P_o \rangle_R$ unless we keep the $\langle P_1 \rangle$ sector. But the $\langle P_1 \rangle$ sector is hopelessly complicated.

CHAPTER 8
CONCLUSION

8.1 SUMMARY OF THIS THESIS

Travelling into the uncharted frontier is always dangerous. The quantum algebra journey followed a path fraught with peril and often impassible.

At the trail head was a method, for examining the spin $\frac{1}{2}$ Anderson model, invented by Matsumoto and Umezawa, called "thermo field dynamics of a quantum algebra", and its purported extension to the N-fold degenerate case by Whitehead, Matsumoto, and Umezawa. Shortly thereafter came the discovery of non-cancelling vacuum diagrams, also by Whitehead, Matsumoto, and Umezawa. Beyond this was the unknown.

At the beginning of chapter 3 came the ominous sign that canonical quantization itself was broken, indicating the need to rework all of quantum field theory from the ground up. This process started with finding an annihilation operator, and making a generalized Wick's theorem. Then came the first peril: zero-energy boson eigenoperators for which this generalized Wick's theorem breaks down.

Following this, a study, of how non-cancelling vacuum diagrams arise in a quantum algebra, revealed the second peril: vacuum diagrams in the presence of zero-energy boson eigenoperators which are noncommuting. The pioneering work of Whitehead, Matsumoto, and Umezawa, which nicely demonstrated the effect of vacuum diagrams when the zero-energy boson eigenoperators are mutually commuting, was realized to be hopelessly inadequate when dealing with the Anderson model.

Taking it slowly, chapter 4 gave a thorough and detailed account of a precursor to the Anderson model. This precursor had no interaction

Hamiltonian, and no conduction electrons. It was simply a single, localized, N-fold degenerate fermionic state, restricted to a maximum occupancy of one fermion. And yet it was found to be incredibly complicated. There were two sectors, the $\langle P_o \rangle$ sector and the $\langle P_1 \rangle$ sector, having different Feynman rules. By careful consideration, it was realized that the three sector structure of Matsumoto, Umezawa, and Whitehead was an unnecessary complication that would only lead to trouble when considering the vacuum diagrams.

Spontaneous vertices were found, due to the quantum algebra, which arise in the absence of any interaction.

Next came the reduction of the zero-energy boson eigenoperator T-product, for which the generalized Wick's theorem breaks down. This was done using Matsumoto's ingenious method of time-splitting. It was found that the time-splitting method was incorrectly applied in Matsumoto, Umezawa, and Whitehead's extension of the spin 1/2 case to the N-fold degenerate case. The Feynman rules were found to be horrendously complicated, due to the nature of the SU(N) group. A method of reduction was found without the SU(N) group. The rules are intuitively simpler, but intractable in any practical calculation, because all possibility of a self-energy expansion in the $\langle P_1 \rangle$ sector is blocked. There are no one-particle irreducible diagrams in the $\langle P_1 \rangle$ sector. Everything is multiply connected by a tangled undergrowth of impassible linear chains having an arbitrary number of vertices in each link. And all this without any interaction! The only saving grace of the SU(N) rules is that they may be expressed in terms of broken chains which *might* lend themselves to a self-energy expansion. Both schemes were presented in chapter 4, and incredibly complex, yet systematic, Feynman rules were given.

Having developed a methodology for reducing the zero-energy boson T-product, it was time to face the next uncompromising peril: vacuum diagrams. Gently easing into it, chapter 5 considered the model of chapter 4 with a very elementary interaction term added to it: a simple shift of energy. Of course, the solution is exactly known. The trick was to make perturbation theory reproduce this solution. It was found that the non-cancelling vacuum diagrams at $\mathcal{R}e\, t = \pm\infty$ are essential, in order to renormalize the expectation value of the sector projection operators.

This result was not without its technical snags. It was found that the effects of the time evolution operators at $\mathcal{R}e\, t = \pm\infty$ must be determined before the time-splitting is performed. Such a determination could be done in this case because all the zero-energy boson eigenoperators are mutually commuting. Such a determination cannot be done in general, when the zero–energy boson eigenoperators do not commute (such as in the Anderson model itself). In this case, the reduction of zero–energy boson eigenoperators at $\mathcal{R}e\, t = \pm\infty$ cannot be separated from the reduction of zero-energy boson eigenoperators at finite time. This has the effect of connecting the "vacuum diagrams" to the main diagrams in the $\langle P_1 \rangle$ sector. The entanglement of the $\langle P_1 \rangle$ sector was thus found to be worse than previously imagined.

Forging deeper into the uncharted frontier, chapter 6 carefully and thoroughly considered the single-site Anderson model itself. Chemical potentials were kept explicit. A particle/hole sum rule was derived, which must be satisfied if the result is to be physical. Clues were obtained from the Heisenberg equations and the Bethe-Salpeter equations. The Feynman rules were laid out. After much consideration, it was found that the vacuum diagrams at $\mathcal{R}e\, t = \pm\infty$ can be extricated from the tangled web, disentangled and disconnected. But then another problem arose. The regular finite-t vacuum diagrams were not disconnected in the $\langle P_1 \rangle$ sector. Furthermore, the methods used to disconnect the $\mathcal{R}e\, t = \pm\infty$ vacuum diagrams would not work on the finite-t vacuum diagrams. Using the SU(N) rules, a partial disconnection was found, in which some of the vacuum diagrams go into renormalizing the chains, which arise from the zero-energy boson reduction. The rest of the vacuum diagrams factorize, yielding the desired projection operator renormalization. (This last result is not certain.) It therefore appears that the vacuum diagrams serve the purpose of renormalizing the sector projection operator expectation values, as in chapter 5. A method was found for self-consistently solving for these renormalized projection operator expectation values.

Chapter 7 presents the results of the method of thermo-field dynamics of a quantum algebra, applied to the Anderson model. In the $\langle P_o \rangle$ sector, a self-energy expansion was found. These self-energies are classified according to their topological classes. There is also a "starting point function", which connects right to the starting point of the f-electron propagator itself. Self-consistent Dyson equations were given to 3–loop order. The order $1/N^0$ approximation was found to coincide with the 1-loop self-consistent approximation. This 1-loop self-consistent calculation was performed, yielding two coupled self-consistent equations.

As usual, the $\langle P_1 \rangle$ sector remains noncompliant. No self-energy expansion could be found. A scheme was proposed for calculating the order $1/N^0$ approximation. This involved an infinite sum of loop diagrams up to infinite order. The result would be a very complicated integral expression which must be solved numerically. It was not done.

The $\langle P_1 \rangle$ sector was ignored, with the expectation that the desired Kondo behaviour would come from the $\langle P_o \rangle$ sector. Numerical solutions of the coupled self-consistent equations were plotted versus temperature. Indeed, it was found that at T_K the usual Kondo temperature, there is a phase transition in which a resonance of width $k_B T_K$ forms at the Fermi surface. It was found that this solution is well within unitary limits. These positive features were offset by the fact that the Friedel sum rule was violated, and so was the particle/hole sum rule. It was concluded that these problems arose due to neglecting the $\langle P_1 \rangle$ sector.

A curious feature of this solution came to light when comparing it to the results of Coleman's slave boson method. Namely, my solution, which was supposed to restrict the single-site occupancy to a maximum of one, corresponded exactly to Coleman's mean field solution for a macroscopic single-site occupancy of $\sim N/2$, where $N \to \infty$. It was concluded that this artifact was probably due to the Friedel sum rule violation, rather than being due to an actual site-occupancy violation.

Next, the lattice Anderson model was presented. It was found to be a direct extension of the single-site model, with the two-sector structure now at every localized lattice site. Keeping track of sector indices for each site in the lattice is a formidable problem, which inhibits the Fourier transformability. This gave even further incentive to ignore the $\langle P_1 \rangle$ sector, keeping only the $\langle P_0 \rangle$ sector.

Site summation restrictions were also found to interfere with the Fourier transformability. A method was devised by which these site summation restrictions were apparently removed. Closer examination revealed that there were still "hidden" site summation restrictions. It was found that these restrictions disappear only when $\langle P_0 \rangle_\ell \simeq 1$. The fact that one expects $\langle P_0 \rangle_\ell << 1$ in the Kondo regime is bad news, but the calculation was proceeded with in spite of this.

As in the single-site case, self-energies and a "starting point function" were found and classified. Self-consistent Dyson equations were given to

3-loop order. The 1-loop self-consistent calculation was performed, yielding a renormalized 2-band hybridization picture, in qualitative agreement with the methods discussed in section 1.8. Also in qualitative agreement was the f-electron spectral function, which had two peaks separated by a band gap.

Numerical calculations were performed, and a Kondo-like solution was found, although all quasi-particle widths remained equal to zero, in conformity with the Luttinger picture of sect. 1.8.3. The band renormalization parameter was found to be in partial agreement with Kuramoto's XNCA result (sect. 1.8.5), i.e. that it is considerably stronger than Brandow's renormalization parameter (sect. 1.8.4).

As in the single-site case, there is a finite temperature phase transition at $T = T_K$, the Kondo temperature. When $T > T_K$, the band gap is well below the Fermi surface and has no effect. When $T \leq T_K$, band gap is suddenly shifted to the Fermi surface, so that for very low T the upper band is almost completely empty and the lower band is almost completely full. This yields an expression for the ***effective mass enhancement***, which is the ***correct size.***

There is some confusion as to the magnitude of $\langle P_o \rangle_R$. If we want this calculation to be a good approximation, then we need $\langle P_o \rangle_R \simeq 1$, in order to remove the hidden site-summation restrictions. Conversely, if this calculation represents the standard Kondo regime, then we need $\langle P_o \rangle_R << 1$. It seems odd that the size of our effective mass enhancement agrees with Kuramoto's, when his results are only valid for $\langle P_o \rangle_R << 1$. Evidently, this contradiction comes from ignoring the $\langle P_1 \rangle$ sector.

8.2 REMARKS

What about the motivations expressed in sect. 1.9 ? I was hoping to establish the quantum algebra approach as a viable field theoretic tool. To this end I have not succeeded. Certainly, this work was original, and many previously unknown things were discovered. But this newly discovered knowledge is of a highly esoteric nature, even for theoretical physics. As to its practical utility, one seems to be at a nonplus until some of the tangled undergrowth in the $\langle P_1 \rangle$ sector falls to the scythe. Many results were obtained which agree with established results, but at what cost? The price is high, the results are few, there seems to be no amenable way to better the approximation, and the results break conditions which should not be broken.

What is the source of all this difficulty? Virtually all other authors either ignore the algebra, or they re-express it in a manner in which the occupied and unoccupied states are carried by two different propagators. With our method, the occupied and unoccupied states are carried by the same propagator. Which state is actually being propagated depends upon the particular time-ordering at any instant. This has been done in order to have a Feynman formalism.

Herein lies the source of all the difficulty: the dogmatic philosophy that Feynman diagrams are "good". The Anderson model is, at its heart, non-Feynman, and amenable to a fixed-time-ordering Goldstone type expansion. We have ***forced*** it into a Feynman mode. But all the θ-functions are still there; they are hiding in the wiggle lines of the $\langle P_1 \rangle$ sector. In spite of our attempts to make it look Feynman-like, it retains its Goldstone-like nature. The system takes its revenge; the treacherous web of wiggle lines in the $\langle P_1 \rangle$ sector is its form of civil disobedience.

The details of the quantum algebra approach are preserved here for posterity. May this find a practical use someday. To my knowledge, nobody before has thoroughly dealt with quantum field theory in the context of an algebra. This thesis has done so in an honest, thorough, and exhaustive manner. I've gone where no man has gone before. At the trail head, I feel obliged to post this warning, "Enter at Your Own Risk."

REFERENCES

1. F. Steglich, J. Aarts, C.D. Bredl, W. Lieke, D. Meschede, W. Franz, and J. Schäfer, Phys. Rev. Lett. 43, 1892 (1979).

2. G.R. Stewart, "Heavy Fermion Systems", Rev. Mod. Phys. 56, 755 (1984).

3. H.R. Ott, H. Rudigier, Z. Fisk, and J.L. Smith, Phys. Rev. Lett. 50, 1595 (1983).

4. G.R. Stewart, Z. Fisk, J.O. Willis, and J.L. Smith, Phys. Rev. Lett. 52, 679 (1984).

5. H.H. Hill, in "Plutonium 1970 and Other Actinides", edited by W.H. Miner, AIME, New York, 1970, pg. 2.

6. P.A. Lee, et al. "Theories of Heavy-Electron Systems", Comm. Cond. Matt. Phys. 12, 99 (1986)

7. J. Kondo, Prog. Theor. Phys. 32, 37 (1964).

8. J. Kondo, in "Solid State Physics", edited by F. Seitz, D. Turnbull, and H. Ehrenreich, Academic Press, New York, vol. 23 (1969).

9. S. Doniach, and E.H. Sondheimer, "Green's Functions for Solid State Physicists", W.A. Benjamin Inc., USA, 1974.

10. P.W. Anderson, "Basic Notions of Condensed Matter Physics", Benjamin/ Cummings, USA, 1984.

11. P.W. Anderson, Phys. Rev. 124, 41 (1961).

12. J.R. Schrieffer and P.A. Wolff, Phys. Rev. 149, 491 (1966).

13. J.G. Bednorz and K.A. Müller, Z. Phys. B 64, 189 (1986).

14. H. Takagi, S. Uchida, K. Kitazawa, and S. Tanaka, Jpn. J. Appl. Phys. Lett. 26, #2 (1987).

15. M.K. Wu, J.R. Ashburn, C.J. Torng, and P.H. Hor, R.L. Meng, L. Gao, Z.J. Huang, Y.Q. Wang, and C.W. Chu, Phys. Rev. Lett. 58, 908 (1987).

16. P.H. Hor, L. Gao, R.L. Meng, Z.J. Huang, Y.Q. Wang, K. Forster, J. Vassilious, C.W. Chu, M.K. Wu, J.R. Ashburn, and C.J. Torng, Phys. Rev. Lett 58, 911 (1987).

17. J. Hubbard, Proc. R. Soc. London, Ser. A, 277, 237 (1964).

18. F.D.M. Haldane, "Scaling Theory of the Asymmetric Anderson Model", Phys. Rev. Lett. 40, 416 (1978).

19. B. Coqblin and J.R. Schrieffer, Phys. Rev. 185, 847 (1969).

20. O. Gunnarson and K. Schonhammer, Phys. Rev. Lett. 50, 604 (1983).

21. K. Sur and T.V. Ramakrishnan, Phys. Rev. B 26, 1798 (1982).

22. J.W. Rasul and A.C. Hewson, J. Phys. C 17, 2555 (1984).

23. N. Read, "Role of Infrared Divergences in the 1/N Expansion of the U=∞ Anderson Model", J. Phys. C 18, 2651 (1985).

24. N. Read and D.M. Newns, "On the Solution of the Coqblin–Schrieffer Hamiltonian by the Large–N Expansion Technique", J. Phys. C 16, 3273 (1983).

25. P. Coleman, "New Approach to the Mixed Valence Problem", Phys. Rev. B 29, 3035 (1984).

26. N. Andrei, K. Furuya, and J.H. Lowenstein, Rev. Mod. Phys. 55, 331 (1983),

27. A.M. Tsvelick and P.B. Wiegmann, Adv. Phys. 32, 453 (1983).

28. A. Okiji and N. Kawakami, "Thermodynamic Properties of the Anderson Model", J. App. Phys. 55, 1931 (1984).

29. P. Schlottmann, "Thermodynamics of the SU(N) Anderson Impurity", Z. Phys. B 54, 207 (1984).

30. P. Schlottmann, "Bethe–Ansatz Solution of the Degenerate Anderson Model: Applications to Ce and Yb Impurity Systems", in ref. [31], pg. 68 (1985).

31. T. Kasuya and T. Saso, editors, "Theory of Heavy Fermions and Valence Fluctuations – Proceedings of the Eighth Taniguchi Symposium", Springer–Verlag, Berlin, 1985.

32. H. Keiter and J.C. Kimball, "Diagrammatic Perturbation Technique for the Anderson Hamiltonian, and the Relation to the s–d Exchange Hamiltonian", Int. J. Magn. 1, 233 (1971).

33. Y. Kuramoto, "Self–Consistent Perturbation Theory for Dynamics of Valence Fluctuations I", Z. Phys. B 53, 37 (1983).

34. H. Kojima, Y. Kuramoto, and M. Tachiki, "Self–Consistent Perturbation Theory for Dynamics of Valence Fluctuations II", Z. Phys. B 54, 293 (1984).

35. F.C. Zhang and T.K. Lee, "1/N Expansion for the Degenerate Anderson Model in the Mixed Valence Regime", Phys. Rev. B 28, 33 (1983).

36. N.E. Bickers, D.L. Cox, and J.W. Wilkins, "Thermodynamic, Transport, and Excitation Properties of Ce Impurities in a Model Metal: Kondo Resonance and Universality in the Mixed Valence Regime", Phys. Rev. Lett. 54, 230 (1985).

37. P. Coleman, "Modelling Mixed Valence Systems Using the Generalized Anderson Model", in ref. [31], pg. 163 (1985).

38. P. Coleman, "Mixed Valence as an Almost Broken Symmetry", Phys. Rev. B 35, 5072 (1987).

39. P. Coleman and N. Andrei, "Diagonalization of the Generalized Anderson Model", J. Phys. C 19, 3211 (1986).

40. K.G. Wilson, "The Renormalization Group: Critical Phenomena and the Kondo Problem", Rev. Mod. Phys. 47, 773 (1979).

41. P. Nozières, "A Fermi–Liquid Description of the Kondo Problem at Low Temperatures", J. Low Temp. Phys. 17, 31 (1974).

42. L.D. Landau, "The Theory of a Fermi Liquid", J. Exptl. Theoret. Phys. (U.S.S.R.) 30, 1058 (1956); Soviet Phys. – JETP 3, 920 (1957).

43. A.A. Abrikosov, L.P. Gorkov, and I.E. Dzyaloshinski, "Methods of Quantum Field Theory in Statistical Physics", Dover, New York, 1975.

44. D.M. Newns and A.C. Hewson, "A Local Fermi Liquid Theory of Intermediate Valence Systems", J. Phys. F 10, 2429 (1980).

45. D.C. Langreth, "Friedel Sum Rule for Anderson's Model of Localized Impurity States", Phys. Rev. 150, 516 (1966).

46. P. Coleman, private communication.

47. B.H. Brandow, "Variational Theory of Valence Fluctuations: Ground States and Quasiparticle Excitations of the Anderson Lattice Model", Phys. Rev. B 33, 215 (1986).

48. N.W. Ashcroft and N.D. Mermin, "Solid State Physics", Saunders College, Philadelphia, 1976.

49. J.M. Luttinger, "Fermi Surface and Some Equilibrium Properties of a System of Interacting Fermions", Phys. Rev. 119, 1153 (1960).

50. N. Grewe and H. Keiter, "Diagrammatic Approach to the Intermediate–Valence Compounds", Phys. Rev. B 24, 4420 (1981).

51. Y. Kuramoto, "Self–Consistent Perturbation Theory for Valence–Fluctuating Lattice Systems", in ref. [31], pg. 152 (1985).

52. N. Read and D.M. Newns, "Mean Field Solution to the Intermediate Valence Problem", Solid State Comm. 52, 993 (1984).

53. Assa Auerbach and K. Levin, "Slave Bosons and the Kondo Lattice: Microscopic Basis for the Heavy Fermi Liquid", Phys. Rev. Lett. 57, 877 (1986).

54. M. Roberts and K.W.H. Stevens, "A Green Function Method for the Intermediate Valence Model", J. Phys. C 13, 5941 (1980).

55. T. Koyama and M. Tachiki, "Heavy Fermion State in the Anderson Lattice", Phys. Rev. B 34, 3272 (1986).

56. H. Matsumoto and H. Umezawa, "Thermo Field Dynamics of a Quantum Algebra", Phys. Lett. 103A, 405 (1984).

57. H. Umezawa, H. Matsumoto, and M. Tachiki, "Thermo Field Dynamics and Condensed States", North–Holland, Amsterdam, 1982.

58. H. Matsumoto and H. Umezawa, "Anderson Model in Thermo Field Dynamics: Generalized Feynman–Diagram Method", Phys. Rev. B 31, 4433 (1985).

59. H. Matsumoto, H. Umezawa, and J.P. Whitehead, "Feynman Rules in the Anderson Model: Generalization to the (2J+1)–Component Case", J. Math. Phys. 27, 1711 (1986).

60. H. Matsumoto, H. Umezawa, and J.P. Whitehead, "Vacuum Diagrams in Perturbative Thermo Field Dynamics", Prog. Theor. Phys. 76, 260 (1986).

61. H. Umezawa, "Thermo Field Dynamics", U of A preprint, 1988.

62. H. Matsumoto, Y. Nakano, and H. Umezawa, "Tilde Substitution Law in Thermo Field Dynamics: Thermal State Conditions", Phys. Rev. D 31, 429 (1985).

63. H. Matsumoto, Y. Nakano, and H. Umezawa, "An Equivalence Class of Quantum Field Theories at Finite Temperature", J. Math. Phys. 25, 3076 (1984).

64. H. Matsumoto, in "Progress in Quantum Field Theory", Edited by H. Ezawa and S. Kamefuchi, Elsevier Science Publishers B. V., 1986.

65. E. Leader and E. Predazzi, "An Introduction to Gauge Theories and the 'New Physics' ", Cambridge University Press, Cambridge, 1982, Appendix A.

APPENDIX A
USEFUL FORMULAE

A.1 PROPERTIES OF PROPAGATORS AND U-MATRICES

GENERAL PROPAGATOR OF FERMIONS (F) OR BOSONS (B):

$$G_F(\omega;\mu) = U_F(\omega-\mu)\ \bar{G}_F(\omega)\ U_F^\dagger(\omega-\mu) \tag{A.1}$$

$$G_B(\omega;\mu) = U_B(\omega-\mu)\ \tau\ \bar{G}_B(\omega)\ U_B^\dagger(\omega-\mu) \tag{A.2}$$

$$\tau \equiv \begin{bmatrix} 1 & 0 \\ 0 & -1 \end{bmatrix} \tag{A.3}$$

THERMAL BOGOLIUBOV MATRICES:

$$U_F(\omega) = \frac{1}{\sqrt{e^{\beta\omega}+1}} \begin{bmatrix} e^{\beta\omega/2} & 1 \\ -1 & e^{\beta\omega/2} \end{bmatrix} \tag{A.4}$$

$$U_B(\omega) = \frac{1}{\sqrt{e^{\beta\omega}-1}} \begin{bmatrix} e^{\beta\omega/2} & 1 \\ 1 & e^{\beta\omega/2} \end{bmatrix} = U_B^\dagger(\omega) \tag{A.5}$$

$$U_F(\omega)\ U_F^\dagger(\omega) = U_F^\dagger(\omega)\ U_F(\omega) = \mathbb{1} \tag{A.6}$$

$$U_B(\omega)\ \tau\ U_B(\omega) = \tau \tag{A.7}$$

$$U_F(\omega)\ \tau\ U_F^\dagger(\omega) = \frac{1}{\cosh\frac{\beta\omega}{2}} \begin{bmatrix} \sinh\frac{\beta\omega}{2} & -1 \\ -1 & -\sinh\frac{\beta\omega}{2} \end{bmatrix} \tag{A.8}$$

$$U_F^\dagger(\omega)\ \tau\ U_F(\omega) = \frac{1}{\cosh\frac{\beta\omega}{2}} \begin{bmatrix} \sinh\frac{\beta\omega}{2} & 1 \\ 1 & -\sinh\frac{\beta\omega}{2} \end{bmatrix} \tag{A.9}$$

$$U_B^2(\omega) = \frac{1}{\sinh\frac{\beta\omega}{2}} \begin{bmatrix} \cosh\frac{\beta\omega}{2} & 1 \\ 1 & \cosh\frac{\beta\omega}{2} \end{bmatrix} \tag{A.10}$$

$$U_F(-\omega)\ \tau\ U_F^\dagger(-\omega) = -\ U_F^\dagger(\omega)\ \tau\ U_F(\omega) \tag{A.11}$$

$$U_B^2(-\omega) = -\ U_B^2(\omega) \tag{A.12}$$

SPECTRAL FUNCTIONS:

$$\bar{G}(\omega) = \int d\kappa \, \frac{\sigma(\kappa)}{\omega - \kappa + i\delta\tau} \tag{A.13}$$

Note
$$\frac{1}{\omega - \kappa + i\delta\tau} = \frac{\wp}{\omega - \kappa} \, \mathbb{1} - i\pi\tau \, \delta(\omega - \kappa) \quad . \tag{A.14}$$

Therefore
$$\tilde{G}(\omega) = \wp\int d\kappa \, \frac{\sigma(\kappa)}{\omega - \kappa} \, \mathbb{1} - i\pi\tau \, \sigma(\omega) \quad , \tag{A.15}$$

yielding
$$\sigma(\omega) = -\frac{1}{\pi} \mathscr{Im} \bar{G}^{11}(\omega) \tag{A.16}$$

and
$$G_F(\omega;\mu) = \wp\int d\kappa \, \frac{\sigma_F(\kappa)}{\omega - \kappa} \, \mathbb{1} - i\pi \, \sigma_F(\omega) \, U_F(\omega-\mu) \, \tau \, U_F^\dagger(\omega-\mu) \quad , \tag{A.17}$$

$$G_B(\omega;\mu) = \wp\int d\kappa \, \frac{\sigma_B(\kappa)}{\omega - \kappa} \, \tau - i\pi \, \sigma_B(\omega) \, U_B^2(\omega-\mu) \quad . \tag{A.18}$$

Note:
$$G^{\alpha\gamma}(\omega) = G^{\gamma\alpha}(\omega) \quad . \tag{A.19}$$

A.2 PROPERTIES OF THE SU(N) GROUP

GENERATORS OF THE SU(N) GROUP: λ_j

λ_j are traceless, Hermitian, N × N matrices.

There are $N^2 - 1$ of them.

NORMALIZATION:

$$\mathrm{Tr}(\lambda_i \, \lambda_j) = 2 \, \delta_{ij} \tag{A.20}$$

STRUCTURE FACTORS:

$$[\lambda_i \, , \lambda_j] = 2i \, f_{ijk} \, \lambda_k \tag{A.21}$$

$$\{\lambda_i \, , \lambda_j\} = \frac{4}{N} \, \delta_{ij} \, \mathbb{1} + 2 \, d_{ijk} \, \lambda_k \tag{A.22}$$

$$f_{ijk} \equiv -\frac{i}{4} \, \mathrm{Tr}(\lambda_i \, \lambda_j \, \lambda_k - \lambda_j \, \lambda_i \, \lambda_k) \tag{A.23}$$

$$d_{ijk} = \frac{1}{4} \, \mathrm{Tr}(\lambda_i \, \lambda_j \, \lambda_k + \lambda_j \, \lambda_i \, \lambda_k) \tag{A.24}$$

IDENTITIES:

$$\mathrm{Tr}(\lambda_i \, \lambda_j \, \lambda_k) = 2 \, (i f_{ijk} + d_{ijk}) \tag{A.25}$$

$$\lambda_i \, \lambda_j = (i f_{ijk} + d_{ijk}) \, \lambda_k + \frac{2}{N} \, \delta_{ij} \, \mathbb{1} \tag{A.26}$$

$$\sum_i \lambda_i^2 = \frac{2}{N} (N^2 - 1) \, \mathbf{1} \tag{A.27}$$

$$\sum_i d_{iik} = 0 \tag{A.28}$$

$$f_{ij\ell} f_{\ell km} = \frac{2}{N} (\delta_{ki} \delta_{jm} - \delta_{kj} \delta_{im}) + (d_{ki\ell} d_{\ell jm} - d_{kj\ell} d_{\ell im}) \tag{A.29}$$

$$f_{ij\ell} f_{kj\ell} = N \, \delta_{ik} \tag{A.30}$$

$$d_{ij\ell} d_{kj\ell} = \frac{N^2 - 4}{N} \delta_{ik} \tag{A.31}$$

$$f_{ijk} f_{ijk} = N \, (N^2 - 1) \tag{A.32}$$

$$d_{ijk} d_{ijk} = \frac{(N^2 - 4) \, (N^2 - 1)}{N} \tag{A.33}$$

JACOBI IDENTITIES:

$$f_{ij\ell} f_{\ell km} + f_{kj\ell} f_{\ell mi} + f_{mj\ell} f_{\ell ik} = 0 \tag{A.34}$$

$$f_{ij\ell} f_{\ell km} + f_{kj\ell} f_{\ell mi} + f_{mj\ell} f_{\ell ik} = 0 \tag{A.35}$$

TRACE RELATIONS:

$$\begin{aligned} \lambda_{i_1} \lambda_{i_2} \cdots \lambda_{i_n} \mathrm{Tr}(\lambda_{i_1} \lambda_{i_2} \cdots \lambda_{i_n}) &= -\frac{4}{N} \lambda_{i_1} \lambda_{i_2} \cdots \lambda_{i_{n-1}} \mathrm{Tr}(\lambda_{i_1} \lambda_{i_2} \cdots \lambda_{i_{n-1}}) + \\ &+ \frac{4}{N^2} (N^2 - 1) \, \lambda_{i_1} \lambda_{i_2} \cdots \lambda_{i_{n-2}} \mathrm{Tr}(\lambda_{i_1} \lambda_{i_2} \cdots \lambda_{i_{n-2}}) \end{aligned} \tag{A.36}$$

$$\begin{aligned} &\lambda_{i_1} \lambda_{i_2} \cdots \lambda_{i_n} \mathrm{Tr}(\lambda_{i_n} \cdots \lambda_{i_2} \lambda_{i_1}) = \\ &= \frac{2 \, (N^2 - 2)}{N} \lambda_{i_1} \lambda_{i_2} \cdots \lambda_{i_{n-1}} \mathrm{Tr}(\lambda_{i_{n-1}} \cdots \lambda_{i_2} \lambda_{i_1}) + \\ &+ \frac{4}{N^2} (N^2 - 1) \, \lambda_{i_1} \lambda_{i_2} \cdots \lambda_{i_{n-2}} \mathrm{Tr}(\lambda_{i_{n-2}} \cdots \lambda_{i_2} \lambda_{i_1}) \end{aligned} \tag{A.37}$$

In general:

$$\lambda_{i_1} \lambda_{i_2} \cdots \lambda_{i_n} \mathrm{Tr}(\lambda_{i_1} \lambda_{i_2} \cdots \lambda_{i_n}) \propto \mathbf{1} \tag{A.38}$$

$$\lambda_{i_1} \lambda_{i_2} \cdots \lambda_{i_n} \mathrm{Tr}(\lambda_{i_n} \cdots \lambda_{i_2} \lambda_{i_1}) \propto \mathbf{1} \tag{A.39}$$

In particular:

$$\lambda_i \lambda_j \mathrm{Tr}(\lambda_i \lambda_j) = \lambda_i \lambda_j \mathrm{Tr}(\lambda_j \lambda_i) = \frac{4}{N} (N^2 - 1) \, \mathbf{1} \tag{A.40}$$

$$\lambda_i \lambda_j \lambda_k \mathrm{Tr}(\lambda_i \lambda_j \lambda_k) = -\frac{16}{N^2} (N^2 - 1) \, \mathbf{1} \tag{A.41}$$

$$\lambda_i \lambda_j \lambda_k \, \mathrm{Tr}(\lambda_k \lambda_j \lambda_i) = \frac{8}{N^2} (N^2-2)(N^2-1) \; \mathbb{1} \qquad \text{(A.42)}$$

OTHER RELATIONS:

$$f_{ijk} \lambda_i \lambda_j \lambda_k = - f_{ijk} \lambda_k \lambda_j \lambda_i = 2i(N^2-1) \; \mathbb{1} \qquad \text{(A.43)}$$

$$d_{ijk} \lambda_i \lambda_j \lambda_k = d_{ijk} \lambda_k \lambda_j \lambda_i = \frac{2}{N^2} (N^2-4)(N^2-1) \; \mathbb{1} \qquad \text{(A.44)}$$

$$\sum_i \lambda_i^{\ell\ell'} \lambda_i^{mm'} = 2 \left[- \frac{1}{N} \delta_{mm'} \delta_{\ell\ell'} + \delta_{\ell m'} \delta_{m\ell'} \right] \qquad \text{(A.45)}$$

Equivalently:

$$- \delta_{mm'} \delta_{\ell\ell'} + \delta_{\ell m'} \delta_{m\ell'} = - \left[1 - \frac{1}{N} \right] \delta_{mm'} \delta_{\ell\ell'} + \frac{1}{2} \sum_i \lambda_i^{mm'} \lambda_i^{\ell\ell'} \qquad \text{(A.46)}$$

APPENDIX B
VIOLATING THE CANONICAL QUANTIZATION CONDITION

The purpose of this appendix is to show how one may violate the canonical quantization condition, and yet have the Euler–Lagrange equations of the Lagrangian agree with the Heisenberg equations of the Hamiltonian.

Suppose there exists a Lagrangian density $\mathscr{L}(x)$ which has the form of a type 1 fermion field as follows:

$$\mathscr{L}(x) = \psi^{\dagger}(x)\left[i\frac{\partial}{\partial t} - \varepsilon(\vec{\nabla})\right]\psi(x) \quad . \tag{B.1}$$

The canonical momentum of $\psi(x)$ is given by:

$$\Pi_{\psi}(x) = \frac{\delta\mathscr{L}(x)}{\delta\dot{\psi}(x)} = i\,\psi^{\dagger}(x) \quad , \tag{B.2}$$

and the Euler–Lagrange equations of eq. (B.1) are:

$$\left.\begin{aligned} \frac{\delta\mathscr{L}(x)}{\delta\psi^{\dagger}(x)} &= \frac{d}{dt}\,\frac{\delta\mathscr{L}(x)}{\delta\dot{\psi}^{\dagger}(x)} \Rightarrow \left[i\frac{\partial}{\partial t} - \varepsilon(\vec{\nabla})\right]\psi(x) = 0 \\ \frac{\delta\mathscr{L}(x)}{\delta\psi(x)} &= \frac{d}{dt}\,\frac{\delta\mathscr{L}(x)}{\delta\dot{\psi}(x)} \Rightarrow \left[-\,i\frac{\partial}{\partial t} - \varepsilon(\vec{\nabla})\right]\psi^{\dagger}(x) = 0 \end{aligned}\right\} \tag{B.3}$$

The Hamiltonian density is given by the usual Legendre transform $\mathscr{H}(x) = \Pi(x)\dot{\psi}(x) - \mathscr{L}(x)$, which yields:

$$\mathscr{H}(x) = \psi^{\dagger}(x)\,\varepsilon(\vec{\nabla})\,\psi(x) \tag{B.4}$$

Up to this point, we have used the usual canonical procedure of classical field theory. Now, to quantize the field, one would normally impose the canonical quantization condition, namely: $\left\{\psi(\vec{x},t),\Pi_{\psi}(\vec{y},t)\right\} = i\delta^{3}(\vec{x}-\vec{y})$. Using eq. (B.2), this would lead to $\left\{\psi(\vec{x},t),\psi^{\dagger}(\vec{y},t)\right\} = \delta^{3}(\vec{x}-\vec{y})$.

Let us instead impose the following condition:

$$\left\{\psi(\vec{x},t)\,,\,\Pi_{\psi}(\vec{y},t)\right\} = i\,\delta^{3}(\vec{x}-\vec{y})\;M(\vec{x},t) \tag{B.5}$$

where $M(\vec{x},t)$ is an operator. This yields:

$$\left\{\psi(\vec{x},t)\,,\,\psi^{\dagger}(\vec{y},t)\right\} = \delta^{3}(\vec{x}-\vec{y})\;M(\vec{x},t) \tag{B.6}$$

Now let us check to see if the Heisenberg equations agree with eqs. (B.3). They are given by:

$$i\frac{\partial}{\partial t}\psi(\vec{x},t) = -\left[H,\psi(\vec{x},t)\right] = -\int d^3y \left[\psi^\dagger(\vec{y},t)\,\varepsilon(\vec{\nabla}_y)\,\psi(\vec{y},t)\,,\,\psi(\vec{x},t)\right] =$$

$$= \int d^3y \left\{\psi^\dagger(\vec{y},t)\,,\,\psi(\vec{x},t)\right\}\varepsilon(\vec{\nabla}_y)\,\psi(\vec{y},t) = M(\vec{x},t)\,\varepsilon(\vec{\nabla})\,\psi(\vec{x},t) \tag{B.7}$$

Similarly:

$$i\frac{\partial}{\partial t}\psi^\dagger(\vec{x},t) = -\,\psi^\dagger(\vec{x},t)\,\varepsilon(\overleftarrow{\nabla})\,M(\vec{x},t) \tag{B.8}$$

These Heisenberg equations are consistent with the Euler–Lagrange equations only if

$$\left.\begin{aligned} M(\vec{x},t)\,\psi(\vec{x},t) &= \psi(\vec{x},t) \\ \psi^\dagger(\vec{x},t)\,M(\vec{x},t) &= \psi^\dagger(\vec{x},t) \end{aligned}\right\} \tag{B.9}$$

The usual solution is to take $M = \mathbb{1}$, which corresponds to the canonical quantization condition. This is not the only solution. M may differ from $\mathbb{1}$ if ψ is a singular operator: $\det\psi = 0$. That is, when one chooses a space in which to represent ψ and M, M must act as a unit matrix in the subspaces in which ψ has non–zero components, and ψ must be zero in the subspaces in which M is not 1.

To illustrate, let P and P' be projection operators which satisfy:

$$\left.\begin{aligned} &P^2 = P\,, \qquad P'^2 = P'\,, \qquad P\,P' = 0\,, \\ &P\,\psi(\vec{x},t) = \psi(\vec{x},t)\,, \qquad P'\,\psi(\vec{x},t) = 0\,. \end{aligned}\right\} \tag{B.10}$$

Then:

$$M(\vec{x},t) = P + X(\vec{x},t)\,P'\,, \tag{B.11}$$

where $X(\vec{x},t)$ is an arbitrary operator. The choice of $X(\vec{x},t)$ will depend upon the algebra one wishes to consider in eq. (B.6).

Thus one sees that the canonical quantization procedure may be consistently violated, within the above constraints.